Copyright is owned by the Author of the thesis. Permission is given for a copy to be downloaded by an individual for the purpose of research and private study only. The thesis may not be reproduced elsewhere without the permission of the Author.

Performance Optimisation of a Solar Air Heater for Heating and Ventilating: A Comparative Study Contributing to New Zealand Classrooms

A thesis submitted in partial fulfillment of the requirements for the degree of

Doctor of Philosophy (Ph.D.)

in

Built Environment

at Massey University, Auckland,

New Zealand

Poonam Pardeshi

2025

Declaration of authorship

I, Poonam Subhash Singh Pardeshi, declare that this thesis titled "Performance Optimisation of a Solar Air Heater for Heating and Ventilating: A Comparative Study Contributing to New Zealand Classrooms" and the work presented in it is my own. I confirm that:

- This work was composed by myself, and where I have used ideas, text, images, or other materials from the work of others, I have appropriately acknowledged and referenced them according to the guidelines provided by Massey University.
- I have not previously submitted this work or any part to be examinimumed at this or any other institution for a degree or as part of any other academic qualifications.
- Any contributions to this work by other individuals or groups are clearly stated and acknowledged in the text or a separate section.

By signing below, I declare that this statement is accurate and truthful.

Poonam Subhash Singh Pardeshi
15/12/2025

Abstract

New Zealand primary schools often fail to meet the World Health Organization (WHO) and American Society of Heating, Refrigerating, and Air-Conditioning Engineers (ASHRAE) standards for winter ventilation and temperature. Poor indoor air quality affects health, well-being, and learning, highlighting the need for better ventilation. Furthermore, strict energy caps in schools make affordable heating and ventilation solutions essential. Since school hours largely coincide with peak solar radiation, solar energy presents a cost-effective pathway to address these challenges.

Solar air heaters (SAHs) have the potential to provide space heating and ventilation simultaneously. However, their application is limited by low thermal efficiency, primarily due to internal and external heat losses. The central research question of this study is: how can the performance of SAHs be optimised to provide effective, low-cost heating and ventilation for New Zealand classrooms?

To address this question, three optimisation strategies were explored at Massey University in 2023. The first examined operational adjustments to a finned-tube SAH with corrugated fins (FT-SAH) under different fan speeds and seasons. The second experiment tested the finned tube SAH with fin inserts (treatment) and without fin inserts (control) to investigate the effect of fin inserts on its thermal performance. The third investigated material optimisation using nanocoated absorber tubes. These approaches collectively aimed to identify pathways for improving SAH performance for classroom heating and ventilation.

The first experiment tested a novel FT-SAH under New Zealand climatic conditions: Case Study 1 at 100% fan speed in winter, and Case Study 2 at 50% fan speed in spring. Results showed a trade-off between airflow, temperature gain, and thermal efficiency. At higher fan speeds (Case Study 1), the system achieved higher mass flow rates, with daily averages ranging from 0.054 to 0.059 kg/s (mean: 0.056 kg/s), and ventilation capacity ranging from 164.2 to 175.3 m^3/h (mean: 172.4 m^3/h). However, this resulted in only moderate outlet temperatures (17.3–49.3 $^{\circ}C$, mean: 29.4 $^{\circ}C$), lower temperature rise (ΔT) values (6.0–32.6 $^{\circ}C$, mean: 15.9 $^{\circ}C$), and decreased thermal efficiency (38.6–83.8%, mean: 69.6%). In contrast, under lower fan speeds (Case Study 2), the FT-SAH produced higher outlet temperatures (24.4–59.0 $^{\circ}C$, mean: 39.9 $^{\circ}C$) and greater ΔT values (10.2–41.3 $^{\circ}C$, mean: 24.1 $^{\circ}C$). However, this was accompanied by reduced airflow (0.022–0.025 kg/s, mean: 0.024 kg/s), lower ventilation (69.9–77.0 m^3/h, mean: 74.8 m^3/h), and decreased thermal efficiency (23.8–34.7%, mean: 29.4%). These findings highlight that high fan speeds favour ventilation, while low fan speeds enhance

heating. However, in both cases, the FT-SAH alone did not meet the minimum ventilation rates recommended by the New Zealand Ministry of Education (MOE). Future work should focus on optimising FT-SAH operation to balance ventilation and heating, particularly by increasing the volume of warm air supplied while maintaining outlet air temperatures near 18.0 °C to support classroom comfort.

In the second experiment, the FT-SAH was tested under two configurations: tubes with corrugated fins (treatment) and tubes without fins (control). At high fan speed ($\dot{m}$ = 0.07 kg/s), the treatment achieved higher outlet temperatures of 25.4 °C compared to 22.3 °C for the control, along with a larger temperature rise of 7.0 °C compared to 4.4 °C, and a greater efficiency of 72.6% compared to 44.5%. At a low fan speed ($\dot{m}$ = 0.04 kg/s), the treatment again outperformed the control, reaching outlet temperatures of 29.4 °C, a temperature rise of 10.4 °C, and an efficiency of 57.0%, compared to 25.3 °C, 6.3 °C, and 33.4%, respectively. These results demonstrate that the addition of corrugated fins substantially enhanced heat transfer and overall thermal efficiency under both operating conditions, confirming the effectiveness of the modified finned-tube design for classroom heating and ventilation applications.

The third experiment investigated nanocoated absorber tubes using aluminium oxide (Al_2O_3) and copper oxide (CuO) in black paint. A 4% Al_2O_3/black paint coating with fin inserts improved thermal efficiency by 37.5% compared to the control and increased outlet air temperatures by up to 16.4 °C. Although these tubes were tested without a cover, insulation, or frame, the results demonstrated the potential of nanocoating to improve performance further. Tubes integrated into a box (SAH) must be investigated for thermal performance.

Overall, the study shows that while a single FT-SAH unit cannot independently achieve the required classroom ventilation rates, performance optimization through fin design and nanocoating can substantially improve thermal output. For practical classroom application, multiple SAH units, integrated with insulation and proper casing, would be required to meet both heating and ventilation demands.

Acknowledgment

I would like to thank my primary supervisor, Dr. Mikael Boulic, for his guidance, encouragement, and generous assistance throughout the research process. It was a great experience working under his supervision. This thesis would not have been possible without his critical and honest feedback, suggestions, ideas, and assistance. Thank you for teaching me how to write literature, research proposals, and presentations. Thank you for being so patient and kind towards me.

I would like to express my gratitude to my co-supervisors, Dr Hennie van Heerden and Professor Chris Cunningham, for their guidance and help in achieving this milestone. I am grateful to Prof Chris Cunningham for hosting me at the Massey Wellington campus. Thank you for arranging the access card and campus facilities. Thank you, Dr Hennie, for always being a call away whenever I needed guidance or was confused. This journey would not have been possible without your support. I would like to thank you both for giving your valuable suggestions, feedback, comments and ideas on the papers and chapters.

A big thanks to my advisor, Professor Robyn Phipps, for agreeing to supervise me. You are the best advisor I have ever met. My visit to New Zealand would not have been possible without your support. You helped me get the Massey Doctoral Scholarship. You have always motivated and supported me. Thank you for helping me get the required instruments for the experiment. Thank you for giving me the tutoring opportunity and for being one of my referees. I appreciate your technical and scientific advice during the experimental test.

I would like to thank Grace from Sojol Pvt Ltd for allowing me to work on the solar air heater design and for helping with the installation and data collection.

I would like to thank Prachee (admin) and Linda (Wellington campus facilities and services) for helping me make the experiment run smoothly. They both helped me access the labs, car park, and tools needed to carry out the research safely on the campus.

Thank you to APL Window LTD and Resene Paints for sponsoring the aluminium tubes and paint needed for the research.

I would like to thank Massey University, both the School of Built Environment and the College of Health (Research Centre for Hauora and Health), for the information technology, technical, and administrative support. Thank you to the staff and fellow students for always motivating and encouraging me.

I would like to thank Vivian Fang and Bill Trompetter, GNS Science, Wellington, for their guidance on nanofluid coating.

Lastly, I would like to thank my parents, parents-in-law, sister-in-law, siblings, niece, and friends for their emotional support and availability when I needed them the most. Special thanks to my husband for being patient and kind throughout our journey. He has stood by my side through both good and challenging times. This journey would be impossible without his support.

During this journey and at this moment, I have often thought about my late father and father-in-law. They would be immensely proud of me.

Abbreviations/Nomenclature

ASHRAE	American Society of Heating, Refrigeration, and Air Conditioning Engineers
BRANZ	Building Research Association Of New Zealand
CO_2	Carbon dioxide
ETC	Evacuated tube collector
ET-SAH	Evacuated tube solar air heater
FT-SAH	Finned tube-type SAH with corrugated fin inserts
IAQ	Indoor air quality
IEA	International Energy Agency
l/s/person	Litres of fresh air per second per person
MHPA	Micro-heat pipe array
NZMOE	New Zealand Ministry of Education
NZ	New Zealand
NZS	New Zealand Standards
PCM	Phase change material
PTC	Parabolic trough collectors
SAH	Solar air heater
SARS-CoV	Severe acute respiratory syndrome coronavirus
TES	Thermal energy storage
TSAH	Tube-type solar air heater
WHO	World Health Organization
NIWA	National Institute of Water and Atmospheric Research
RH	Relative humidity
SD	Standard deviation
CNT	Carbon nanotubes

Glossary

Fin	A fin is an extended surface attached to a heat exchanger to increase its surface area and enhance heat transfer.
Heat Transfer	Heat transfer is the movement of thermal energy from one object or substance to another.
Hybrid Nanofluid	A hybrid nanofluid contains two or more different types of nanoparticles suspended in a base fluid, such as water, ethylene glycol, or oil. A hybrid nanofluid aims to influence the unique properties of each nanoparticle to achieve superior thermal performance and heat transfer capabilities.
Indoor Air Environment	Indoor air quality refers to the quality of the air inside buildings and structures, particularly concerning the health and comfort of occupants.
Nanofluid	Nanofluid is a fluid containing metallic particles with an average particle size of 10.0 nanometres (nanoparticles) uniformly and stably suspended in a base fluid such as water, oil, or ethylene glycol. The primary goal of adding nanoparticles to a fluid is to enhance its thermal properties, particularly its heat transfer capabilities.
Overall Efficiency	The ratio of useful energy output to the total energy input in a system expressed as a percentage.
Solar Air Heaters	Solar air heaters use solar energy to heat air, typically for space heating or drying.
Specific Heat	Specific heat is the amount of heat energy required to raise the temperature of a unit mass of a substance by one degree Celsius (or Kelvin)
Temperature Difference	The difference in temperature between air entering and exiting a solar air heater
Ventilation	Ventilation is supplying fresh air to an indoor space and removing stale air, typically to control temperature, humidity, and air quality.
Ventilation Rate	The ventilation rate is the air (measured in cubic meters per second or cubic feet per minute) introduced into or removed from a space over a certain period. Higher ventilation rates typically improve air quality but may increase energy usage.

Publications and my contributions

The literature study on artificial roughness (chapter 2) has been published in the Journal of "***Renewable and Sustainable Energy Reviews***" and the details are as follows:

1) Pardeshi, Poonam S., Mikael Boulic, Andries van Heerden, Robyn Phipps, and Chris W. Cunningham. 2024. "Review of the thermal efficiency of a tube-type solar air heater." Renewable and Sustainable Energy Reviews 199. https://doi.org/10.1016/j.rser.2024.114509.

Expected future publication outcomes from the thesis chapters

Sr No	Paper title	Submission status
1)	Experimental investigation of a finned tube-type solar air heater with corrugated fin inserts for heating and ventilating – a New Zealand study	In preparation
2)	Thermal Performance of a Finned Tube-Type Solar Air Heater with and without Corrugated Fin Inserts	In preparation
3)	Thermal efficiency of Nanocoated tubes with and without Fin Inserts	In preparation
4)	Literature Review on Nanofluids for Solar Thermal Engineering Systems	In preparation

My contributions to the papers

For the literature review paper (Chapter 2), **"Review of the thermal efficiency of a tube-type solar air heater,"** I identified the research gaps, synthesized and organized the existing knowledge, and critically evaluated the previous work. With the help of Dr. Mikael Boulic and Dr. Andries (Hennie) van Heerden, I developed conceptual frameworks. I also proposed new research directions and finally concluded the outcomes. The co-authors made comments and edited the paper.

For a paper titled "Experimental investigation of a finned tube-type solar air heater with corrugated fin inserts for heating and ventilating – a New Zealand study" I conducted the experimental work and collected and analyzed the data. Created conceptual frameworks with the help of Dr. Mikael Boulic and Dr. Andries (Hennie) van Heerden. Dr Mikael Boulic helped me with data analysis and calculations. Dr. Andries (Hennie) van Heerden contributed to the paper's structure. I wrote the first draft of the paper. Co-authors made comments and edited the paper.

Table of Contents

Declaration of authorship ……ii
Abstract ……...iii
Acknowledgment ……v
Abbreviation/Nomenclature ……vii
Glossary ……viii
Publications and my contributions ……ix
1. Introduction 1
1.1 Background 1
1.2 Research aims, questions, and objectives 5
1.2.1 Research aim 5
1.2.2 Research questions 5
1.2.3 Research objectives 5
1.2.4 Research philosophy 6
1.3 Scopes and limitations 6
1.3.1 The limitations of this research 7
1.3.2 The delimitations of this research 8
1.4 Conceptual framework 9
1.5 Thesis outline 11
1.6 Research phases 13
2 Review of the thermal efficiency of a tube-type solar air heater 15
2.1 Introduction 15
2.2 Tube-type SAH components and airflow through SAH 18
2.3 Equation used to determine the thermal efficiency of SAHs 19
2.4 Review methodology 19
2.5 Results: Different techniques to improve the thermal efficiency of the SAH 21
2.5.1 Adding artificial roughness to a tube-type SAH 22
2.5.2 Adding a thermal energy storage to increase thermal efficiency 27
2.5.3 Using an Evacuated tube to increase the thermal efficiency of the SAH 31
2.5.4 Micro heat pipe array type SAH 37
2.5.5 Other techniques include applying reflectors, coating, and using high thermal conductivity materials. 41
2.6 Literature review on nanofluids for solar thermal engineering systems 44
2.7 Introduction 44
2.8 Applications and performance of nanofluids in solar thermal systems 45

2.9 Nanocoating of absorber tubes 45
2.10 Nanofluids as working fluids 46
Excluded areas of research and limitations 46
Types of nanofluids based on nanoparticles 46
2.10.1 Metal oxide nanoparticles 47
2.10.2 High thermal conductivity metals 50
2.10.3 Carbon based nanoparticles 51
2.11 Hybrid nanofluids in solar thermal applications 54
2.12 Conclusion 56
2.13 Limitations and future scope 59
2.14 Proposed design: nanocoated corrugated tubes with finned inserts 61
3 Experimental performance of a tube-type solar air heater with corrugated fin inserts in New Zealand 62
3.1 Materials and Methods 65
3.1.1 Structure of the tested finned tube-type solar air heater (FT-SAH) 65
3.1.2 Experimental setup and test procedure 67
3.1.3 Methodological justification and research philosophy 69
3.1.4 Thermal efficiency calculation 70
3.1.5 Effective efficiency calculation 71
3.1.6 Uncertainty analysis 72
3.2 Results and discussion 72
3.2.1 Wellington weather conditions 72
3.2.2 Ambient temperature, solar radiation, wind speed, and rainfall 73
3.2.3 Temperature difference between outlet and inlet air temperature 77
3.2.4 Outlet air temperature and ventilation rate 82
3.2.5 Application of FT-SAH 89
3.2.6 Thermal efficiency of FT-SAH 91
3.3 Conclusion 95
3.4 Limitations and Future Scope 96
4 Effect of fin inserts on the thermal efficiency of the tube-type solar air heater 98
4.1 Introduction 99
4.2 Materials and methods 103
4.2.1 Structure of the tested FT-SAH with and without fin inserts 103
4.2.2 Tube setting 104
4.2.3 Experimental setup and test procedure 105
4.2.4 Thermal efficiency calculation 106

4.3 Results and discussion 107
4.3.1 Ambient temperature, solar radiation, wind speed 107
4.3.2 Investigating the change in Temperature difference (outlet temperature minimum inlet temperature) between the control case (no insert) and the treatment case (insert) ... 108
4.3.3 Ventilation rate 112
4.3.4 Thermal efficiency of FT-SAH 112
4.4 Conclusion and future scope 114
4.5 Limitation 115
5 Experimental investigation of the thermal performance of uncoated and nanocoated tubes 117
5.1 Introduction 119
5.2 Research Methodology 121
5.3 Materials and Methods 124
5.3.1 Tubes setting 124
5.3.2 Experimental setup 124
5.3.3 Nanofluid preparation 125
5.3.4 Nanofluid preparation process 127
5.4 Data collection 128
5.4.1 Thermal efficiency calculation 129
5.5 Results 129
5.5.1 Ambient temperature and solar radiation 129
5.5.2 Outlet air temperature and temperature difference (T_o-T_i) 130
5.5.3 Ventilation rate of tubes 136
5.5.4 Comparison of thermal efficiency of control vs treatment tubes 137
5.5.5 Discussion 145
5.6 Limitations of the experimental setup 146
5.7 Conclusion and future scope 147
6 General Discussion 149
6.1 Finned tube solar air heater with corrugated fin inserts 150
6.2 Finned tube SAH with and without fin inserts 152
6.3 Nanocoated tubes. 153
Summary 155
7 Conclusion and Recommendation 156
7.1 Original contribution 156
7.2 Conclusions drawn from the research objectives 157
7.3 Limitations of the Study 158

7.4 Future scope of research 159
7.5 Significance of the findings 160
8 References 161
Appendices 176

List of Tables

Table 2-1 Summary of the review studies mentioned in Section 2.5.1 26
Table 2-2 Summary of the review studies is mentioned in section 2.5.2 29
Table 2-3 Summary of the review studies is mentioned in section 2.5.3 36
Table 2-4 Summary of the review studies is mentioned in section 2.5.4 40
Table 2-5 Summary of the literature studies discussed in Section 2.12.1 49
Table 2-6 Summary of literature studies discussed in sections 2.12.2 and 2.12.3 53
Table 2-7 A summary of the literature studies is discussed in section 2.13 55
Table 3-1 The characteristics of the monitoring equipment 67
Table 3-2 Air density at different air temperatures (Cengel 2011) 71
Table 3-3 The daily average ± SD values of ambient temperature (T_a), wind speed, and rainfall on each test day 75
Table 3-4 The daily average (± SD) of air mass flow rate ($\dot{m}$), solar radiation incident on the FT-SAH surface (I_T), and temperature difference between the outlet and inlet air ($\Delta T = T_o - T_i$) for Case Study 1 and Case Study 2 77
Table 3-5 The daily average ± SD values of ventilation correspond to the outlet air temperature values when FT-SAH operates at 100% and 50% maximum ventilator speed in good weather conditions 87
Table 3-6 Percentage of the time when the hourly average outlet temperature is above 18°C for Case Studies 1 and 2 90
Table 3-7 Hourly average airflow rates at 20 °C and percentage of time when volume flow rate ≥ 864 m³/h 90
Table 3-8 Thermal efficiency comparison of the present work with work conducted by other researchers 93
Table 4-1 Literature studies on improving the thermal efficiency of SAHs integrated with artificial roughness 100
Table 4-2 The characteristics of the monitoring equipment 105
Table 4-3 Air density at different air temperatures (Cengel 2011) 106
Table 4-4: The daily average ± SD values of ambient temperature and solar radiation on each test day 107
Table 4-5 The daily average values of T_o, T_a, ΔT, and ΔT_1 for control SAH operating at high speed 111
Table 4-6 The daily average values of T_o, T_a, ΔT, and $\Delta T1$ for control SAH operating at low speed 111
Table 5-1 Overview of experimental tests for control, black paint coating, and nanocoated tubes with and without fins 123
Table 5-2 shows the properties of Al_2O_3, CuO nanoparticles, and Lumberside matt black paint 126
Table 5-3 The characteristics of the monitoring equipment used for the experiment 128
Table 5-4 Air-specific capacity and air density at different air temperatures (Cengel 2011) 129
Table 5-5 The daily average ambient temperature (T_a) and solar radiation on the tilted surface (I_T) 130
Table 5-6 The daily average outlet temperature (T_o), ambient temperature (T_a), and temperature difference (ΔT) and change in temp difference between treatment and control tubes (ΔT_1) values for Test 1 133

Table 5-7 The daily average outlet temperature (T_o), ambient temperature (T_a), and temperature difference (ΔT) and change in temp difference between treatment and control tubes (ΔT_1) values for Test 2 134
Table 5-8 The daily average outlet temperature (T_o), ambient temperature (T_a), and temperature difference (ΔT) and change in temp difference between treatment and control tubes (ΔT_1) values for Test 3 135
Table 5-9 The daily average outlet temperature (T_o), ambient temperature (T_a), and temperature difference (ΔT), and change in temp difference between treatment and control tubes (ΔT_1) values for Test 4 135
Table 5-10: Thermal efficiency of tubes with and without fins when coated with black paint and Al_2O_3 142
Table 5-11 Thermal efficiency of tubes with and without fins when coated with black paint and CuO 143

List of Figures

Figure 1-2-1 Sunshine hours (monthly) for the different sites in the Wellington region (Chappell, 2014) 7
Figure 1-2-2 A conceptual framework for the research 10
Figure 1-2-3 Thesis outline, objective, and aim 12
Figure 1-2-4 The sequence of the four research phases 14
Figure 2-1 Schematic diagram of tube-type SAH 18
Figure 2-2 Five-step review process 21
Figure 2-3 SAH efficiency improvement techniques 22
Figure 2-4 Schematic diagram (a) SAH-I, and (b) SAH-II (Fan et al., 2019) 23
Figure 2-5 SAH with increased roughness from ribs (Komolafe et al., 2019) 24
Figure 2-6 Geometry of (a) half-finned turbulator and (b) full-finned turbulator (Afshari et al., 2020) 24
Figure 2-7 (a) SAH experimental setup, (b) modified- iron mesh (Sozen et al., 2020) 25
Figure 2-8 Angular twisted tape of varying length: a) Full-length, b) Short-length, c) Short-length middle (Souayeh et al., 2021) 26
Figure 2-9 A sectional view of SAH with PCM-filled cylindrical tubes (Singh et al., 2021) 28
Figure 2-10 Tubes arrangement: A) Inline shape, B) Circular shape, and C) Staggered shape (Madhulatha et al., 2021) 29
Figure 2-11 ET collector with inserted tubes (Li et al., 2012) 31
Figure 2-12 Cross section of ET; (a) control system, (b) system with copper coil, (c) system with aluminium fins (Abu Hamed & Alkharabsheh, 2020) 32
Figure 2-13 Schematic diagram of thermal storage ET heat pipe solar collector with header section (Abi Mathew & Thangavel, 2021) 32
Figure 2-14 Evacuated Tube with helical tube inserts (Singh & Vardhan, 2021) 33
Figure 2-15 ET SAH without reflectors and B) ET SAH with reflectors (Dabra et al., 2018) 33
Figure 2-16 . Schematic diagram of ET-SAH with CPC (Wang et al., 2015) 34
Figure 2-17 Schematic view of parabolic trough SAH (Nain et al., 2021) 34
Figure 2-18 Schematic diagram of ET with U-shaped Copper tube insert (Pandey et al., 2021) 35
Figure 2-19 Schematic diagram of the SAH with MHPA transparent-vacuum glass tube (T.-y. Wang et al., 2019) 38
Figure 2-20 Schematic diagram of the conventional tube collector and transparent tube collector (Wang, D. Tengyue, Yanhua, et al., 2020) 39
Figure 2-21 Schematic diagram of the MPHA (Norouzi et al., 2020) 40
Figure 2-22 An experimental set of ETSC-HP (Abo-Elfadl et al., 2020) 43
Figure 2-23 Picture of proposed SAH 61
Figure 3-1 A study conducted by various researchers on the thermal efficiency of SAHs 63
Figure 3-2 . An experimental set of FT-SAH 65
Figure 3-3 Schematic diagram of FT-SAH (A. transversal section) and air circulation through the absorber tube (B. longitudinal section) 66

Figure 3-4 The mean (±SD) values of the temperature difference between outlet and inlet air on each test day for FT-SAH operating at 100% (left) and 50% (right) maximum speed of the ventilator 81
Figure 3-5 Mean (±SD) outlet air temperature and solar radiation for FT-SAH under Case Study 1 (left, winter, 100% fan speed) and Case Study 2 (right, spring, 50% fan speed). Data points are hourly averages; straight-line connections only (no polynomial smoothing). Comfort thresholds (18.0–25.0 ˚C) are shown according to ASHRAE and MOE guidelines 83
Figure 3-6 The time lag between the optimum temperature and the optimum solar radiation for FT-SAH operating at 100% (Case Study 1) and 50% (Case Study 2) maximum speed of the ventilator 85
Figure 3-7 Relationship between thermal efficiency and the temperature difference ratio ($\Delta T/I_T$) for FT-SAH at two mass flow rate ranges: 0.051–0.062 kg/s (Case Study 1, black plain squares) and 0.020–0.026 kg/s (Case Study 2, red plain circles). Data points represent hourly averages calculated from one-minute sampling intervals. 92
Figure 3-8 The overall efficiency of FT-SAH for Case Studies 1 and 2 94
Figure 4-1 Sections discussed in the chapter 99
Figure 4-2 The experimental set of FT-SAH 103
Figure 4-3 Tube setting for treatment and control SAH 103
Figure 4-4 Schematic diagram of the FT-SAH 104
Figure 4-5 Comparison of outlet temperature for control and treatment SAH with solar radiation operating at high fan speed (21/12/2023 and 22/12/2023) 109
Figure 4-6 Comparison of outlet temperature for control and treatment SAH with solar radiation operating at low fan speed (23/12/2023 and 24/12/2023) 110
Figure 4-7 Thermal efficiency comparison for treatment and control SAH at high (0.07 kg/s) and low (0.04 kg/s) mass flow rates 113
Figure 5-1 chapter 4 framework 119
Figure 5-2 Studies on nanofluid-coated solar collectors 120
Figure 5-3 Research process for experimental test results of nanocoated tube 122
Figure 5-4 Experimental set of control and modified tubes 124
Figure 5-5 Experimental setup of data acquisition and outlet system 125
Figure 5-6 The materials used and setup of the test tube and sonicator bath 126
Figure 5-7 The nanofluid preparation process 127
Figure 5-8 Mean outlet temperature vs Solar radiation plot on a tilted surface for Test 1 (14/11/2023, 16/11/2023 and 21/11/2023) 131
Figure 5-9 Mean outlet temperature vs Solar radiation plot on a tilted surface for Test 2 (22/11/2023, 23/11/2023 and 24/11/2023) 131
Figure 5-10 Mean outlet temperature vs Solar radiation plot on a tilted surface for ... 132
Figure 5-11 Mean outlet temperature vs Solar radiation plot on a tilted surface for ... 132
Figure 5-12: Test 1 ηth vs. $\Delta T/IT$ plot over three days (14/11, 16/11, and 21/11/2023) 138
Figure 5-13: Test 2 ηth vs. $\Delta T/IT$ plot over three days (22/11, 23/11 and 24/11/2023) .. 140
Figure 5-14: Test 3 and Test 4 ηth vs. $\Delta T/IT$ plot (27/11 and 29/11/2023) 141
Figure 5-15: Comparison of thermal efficiency of tubes with 4% nanofluid coating (present study) 145

1. Introduction

Around 90% of New Zealand classrooms are naturally ventilated through opening windows (McIntosh, 2011a). Studies showed that only 40.0% of teachers opened the windows during teaching times (N. Z. Ministry of Education, 2014). Conventional mechanical ventilation systems have a high capital cost and need maintenance (Cutler-Welsh, 2006a). Introducing mechanical or mixed systems will add to the school's expenses (M. Ministry of Education, 2014). This means an alternative, affordable method is required to provide sufficient winter ventilation in the classroom. The school hours (9 a.m. to 3 p.m.) closely align with the optimal solar radiation. Therefore, schools are an ideal environment for harnessing solar energy.

In December 2019, severe acute respiratory syndrome coronavirus 2 (SARS-CoV-2) spread rapidly, raising global public health concerns. SARS-CoV-2 (Covid-19) spreads through close contact, contaminated surfaces, respiratory droplets, and fomites (Azuma et al., 2020). Students are in close contact with one another for prolonged periods in classrooms and other activities. Therefore, educational facilities pose a significant risk of infection in various environments (Azuma et al., 2020; Lorenc et al., 2021). The researchers found that SARS-CoV-2 transmission can be reduced by masking, frequent hand sanitizing, social distancing, improving ventilation, avoiding air recirculation, implementing air filters and purifiers with existing ventilation systems in closed spaces, and exposure to sunlight (Lorenc et al., 2021; Morawska et al., 2020; Prevention, 2022). Research indicates that improved ventilation is important for mitigating the effects of COVID-19, as discussed in Section 1.1 (Background).

Primary schools in New Zealand fail to maintain temperatures or ventilation levels that comply with WHO and ASHRAE recommendations during the winter (Cutler-Welsh, 2006b; McIntosh, 2011a). Studies show that the classroom environment is vital to student health and academic learning (Kabirikopaei et al., 2021; Sunyer et al., 2015; Wargocki et al., 2020). Therefore, it is essential to provide the students with a healthy environment.

This PhD study aims to investigate changes in the thermal performance of solar air heater (SAH) when fins are inserted (as a design modification) and when a nanofluid coating is applied. Practical applications of SAH in school environments are investigated.

1.1 Background

It is well established that children are more vulnerable than adults to environmental conditions (Wargocki & Wyon, 2007b). Therefore, providing the students with a healthy classroom environment is necessary, as they spend the second most time in school.

Children have an underdeveloped immune system. They breathe a higher volume of air per body mass than adults (Miller et al., 2002). Indoor air pollutants often trigger respiratory illnesses (WHO, 2010). Australian and New Zealand research has confirmed that an increase in hospital admissions (pneumonia and acute bronchitis in children aged less than four years old, respiratory disorders in children less than 14 years old, and asthma in children between 5 and 14 years old) was linked to an unhealthy indoor environment, such as cold, damp, mouldy, crowded, and exposed to smoke (Kulkarni & Grigg, 2008; McNamara et al., 2020). Research conducted in schools showed that children from highly polluted schools had less cognitive performance growth than those from less polluted schools (Kabirikopaei et al., 2021; Sunyer et al., 2015; Wargocki et al., 2020). Therefore, it is essential to investigate the impact of indoor air quality (IAQ) in classrooms on children's well-being.

Indoor temperature, humidity, and ventilation are associated with IAQ and deteriorate work and cognitive performance. These three parameters must be studied together as they are interdependent (Wolkoff et al., 2021).

Inadequate ventilation in elementary schools reduces the comfort, performance, and attendance of the pupils and increases the occurrence of negative health symptoms (Bako Biro et al., 2012; Daisey et al., 2003; Gaihre et al., 2014; Shaughnessy et al., 2006; Wargocki et al., 2020; Wargocki & Wyon, 2007b). For instance, raising ventilation rates from 1.70 to 6.61 L/s per person improved short-term attention and logical thinking (Petersen et al., 2016), while increasing ventilation from 5.0 to 10.0 L/s per person enhanced students' cognitive performance (Wargocki & Wyon, 2007a). Similarly, classrooms in California reported better learning outcomes in English and Mathematics when ventilation rates were increased (Mendell et al., 2016). These findings highlight that good IAQ, particularly through adequate ventilation, is essential for student health and learning.

NZ classrooms are high-density, with over 25,000 teaching spaces (MOE, 2022). Many NZ classrooms are naturally ventilated by opening doors and windows. A study conducted in forty-nine NZ primary schools found that only 15.0% to 40.0% of teachers open windows during winter (Branz, 2019; Gully, 2015; Liaw, 2015). It is challenging to provide an acceptable IAQ due to a combination of the high density of occupants and reliance on natural ventilation (Almeida et al., 2016; Duarte et al., 2017; Jurelionis & Seduikyte, 2008; Luca et al., 2019). In naturally ventilated classrooms and other areas, people are typically not motivated to open windows during the winter. The SARS-CoV-2 pandemic has highlighted the importance of ventilation in reducing viral and other pathogen transmission.

Ventilation creates air movement that helps in the dilution and distribution of tiny particles (Nembhard et al., 2020). However, there is a common concern that lower external temperatures during winter may affect thermal comfort in naturally ventilated classrooms. Fully opening doors and windows in winter may not be convenient. However, adequate ventilation can be achieved by partially opening the windows. Preheating classrooms in the morning and partially opening the windows help ensure sufficient ventilation. Taking refresher breaks at different times of the day by exiting the space with doors and windows open may clear the air and maintain indoor temperatures. Recirculating air is not preferred, as it may recirculate the contaminants (Alexis Sutherland et al., 2022). It can be concluded that natural ventilation can help mitigate the challenges of COVID-19 transmission.

The carbon dioxide (CO_2) level in the classroom or room can be used to estimate the ventilation rate. The NZ Building Code compliance document G4 and the cited NZS 4303 (Standards New Zealand, 1990) recommend a ventilation rate of 8 litres per second and per child in a classroom (with an assumed maximum occupant density of 0.5 users/m^2) to maintain a CO_2 level below 1000 ppm (MBIE, 2017). However, there is insufficient justification for using CO_2 as an indicator of indoor air quality. The American Society of Heating, Refrigerating, and Air-Conditioning Engineers (ASHRAE 62.1) has not included the CO_2 concentration limitation in its standards. Although new research is being done to investigate the direct effects of indoor CO_2 concentrations on human health, comfort, and performance (Persily, 2020).

The optimal temperature levels should be maintained between 18 ℃ and 25 ℃ during the winter (Branz). A study found that cognitive and work performance were best at the temperature between 22.0 ℃ and 24.0 ℃. Cognitive and work performance decrease at higher or lower temperatures. However, temperature values may vary between hot and cold regions. The humidity should be between 40.0% and 60.0% (Wolkoff et al., 2021). Several studies showed that the infectivity of numerous influenza viruses is significantly decreased when the relative humidity is greater than 40.0% (Dietz et al., 2020; Moriyama et al., 2020; Wolkoff, 2018)

Despite these standards, maintaining CO_2 levels below 1000.0 ppm remains challenging. However, this could be achieved by installing a mechanical ventilation system in the classroom. The Ministry of Education (MOE) reports indicate that schools operate under capped budgets, and the introduction of mechanical ventilation systems would significantly increase heating and ventilation costs (N. Z. Ministry of Education, 2014). Instead, the MOE recommends maintaining thermal comfort by distributing temperature and fresh air evenly throughout classroom spaces, with adequate air filtration, low noise levels, and systems that are economical and easy to operate. Such systems must also provide sufficient airflow to meet mechanical

ventilation requirements. Recent studies suggest that SAHs could offer an affordable alternative for classrooms, aligning with these MOE guidelines (Matsunaga et al., 2023; N. Z. Ministry of Education, 2014; Wang et al., 2016).

Following the Paris Climate Change Agreement 2015, New Zealand has launched the Building for Climate Change Programme (Building for Climate Change, 2020), which places strong emphasis on reducing carbon emissions from building operations such as heating, cooling, lighting, and ventilation. In this context, SAHs offer a sustainable solution by utilising solar energy for space heating and ventilation, thereby reducing reliance on fossil-fuel-based energy systems.

SAHs capture incident solar radiation and convert it into useful thermal energy, which is then transferred to the air and circulated indoors (Ravi & Saini, 2016b). SAH is more affordable, easier to operate, requires less maintenance, and creates less noise (due to fewer mechanical components) than a mechanical ventilation system. These attributes make SAHs a practical and sustainable option for ventilating and warming classrooms in alignment with national carbon-reduction goals.

SAH can be classified into two types: flat plate type (FSAH) and tube type (TSAH). The heat transfer fluid will be air in SAH or water in solar liquid heaters (Ravi & Saini, 2016b). SAHs are used for low and moderate-temperature applications such as space heating, preheating, crop drying, and the food industry (Bezbaruah et al., 2020). Typical thermal efficiencies range from 38.0–45.0% (Ansari & Bazargan, 2018), but performance is limited by internal and external energy losses (Lakshmi et al., 2017). TSAHs remain under-researched, with only ~40.0% of studies addressing their performance, presenting an opportunity to further investigate their ability to meet ventilation standards (8 litres/second/person).

The researchers have investigated different modified techniques, such as artificial roughness, integrating thermal energy storage (TES), evacuated tubes, micro heat pipe array, reflectors, nanofluid coatings, and conductive materials to improve the thermal efficiency of SAH (Abdelkader et al., 2020; Abi Mathew & Thangavel, 2021; Abo-Elfadl et al., 2020; S Abo-Elfadl et al., 2021; Kalaiarasi et al., 2016; Lakshmi et al., 2017; Madhulatha et al., 2021; Mandal & Ghosh, 2020; Misra et al., 2020; Murali et al., 2020; Ravi & Saini, 2016a; Shamshirgaran et al., 2017; Singh & Vardhan, 2021; Wadhawan et al., 2018; Zhu et al., 2015; Zhu et al., 2016). These techniques are discussed in detail in Chapter 2, a review of the literature.

Building on this foundation, the present thesis aims to optimize the thermal and ventilation performance of TSAHs under Wellington, New Zealand, weather conditions. Three sets of experimental studies were conducted:

Chapter 3 – Experimental performance of a finned tube-type solar air heater with corrugated fin inserts in New Zealand.

Chapter 4 – Effect of fin inserts on the thermal efficiency of the tube-type solar air heater.

Chapter 5 – Experimental investigation of the thermal performance of uncoated and nanocoated tubes (sponsored by APL Window Solutions, tested under clear-sky days).

The results of these experiments, presented in Chapters 3–5, provide new insights into the performance optimization of tube-type SAHs and their potential role as sustainable ventilation solutions for New Zealand classrooms.

1.2 Research aims, questions, and objectives

1.2.1 Research aim

This thesis aims to investigate potential treatments (design and nanofluid coating) to optimize the thermal and ventilation performance of tube-type SAHs.

1.2.2 Research questions

The fundamental question of this investigation was:

"How efficient is nanocoating the tubes, and which nanofluid type is best for coating? Did the nanocoating of tubes impact the performance of SAH?"

The following sub-questions were framed:

1) How will FT-SAH with corrugated fin inserts perform under Wellington, NZ, conditions in winter when operated under different mass flow rates?
2) How will the FT-SAH with fin (treatment) and without fin (control) perform under Wellington, NZ, conditions in winter when operated under different mass flow rates
3) How will the nanocoated tubes with and without fin inserts perform under Wellington, NZ, weather conditions in winter?

1.2.3 Research objectives

The research objectives are as follows:

Objective 1: To investigate the thermal and ventilation performance of FT-SAH under Wellington, New Zealand, winter conditions at different mass flow rates, with a specific focus on assessing the effect of corrugated fin inserts by comparing configurations with fins (treatment) and without fins (control).

Objective 2: To investigate the thermal and ventilation performance of nanocoated tubes. It is crucial to examine the performance of the optimized tubes in Wellington, NZ, under various weather conditions, and advise on their potential use in schools.

1.2.4 Research philosophy

A pragmatic–constructivist informs the methodological choices in this thesis research philosophy, which is well established in building performance and environmental engineering research (Denscombe et al., 2014; Weyant, 2022). Constructivism recognises that system performance is shaped by contextual and environmental factors, and that knowledge emerges from the interaction between the researcher, the prototype, and real operating conditions (Guba & Lincoln, 1994). This is relevant because the performance of a solar air heater depends on variables such as solar irradiance, ambient temperature, and airflow. Pragmatism, on the other hand, emphasises practical problem-solving and the use of methods that best address real-world challenges (Morgan, 2014; Patton). This aligns with the thesis's intention to optimise a functional FT-SAH system suitable for New Zealand classrooms.

This philosophical perspective supports the use of an experimental, quantitative, and case-based research design. Experimental testing is necessary to measure key performance variables—including outlet temperature, temperature difference, thermal efficiency, mass flow rate, and ventilation supply rates—and to evaluate the influence of fin inserts, coatings, and operating scenarios (John & Beckman, 2013). A case study structure (winter high-flow and spring reduced-flow operation) is justified because solar air heater behaviour is context-dependent and influenced by seasonal variations (Crawley et al., 2008). Quantitative analysis, including statistical comparisons, ventilation calculations, and thermodynamic interpretation, provides objective and decision-relevant evidence consistent with requirements from organisations such as the Ministry of Education, WHO, and ASHRAE (ASHRAE, 2021; WHO, 2021).

Overall, the pragmatic–constructivist philosophy provides a coherent foundation for the selected methods, enabling flexible, problem-focused inquiry and the generation of empirical, context-specific insights. The methodological choices, therefore, align directly with the research aim and offer a robust pathway to answer the thesis questions.

1.3 Scopes and limitations

Wellington is located at 41.2924 °S and 174.7787 °E and has a temperate maritime climate. It is located between the Cook Strait and the Remutaka Range at the Southwestern tip of the North Island. The winters are wet and cold, whereas the summers are comfortable. Strong winds frequently occur in Wellington due to its proximity to the Cook Strait, and it is partly cloudy year-round. The southwestern part of Wellington receives 2100 hours of bright sunshine. Cloud cover increases as one approaches the Tararua and Rimutaka Ranges. The bright sunshine hours are less than 1750 hours in the Tararua Ranges. Due to Wellington's complex topography, there

is significant variation in solar energy, wind, and cloud cover. Solar radiation is minimal in June and maximum in December and January (Chappell, 2014). Figure 1-1 below shows the lowest, highest, and mean recorded bright sunshine hours (monthly) for the different sites in the Wellington region.

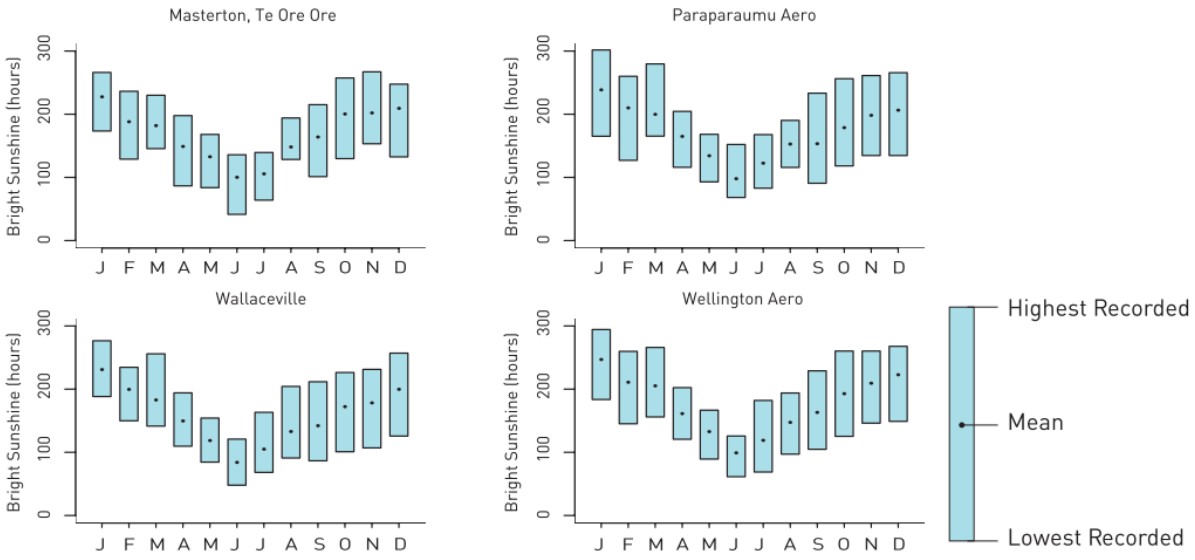

Figure 1-1 Sunshine hours (monthly) for the different sites in the Wellington region (Chappell, 2014)

Considering Wellington's climatic conditions and the significant deviation in solar, wind, and cloud cover distribution, the SAH will not operate at its best compared to other NZ locations. This study, therefore, focuses on experimental testing under real Wellington weather conditions. The scope includes:

- Testing a finned-tube solar air heater (FT-SAH) with corrugated fin inserts to evaluate its thermal and ventilation performance.
- Investigating the impact of fin inserts on FT-SAH performance under varying mass flow rates.
- Proposing enhancement methods, including nanocoating tubes with aluminium oxide and copper oxide dispersed in black paint.

1.3.1 The limitations of this research

The limitations of this research are listed below:

1) COVID-19 restrictions delayed fieldwork by more than a year due to lockdowns, shipping delays, and the psychological impact of uncertainty.
2) Auckland was experiencing a continuous lockdown, so the components were shifted to Massey, Wellington Campus. This took longer than anticipated.

3) The variable fans were shipped from China and had to be tested for conformity in NZ, ensuring each fan had been tested individually, met the relevant NZ standards, and was safe to use. This was done at Victoria University in Wellington, which took more time.
4) The FT-SAH designed by SOJOL Pvt Ltd was very bulky (nearly 80kgs). Shifting the assembled SAH from the laboratory to the experiment location was difficult. Efforts should be made to reduce its weight.
5) In the first month of data collection (May 2023), the efficiency of SAH was calculated, and the efficiency was above 100%. It was found that the anemometer was incorrectly placed (close to the fan inlet) and that the duct was stuffed, which caused the air velocity to vary and be high, resulting in continuous higher efficiency. The anemometer was then placed at the duct outlet, away from the fan (as per the literature study). The duct was extended and sealed with duct tape to prevent air leakage.
6) Condensation was observed inside the glass at low temperatures in winter. This could be eliminated by running the fan throughout the day and night.
7) Frost was formed on the surface of the glass on wet days and when the temperature dropped below 8.0 ℃. Defrosting took 1.5 hours in bright sunlight and longer on cloudy days.
8) The tube holder at each end of the collector was made of wood, and at higher flow rates, the material that settled on the tube surfaces was chipped. This could shade the collector surface, affecting its thermal efficiency. Air filters should be installed in such cases, as the mixing of wood chips will pollute the air.
9) Supply of nanoparticles (Al_2O_3 and CuO) from the USA was delayed by one month due to stock shortages.
10) The first batch of nanofluid was improperly prepared due to unmonitored sonication. Subsequent preparation required restarting the process in 30-minute monitored intervals.
11) The tubes were nanocoated manually using a brush, which was time-consuming. Spray paint could be easy and less time-consuming.

1.3.2 The delimitations of this research

The delimitations of this research are listed below:

1) The experiment was conducted from 9 a.m. to 4 p.m., considering NZ school time and solar timing. Therefore, the data was not collected 27/7.

2) Due to time constraints, hybrid nanofluid-coated tubes were not tested for thermal performance.
3) The SAH was mounted on the aluminium metal frame at the Massey University car park, making it easily accessible for inspection and cleaning of the SAH periodically.
4) The numerical study of the SAH was out of scope.
5) Due to the space and financial constraints, only one FT-SAH prototype was available. Therefore, both phases (Case Studies 1 and 2) were conducted progressively using the same setup to maintain consistency across test conditions.

1.4 Conceptual framework

Figure 1-2 shows the conceptual framework for this research. This conceptual framework examines the performance of FT-SAH under various treatments, with a focus on design modifications and nanofluid coatings.

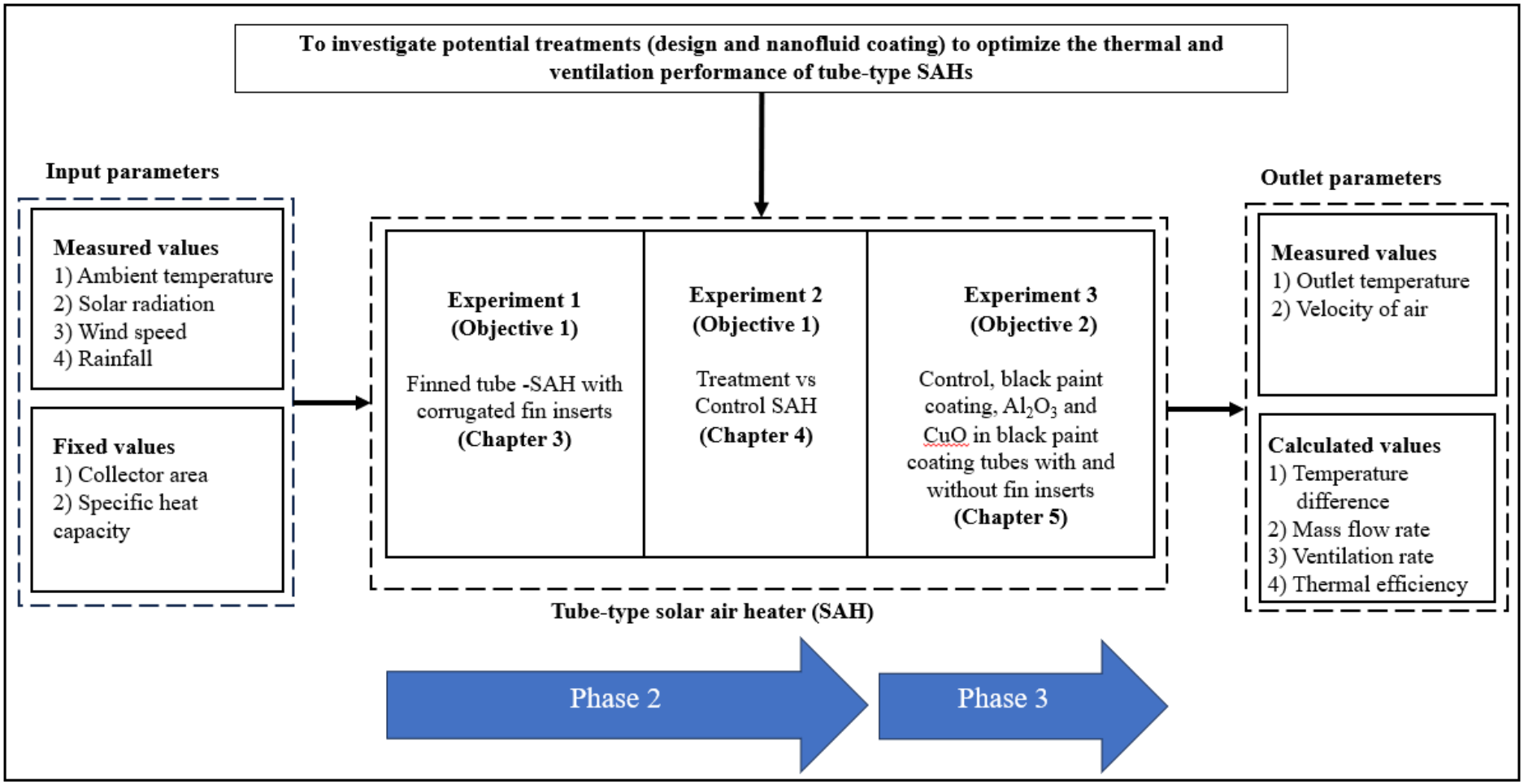

Figure 1-2 A conceptual framework for the research

The input parameters include measured environmental factors, such as ambient temperature, solar radiation, wind speed, and rainfall, as well as fixed values like collector area and specific heat capacity.

There are three experiments outlined:

Experiment 1 (Objective 1): Evaluates the thermal and ventilation performance of finned tubes with corrugated inserts (see Chapter 3).

Experiment 2 (Objective 1): Compares the performance of the treatment SAH (with fin inserts) against a control SAH (without inserts), with results reported in Chapter 4.

Experiment 3 (Objective 2): Investigates the impact of surface treatments, including black paint and nanoparticle coatings (Al_2O_3 and CuO), applied to tubes with and without fin inserts (see Chapter 5)

The outputs include the outlet temperature and the air velocity (measured values), along with calculated parameters such as temperature difference, mass flow rate, ventilation rate, and thermal efficiency.

The framework consists of two phases: Phase 2 and Phase 3 (discussed in detail in section 1.6), which indicate the progression of the research work and experiments. The framework connects input parameters to experiments and, finally, to output parameters, providing a structured approach to optimizing the thermal and ventilation performance of the SAHs.

1.5 Thesis outline

This thesis comprises seven chapters, as shown in Figure 1-3. It aims to investigate potential treatments (e.g., design modifications such as fin inserts and nanofluid coatings) to optimize the thermal and ventilation performance of TSAHs.

This aim is achieved through the research presented in Chapters 3, 4, and 5, which involve experimentation and analysis, leading to general discussions and conclusions in Chapters 6 and 7. The aim is supported by specific objectives, each corresponding to the investigation conducted in a particular chapter.

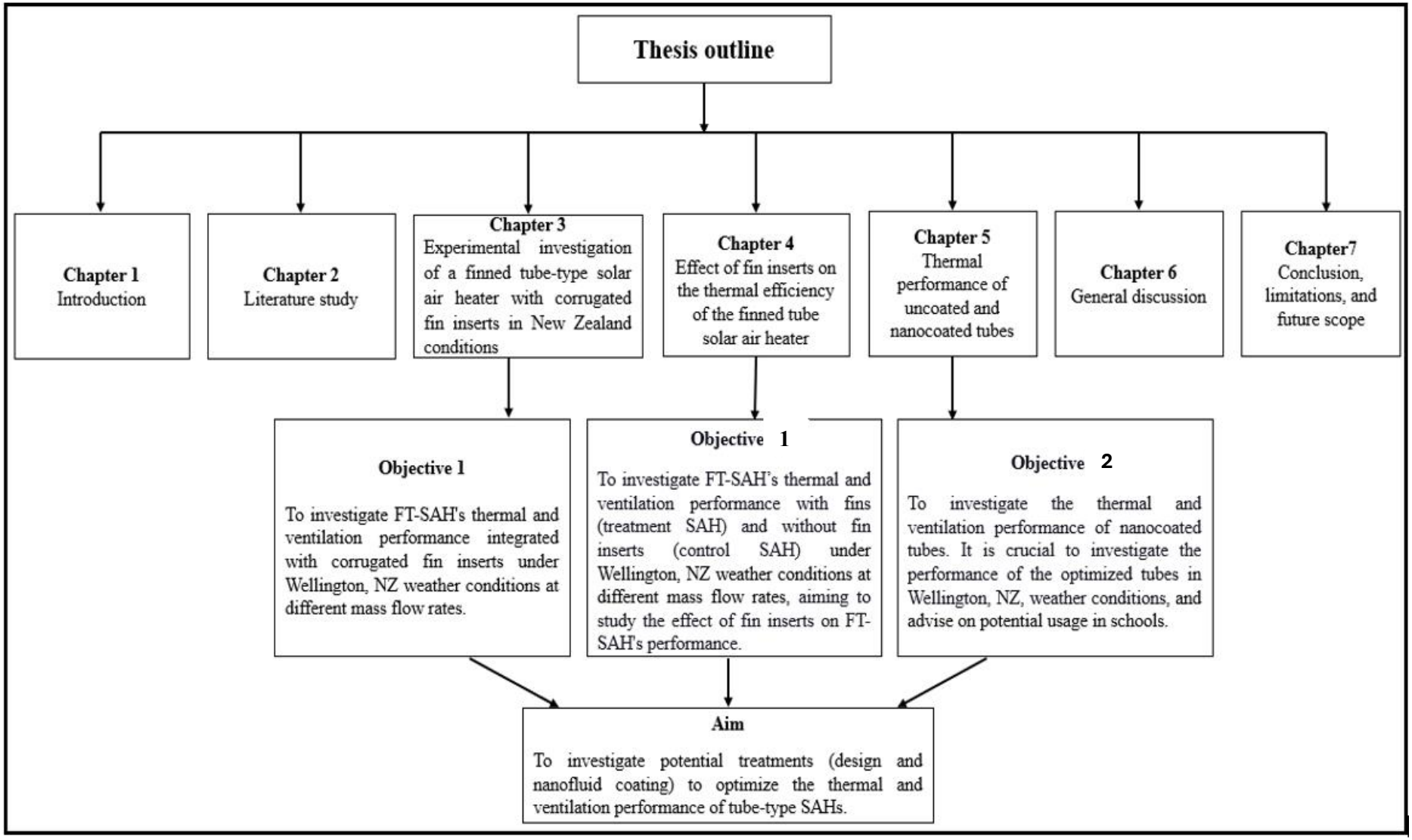

Figure 1-2 Thesis outline, objective, and aim

The objectives align directly with specific chapters that present the research experiments and findings, which are explained as follows:

1 **Chapter 1 (Introduction)**:

Introduces the problem and research scope, outlining the need for improved SAH performance, thereby setting the aim and objectives of the research.

2 **Chapter 2 (Literature Study)**:

Reviews existing research and technologies related to SAHs, fin inserts, and nanocoating. This provides the foundation and justification for pursuing the objectives.

3 **Chapters 3, 4, and 5**:

These chapters report the results of the three experiments. Chapters 3 and 4 discuss the experimental test results of FT-SAH with corrugated fin inserts, treatment FT-SAH, and control FT-SAH operating under the Wellington, NZ weather conditions at different air mass flow rates. These experiments aim to estimate the thermal and ventilation performance of the studied SAH.

Chapter 5 demonstrates the test results of nanocoated tubes. The tubes were experimentally tested under Wellington weather conditions. They were coated with black paint and nano-coated with 1, 2, 3, and 4% CuO and Al_2O_3, integrated with and without fins, and compared to control tubes. Four tests were performed during this phase. Each chapter addresses an objective that collectively supports the optimization of SAH performance.

4 **Chapter 6 (General Discussion)**:

This chapter presents a discussion that synthesizes the findings from the experimental chapters (3, 4, and 5), integrating how different treatments (fins, nano-coatings) affect performance and how they contribute to achieving the overall aim.

5 **Chapter 7 (Conclusion, Limitations, and Future Scope)**:

The research concludes by summarizing how the objectives and aims were achieved, discussing the practical applications of the findings in schools, and suggesting areas for future study or improvements.

1.6 Research phases

Figure 1-4 represents the sequence of the four research phases.

Phase 1 (documentation): The literature review will examine SAH performance and document potential SAH optimization opportunities. This phase is included in Chapter 2 of the writing.

Phase 2 (experiment): Chapters 3 and 4 report phase 2 of this study. FT-SAH with corrugated fin inserts, treatment FT-SAH, and control FT-SAH were to be experimentally tested under the Wellington, NZ, weather conditions. These experiments aim to estimate the thermal and ventilation performance of the studied SAH.

Phase 3 (experiment): Nanocoated tubes will be experimentally tested under Wellington weather conditions (Chapter 5). The tubes were nanocoated with 1, 2, 3, and 4% CuO and Al_2O_3, integrated with and without a fin. Four tests were performed during this phase.

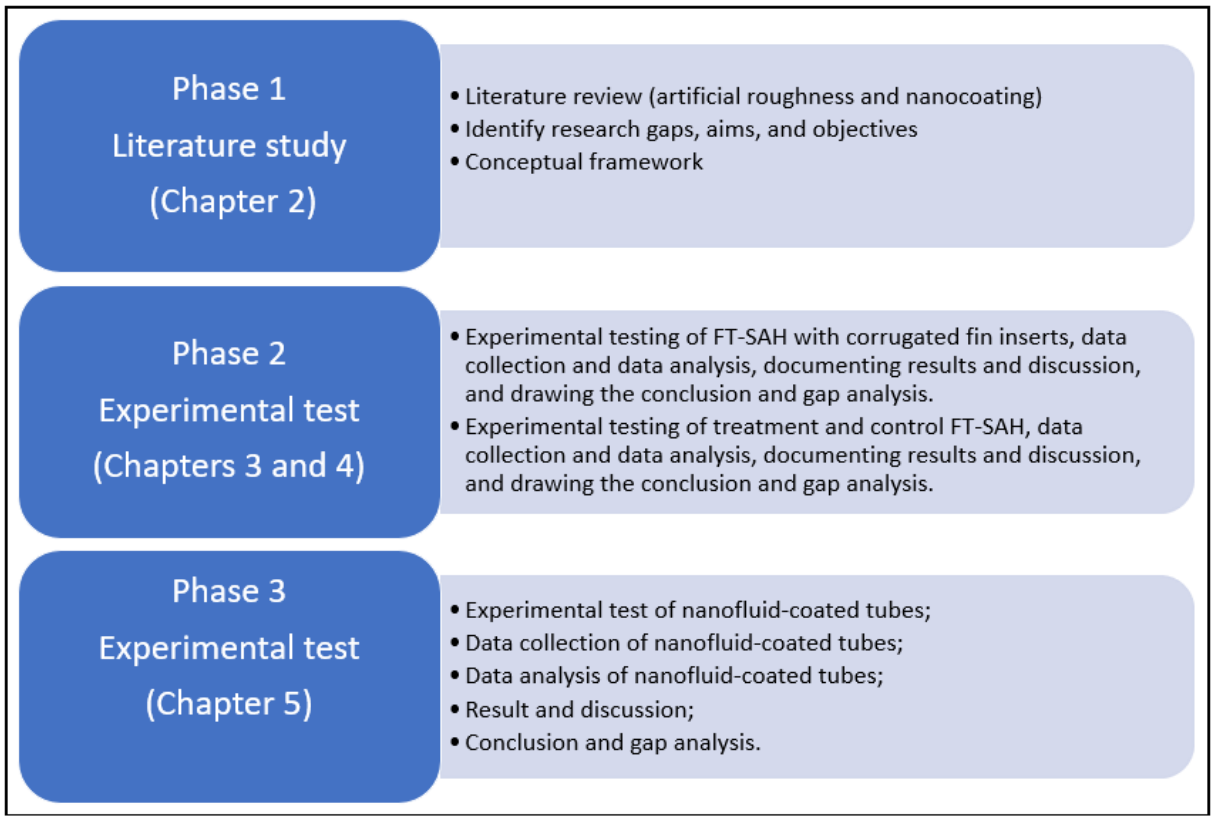

Figure 1-3 The sequence of the four research phases

The next chapter presents the literature reviews on the thermal efficiency modification of TSAH and nanocoating. The study aims to provide up-to-date information on TSAHs to advance the development and uptake of SAHs. The research demonstrated that thermal efficiency gains could be achieved by modifying the design of the SAHs, including various artificial roughness geometries within the tubes, integrating solar thermal energy systems, applying coatings or reflectors inside the SAHs, or utilizing evacuated tubes and micro heat pipe array systems. Chapter 2 primarily focused on design alterations and nanofluid technology used to enhance the SAH thermal performance. A part of the literature study (focusing on design alteration) is peer-reviewed and published in the Journal of "Renewable and Sustainable Energy Reviews." The paper is attached in the appendix

2 Review of the thermal efficiency of a tube-type solar air heater

There is an urgent need to prove that SAHs can be effective for heating and ventilating low-rise buildings. SAHs can convert solar energy into thermal energy for moderate- and low-temperature applications, such as space heating, preheating, crop drying, and food processing. However, its efficiency is low due to the low heat transfer coefficient between the absorber and the flowing air. Nonetheless, SAHs remain attractive because they are simple to construct and operate and, unlike liquid-based collectors, pose minimal risk of leakage.

The two main types of SAHs are flat plate and tube-type. Flat plate SAHs have received the most attention in the research literature, but evidence of the efficiency gains from TSAH is growing. The chapter aims to provide up-to-date information on TSAHs to advance the development and uptake of SAHs. The research demonstrated that thermal efficiency gains could be achieved by modifying the design of the SAHs, including various artificial roughness geometries within the tubes, integrating solar thermal energy systems, applying coatings or reflectors inside the SAHs, or utilizing evacuated tubes and micro heat pipe array systems. Among these, evacuated tubes and micro heat pipe array systems demonstrate higher thermal efficiency than other techniques. The study revealed the potential of nanocoated SAHs to enhance thermal performance significantly. However, more research is needed to address the gaps in long-term stability, economic feasibility, and broader geographic testing. A new roughness geometry was proposed following a detailed discussion of various techniques to improve the thermal efficiency of SAHs.

Some parts of the research presented in this thesis (such as Sections 2.1–2.5) have already been published in peer-reviewed journals, while other sections are currently under preparation for submission. Despite the inclusion of published material, the thesis adheres to a traditional format rather than a publication-based approach. The published work has been fully integrated into the overall structure to provide a coherent narrative, ensuring that the thesis reads as a single, unified study.

2.1 Introduction

In 2019, renewable energy sources supplied only 11.0% of global energy demand (Ritchie et al., 2020). Around 80.0% of global energy demand for heat, electricity, and transportation is still met by the combustion of fossil fuels, namely coal, oil, and gas. Burning fossil fuels releases carbon dioxide and greenhouse gases, leading to global warming and climate change. One hundred and ninety-three states and the European Union have committed to the 2015 Paris

Agreement to reduce greenhouse gas emissions and adapt to the impacts of climate change. Renewable, non-polluting heat sources are essential to meet this commitment (Nunez, 2019). Therefore, there is a need to reduce greenhouse gas emissions (Jia et al., 2019) and find alternate, renewable, and affordable energy solutions (Li, 2011).

The International Energy Agency reports that space heating in residential and commercial buildings uses around 46.0% of global energy (International Energy Agency-Renewables. 2019, Paris.). A New Zealand study reports similar results that about 34.0% of New Zealand's energy is used in households for space heating (Isaacs et al., 2006). The World Energy Outlook 2022 report shows that energy consumption for building space heating is eight times higher than for space cooling, despite increased cooling demand (IEA, 2022). Indoor spaces that are under-heated or under-ventilated can cause poor health outcomes for the occupants and be damp and mouldy (Holden et al., 2023). With 10.0 % of the world living in energy poverty (*International Energy Agency*, 2020). There is a dire need to identify heating solutions that are both renewable and low-cost. The researchers will address the question: What is the most affordable renewable energy source technology that could fulfil the heating demand for low-rise buildings?

Heating with solar energy could reduce the dependence on fossil fuels (Choudhury & Baruah, 2017). The amount of solar energy that reaches the Earth in one hour is $4.3x10^{20}$ J, which is slightly higher than the annual worldwide consumption of energy used for space heating of $4.1x10^{20}$ J (Energy, 2005). Therefore, harvesting even a fraction of available solar energy can contribute to space heating and offset fossil fuel dependence. Solar energy utilization could potentially reach an annual growth rate of about 34.0% within the next decade, meaning immense energy can be harvested from the sun, contributing to the growing energy demand (Calderone, 2020). A positive trend in the utilization of solar thermal technologies (10.0% - 40.0%) is seen across European countries for the decarbonization of heating and cooling (Sutu, 2023).

Solar energy can be converted to thermal energy using solar collectors (Ravi & Saini, 2016b). Solar collectors are classified as concentrating types or non-concentrating types. Concentrating collectors use direct (beam) radiation and a tiny portion of the available diffuse (scattered by the atmosphere) radiation. Concentrating collectors must, therefore, track to follow the sun's location across the sky. Non-concentrating collectors use direct solar radiation at different angles and diffuse radiation. They can have a fixed orientation and do not need to track the sun's position. Non-concentrating types are further classified as flat plate or tube-type collectors (Eggers-Lura, 1979). Flat plate and tube-type collectors are used for low-temperature

applications requiring air temperatures ranging from 45.0 ℃ to 100.0 ℃, and the more complex concentrating collectors are typically used for higher-temperature applications (Gupta et al., 1997). The solar collectors contain a heat transfer medium: liquid (solar liquid heater, SLH) or air (SAH). SLHs have higher efficiency than SAHs, but they require higher construction standards to prevent liquid leakage (Ravi & Saini, 2016b). Heating air, rather than liquid, has the advantage of being a low-technology system that does not use rare metals or moving components. SLH uses a pump to circulate liquid, and SAH uses a fan to circulate air around the system. The energy required to pump the heated liquid medium is greater than the energy required by the fan to move the heated air. Furthermore, a secondary heat transfer system, such as a radiator heater, is necessary to extract heat from the liquid medium and distribute it to the space. With SAHs, there are no risks of liquid leaks from the pipework or freezing in winter. SAHs avoid this risk, as leaked air is unlikely to cause consequential damage (John & Beckman, 2013). In addition to the advantages mentioned above, the heated air from the SAH can be used directly for space ventilation (Boulic et al., 2016).

During the COVID-19 pandemic, in addition to sanitizing, masking, and social distancing, opening classroom windows to increase ventilation was a key requirement for reopening schools and maintaining a healthy environment. A Report by the Ministry of Education showed that only a third of the teachers opened windows during teaching time (*MOE*, 2017). Achieving an appropriate ventilation level should not depend on occupants' awareness of the need to open windows. Mechanical ventilation systems are not affordable for most schools. Consequently, an alternative and affordable method will be needed to increase the ventilation rate in under-ventilated school buildings to decrease virus transmission (Morawska et al., 2020). A field study conducted in twelve NZ classrooms showed that SAHs can be used effectively in preheating and ventilating classrooms (Y. Wang et al., 2020). However, there is a need for additional research and evidence on the effectiveness of using SAHs for heating and ventilating buildings, and the technologies available to increase the efficiency of the SAH. It was found that the SAHs have low thermal efficiency (from 38.0% to 45.0%) due to heat losses; hence, SAHs are limited to space heating, preheating, and crop drying (Kumar & Layek, 2020).

A systematic literature review was conducted to understand the available thermal efficiency improvement techniques of tube-type SAH for low- and medium-temperature space heating applications and modify them further for efficiency improvement. Thermal efficiency equations are also discussed to identify the modifiable factors affecting the SAH performance. One finding was that few studies have been published on tube-type SAHs, but this is an emerging and promising area of research. Compared with flat panel designs, tube-type solar panels have

two theoretical advantages due to the tube's curvature: greater surface area and better orientation to the sun's path during the day. These advantages can be further enhanced to produce positive effects on thermal efficiency. This review provides up-to-date information on design innovations for tube-type SAHs, which will be helpful for engineers and researchers alike to engineer improved SAHs. Based on the analysis of various techniques for improving the thermal efficiency of SAH, a new roughness geometry is proposed to be investigated.

The research started by describing typical SAH components to allow comparison between papers and the factors that impact the efficiency of the tubes.

2.2 Tube-type SAH components and airflow through SAH

A typical SAH comprises a transparent top plate, an absorber, an insulated frame, and a backplate. Figure 2-1. shows the schematic diagram of SAH. The transparent top cover can be made from either glass or a transparent polymer to absorb solar radiation. The solar energy is then transferred to the absorber tubes. Substantial heat is lost through various SAH parts; therefore, the insulating material is applied to the sides and the back plate to increase the thermal resistance and reduce the heat losses. Different SAH systems have used various insulating materials such as mineral wool, glass wool, natural fiber, or foam to reduce heat loss. Due to the heat losses, most SAHs have low thermal efficiency (from 38.0% to 45.0%); hence, SAHs are limited to space heating, preheating, and crop drying (Kumar & Layek, 2020).

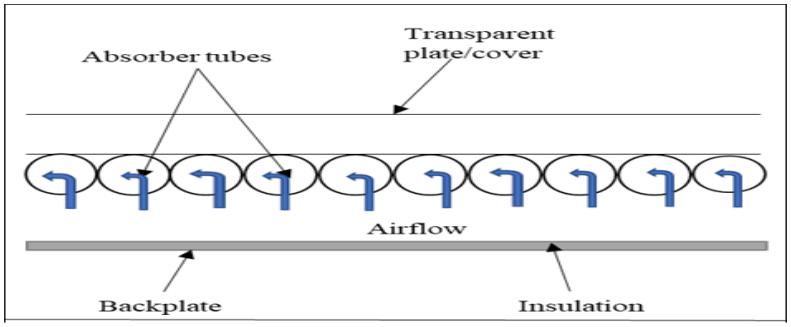

Figure 2-1 Schematic diagram of tube-type SAH

As shown in Figure 2-1, the ambient air is typically admitted at the lower edge of the SAH and flows through the absorber tube, using the natural buoyancy of the air as it is heated. The heat from the absorber surfaces is transferred to the air circulating inside the SAH, which is then supplied to an adjacent area for space heating and ventilation. The airflow through the SAH can be either a single or double pass. In a single-pass flow, the air passes through the absorber only once, and in a double-pass flow, the air passes twice through the absorber to increase the time that the air is in contact with the absorber surfaces (Kabeel, Hamed, et al., 2017). A typical

double-pass SAH is 10.0%-15.0% more efficient than a single-pass SAH due to the increased heat transfer area (Alam & Kim, 2017).

2.3 Equation used to determine the thermal efficiency of SAHs

The thermal efficiency of SAH can be calculated using Equation 1 (John & Beckman, 2013).

$$\eta = \frac{\dot{m}Cp(To-Ti)}{IAc} = \frac{\rho vAdCp(To-Ti)}{IAc} \quad \textbf{2.1}$$

For tube type SAH, the collector area is calculated from Equation 2 (Abu Hamed & Alkharabsheh, 2020).

$$A_c = n\pi TDL \quad \textbf{2.2}$$

Where,

A_c	SAHs effective area (m^2)
A_d	Outlet duct cross-section area (m^2)
C_P	Specific heat capacity of air [J/(kg*K)], constant =1007 J/kg*K
I	Solar radiation on the tilted SAH surface (W/m^2)
T_i	Inlet air temperature (K)
T_o	Outlet air temperature (K)
$\dot{m}$	Air mass flow rate (kg/s)
η	Efficiency (%)
ρ	Density of air (kg/m^3)
v	Air velocity (m/s)
n	Number of tubes
π	Pie (constant) =3.14
D	The outer diameter of the tube (m)
L	Tube length (m)

Equation 1 shows that the thermal efficiency of SAH depends on the air mass flow rate, the collector area, and the ratio of the temperature difference between the air at the outlet and the inlet air (that is, the ambient temperature) to global solar radiation.

2.4 Review methodology

A systematic literature review was conducted by searching journal papers published in relevant research areas through search engines (Google Scholar, Web of Science, Scopus, and Discover – the Massey University library database) from 1 January 2010 to 31 July 2023. Figure 2-2 shows the process for conducting the review study. The research methodology involved a five-step review process. The first step for the study was to identify the research area demanding 1) explore cost-effective solutions for heating and ventilating low-rise buildings as more energy

is used in space heating and cooling and 2) extensive research that will contribute to reducing greenhouse emissions and help in combating energy poverty which is a significant concern worldwide. Extensive research has found that SAHs could be a potential technology that could be used for heating and ventilating buildings. In step 2, keywords were grouped in different combinations to create a search string. The keywords were selected and grouped to appear at least once in the title or the article. The chosen keywords were "SAH," "TSAH," "thermal efficiency," "artificial roughness," "coating," "evacuated tubes," "micro heat pipe array," and " reflectors. The keywords grouping was crucial. Using the keywords simultaneously gave no results. The keywords were grouped randomly. The keywords in group 1 were "solar air heater," "tube type solar air heater," and "thermal efficiency," group 2 were "artificial roughness," "coating," and "evacuated tubes," and group 3 was "micro heat pipe array" "reflectors." A total of one hundred and fifty-three papers were identified. These papers were filtered by year in the date range of 1 January 2010 -31 July 2023. Filters were applied to exclude review articles and citations but include peer-reviewed articles (filter). When the filters were applied, the number of papers identified was eighty-three. In step 3, the articles were categorized into five categories based on the techniques used to increase thermal efficiency.

The papers were categorized as a) SAH with artificial roughness, b) SAH with thermal energy storage, c) evacuated tubes SAH, d) Micro heat pipe arrays SAH, and e) application of coatings, high thermal conductivity material, or reflectors. The papers focussing on the thermal efficiency of tube-type SAH were selected (Step 4). Only thirty-seven papers focussed on the thermal efficiency of tube-type SAH for space heating. The remaining papers focussed on agricultural drying, hot water generation, and industrial applications and are excluded from this paper. Step 5 was the critical review and identification of conclusions from the thirty-seven papers.

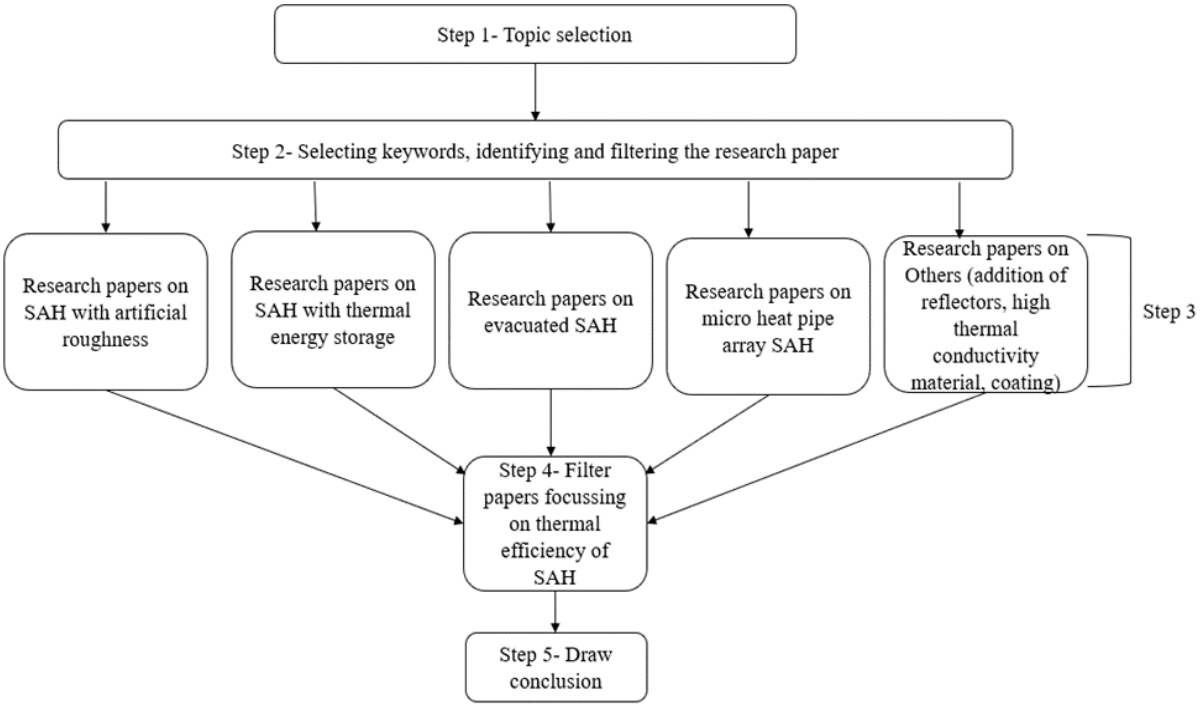

Figure 2-2 Five-step review process

In this review study, some SAHs combine two improvement techniques—for example, SAHs with artificial roughness and thermal energy storage. If the significant thermal efficiency is influenced by the application of artificial roughness and not the thermal storage, then it is categorized under the artificial roughness sections and vice versa.

2.5 Results: Different techniques to improve the thermal efficiency of the SAH

The literature review showed that 60% of research papers identified in step 1 investigated the thermal performance of flat plate SAHs, and 40% focussed on tube type SAHs, but this is an emerging and promising area of research. Compared with flat panel designs, tube-type solar panels have two theoretical advantages due to the tube's curvature: greater surface area and better orientation to the sun's path during the day. These advantages can be further enhanced to produce positive effects on thermal efficiency. Therefore, this review synthesizes the results of experimental modifications to TSAHs and identifies further advantages that might be delivered through innovative design additions. The literature review showed that the thermal efficiency of SAH could be improved by the following:

1) providing some artificial roughness, which increased the absorber surface area and air turbulence,
2) adding reflectors to focus the solar radiation on the absorber,

3) integrating the SAH with thermal energy storage to make the heat available after sunset,
4) using evacuated tubes and multi-heat pipe arrays to improve heat absorption and
5) Using high thermal conductivity material or selective coatings to increase heat transfer between the absorber and the airflow.

Figure 2-3. illustrate SAH's different thermal efficiency improvement techniques, detailed in the sections below.

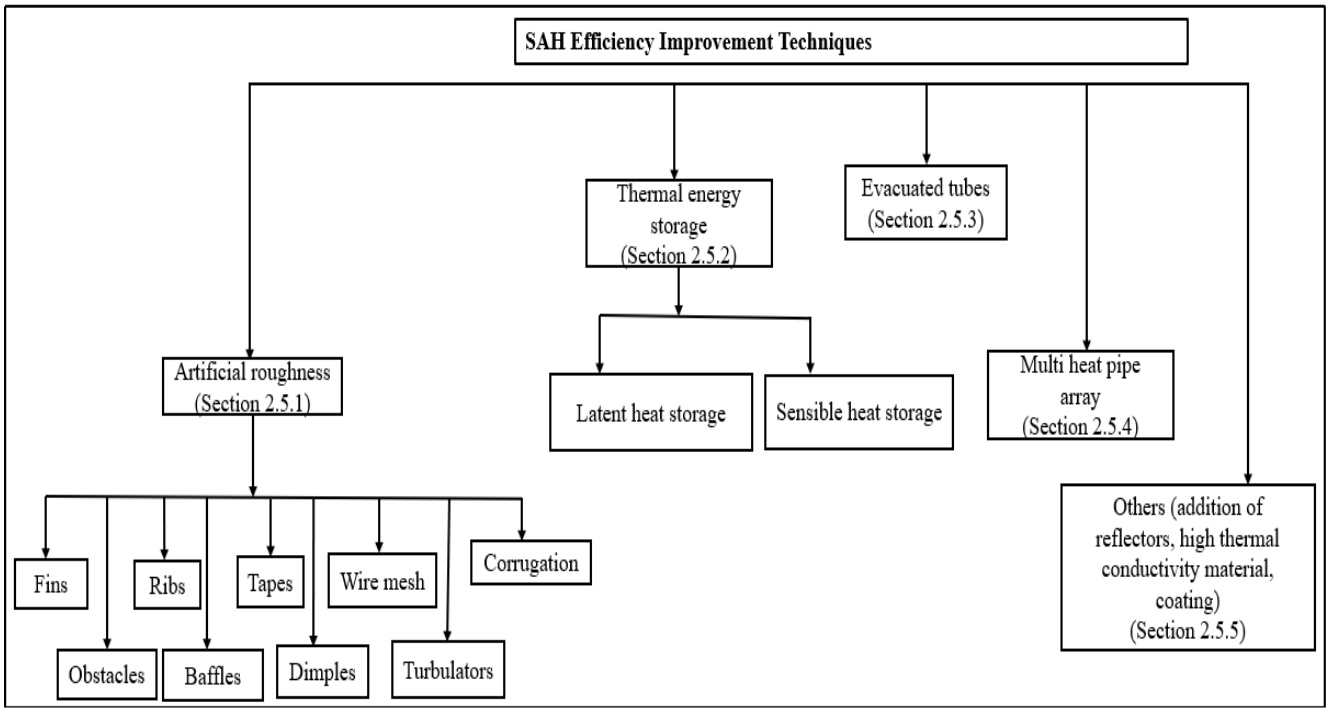

Figure 2-3 SAH efficiency improvement techniques

2.5.1 Adding artificial roughness to a tube-type SAH

Providing artificial roughness on the absorber tube increased the surface area for transferring heat from the absorber to the airflow. Increased surface area results in higher heat transfer and converts the laminar sublayer to turbulent airflow, increasing the SAH thermal efficiency. Artificial roughness could include fins (Foued Chabane, Noureddine Moummi, et al., 2014), ribs (Ansari & Bazargan, 2018), baffles (Khanlari et al., 2022), obstacles (Akpinar & Kocyigit, 2010), dimples on the interior surface of tubes (Saini & Verma, 2008), tapes within the tubes (Souayeh et al., 2021), corrugation (Bhattacharyya et al., 2020), wire mesh (Sozen et al., 2020), and turbulators(Afshari et al., 2020). Each type of roughness is discussed in this section.

2.5.1.1 Application of fins

Figure 2-4a. show SAH without fins (SAH I) and Figure 2-4b. show the SAH with fins and heat pipes (SAH II). The thermal efficiency of both the SAHs was evaluated, and it was found that the thermal efficiency of SAH-II was increased by 7.5% compared to SAH-I. It was concluded

that inserting the longitudinal fins increased the surface area, and the heat pipe transferred heat to a longer distance. The heat pipe's higher heat transfer efficiency increased the outlet air temperature of the SAH II. The uniform temperature difference and more substantial cooling effects of the photovoltaic panels were observed using heat pipes. However, integrating heat pipes into SAH is not economical (Fan et al., 2019).

Figure 2-4 Schematic diagram (a) SAH-I, and (b) SAH-II (Fan et al., 2019)

2.5.1.2 Application of ribs

Another technique used to increase the thermal efficiency was rectangular rib roughness on the black-coated absorber plate integrated with copper pipes. Figure 2-5 shows the SAH with ribs roughness. The study proved that the attachment of ribs on a black-coated absorber plate increased the surface area and provided uniform air mixing, thus increasing the collector efficiency. The maximum thermal efficiency was 56.5%. The author did not explain why copper pipes were selected except to pass air through the tubes. However, the copper pipes have a thermal conductivity of 390.0 W/m-k and corrosion resistance; it is assumed these were the preferred material characteristics (Komolafe et al., 2019).

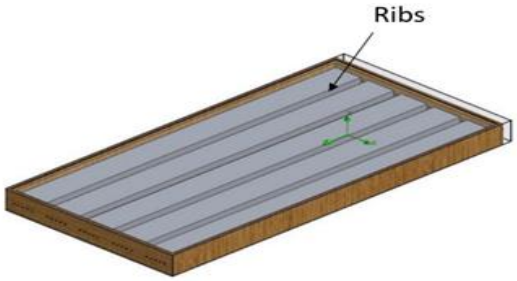

Figure 2-5 SAH with increased roughness from ribs (Komolafe et al., 2019)

2.5.1.3 Application of turbulators

A comparative study of three types of SAH was conducted: 1) a smooth tubed SAH, 2) SAH with a half-finned turbulator inside the tubes, and 3) SAH with a full-finned turbulator inside the tubes. Figure 2-6 shows the geometry of (a) a half-finned turbulator and (b) a full-finned turbulator. A turbulator consisting of fins is a device that changes a laminar airflow into a turbulent flow. Applying a turbulator increased the thermal efficiency from 60.7% to 64.1% with a half-finned turbulator and to a maximum of 72.4% with a full-finned turbulator. Using elbow-shaped tubes decreased the occupied space compared to straight tubes, thus requiring only forced convection for airflow. However, the effect of various placement angles of turbulators on the thermal efficiency of TSAH requires further investigation. It can be concluded that the SAH with a full finned turbulator had the maximum thermal efficiency (72.4%) compared to other artificial geometries discussed in section 2.5.1 (Afshari et al., 2020).

Figure 2-6 Geometry of (a) half-finned turbulator and (b) full-finned turbulator (Afshari et al., 2020)

2.5.1.4 Application of iron mesh

Figure 2-7(a) shows the experimental setup of SAH, and Figure 2-7(b). shows the iron mesh inserts used in the modified SAH. The results showed that adding iron mesh increased the thermal efficiency by 10.0% (from an average of 53.8% to 63.8%). However, the modified SAH did not have a transparent cover, insulation, backplate, and frame, which reduced the

fabrication cost for the experiment but increased the effect of wind chill and heat loss. Therefore, it can be concluded that the effects of the techniques mentioned above are difficult to compare to other SAHs with insulation and a transparent cover. A separate study to investigate the effect of the orientation of the tubes is warranted (Sozen et al., 2020).

Figure 2-7 (a) SAH experimental setup, (b) modified- iron mesh (Sozen et al., 2020)

2.5.1.5 Using corrugated tubes

A SAH with a helically corrugated tube and a perforated circular disc insert was tested. The study revealed that adding the perforated circular disc insert augmented heat transfer by 50.0%-60.0%. The authors did not estimate the thermal efficiency of the developed SAH. However, studies have indicated that augmented heat transfer results in higher thermal efficiency (Bhattacharyya et al., 2020)

2.5.1.6 Application of twisted tape inserts in the tubes

An experimental investigation of an SAH with varied lengths of twisted tape inserts, angular cuts, and plain triangular tubes was performed. Three geometrical configurations of twisted tapes, full-length, short-length, and short-length middle, are shown in Figure 2-8. The results showed that the heat transfer in the triangular tube was equipped with different configurations of twisted tapes, and the angular cut had higher heat transfer than the plain triangular tube. The three geometries have shown improvements in heat transmission. The flow field is disturbed by tape inserts, leading to improved heat transfer. The tape inserts boost fluid mixing, which breaks the thermal and hydrodynamic boundary layer and increases secondary flow. It was concluded that the SAH with full-length twisted tapes performed better than the other twisted tape geometries. The thermal efficiency values are not discussed in the article. However, the thermal performance factor is estimated. The Thermal Performance Factor, which measures the relationship between the relative impacts of change in heat transfer rate to change in friction

factor, can be used to assess the effectiveness of a heat transfer enhancement technology (Souayeh et al., 2021).

Figure 2-8 Angular twisted tape of varying length: a) Full-length, b) Short-length, c) Short-length middle (Souayeh et al., 2021)

Table 2-1 summarizes the roughness geometries. The studies discussed in section 2.5.1 conclude that adding roughness to the absorber increases the surface area, thereby increasing the heat transfer rate and the thermal efficiency of SAH.

Table 2-1 Summary of the review studies mentioned in Section 2.5.1

Sr No	Author	Year	Research Methodology	Modification type	Thermal efficiency (%)
1.	(Fan et al., 2019)	2019	Analytical	**SAH without heat pipe and fins**	60.2 - 61.7
				SAH with heat pipe and fins	67.2 - 69.2
2.	(Komolafe et al., 2019)	2019	Experimental and Numerical	**SAH with rectangular rib roughness on the black coated absorber plate integrated with copper chrome pipes**	14.0 - 56.5
3.	(Afshari et al., 2020),	2020	Experimental and Numerical	η_{th}(full finned) > η_{th}(half finned)> η_{th}(no fin)	
				SAH with smooth tube type	47.7 - 60.7, at 0.009kg/s - 0.015kg/s
				SAH with half finned turbulator	53.0 - 64.1, at 0.009kg/s - 0.015kg/s

				SAH with full finned turbulator	67.6 - 72.4, at 0.009kg/s - 0.015kg/s
4.	(Sozen et al., 2020)	2020	Experimental and Numerical	**SAH with iron mesh**	59.9 - 67.6
				SAH without iron mesh	51.1 - 56.5
5.	(Bhattacharyya et al., 2020)	2020	Experimental	**SAH with and without helically corrugated tubes with perforated disc**	SAH with helically corrugated tubes with perforated discs augmented heat transfer by 50.0-60.0% compared to SAH without corrugated and perforated tubes.
6.	(Souayeh et al., 2021)	2021	Experimental and Numerical	**A triangular SAH tube fitted with angular cut and varied length twisted tape inserts**	Full-length angular-cut twisted tape performed better than small-length twisted tape and small-length, and middle-length twisted tape.

2.5.2 Adding a thermal energy storage to increase thermal efficiency

The above studies have shown that SAHs can provide heating during the day, which makes these technologies especially useful for schools and low-rise workplace buildings. SAH can add warmth to a home during the day, but does not provide evening or nighttime heating unless there is a means of thermal energy storage (TES). High-quality TES overcame a lower level of solar energy harvesting (Tyagi et al., 2012). Different types of material could be used as TES media. Paraffin wax, a latent heat storage phase change material (PCM), is used for TES (Shalaby et al., 2014). Sand (Shalaby et al., 2014), gravel (Lakshmi et al., 2017), tin cans (Murali et al., 2020), and synthetic fluids like therminol (Kalaiarasi et al., 2016) can be used as sensible heat storage materials.

2.5.2.1 SAH with latent heat storage

SAH with a bed of small cylindrical hollow tubes (Type -I) and SAH with a bed of small cylindrical tubes filled with PCM (Type -II) are shown in Figure 2-9. The results showed that the Type-II SAH's thermal efficiency was 12.0% higher than that of Type-I. The PCM stores

the useful heat for longer but solidifies after sunset due to a higher mass flow rate. PCMs are limited due to the super cooling effect, which is cooling a liquid or a gas below its freezing point without becoming a solid. The study showed that integrating SAH with TES and a phase change material effectively increased thermal efficiency during periods of lower solar radiation. However, the authors have not addressed the effect of supercooling, and this may not give more accurate results (Singh et al., 2021).

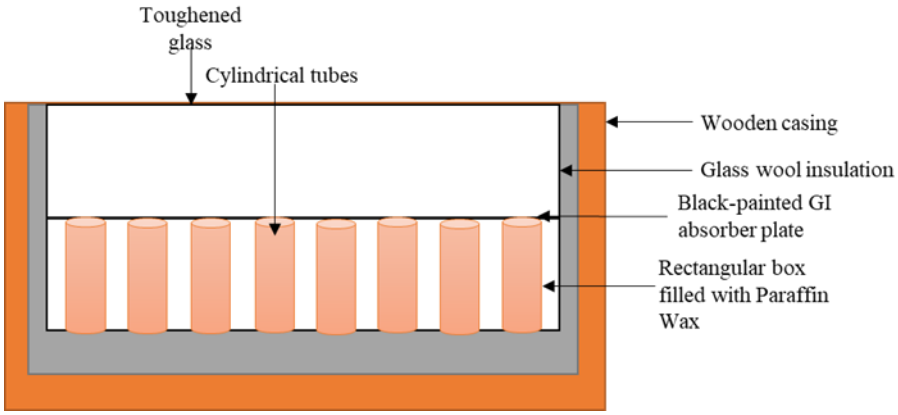

Figure 2-9 A sectional view of SAH with PCM-filled cylindrical tubes (Singh et al., 2021)

A SAH with copper tubes filled with Lauric acid (which has a melting temperature of 85 ℃) as a PCM and a SAH without any PCM were investigated experimentally and numerically for the output temperature rise. The results showed that the SAH with PCM performed better than the SAH without PCM in terms of temperature level rise (average temperature rise of 86.5%). The authors did not calculate the SAH efficiency. However, it can be concluded from Equation 1 that the SAH efficiency depends on the temperature difference (Wadhawan et al., 2018). TES integrated into SAH with PCM-filled tubes was investigated. The tubes are arranged in an inline, staggered, and circular pattern, as shown in Figure 2-10. The PCMs considered were paraffin wax, n-octadecane, and calcium-chloride hexahydrate. Compared to paraffin wax and n-octadecane, the calcium chloride hexahydrate showed better results when arranged in a staggered pattern. The same study also showed that the tube arrangement impacted the heat transfer with a circular pattern due to the uniform airflow. The tubes in a circular pattern increased the heat absorption by 1.1%, 1.6%, and 9.2% using calcium chloride hexahydrate, n-octadecane, and paraffin wax. It can be concluded that the higher heat absorption is due to its high thermal conductivity and heat capacity per unit volume. It was noted that the air inlet temperature significantly impacted the heat transfer rate between air and PCM compared to air inlet velocity. However, the author did not calculate the thermal efficiency. The experimental test results should validate the numerical results (Madhulatha et al., 2021).

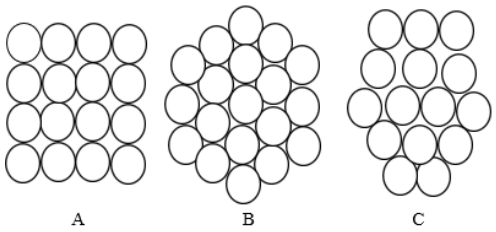

Figure 2-10 Tubes arrangement: A) Inline shape, B) Circular shape, and C) Staggered shape (Madhulatha et al., 2021)

2.5.2.2 SAH with sensible heat storage

A porous medium, such as aluminum fibers, could also increase thermal efficiency. Thermal efficiency increased from 60.0% to 90.0% when using a porous material. These were tested at a mass flow rate of 0.075 kg/s (Saleh Abo-Elfadl et al., 2021). Another study used aluminium strips and black pebble stones as TES. Aluminium strips had 6.8 % higher thermal efficiency than black pebbles at a mass flow rate of 0.025 Kg/s. The same SAH without TES had a lower thermal efficiency (60.0%). It can be concluded that the aluminium strips have higher thermal conductivity, thereby increasing the SAH efficiency. TES with aluminium strips achieved the highest thermal efficiency among the SAHs with phase change materials studied in this research. However, the high air mass flow rate may slowly erode the aluminium strips, thereby needing the airflow to be filtered before supplying the occupied space. While pebble stones are a low-cost option compared to aluminium strips, the weight of the SAH will be increased (Murali et al., 2020).

Three types of TES were investigated: graphite powder, brick powder, and desert sand. The SAH with graphite powder as TES showed the highest thermal efficiency (37.6%) compared to brick powder (35.0%) and desert sand (30.2%). Graphite's thermophysical properties are higher than brick and sand, increasing its efficiency. The thermal and mechanical stability of the TES materials should be studied.(Algarni et al., 2022).

The studies mentioned in section 5.2 show that integrating SAH with TES and PCM effectively increased thermal efficiency during periods of lower solar radiation. Table 2-2 summarizes section 2.5.2.

Table 2-2 Summary of the review studies is mentioned in section 2.5.2

Sr No	Author	Year	Research Methodology	Modification type	Thermal efficiency (%)
1	(Singh et al., 2021)	2021	Experimental	**SAH with a bed of small cylindrical hollow tubes**	53.3

				SAH with a bed of small cylindrical tubes filled with PCM	59.0
2.	(Wadhawan et al., 2018),	2018	Experimental and Numerical	**SAH with PCM**	SAH with PCM performed better than SAH without PCM
3.	(Madhulatha et al., 2021)	2021	Numerical	**SAH with PCM-filled tubes**	CaCl2•6H2O absorbed higher heat (48.03%) compared to paraffin wax and n-octadecane when arranged in a staggered pattern. Higher heat augmentation increased the thermal efficiency of SAH with CaCl2•6H2O.
4.	(S Abo-Elfadl et al., 2021)	2021	Experimental	**SAH without porous medium**	60 .0
				SAH with porous medium	90.0
5.	(Murali et al., 2020)	2020	Experimental	ηth (with Aluminium)> ηth (with pebbles)> ηth(without strips)	
				SAH without strips	60.0, at 0.025 kg/s
				SAH with pebbles	63.0, at 0.025 kg/s
				SAH with aluminium	69.8, at 0.025 kg/s
6.	(Algarni et al., 2022)	2022	Experimental	ηth (graphite)> ηth (brick powder)> ηth(sand)> ηth (no TES)	

				SAH with graphite powder	37.6
				SAH with brick powder	35.0
				SAH with sand	30.2
				SAH without TES	23.1

2.5.3 Using an Evacuated tube to increase the thermal efficiency of the SAH

Figure 2-11. show the evacuated tube collector with inserted tubes. Evacuated (vacuum) tubes (ET) have low conduction and convection losses between the absorbing surface and the air and can deliver high thermal efficiency compared to conventional SAHs (Abo-Elfadl et al., 2020). The operating temperature range of evacuated tube collectors (ETCs) is between 50.0 ℃ and 200.0 ℃ (Luo et al., 2022). It was estimated that the SAH average thermal efficiency was 50.0% for heating purposes on sunny days (Li et al., 2012).

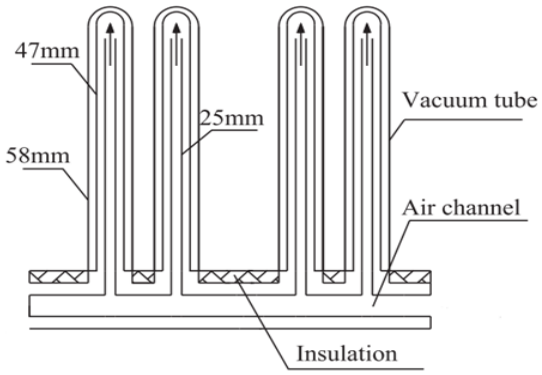

Figure 2-11 ET collector with inserted tubes (Li et al., 2012)

Figure 2-12 shows three ET configurations : (a) control system, (b) tube coated with copper coil, and (c) tube with aluminium fins. As discussed in Section 2.5.1, using fins increased the heat transfer area. Abu Hamed and Alkharabsheh (2020) found that adding fins with ET increased thermal efficiency from 24.0% to 37.0%. The maximum thermal efficiencies of the plain ET, the ET with a copper coil, and the ET with aluminium fins outside the tube were 24.0%, 29.0%, and 37.0%, respectively, at a mass flow rate of 0.013 kg/s. However, the author has not explained the effect of varying the tube material, fin size, and shape on the thermal efficiency of the evacuated collector (Abu Hamed & Alkharabsheh, 2020).

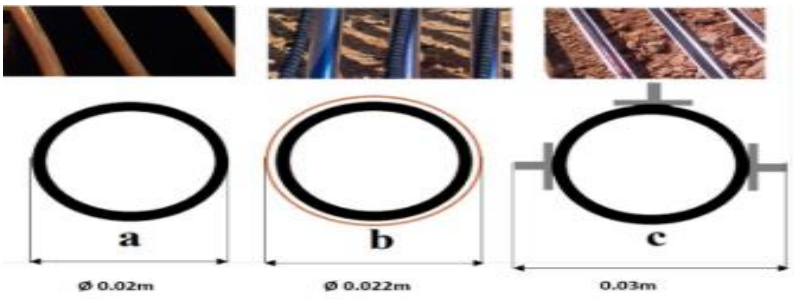

Figure 2-12 Cross section of ET; (a) control system, (b) system with copper coil, (c) system with aluminium fins (Abu Hamed & Alkharabsheh, 2020)

SAHs with evacuated tubes, energy storage, and fins were tested experimentally. The thermal storage efficiency of the modified ET SAHs during the experiment period ranged from 56.1% to 67.5%. It was concluded that integrating fins to ET with TES improved the thermal efficiency of the SAH. The study found that more SAHs are required to meet the heating demand, which is not a cost-effective solution (Wang, Zeyu, et al., 2020). Figure 2-13 illustrates the experimental investigation of the thermal storage ET heat pipe solar collector. The maximum thermal efficiency for the system was 89.8%, at a mass flow rate of 0.3 kg/s. The results indicate that the air mass flow rate has a significant impact on the collector's performance. The high efficiency is due to the experiment conducted in Chennai in March, where the average ambient air temperature ranges between 25.0 ˚C and 29.0 ˚C and has bright solar radiation. The cloud cover, lower ambient temperatures, wind, and humidity will affect efficiency during the winter and rainy seasons. The author has not considered the SAH efficiency under various weather conditions (Abi Mathew & Thangavel, 2021).

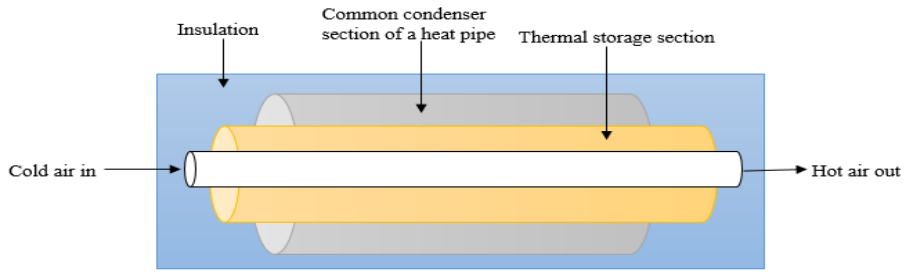

Figure 2-13 Schematic diagram of thermal storage ET heat pipe solar collector with header section (Abi Mathew & Thangavel, 2021)

Figure 2-14. shows the geometry of ET with helical inserts. The performance of inserting helically coiled components was investigated for SAH with evacuated tubes. The addition of the helical coil inserts increased the maximum thermal efficiency by 6.1% (from 64.8% to 70.9%) at the mass flow rate of 0.015kg/s. The authors did not consider the efficiency between

3:00 and 5:00 pm due to higher and unrealistic efficiency values at low solar radiation. It can be concluded that the helical coils are made of aluminium wires, which store the heat for a more extended period. Therefore, the thermal efficiency kept increasing even at low solar radiation, giving an unrealistic efficiency value (Singh & Vardhan, 2021).

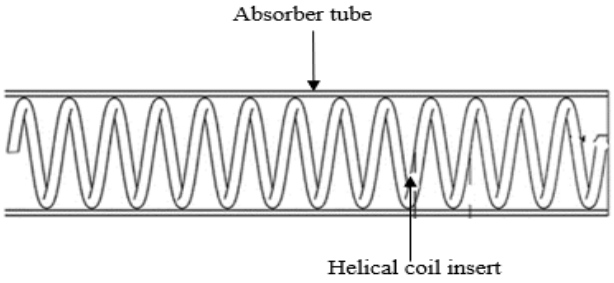

Figure 2-14 Evacuated Tube with helical tube inserts (Singh & Vardhan, 2021)

Figure 2-15 illustrates an experiment on an SAH with ET with and without reflectors. A reflector made of galvanized steel sheet coated with zinc was used to increase the collector's thermal efficiency. Reflectors are used to concentrate more incident solar radiation onto the tube. The tilt angle had a remarkable effect on the performance of ET-SAH. The maximum efficiency of ET-SAH at 45 ˚ with and without reflectors was 68.5% and 63.6%, respectively. The maximum efficiency of ET-SAH mounted at 30˚ with and without reflectors was 79.6% and 65.0%, respectively. It can be concluded that adding the reflector increased the efficiency for both selected tilt angles. Latitude plays a critical role in determinimuming the tilt angle of the SAH. The experiment is conducted in Kurukshetra, India (29 ˚ 58′ North and 76 ˚ 53′ East). Therefore, the ideal tilt angle for ET-SAH is 30 ˚ (Dabra et al., 2018).

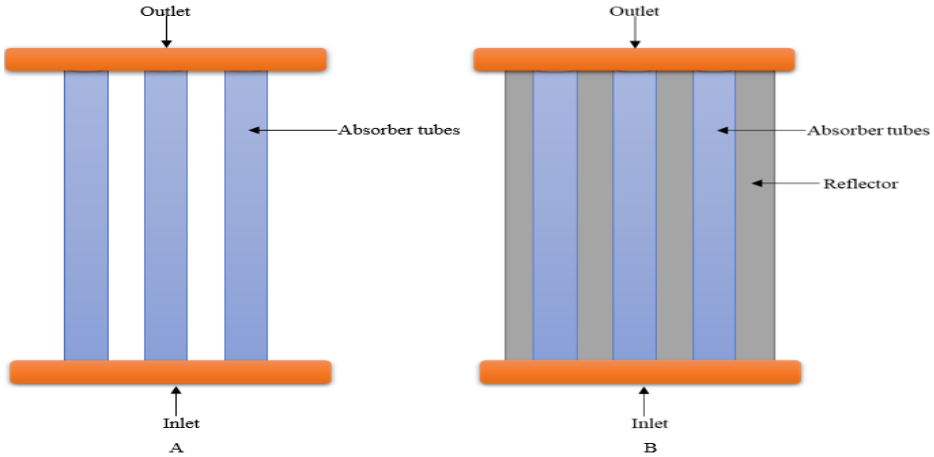

Figure 2-15 ET SAH without reflectors and B) ET SAH with reflectors (Dabra et al., 2018)

Figure 2-16. shows an ET-SAH with a simplified (compound parabolic concentrator and a concentric tube heat exchanger that was tested experimentally. The thermal efficiency at 80.0 ̊C, 150.0 ̊C and 200.0 ̊C was 52.0%, 35.0%, and 21.0%, respectively, for air mass flow rates ranging from 0.160 kg/s - 0.030 kg/s. The collector's efficiency drops to zero when the temperature exceeds 220.0 °C due to the low airflow rate. A variable-speed fan can be employed to adjust airflow velocity and to test airflow rates. The inner tube can be insulated to reduce heat losses, and a solar tracking system can be employed to increase the efficiency (Wang et al., 2015).

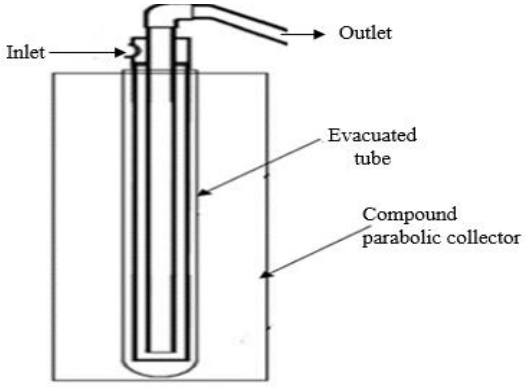

Figure 2-16 . Schematic diagram of ET-SAH with CPC (Wang et al., 2015)

Figure 2-17 shows a parabolic trough SAH with an ET inserted with a U-shaped tube heat exchanger and fitted with a reflector. Comparative performance was evaluated for aluminium U-shaped and copper U-shaped heat exchangers with and without fins. Copper has higher thermal conductivity. Thus, copper U-shaped heat exchangers perform better than aluminium U-shaped heat exchangers. The maximum thermal efficiency for aluminium U-shaped heat exchangers with and without fins was 14.4% and 10.7%, respectively, and for copper U-shaped heat exchangers with and without fins was 14.7% and 11.6%, respectively, at an airflow rate of 0.001 kg/s. The results showed that materializing fins, reflectors, and high thermal conductivity improved the collector's efficiency. However, the percentage of efficiency improved by applying a reflector needs to be studied (Nain et al., 2021).

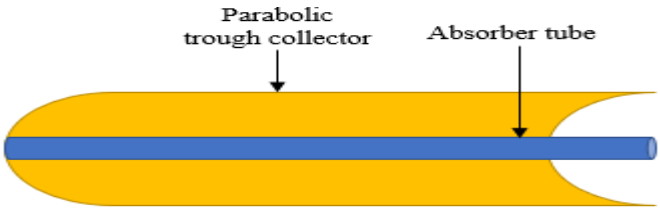

Figure 2-17 Schematic view of parabolic trough SAH (Nain et al., 2021)

A blower increased the air velocity in a U-shaped copper tube fitted into an ET. Figure 2-18 shows the schematic diagram of an ET with a U-shaped copper tube insert. The minimum average thermal efficiency was 15.2 % at a mass flow rate of 0.006 kg/s, while the maximum average thermal efficiency was 21.3 % at a mass flow rate of 0.008 kg/s. The maximum temperature obtained was 151.0 ℃ at a mass flow rate of 0.006 kg/s. It was concluded that the air mass flow rate is an important parameter affecting the collector performance (Pandey et al., 2021).

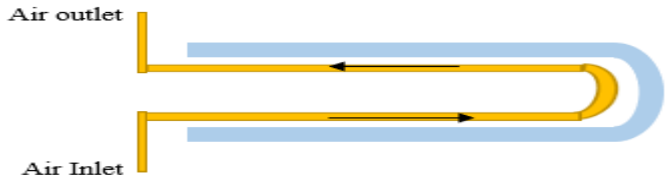

Figure 2-18 Schematic diagram of ET with U-shaped Copper tube insert (Pandey et al., 2021)

The studies show that integrating roughness geometries into ET SAHs and using high-thermal-conductivity materials, reflectors, and TES materials improved their thermal efficiency. Air mass flow rate, collector and tube tilt angle, outlet air temperature, and solar radiation affected the performance of ET SAHs. Using a synthetic fluid (Therminol) yielded the highest thermal efficiency (89.9%) among the studied ET-type SAHs. The summary of 2.5.3 is given in Table 2-3 below.

Table 2-3 Summary of the review studies, is mentioned in section 2.5.3

Sr No	Author	Year	Research Methodology	Modification type	Thermal efficiency (%)
1.	(Li et al., 2012)	2012	Experimental	**ET SAH**	50.0
2.	(Abu Hamed & Alkharabsheh, 2020)	2020	Experimental	**ET-SAH -control**	24.0, at I= 1000.0 W/m^2
				ET-SAH - with copper coil	29.0, at I= 1000.0 W/m^2
				ET-SAH - aluminium fins	37.0, I= 1000.0 W/m^2
3.	(Wang, Zeyu, et al., 2020)	2020	Experimental	**ET-SAH with TES and fins**	56.1 -67.5
4.	(Abi Mathew & Thangavel, 2021)	2021	Experimental	**Thermal storage ET heat pipe solar collector**	38.11, 77.0, 85.7, 89.9 at 0.030 kg/s, 0.10 kg/s, 0.20 kg/s, 0.30 kg/s respectively
4.	(Singh & Vardhan, 2021)	2021	Experimental and Numerical	**ET collector with helical coil insert**	70.9, at 0.015 kg/s
				Simple ETC	64.9, at 0.015 kg/s
6.	(Dabra et al., 2018)	2018	Experimental	**ET-SAH**	68.5 (with reflector, at inclination angle (θ)=45°) 63.5 (without reflector, at θ=45°) 79.6 (with reflector, at θ=30°) 65.0 (without reflector, at θ=30°)

7.	(Wang et al., 2015)	2015	Experimental	**ET- SAH with simplified compound parabolic collector and concentric tube heat exchanger**	52.0, at T_o=80.0 ℃ 35.0, at T_o=150.0 ℃ 21.0, at T_o=200.0 ℃
8.	(Nain et al., 2021)	2021	Experimental	**Aluminium U-shaped heat exchangers with fins**	14.4
				Aluminium U-shaped heat exchangers without fins	10.7
				Copper U-shaped heat exchangers with fins	14.7
				Copper U-shaped heat exchangers without fins	11.6
9.	(Pandey et al., 2021)	2021	Experimental	**ET-SAH with parabolic tough type collector**	21.3 at 0.008 kg/s 15.2 at 0.006 kg/s

2.5.4 Micro heat pipe array type SAH

A micro heat pipe array (MHPA-SAH) can serve as a heat transfer element, transferring large amounts of heat. Flat micro-heat pipe arrays SAH (FMPHA-SAH) had 73.0% and 56.0% thermal efficiency rates in summer and winter, respectively. Efficiency is higher in summer due to clear skies and strong solar radiation (Zhu et al., 2015). Zhu et al. (2016) tested a flat, micro heat pipe array compound parabolic collector SAH. The flat micro-heat-pipe array served as a heat-transfer element, and the compound parabolic collector reflected solar radiation into the tubes. The average thermal efficiency of the collector was approximately 52.0% during the test

period. It can be concluded that combining a flat micro-heat-pipe array with a compound parabolic collector increased the heater's thermal efficiency.

An MHPA integrated with thermal energy storage was tested for its thermal efficiency. Lauric acid was used as a latent heat storage material. The daily mean thermal efficiency increased from 59.8% to 72.4% for airflow rates between 0.022 and -0.050 kg/s in SAH integrated with thermal storage. The result showed that the mass flow rate considerably influences the collector's thermal efficiency. However, the SAH should be tested for different ambient air temperatures (Z. Wang et al., 2019). A SAH with a vacuum glass tube, MHPA, fins, and selective absorption film is shown in Figure 2-19. The SAH was investigated experimentally and numerically. The MPHA SAH's maximum efficiency was 85.2 %, at 0.044 Kg/s, and the average efficiency was 82.7%. The results inferred that the mass flow rate affected the collector efficiency (T.-y. Wang et al., 2019).

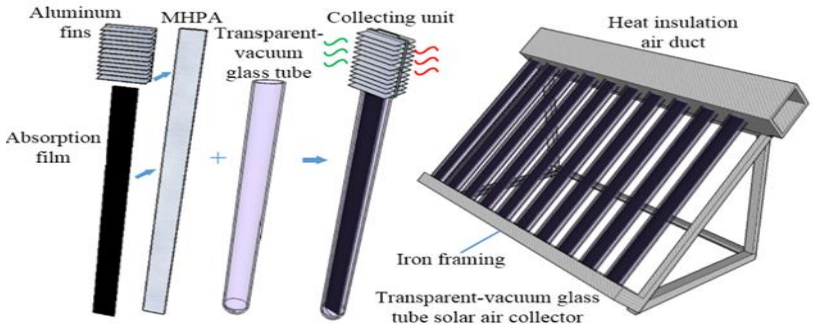

Figure 2-19 Schematic diagram of the SAH with MHPA transparent-vacuum glass tube (T.-y. Wang et al., 2019)

Figure 2-20 shows the schematic diagram of two types of flat micro-heat pipe arrays: transparent-tube collector and conventional tube collector. FMHPA was coated at various locations to increase solar energy absorption in both SAHs. Compared to T-TC, C-TC had a greater absorption coating, which improved its capacity to absorb solar energy. The maximum average thermal efficiency of C-TC and T-TC was 77.6% and 85.0%. It can be concluded that the thermal efficiency of T-TC is higher due to low thermal resistance from the absorption coating to the FMHPA evaporation portion and negligible heat transfer. Integrating coating with MHPA improved the thermal efficiency of SAH (T. Wang et al., 2020)

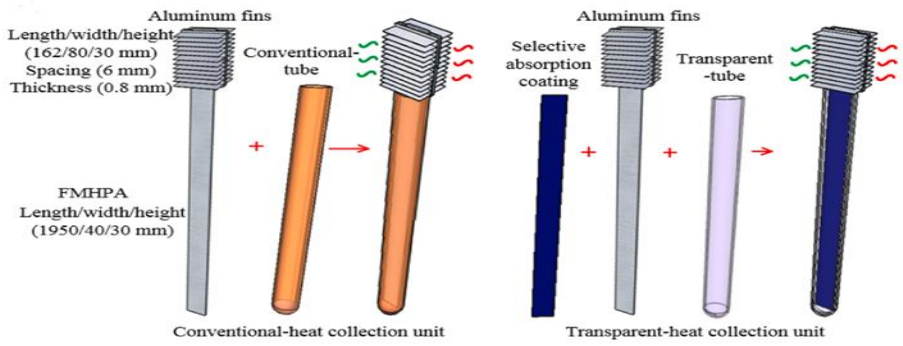

Figure 2-20 Schematic diagram of the conventional tube collector and transparent tube collector (Wang, D. Tengyue, Yanhua, et al., 2020)

A numerical model of MHPA- SAH with fins attached was studied. The thermal efficiency of the MHPA-based SAH increased with increasing ambient temperature and decreasing wind speed. Maximum thermal efficiency was 66.5%, at an air velocity of 3.3 m/s and air layer thickness value of 25.0mm. The air thickness value above or below 25.0 mm reduced the SAH efficiency, as higher heat loss was observed between the air and the glass cover. The optimal fin height, spacing, and aspect ratio values were achieved at 12.0 mm, 6.0 mm, and 0.25 mm. It can be concluded that appropriate fin spacing allows for a trade-off between heat transfer area and air flow dispersion (Zhu & Zhang, 2021). Wang et al. (2021) found that integrating FMHPA and TES into SAH improved the collector's thermal efficiency. The thermal performance of a solar air collection-storage system with PCM based on FMHPA was investigated for its performance. The solar air collection-storage system had a latent thermal storage device with Lauric acid (PCM). SAH outlet temperature ranged from 67.8 ℃ to 88.2 ℃, and the thermal efficiency of the collector was 34.5%, 38.6%, and 50.7% for airflow rates of 0.021, 0.042, and 0.084 kg/s. It can be concluded that a high airflow rate influences the SAH's thermal efficiency. Due to the low mean temperature of the SAH, an increased air flow rate with significant air disturbance improved the heat transfer effect and reduced heat loss (Wang et al., 2017). A thermal storage SAH was proposed by Norouzi et al. (2020), as shown in Figure 2-21. The system consisted of a vacuum tube (which acts as thermal insulation), flat, micro heat pipe arrays (FMHPA- acts as heat transfer element), and paraffin (PCM), which was filled inside the vacuum tube to make it compact. The PCM has a low heat transfer coefficient, limiting the heat transfer rate; therefore, louver aluminium fins were used to improve the heat transfer rate. It was observed that the thermal collection efficiency of TSSAH was 80.5%. It can be concluded that the flat MPHA integrated with thermal storage improved the SAH efficiency.

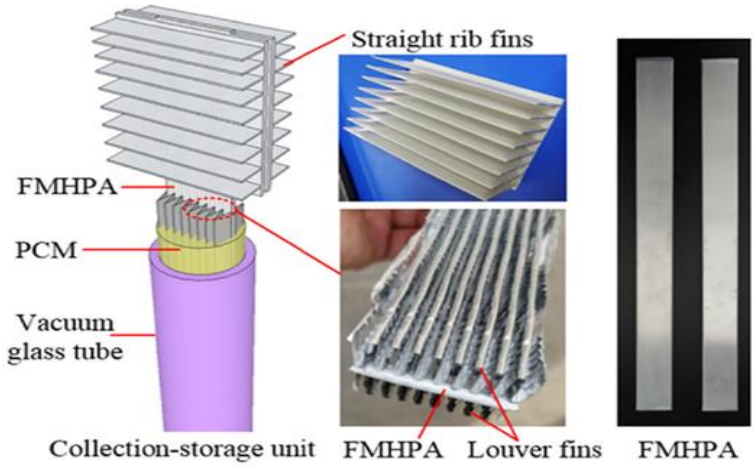

Figure 2-21 Schematic diagram of the MPHA (Norouzi et al., 2020)

Section 2.5.4 showed that the thermal efficiency for SAH integrated with MHPA improved from 35.0% to 85.0%. Applying transparent tubes, MHPA, coating, and TES further improved the SAH efficiency. The airflow rate and the ambient temperature dominated the MHPA-SAH performance. Different design configurations should be investigated, such as integrating MHPA, coating, and TES or vacuum tube, MHPA, and TES. A study on high thermal conductivity material to design MHPA for improving efficiency should be investigated. The summary of section 2.5.4 is given in Table 2-4.

Table 2-4 Summary of the review studies is mentioned in section 2.5.4

Sr No	Author	Year	Research methodology	Modification type	Thermal efficiency (%)
1.	(Zhu et al., 2015)	2015	Experimental	**Flat MPHA-SAH**	73.0 and 56.0 for summers and winters, respectively.
2.	(Zhu et al., 2016)	2016	Experimental	**Flat MHP array compound parabolic collector SAH**	53.0
3.	(Z. Wang et al., 2019)	2019	Experimental	**SAH integrated with storage**	59.8 - 72.4
4.	(T.-y. Wang et al., 2019)	2019	Numerical	**MPHA based SAH**	85.2
5.	(Wang, D. Tengyue, Yanhua, et al., 2020)	2020	Experimental	**Conventional tube collector**	77.6
				Transparent tube collector	85.0
6.	(Zhu & Zhang, 2021)	2021	Experimental and numerical	**MPHA based SAH**	66.5, at velocity =3.3m/s

7.	(Wang et al., 2017)	2017	Experimental	**Latent thermal storage device - Flat MHPA**	34.5 - 50.7
8.	(Wang et al., 2021)	2021	Experimental	**Thermal storage SAH based on Flat MHPA**	80.6, at Ta=30.3°C and I= 810.0 W/m^2 70.2 - 77.3, at Ta= 20.8 –23.3 °C and I= 675.0 – 835.0 W/m^2

2.5.5 Other techniques include applying reflectors, coating, and using high thermal conductivity materials.

2.5.5.1 Coating with paints (black paint, matte paint) and nanofluids

Nanomaterials, such as nanofluids, nanocomposites, and nanofluid PCMs, can improve heat transfer phenomena by changing heat transfer fluids' thermal and optical characteristics. SAH can be coated with paints (black paint, matte paint) and nanofluids to increase its efficiency. The theoretical and experimental studies show that combining nanoparticles with base fluids may significantly increase the performance and efficiency of solar heaters (Shamshirgaran et al., 2017). Two SAHs were experimentally tested in Wuhan (China). Aluminium plates were used as absorbers: one set was painted with black paint, and the other was painted with a nanofluid, a mixture of black paint and nanoparticles. Nanoparticles, cupric oxide (CuO), and carbon nanotubes (CNTs) powder or CNTs with a mass ratio of 1:1 was mixed. Then, other mass percentages ranging from 0% to 5% of CNT powder or the composite were distributed in black paint. The study revealed that adding CuO or CNTs is a cheap and easy way to improve the efficiency of SAH (Abdelkader et al., 2020). A triangular SAH was experimentally tested for its thermal efficiency. One side had a glass cover, whereas the other had two aluminium plates (absorber plates) that collect solar energy from the sun. One set of aluminium plates was sprayed with black paint, while the second set was sprayed with 1% graphene nanomaterial embedded in black paint. Investigation revealed that for a 1% graphene nanoparticle black paint coating, the maximum efficiency was 48.2% at 12 hours at an air speed of 1 m/s, and for the black paint coating, it was 43.2%. Applying a graphene nanomaterial coating to the absorber plate increased the average thermal efficiency by 4.9 %. The authors have conducted an experiment using 1% graphene mixed in black paint. Testing the SAH with different concentrations of graphene coating is recommended, as the nanoparticle concentration affects the SAH performance (Kumar et al., 2020).

The studies in section 2.5.5 show that SAH with the nanofluid coating could be more efficient than SAH with a black paint coating. This is because the nanofluid coating increases the heat transfer area and has higher thermal conductivity. A study on SAH with a nanofluid coating needs more attention. The effect of varying nanofluid volume concentration, nanoparticle size, and stability should be further investigated. Studies have shown that one of the most promising technologies for improving SAH performance is the application of nanofluids to absorber tubes. This technique is discussed in detail in section 2.6.

2.5.5.2 Utilizing high thermal conductivity material

Using high thermal conductivity material (metals) to design the absorber (tubes/plate) improved the thermal efficiency of the collector (Nain et al., 2021). Two SAHs were designed and fabricated from plastic and metal materials. The experimental results showed that the plastic and metal SAHs had maximum average thermal efficiencies of 47.7% and 60.0%, respectively, at a mass flow rate of 0.012 kg/s and a tilt angle of 32 ° off the horizontal. The airflow rate, tilt angle, and solar radiation affect the SAH's thermal efficiency. The thermal conductivity of metal is higher compared to plastic, thereby increasing the thermal efficiency of the heater (Khanlari et al., 2021). The effect of tube material on the thermal efficiency of parabolic trough collectors (PTC) was investigated. Six different materials, including aluminium, brass, copper, steel, and nickel, were used for the tube, and their effects on the results were studied. It was found that the aluminium tube had a higher thermal efficiency (15.0% higher) and was lighter than other tubes. Steel had the lowest thermal efficiency compared to other tubes. Copper has higher thermal conductivity compared to aluminium. However, it loses heat, so its efficiency is lower than aluminium. An extensive study for selecting material to design TSAH that is low-cost, light, and highly efficient is required (Norouzi et al., 2020).

2.5.5.3 Application of reflectors

The heat input to SAH can be improved by using reflectors, thereby increasing SAH efficiency (Abdullah, Amro, et al., 2020). A study found that adding reflectors to double-pass solar water heaters improved their efficiency by 9.0-15.0% compared to single-pass water heaters (Mandal & Ghosh, 2020). A solar collector was fabricated, integrating flat-plate reflectors made of aluminium, oriented at the bottom, top, left, and right. The objective was to find the optimal tilt angle for the solar collector and the optimal inclination angle for the reflectors to achieve maximum solar concentration. The results showed that the bottom reflector had a greater effect (double) than the top reflector, and both increased solar intensity by about 50.0%. The solar radiation intensity on the solar collector increased to about 80.0% when the reflector was placed

at the top, bottom, left, and right (in summer), thereby improving the collector efficiency. It can be concluded that solar tracking could further boost the thermal efficiency of the SAH with reflectors. (Pavlovic & Kostic, 2015). ET solar collector heat pipes integrated with and without reflectors for water heating were experimentally tested. Reflectors were attached to the collector's upper and lower sides, as shown in Figure 2.22. The daily average thermal efficiency of ET solar collector heat pipes with and without reflectors was 76.3% and 60.6%, respectively. In summer, the lower reflectors had a more significant effect on the performance of the ET solar collector heat pipes than the upper reflectors, due to the greater beam width on the lower reflectors. The opposite happens in winter. Therefore, two reflectors (upper and lower) are integrated into the ET solar collector heat pipes. It was found that combining reflectors with SAH improved its thermal efficiency and reduced the convective losses from the collector tubes. However, the effects of integrating reflectors on the left or right side and of different reflector materials should be investigated (Abo-Elfadl et al., 2020).

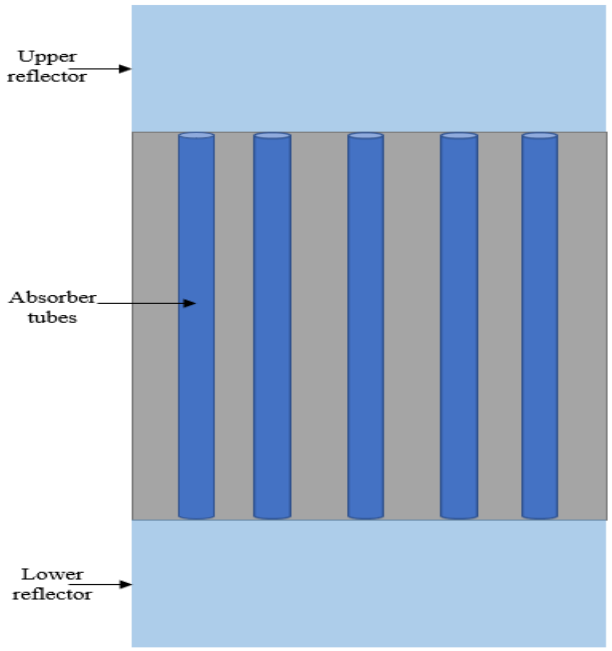

Figure 2-22 An experimental set of ETSC-HP (Abo-Elfadl et al., 2020)

The studies in section 2.5.8 showed that integrating reflectors into the solar collector improved efficiency. A solar collector with reflectors at the bottom performs better than one with reflectors at the top. Incorporating reflectors on top, bottom, left, and right further increases its thermal efficiency, but at the expense of cost and weight. More investigation is required to design and implement SAH's tracked reflectors with reduced cost, weight, design, material, and efficiency.

The literature study identified that nanocoating the absorber surface could improve the SAH's thermal efficiency. However, the literature shows limited research on SAHs with nanofluid coatings, warranting further investigation. This motivated me to examine the potential of nanofluids in solar thermal applications; therefore, section 2.6 further reviews nanocoated solar collectors.

2.6 Literature review on nanofluids for solar thermal engineering systems

Nanofluids have transformed solar thermal engineering by improving the thermal performance of solar collectors, SAHs, solar stills, and solar dryers. This review presents the existing research on the application of nanofluids, focusing on their use in improving the thermal performance of solar thermal systems. Kim et al. (2017) reported performance improvements ranging from 6.8% to 62.0%, depending on the type and concentration of nanoparticles used. Standard nanoparticles, including copper oxide (CuO), aluminium oxide (Al_2O_3), and titanium dioxide (TiO_2), enhance heat transfer and increase solar radiation absorption. This review of nanofluids also explores the emerging role of hybrid nanofluids, which combine multiple nanoparticles to improve efficiency. However, stability, environmental impact, and long-term feasibility remain unsolved. This chapter presents recommendations for future research to optimize the use of nanofluids in solar thermal applications, focusing on long-term testing, cost analysis, and environmental assessments.

2.7 Introduction

The continuous search for efficient and sustainable energy solutions has increased the development of advanced technologies in solar thermal engineering (Kabeel, Hamed, et al., 2017). Solar thermal systems, including SAHs, solar stills, and solar dryers, are crucial for harnessing solar energy for applications such as water heating, drying, and desalination. However, one of these system's main challenges is the relatively low thermal efficiency due to heat loss and low energy absorption (Kumar & Layek, 2020). Pardeshi et al. (2024) reported that applying nanofluid coatings on absorber tubes could significantly improve thermal performance.

The term "nanofluid" refers to a fluid containing metallic particles with an average particle size of 10.0 nanometres (known as nanoparticles) uniformly and stably suspended in a base fluid (Choi & Eastman, 1995). Their study found that adding nanoparticles, such as copper oxide (CuO), aluminium oxide (Al_2O_3), and titanium dioxide (TiO_2), and carbon-based materials, such as graphene and carbon nanotubes (CNTs), improved the efficiency of solar collectors by enhancing heat transfer.

Kim et al. (2017) observed that nanofluids could enhance the thermal efficiency of solar collectors by 6.8% to 62.0%, depending on the type and concentration of nanoparticles used. These findings suggest that nanofluids are effective at improving energy absorption and optimizing heat retention in solar collectors, thereby improving performance.

This review aims to comprehensively analyse the literature on nanofluids, with a particular focus on their application in solar thermal systems. The discussion will cover the classification of nanofluids based on the types of nanoparticles used, their application methods, performance improvements, and the challenges faced using these fluids. Additionally, the review will explore the growing field of hybrid nanofluids, which combine multiple types of nanoparticles to achieve even greater efficiency gains. Finally, recommendations for future research and long-term testing will be provided.

2.8 Applications and performance of nanofluids in solar thermal systems

In recent years, nanofluids have gained massive attention for their potential to improve the performance of solar thermal systems. SAHs, solar distillation systems, and solar dryers are among the most common applications where nanofluids have proven significant performance improvements (Kabeel, Hamed, et al., 2017). There are two ways to use nanofluids. One method is to apply a nanofluid coating to the absorber tube, and the other is to use nanofluid as a working fluid for heat absorption in solar collectors. These two methods are discussed in Sections 2.11 and 2.12.

2.9 Nanocoating of absorber tubes

One of the most promising applications of nanofluids is the nanocoating of absorber tubes in solar thermal collectors. For example, (Khanlari et al., 2022) reported that SAHs coated with 2% CuO in black paint improved thermal efficiency by 4.0% compared to uncoated systems. Additionally, (Sivakumar et al., 2020) found that nanocoating improved the solar dryer's efficiency by 7.3%, with CuO coatings absorbing 6.3% more solar energy than conventional black paint. Studies by (Khanlari et al., 2022) and (Sivakumar et al., 2020) show that applying CuO or Al_2O_3/nanoparticles to absorber tubes can significantly increase the efficiency of SAHs and dryers.

Other studies have focused on the benefits of using different nanoparticle materials for absorber coatings. For instance, the use of TiO_2 nanoparticles has been shown to improve light absorption and increase freshwater production in solar stills by 6.3% (Kabeel et al., 2019). Similarly, Ozturk and Ciftci (2023) reported that combining graphene and black paint improves the thermal efficiency of SAHs by 11.6%.

2.10 Nanofluids as working fluids

Another application of nanofluids is their use as working fluids in solar collectors. Due to the high surface area of the nanoparticles, nanofluids have superior heat transfer properties compared to traditional working fluids like water or oil, which allows for better heat exchange. Sethi et al. (2023), reported that using nanofluids like CuO, TiO_2, and Al_2O_3 in solar thermal systems can enhance heat transfer efficiency by increasing the working fluid's thermal conductivity and optical absorption.

Elbrashy et al. (2023) conducted an experimental study on the performance of SAHs using nanofluids as working fluids. Their findings revealed that nanofluids significantly improved the thermal performance of evacuated tube solar collectors by increasing heat storage in the system, thereby enabling more efficient heat transfer to the absorber. In some cases, nanofluids improved heat transfer efficiency by up to 45%, particularly when high-conductivity nanoparticles such as Ag or Cu were used.

In summary, using nanofluids in solar thermal systems has demonstrated significant potential for improving heat transfer and energy absorption. The following section examines the classification of nanofluids by nanoparticle type and their respective applications in solar thermal systems.

Excluded areas of research and limitations

1. Literature studies indicate that much of the research has focused on solar distillation, solar stills, solar water heating, and solar dryers, where nanofluids are primarily used as working fluids. However, there is limited research on SAHs that utilize nanofluid coatings. Therefore, this chapter aims to investigate the thermal efficiency of solar thermal systems when improved with nanocoating.
2. Nanoparticles in carbide form (e.g., silicon carbide) are not explored as they have not yet been tested or reported in the literature on solar thermal systems.

Types of nanofluids based on nanoparticles

Nanofluids are classified based on the types of nanoparticles used, which are selected for their unique thermal properties and ability to improve base fluids' heat transfer capabilities. The primary categories of nanoparticles used in solar thermal systems include metal oxides, high thermal conductivity metals, and carbon-based materials (Modi et al., 2023). Each type offers distinct advantages in thermal conductivity, stability, and overall performance. The following sections present the research on the nanofluid classification.

2.10.1 Metal oxide nanoparticles

Metal oxides are commonly preferred in the formulation of nanofluids due to their chemical stability, which can be attributed to their resistance to oxidation. Additionally, some metal oxides exhibit fewer particle-settling issues because their densities are lower than those of the corresponding metals (Sundar et al., 2013). Although metal oxides generally have lower thermal conductivity than metals, their chemical stability makes them the favoured nanomaterials for forming nanofluids. The following section outlines various studies that show the application of metal oxide nanofluids in solar collectors.

A study by Khanlari et al. (2022) investigated a SAH coated with 2% CuO/black paint and reported a 4.0% improvement in thermal efficiency compared to uncoated SAHs. The same study also found that nano-embedded absorber material and air mass flow rate significantly influenced SAH thermal performance. However, the study did not explore the effects of different nanofluid concentrations.

Sivakumar et al. (2020) examined solar dryers and found that using a 0.04% CuO/black paint coating improved thermal efficiency by 7.3% compared to a 0.02% CuO/black paint coating and 4% conventional black paint. The CuO-coated collector absorbed 6.3% more solar energy than a black paint-coated collector. Increasing the CuO concentration further enhanced the solar dryer's efficiency. Studying the long-term stability and economic feasibility of nanofluids in future research is recommended.

Selimefendigil et al. (2022) tested the thermal efficiency of solar dryers with nanocoated and uncoated absorbers. The thermal efficiency of the nanocoated dryer was 75.1%, compared to 70.4% for the uncoated dryer. Nanocoating also reduced drying time from 220 minutes to 180 minutes, indicating that nanocoating improves heat transfer and drying temperature, thereby reducing drying time.

In addition to solar drying systems, CuO nanofluids have proven effective in solar distillation. Research by Abdullah, Essa, et al. (2020) demonstrated that coating a solar distiller with CuO/black paint increased the overall freshwater yield by 14.0%, boosting the usefulness of nanofluids in solar applications. Meanwhile, (Kabeel, Omara, et al., 2017) reported that using CuO nanofluids in conventional basin solar stills increased water productivity by 16.0% to 24.0%, depending on the nanofluid concentration (ranging from 10% to 40%).

While CuO nanofluids have dominated much of the research, other metal oxides, such as aluminium oxide (Al_2O_3), have also shown notable potential in solar thermal systems. Al_2O_3/black paint coatings, for instance, increased water productivity in solar stills by 38.1%

and boosted thermal efficiency by 12.2% (Manoj Kumar Sain & Kumawat, 2015). Moreover, when used in higher concentrations (10%, 15%, and 20%), Al_2O_3 enhanced solar still productivity by 134.9% (Caturwat et al., 2023). These findings highlight Al_2O_3's ability to maximize heat absorption and retention, making it an ideal nanoparticle for improving solar distillation systems. However, little information is available on Al_2O_3-coated SAHs, while many studies focus on using Al_2O_3 as a working fluid to improve performance in SAH applications.

TiO_2 has emerged as another promising metal oxide for solar collectors. The effectiveness of TiO_2/black paint coatings in improving light absorption was demonstrated by (Pfeffer et al., 2016) and (Samneang et al., 2021). Kabeel et al. (2019) showed that daily freshwater production increased by 6.3% when TiO_2/black paint was used in a solar still and found the method economically viable and feasible.

SiO_2 nanofluids have also gained attention due to their stability. (Sathyamurthy et al., 2020) explored using SiO_2/black paint in solar stills and found improvements of 27.2% and 34.3% for 10% and 20% SiO_2 concentrations, respectively. Their research showed that moderate concentrations of SiO2 optimized thermal efficiency, whereas higher concentrations of SiO_2 reduced thermal conductivity. (Arani et al., 2021) examined tubular solar stills coated with SiO_2 at varying concentrations. Their results showed that a 20% SiO_2 coating achieved the highest thermal efficiency (52.5%), while higher concentrations led to diminished performance. These findings suggest that while SiO_2 nanofluids have great potential, further research is needed to optimize their applications fully.

In addition to SiO_2, ceria (CeO_2) has also been explored for its potential to enhance solar thermal systems. (Khanlari et al., 2023) found that CeO_2/black paint coatings improved the thermal efficiency of SAHs by 7.8% at low airflow rates and by 6.7% at high airflow rates, further demonstrating the potential of nanofluids to boost system performance under varying conditions.

Tuncer et al. (2023) explored the thermal efficiency of an infrared-assisted solar drying system that used a vertical SAH with perforated baffles and ZnO nano-enhanced black paint coatings. The thermal efficiency ranged from 53.5% to 65.1%, and drying time was reduced by 43.8%. The authors emphasized the need for further study on long-term stability, cost-effectiveness, and performance testing under different climatic conditions

Finally, Gurbuz et al. (2023) examined SAHs with meshed tubes coated with Fe_2O_3/black paint. Their study showed that the thermal efficiency was 40.5% higher than that of uncoated SAHs

without meshed tubes. The increased thermal efficiency was attributed to the meshed tubes' extended surface area and the nanomaterials' thermal conductivity.

Tables 2-5 summarize the literature studies. They note that CuO/black paint is the best coating and provides higher thermal efficiency.

Table 2-5 Summary of the literature studies discussed in Section 2.12.1

Sr No	Author and year	Coating type	SAH performance (%)
1.	Khanlari et al. (2022)	Black paint	72.1
		CuO /black paint	76.2
2.	Sivakumar et al. (2020)	0.04% Black paint	55.0
		0.02 % CuO/black paint	62.3
3.	Selimefendigil et al. (2022)	CuO/black paint	70.4 - 75.1
4.	Abdullah, Essa, et al. (2020)	CuO/black paint+reflectors+paraffin wax	51.5
5.	Kabeel, Omara, et al. (2017)	(CuO/black paint	Productivity rise from 16.0%-24.0%.
6.	Manoj Kumar Sain and Kumawat (2015)	Al_2O_3/black paint	38.7
7.	Caturwat et al. (2023)	Al_2O_3/black paint	The distillate productivity increases for 20% Al_2O_3/black paint by 134.9%.
8.	Kabeel et al. (2019)	TiO_2/black paint	Daily freshwater production was improved by 6.3%
9.	Sathyamurthy et al. (2020)	SiO_2/black paint	Productivity increased by 34.3%
10.	Arani et al. (2021)	10% SiO_2/black paint 20% SiO_2/black paint	38.5 52.5
		30% SiO_2/black paint 40% SiO_2/black paint	40.8 28.7
11.	Khanlari et al. (2023)	Uncoated	46.2
		CeO_2 /black paint coating	67.4
12.	Tuncer et al. (2023)	Vertical SAH with perforated baffles and a ZnO/black paint coating	53.5 - 65.1
13.	Gurbuz et al. (2023)	uncoated	31.1 – 53.5
		Fe_2O_3/black paint	37.9 – 73.3

Section 2.12.1 Summary: The reviewed literature demonstrates that metal oxide nanofluids, particularly CuO, Al_2O_3, TiO_2, SiO_2, CeO_2, ZnO, and Fe_2O_3, significantly enhance the thermal performance of solar thermal systems, including SAHs, solar dryers, and solar stills. These

nanofluids improve thermal efficiency, solar energy absorption, and water productivity, with CuO and Al_2O_3 showing promising results. CuO is particularly effective at enhancing solar energy absorption and heat transfer, while Al_2O_3 is known for its strong heat retention and solar radiation absorption. The mentioned improvements can make solar thermal systems more efficient and sustainable, reducing the time and energy required for drying and water distillation processes. However, further research is needed to investigate the long-term stability, optimal nanoparticle concentrations, and cost-effectiveness of these nanofluids.

2.10.2 High thermal conductivity metals

Nanoparticles made from high thermal conductivity metals, such as silver (Ag), copper (Cu), and gold (Au), offer superior heat transfer capabilities compared to metal oxides. These metals have higher thermal conductivities, which allow them to transfer heat more efficiently (Abdullah et al., 2022; Parsa et al., 2021). However, their higher cost often limits their widespread use.

Silver nanoparticles are among the most effective for improving heat absorption due to their high thermal conductivity. Research by Abdullah et al. (2022) showed that using Ag nanoparticles in solar stills increased daily average distillation by 34.0%, compared to 30.0% for Au and 28.5% for TiO_2. Similarly, Parsa et al. (2021) found that Ag/black paint coatings achieved the highest instantaneous thermal efficiency, outperforming other metallic nanoparticles, such as Au and TiO_2, by up to 10.9% in solar stills. Despite these promising results, the high cost of silver nanoparticles limits their use in practical applications. Future research may explore ways to reduce costs or use less silver in hybrid nanofluids to maintain performance while improving cost-effectiveness.

Copper nanoparticles also offer high thermal conductivity and are more affordable than silver. They have been combined with other materials to improve the thermal performance of solar thermal systems. Abdullah, Essa, et al. (2020) and Elbrashy et al. (2022) demonstrated that Cu nanoparticles enhanced the heat absorption and transfer efficiency in SAHs and stills. Combining Cu nanoparticles with other nanomaterials, such as graphene or carbon nanotubes, can further improve performance, as discussed later in the section on hybrid nanofluids. Literature on nanocoating with high-thermal-conductivity materials is limited, but much research is available on utilizing nanofluids of high-thermal-conductivity metals as working fluids.

Section 2.12.2 Summary: The reviewed literature highlights the significant potential of high thermal conductivity metal nanoparticles (Ag, Cu, Au) and carbon-based nanoparticles

(graphene, CNTs) in enhancing the thermal efficiency of solar thermal systems. Silver nanoparticles, while costly, offer superior heat transfer, boosting solar still efficiency by up to 34.0%. Copper nanoparticles provide a more affordable alternative with promising performance in SAHs and stills.

2.10.3 Carbon based nanoparticles

Carbon based nanoparticles, including graphene, carbon nanotubes (CNTs), and fullerenes, have attracted attention for their exceptional thermal conductivity and high surface area. These nanoparticles significantly improve the efficiency of solar thermal systems by enhancing heat absorption and retention. The following section discusses research on carbon-based nanoparticles, and the summary of this section is presented in Table 2-6.

Graphene has emerged as one of the most promising materials for improving solar thermal efficiency. Its high thermal conductivity, specific heat capacity, and optical absorption properties make it an ideal candidate for solar collectors. Studies showed that applying graphene and its derivatives increased the collector's thermal conductivity by 17.0% and 40.0%, respectively. Utilizing graphene nanoparticles increases viscosity by almost 50.0% and is stable. Therefore, they are used in solar collectors for efficiency improvement (Mahamude et al., 2021). Research by Alami and Aokal (2018) showed that graphene-coated solar absorbers were 29.9% more efficient than those coated with conventional black paint. SAH coated with 1% graphene/black paint showed an average increment in thermal efficiency of 4.9%. The increase in efficiency is due to the nanofluid's heat-storage capability. However, the authors have not mentioned the SAH thermal efficiency with different nanofluid concentrations (Kumar et al., 2020). The thermal efficiency of SAH coated with graphene/black paint was 6.25% higher compared to black paint-coated SAH. Thermal efficiency depends on the thermal conductivity and the optical properties of the absorber material and coating (Senthil et al., 2020).

Kumar et al. (2021) reported that the optimal graphene concentration for maximum thermal efficiency (73.3%) was 0.2%, as higher concentrations led to a significant pressure drop, reducing overall efficiency. This indicates that while graphene is highly effective at improving heat transfer, carefully considering its concentration is crucial to avoid diminishing returns. compared two types of SAHs, one coated with black paint and the other with graphene/black paint. The SAH with graphene/black paint achieved an 11.6% improvement in thermal efficiency compared to the black-paint-coated system. The sustainability index of the graphene-enhanced system was higher, indicating better long-term performance and reduced environmental impact. However, the study highlighted the need for testing in varied geographic

regions and long-term assessments to understand the durability of nanoparticle coatings over time. SAH with inclined and winglet baffles with different coatings was investigated for thermal efficiency. The average thermal efficiency of SAH with graphene-based nanopaint (72.5%) was 9.6% higher than that of black-painted SAH (62.9%). However, the authors conducted the experiment in April in India, which has hot weather. The winter result needs to be estimated (Dharmaraj et al., 2023).

Single-wall and multi-wall carbon nanotubes were studied for their potential to improve the efficiency of solar thermal systems. (Madhu et al., 2020) reported that CNT/black paint coatings on SAHs with staggered fin arrangements improved thermal efficiency by 6.6% compared to conventional black paint coatings. CNT's high surface area and thermal conductivity make them highly effective at enhancing heat transfer, particularly when combined with advanced absorber designs like staggered fins.

Due to their unique properties, carbon-based materials such as graphene and CNTs hold exceptional promise for improving solar thermal efficiency. However, their optimal concentrations must be carefully managed to prevent adverse side effects, such as pressure drops.

A study conducted by GaneshKumar et al. (2024) compared the thermal efficiency of the conventional SAH with activated carbon/black paint-coated SAH integrated with V corrugation and black pebble stones (modified SAH). The thermal efficiencies of conventional and modified SAH ranged from 10.5% to 31.5% and 12.6% to 42.4%, respectively, at mass flow rates between 0.01 kg/s and 0.02 kg/s. The activated carbon/black paint-coated V corrugated and shot-blasted absorber improved heat transfer, and the black pebble stone stored heat effectively. This modification maintained the temperature distribution and improved the thermal efficiency of the SAH. However, the study primarily focuses on mass flow rate and solar radiation, with limited discussion of other factors such as humidity, wind speed, and seasonal variations, which could be explored more thoroughly for their impact on thermal efficiency. The stability of nanomaterials needs to be explored.

Carbon-based nanoparticles, including graphene, CNTs, and fullerene, have demonstrated significant potential to enhance the thermal efficiency of SAHs. Graphene, in particular, stands out for its exceptional thermal conductivity, specific heat capacity, and optical absorption, leading to notable improvements in solar energy absorption and heat retention. Various studies have shown that graphene-coated absorbers can outperform conventional black paint coatings by a substantial margin, with thermal efficiency improvements ranging from 4.9% to 11.6%, depending on the design and concentration used. However, the optimal concentration of

graphene must be carefully considered, as excessively high concentrations can lead to undesirable effects, such as pressure drops, which can diminish overall efficiency.

Table 2-6 Summary of literature studies discussed in sections 2.12.2 and 2.12.3

Sr No	Author and Year	Nanofluid Coating type	SAH performance (%)
14.	Abdullah et al. (2022)	**TiO_2/black paint**	Daily average distillate= 28.5%
		Au/black paint	Daily average distillate= 30.0%
		Ag/black paint	Daily average distillate= 34.0%
15.	Parsa et al. (2021)	**TiO_2/black paint**	27.9
		Au/black paint	31.3
		Ag/black paint	33.7
16.	Alami and Aokal (2018)	**Black paint**	39.5
		Graphene/black paint	69.4
17.	Kumar et al. (2020)	**Black paint**	43.2
		Graphene/black paint	48.2
18.	Senthil et al. (2020)	**Black paint**	36.4
		Graphene/black paint	42.7
19.	Kumar et al. (2021)	**Graphene/black paint**	68.3
		Graphene/black paint	73.3
		Graphene/black paint	72.16
20.	Ozturk and Ciftci (2023)	**Black paint-coated SAH**	62.3
		Graphene/black paint-coated SAH	73.9
21.	Dharmaraj et al. (2023)	**Black paint**	62.9
		Graphene/black paint	72.5
22.	Madhu et al. (2020)	**Black paint-coated SAH with staggered fin inserts**	64.9
23.	GaneshKumar et al. 2024	**Conventional SAH**	10.5 - 31.5
		SAH integrated with V corrugation and black pebble stone	12.6 - 42.4

Section 2.12.3 Summary: Carbon-based nanoparticles, particularly graphene and carbon nanotubes (CNTs), exhibit exceptional potential for improving the thermal efficiency of solar thermal systems due to their high thermal conductivity, surface area, and heat retention capabilities. Studies consistently show that graphene coatings significantly outperform conventional black paint, with efficiency improvements ranging from 4.9% to 11.6%, depending on the design and nanoparticle concentration. CNTs enhance performance, particularly when paired with advanced designs like staggered fins. However, optimal

nanoparticle concentrations must be carefully managed to avoid adverse effects such as pressure drops, and further research is needed to explore long-term stability and the impact of environmental factors on performance.

Despite these advancements, several areas still require further investigation. Key factors such as humidity, wind speed, seasonal variations, and the long-term stability of nanomaterials have not been thoroughly explored. Additionally, future studies should focus on the durability and performance of these coatings across different geographic regions and environmental conditions to fully understand their long-term viability and impact. Careful management of nanomaterial concentration, design optimization, and holistic evaluation of environmental factors will be essential for realizing the full potential of carbon-based nanoparticles in solar thermal systems.

2.11 Hybrid nanofluids in solar thermal applications

Hybrid nanofluids are a recent innovation in solar thermal engineering that combines two or more types of nanoparticles into a base fluid. Their primary advantage is their superior thermophysical properties compared to nanofluids containing only one nanoparticle type. Che Sidik et al. (2017) found that hybrid nanofluids exhibit higher heat transfer performance and better stability than single-nanoparticle fluids. For example, combining carbon nanotubes (CNTs) and copper oxide (CuO) nanoparticles in a base fluid has enhanced heat absorption and thermal conductivity. The improved performance of hybrid nanofluids is primarily due to the increased surface area and synergistic effects of the mixed nanoparticles, which enable more efficient heat transfer between the fluid and the absorber surface. This section reviews critical studies on the application of hybrid nanofluids in SAHs, solar stills, and other solar thermal systems, focusing on the performance benefits and challenges of these materials.

Several studies have demonstrated the effectiveness of hybrid nanofluids in improving SAH's performance. Abdelkader et al. (2020) studied a flat-plate SAH coated with a hybrid nanofluid containing carbon nanotubes (CNTs) and CuO nanoparticles embedded in black paint. Their results showed a 10.0% improvement in thermal efficiency compared to SAHs coated with conventional black paint. Combining CNTs and CuO enhanced the absorber surface's thermal conductivity and optical absorption, thereby improving heat retention and system performance. In another study, Rahul Kumar and Verma (2021) investigated the performance of a tube-type SAH coated with varying concentrations of a hybrid graphene/CuO nanofluid. Their findings revealed that the thermal efficiency of the SAH increased by 4.9% when 0.3% graphene/CuO was used, compared to lower concentrations. The researchers attributed the improved

performance to the large surface area of the graphene and the high thermal conductivity of CuO, which enhanced the system's ability to absorb and retain heat.

Hybrid nanofluids have also been applied in solar stills, where they have been shown to improve water productivity and thermal efficiency significantly. Alami and Aokal (2018) found that using a CuO/graphene hybrid nanofluid in solar stills improved thermal efficiency by 15.6% compared to systems coated with CuO alone. This improvement was due to the synergy between graphene's large surface area and CuO's excellent heat conductivity, which enhanced the system's overall heat absorption and retention.

The thermal efficiency of SAH coated with graphene/CuO/absorptive solution ranged from 57.0% to 68.0%. The increase in thermal performance could be attributed to the thermal properties of the absorber material, the nanocoating material, and its optical properties (Vasantha Malliga & Jeba Rajasekhar, 2017).

SAHs with 1% graphene/black paint and 1% graphene/cerium/black paint were experimentally investigated for thermal efficiency. The thermal efficiency of graphene/cerium/black paint-coated SAH was 3.4% higher than that of SAH with 1% graphene in black paint for solar radiation varying from 700.0-1250.0 W/m^2. The addition of nanofluid increased the heat absorption capacity of the absorber, which improved the solar heater's efficiency (Kumar et al., 2022).

Research by Al-Kayiem et al. (2021) further, their study demonstrated the effectiveness of hybrid nanofluids in improving the thermal efficiency of solar collectors. They compared the performance of solar collectors coated with Al_2O_3/black paint, CuO/black paint, and a hybrid Al_2O_3/CuO/black paint nanofluid. The results revealed that while Al_2O_3/black paint alone increased thermal efficiency by 51.0%, the hybrid Al_2O_3/CuO/black paint nanofluid reduced thermal conductivity slightly but improved overall performance. The study concluded that the optimal combination of nanoparticles in hybrid nanofluids can significantly enhance the performance of solar collectors. However, further research is needed to fine-tune the nanoparticle ratio for maximum efficiency. The summary of the literature studies discussed above is presented in Table 2-7.

Table 2-7 A summary of the literature studies is discussed in section 2.13

Sr No	Author and Year	Nanofluid Coating type	SAH performance (%)
24.	Abdelkader et al; 2020	**Black paint**	49.7
		CNT/CuO/black paint	59.8
25.	Rahul Kumar and Verma (2021)	**0.1% CuO/graphene/black paint**	69.4

		0.2% CuO/graphene/black paint	70.9
		0.3% CuO/graphene/black paint	73.2
		0.4% CuO/graphene/black paint	72.4
26.	Alami and Aokal (2018)	**CuO+graphene/black paint**	53.8
		Graphene/black paint	69.4
27.	Vasantha Malliga and Jeba Rajasekhar (2017)	**Graphene/CuO/absorptive solution**	57.0-68.0
28.	Kumar et al. (2022)	**Graphene/black paint**	35.5-48.4
		Graphene/CeO_2/black paint	37.5-52.3
29.	Al-Kayiem et al. (2021)	**Black paint**	44.9
		CuO/black paint	42.2
		Al_2O_3/black paint	51.0
		Al_2O_3/CuO/black paint	39.8

Section 2.13 Summary: Hybrid nanofluids, which combine multiple nanoparticles such as CNTs, CuO, and graphene, offer significant improvements in the thermal performance of solar thermal systems compared to single-component nanofluids. Studies have consistently shown that hybrid nanofluids enhance thermal conductivity, heat absorption, and retention, leading to notable efficiency gains in SAHs and solar stills. For example, combining CNTs and CuO or graphene and CuO has improved thermal efficiency by 10.0%-15.6%. However, determining the optimal nanoparticle ratio in hybrid nanofluids requires further research to maximize their potential without compromising stability and cost.

2.12 Conclusion

From the review of the above papers, it can be concluded that:

1) Under-ventilated and under-heated indoor spaces can cause health issues to occupants and be damp and moldy. With 10.0% of the world's population living in energy poverty, and studies reporting that most energy is used for heating buildings, there is a dire need to identify heating solutions that are both renewable and low-cost. Tube-type SAHs could be the potential technology for heating and ventilating low-rise buildings.
2) The air mass flow rate, temperature difference, solar radiation, and air layer thickness affected the thermal efficiency of SAH. However, the airflow rate dominated the thermal efficiency of SAH. The slower the air moved through the SAH, the more heat it could absorb. The optimum mass flow rate must be investigated in relation to the climatic conditions and thermal efficiency techniques used.

3) The study showed that latitude plays a vital role in determining the SAH tilt angle. The ideal tilt angle for the SAH is equal to or close to the latitude of the experimental setup location. Tilt angle plays a significant role in evaluating the SAH's thermal efficiency.
4) Artificial roughness (fins, ribs, turbulators, corrugations) increased the surface area, resulting in an improved heat transfer rate and, thus, improving the collector's thermal efficiency. However, a limitation of tube-type SAH is a significant pressure drop, which needs to be investigated.
5) Integrating thermal energy storage (TES) into SAH improved its thermal efficiency. The literature found that SAH with aluminium fibers (a porous material) has a higher thermal efficiency (90.8%) than SAH with other TES materials discussed in this study. Using materials that store energy for more extended periods improves the thermal efficiency of SAH.
6) The supercooling effect is a major issue when using SAHs with phase change materials. Supercooling is the process of cooling a liquid or gas below its freezing point without it becoming solid. The supercooling effect may not give more accurate results due to changes in the thermophysical properties of PCM,
7) The literature study revealed that SAHs with evacuated tubes integrated with heat pipes and thermal energy storage have a higher efficiency of 89.8 % compared to other evacuated tube SAHs studied in this review.
8) A transparent tube flat micro heat pipe array (FMHPA) collector achieved a maximum efficiency of 85.0%. The literature study revealed that SAH integrated with FMHPA had a lower pressure loss than other SAHs.
9) Attaching reflectors to SAHs improved their efficiency. However, this will impact the aesthetics and space required for the SAH. The weight and cost of SAH increase when reflectors are used. However, it increases solar radiation absorption by 80.0%.
10) Applying black paint and nanofluid (nanoparticles dispersed in black paint) coating improved the collector's efficiency. Highly thermal-conductive materials improved SAH efficiency. Copper has higher thermal conductivity than aluminium, but copper is expensive. Therefore, low-cost materials are needed.
11) Applying a nanofluid coating to the tubes increases the thermal efficiency of the collectors. Nanofluid is categorized into three main categories, namely, 1) metal oxide nanofluids, 2) carbon-based nanofluids, and 3) high thermal conductivity based.
12) **Metal oxide nanofluids:** These include nanoparticles like copper oxide (CuO), aluminium oxide (Al_2O_3), and titanium dioxide (TiO_2). CuO and Al_2O_3 nanofluids have

demonstrated significant increases in thermal efficiency, especially when used as coatings on absorber tubes or as working fluids. TiO_2-based coatings have also proven effective, particularly in solar still applications.

13) **Carbon based nanofluids:** Graphene and carbon nanotubes (CNTs) stand out due to their excellent thermal conductivity and large surface area, which enhance heat absorption and retention. Studies show that graphene coatings can improve efficiency by up to 11.6%, and CNTs are effective when integrated into advanced designs such as staggered fins.
14) **Hybrid nanofluids:** These combine multiple nanoparticles, such as CuO, with graphene or CNTs, offering synergistic effects that enhance thermal conductivity and optical absorption. Hybrid nanofluids have shown the potential to improve efficiency by up to 15.6%. Using graphene/CuO composites significantly improved the thermal efficiency of SAH, increasing it by 4.9% compared to graphene/black paint coatings. This improvement can be attributed to the superior optical absorption of CuO and to graphene's large surface area and thermal properties, with thermal efficiency reaching 68.0% under optimal conditions. This suggests that hybrid nanofluids, such as graphene/CuO, are highly effective at enhancing heat transfer and should be further explored for practical applications.
15) **Nanofluids application:** has emerged as a promising solution for enhancing the thermal performance of SAHs and other solar thermal systems. The unique thermal properties of nanoparticles, particularly their ability to increase heat transfer and solar radiation absorption, make them valuable for improving the efficiency of these systems. Analysis of various nanofluids shows that metal oxide-, carbon-, and hybrid-based nanofluids offer significant improvements.
16) Silver (Ag) nanoparticles exhibit the highest thermal efficiency among the nanofluids reviewed due to their superior thermal conductivity. However, their high cost limits their practical applications. Graphene-based nanofluids also perform exceptionally well, with efficiency improvements ranging from 9.6% to 11.6%, making them a strong candidate for future solar thermal applications. Copper oxide (CuO) nanofluids, while slightly less efficient than silver and graphene, provide an excellent balance of performance and cost-effectiveness, making them widely used in practical applications.

However, despite the promising results, artificial roughness and nanofluids have some limitations. The development of more stable formulations, coupled with rigorous environmental and economic assessments, is necessary for the widespread adoption of these technologies.

Further real-world testing is essential to confirm the long-term performance and durability of nanofluid-based solar thermal systems.

2.13 Limitations and future scope

1) Extensive research is required to optimize the different artificial roughness geometries for tube type SAH, roughness material, and orientation to improve thermal efficiency and reduce pressure drop.
2) There is scope to explore low-cost, lightweight thermal energy storage materials that are eco-friendly and will boost the thermal efficiency of SAH.
3) The supercooling effect on the thermal efficiency of SAH must be investigated when using phase change materials.
4) Applying black paint and a nanofluid (nanoparticles dispersed in black paint) coating improved the collector's efficiency. However, the literature shows limited research on SAHs with nanofluid coatings, warranting further investigation. Different concentrations of nanoparticles mixed into black paint, along with hybrid nanofluid technology, should be investigated.
5) All the techniques used to improve the thermal efficiency of SAH require extended research under a range of ambient conditions.
6) Evaluating the thermo-economic benefits and the life cycle analysis of SAHs is important.
7) The thermal efficiency of the proposed SAH needs to be investigated.
8) One of the primary limitations of nanofluids is their stability over time. Nanoparticles tend to agglomerate or settle in the base fluid, reducing heat transfer efficiency. Although surfactants have been used to enhance nanoparticle dispersion, they can alter nanofluid properties and may not provide a long-term solution. Stability remains a concern, particularly for applications that require extended operation periods, such as SAHs.
9) The high cost of nanoparticles, especially those made from precious metals such as silver (Ag) and gold (Au), limits the economic feasibility of nanofluid-based solar thermal systems. These costs hinder scalability for widespread use in regions with stringent budget constraints. At the same time, hybrid nanofluids offer better performance but often involve multiple expensive materials, increasing costs. Future research should aim to lower the production costs of nanofluids, especially by identifying cheaper but effective nanoparticles. Developing hybrid nanofluids with

optimized nanoparticle ratios could also provide cost-effective solutions without compromising performance. Moreover, exploring more affordable materials, such as copper (Cu) and carbon-based nanoparticles, could reduce costs while maintaining efficiency.

10) The potential environmental and health impacts of nanofluids, particularly metallic nanoparticles, have not been thoroughly explored. Nanoparticles can pose significant risks to ecosystems and human health if not properly managed, especially when released into the environment through spills or improper disposal. Addressing these concerns will require further research into eco-friendly, biodegradable alternatives.
11) Standardized theoretical models are lacking to predict the behaviour of nanofluids in varying operating conditions. The current models do not fully capture the effects of particle size, concentration, and temperature variations, limiting the ability to optimize system designs effectively. It will be essential to develop standardized, accurate theoretical models that predict nanofluid behaviour under various operating conditions. Such models would enable more precise optimization of solar thermal systems, ensuring that nanofluids can be effectively utilized across diverse environmental settings.
12) The long-term durability of nanofluid coatings has not been extensively studied. UV exposure, temperature fluctuations, and weather conditions can degrade the coatings over time, reducing their effectiveness. Most studies have been conducted under controlled laboratory conditions, and real-world testing is needed to evaluate their practical durability.
13) Extensive long-term testing of nanofluids and nano-coatings under real-world conditions is needed. Such testing would provide insights into the long-term stability and performance of nanofluid-based solar thermal systems across different climatic regions. Additionally, studies should focus on the effects of environmental variables, such as humidity, wind speed, and seasonal changes, on system performance.
14) Hybrid nanofluids have shown great promise in enhancing the efficiency of solar thermal systems. Future studies should explore optimal combinations of nanoparticles to achieve the best balance between performance, cost, and stability. By optimizing nanoparticle ratios, hybrid nanofluids can achieve higher performance with reduced material costs and improved system stability.

2.14 Proposed design: nanocoated corrugated tubes with finned inserts

Building on these advancements, this chapter introduces a new tube-type SAH design that integrates multiple efficiency-enhancing technologies. The proposed design consists of corrugated absorber tubes combined with corrugated fin inserts coated with nanofluids. The tubes are coated with varying concentrations of copper oxide and aluminium oxide nanoparticles mixed into black paint to maximize solar absorption and heat transfer.

The design, depicted in Figure 2.23, represents a novel approach to improving SAH efficiency. The tube's corrugated structure and fin inserts are expected to enhance heat transfer by increasing surface area and inducing turbulence within the airflow. This innovative geometry and material combination will be studied and experimentally tested in future research.

Figure 2-23 Picture of proposed SAH

The proposed tube design, as discussed in Section 2.16, was integrated into SAH and tested at the Massey University, Wellington campus carpark. However, the finned tubes were not nanocoated due to SOJOL Pvt Ltd.'s availability of only one SAH. Therefore, the effect of adding fins and without fins on the thermal performance of SAH is discussed in

Chapters 3 and 4.

Chapter 3 presents the experimental test setup, results, and key findings of the finned tube SAH integrated with corrugated fin inserts.

3 Experimental performance of a tube-type solar air heater with corrugated fin inserts in New Zealand

This study evaluates the thermal efficiency of a commercially designed finned tube-type solar air heater (FT-SAH). This FT-SAH comprises a glass cover, finned tubes with corrugated fin inserts (absorber), insulation, a back plate, and an aluminium frame. The incoming air, known as inlet air, undergoes heating while traversing the finned tubes fitted with corrugated fin inserts. These fins augment the surface area, enhancing heat transfer efficiency. Subsequently, the heated air is extracted through the exit using a variable-speed fan. Throughout the experiment, the fan speed regulator was set to 100% (Case Study 1, corresponding to 0.051–0.062 kg/s) and 50% (Case Study 2, corresponding to 0.022–0.024 kg/s) of the ventilator's maximum speed. The test was conducted at Massey University's Wellington campus from June 2023 to November 2023 under various weather conditions and at different fan speeds. The study determined that the FT-type SAH exhibited a range of thermal efficiencies, namely 31.6 ± 13.8% - 83.3 ± 3.4% and 30.8 ± 6.7% - 34.6 ± 3.6%, at mass flow rates of 0.051 - 0.062 kg/s and 0.022 - 0.025 kg/s, respectively. The research revealed that the thermal efficiency of FT-SAH was primarily determined by the ratio of the temperature differential (between the outlet and inlet air temperatures) to the solar radiation received on a tilted surface. The maximum hourly average ventilation rate was 176.1 m³/h at an air mass flow rate of 0.056 kg/s, while the minimum rate was 69.0 m³/h at an air mass flow rate of 0.020 kg/s. Across the test period, the outlet air temperature exceeded 18.0 ˚C for 95.8% of the time, indicating that the system consistently maintained the minimum thermal comfort threshold recommended for classrooms.

Introduction

Solar energy can be converted to thermal energy using SAHs. Nonetheless, significant heat loss occurs through various components of SAHs, resulting in low average thermal efficiency (ranging from 38% to 45%), and they are limited to low-temperature applications like space heating, preheating, and crop drying (Ansari & Bazargan, 2018; Bezbaruah et al., 2020). The application of artificial roughness (Saxena et al., 2023), integrating solar thermal energy systems (Tyagi et al., 2012), application of nanofluid coatings (Kumar et al., 2020), reflectors (Abdullah, Amro, et al., 2020) inside the SAHs, using evacuated tubes (Abi Mathew & Thangavel, 2021), and micro heat pipe array systems (Zhu & Zhang, 2021) are techniques investigated to improve the thermal efficiency of SAHs. For example, it was found that applying artificial roughness increased the surface area available for heat transfer from the absorber to the airflow. Increased surface area results in higher heat transfer and converts the laminar

sublayer to turbulent airflow, thereby increasing the SAH thermal efficiency (Pardeshi et al., 2024).

The artificial roughness geometries consist of fins (Foued Chabane, Noureddine Moummi, et al., 2014), ribs (Ansari & Bazargan, 2018), baffles (Khanlari et al., 2022), obstacles (Akpinar & Kocyigit, 2010), dimples on the interior surface of tubes (Saini & Verma, 2008), tapes within the tubes (Souayeh et al., 2021), corrugation (Bhattacharyya et al., 2020), wire mesh (Sozen et al., 2020), and turbulators (Afshari et al., 2020). Figure 3.1 shows the thermal efficiency of different SAHs incorporating artificial roughness.

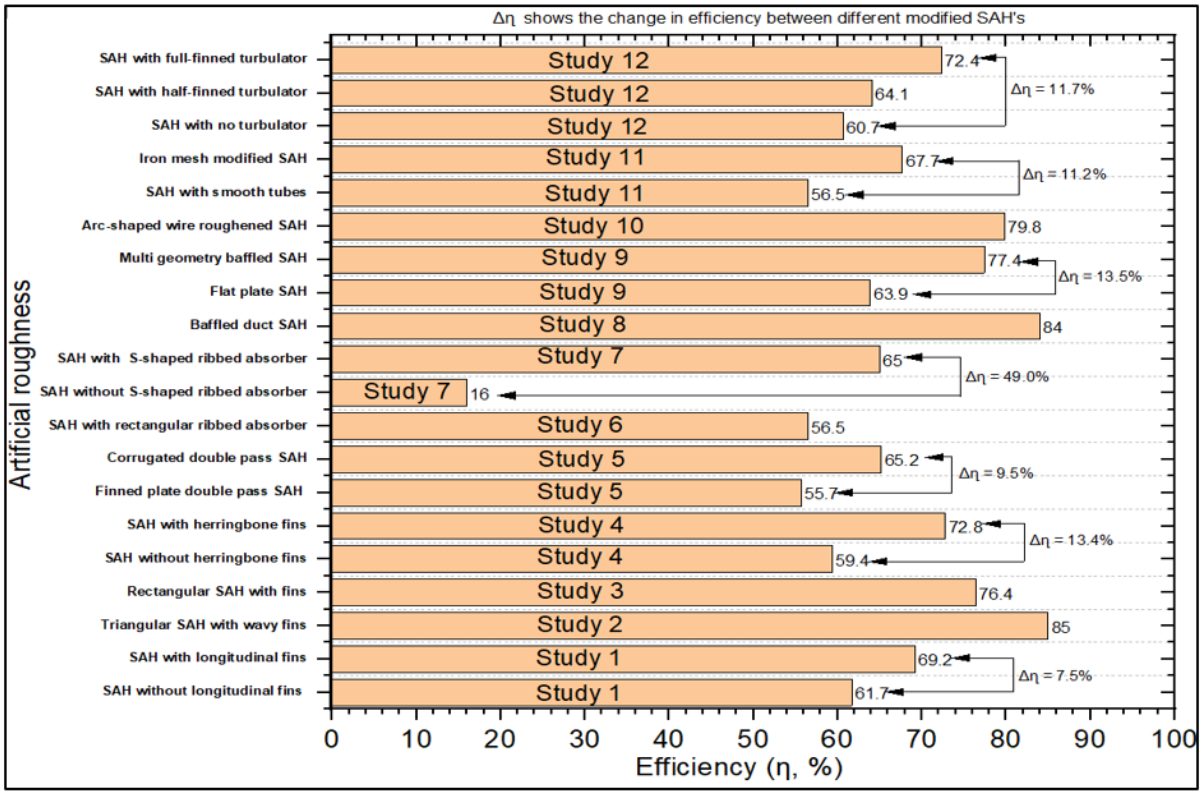

Figure 3-1 A study conducted by various researchers on the thermal efficiency of SAHs

(Figure 3-1, Study 1), shows that SAH equipped with fins demonstrated a 7.5% increase in efficiency compared to SAH without fins (Fan et al., 2019). (Figure 3-1, Study 2) reveals that incorporating wavy fins into the triangular duct increased the efficiency to 85.0% (CJ Thomas Renald et al., 2022). (Figure 3-1, Study 3) showed that the thermal efficiency of rectangular SAH with a wavy fin was 76.4% (Priyam & Chand, 2016). Studies 2 and 3 noted that the thermal efficiency of the triangular duct SAH incorporated with wavy fins was 8.5% higher than that of the rectangular duct SAH incorporated with wavy fins. Thus, studies 2 and 3 concluded that the SAH duct shape and application of fins affected the thermal efficiency of SAH.

Furthermore, Figure 3-1 (Study 4) suggests that using herringbone corrugated fins at the bottom of the absorber plate resulted in a 13.4% increase in efficiency compared to SAH without fins (Kumar & Chand, 2017). (Figure 3-1, Study 5) demonstrates that employing a corrugated plate in double-pass SAH improved the thermal efficiency of SAH by 9.0% - 11.9% compared to double-pass SAH with a finned plate (El-Sebaii et al., 2011a). Another design feature that increased the thermal efficiency was the rectangular rib roughness on the black-coated absorber plate, integrated with copper-chrome pipes (Figure 3-1, Study 6). The maximum thermal efficiency was found to be 56.5% (Komolafe et al., 2019). (Figure 3-1, Study 7) demonstrated that the S-shaped ribbed SAH exhibited a higher efficiency, ranging from 13.0% to 48.0% when compared to the flat plate SAH across various conditions (Wang, 2020).

(Figure 3-1, Study 8) revealed that the baffled duct SAH achieved a thermal efficiency of approximately 84%. This was 22.0%—33.0% greater than the smooth duct SAH (Maheshwari et al., 2012). Figure 3-1, Study 9, shows that the thermal efficiency of the multi-geometry baffled SAH increased by 13.5% compared to the flat SAH, as the air mass flow rate progressively increased from 0.04 to 0.07 kg/s (Rajendran et al., 2022).

(Figure 3-1, Study 10) observed that the highest recorded thermal efficiency of arc-shaped wire roughened SAH amounted to 79.8% (Sahu & Prasad, 2017). Additionally, (Figure 3-1, Study 11) demonstrated that incorporating an iron mesh into a hollow tube augmented the thermal efficiency of the collector by 11.2% (Sozen et al., 2020). Furthermore, (Figure 3.1, Study 12) revealed that the inclusion of a turbulator, a mechanism that alters a smooth flow into a turbulent one, amplified the thermal efficiency from 60.7% (without a turbulator) to 64.1% (with a half-finned turbulator), ultimately reaching a maximum of 72.4% with a full-finned turbulator (Afshari et al., 2020)

Studies 1-12 demonstrate that incorporating artificial roughness into SAHs improves thermal efficiency. Figure 3.1 shows that incorporating wavy fins into the collector had a higher efficiency than other roughness, followed by baffled duct collectors. It was also found that adding fins to the collector increased the thermal mass (Mostafavi, 2022). Thermal mass is the ability of a material to absorb, store, and release heat (Reardon et al., 2020). Studies have shown that fins or corrugated surfaces increase the heat transfer surface area and turbulence within the channel. It is one of the most effective ways to enhance convective heat transfer (Goldstein & Sparrow, 1977; Goldstein & Sparrow, 1976; Ho et al., 2021).

Previous studies have demonstrated that introducing artificial roughness into SAHs is an effective technique for enhancing thermal efficiency. However, to date, no research has evaluated an SAH design that combines finned tube absorbers with inserted corrugated fins. To

address this gap, the present study investigates the thermal efficiency and ventilation performance of a commercially developed finned-tube solar air heater (FT-SAH) incorporating corrugated fin elements. In addition to assessing current performance, this paper identifies opportunities for future research to further optimize tube-type SAH systems. The findings indicate that FT-SAHs have strong potential for space heating applications, with classroom integration a promising area for future exploration. The following section presents results from the experimental testing of the FT-SAH conducted at Massey University, Wellington, New Zealand

3.1 Materials and Methods

3.1.1 Structure of the tested finned tube-type solar air heater (FT-SAH)

Sojol Pvt Ltd (NZ) developed the FT-SAH prototype. The studied FT-SAHs have lengths and widths of 2103.0 mm and 985.8 mm, respectively. The collector height at the lower end was 211.6 mm, and the upper end was 333.8 mm, as shown in Figure 3-2.

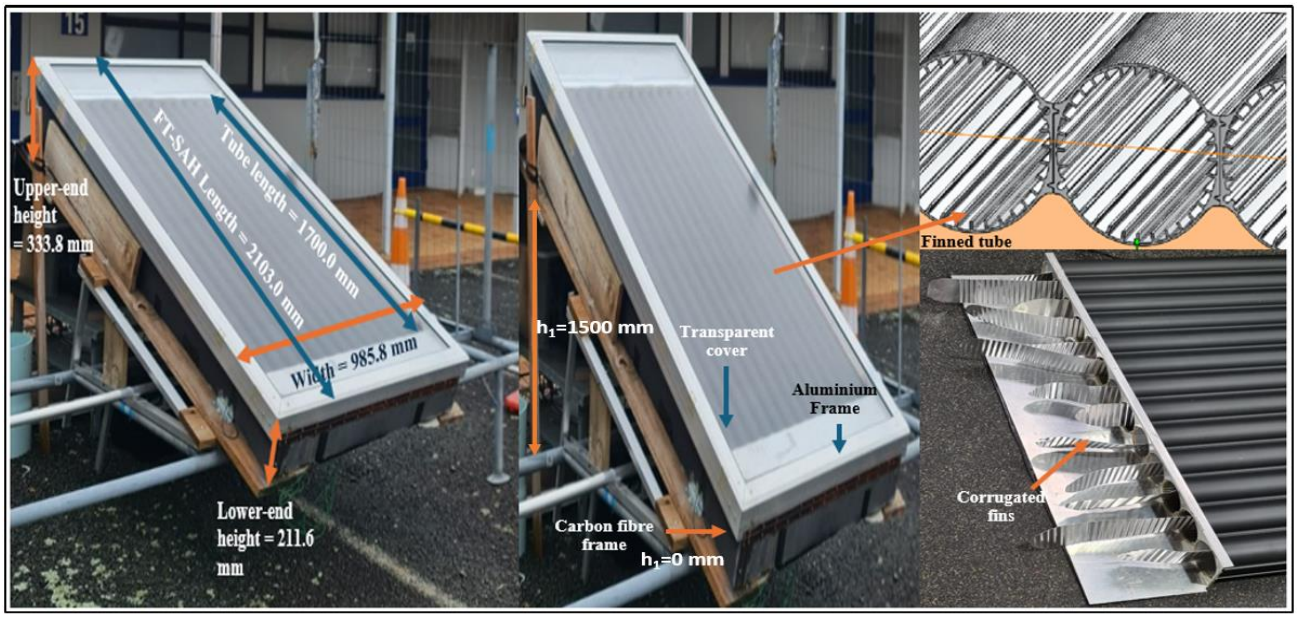

Figure 3-2 . An experimental set of FT-SAH

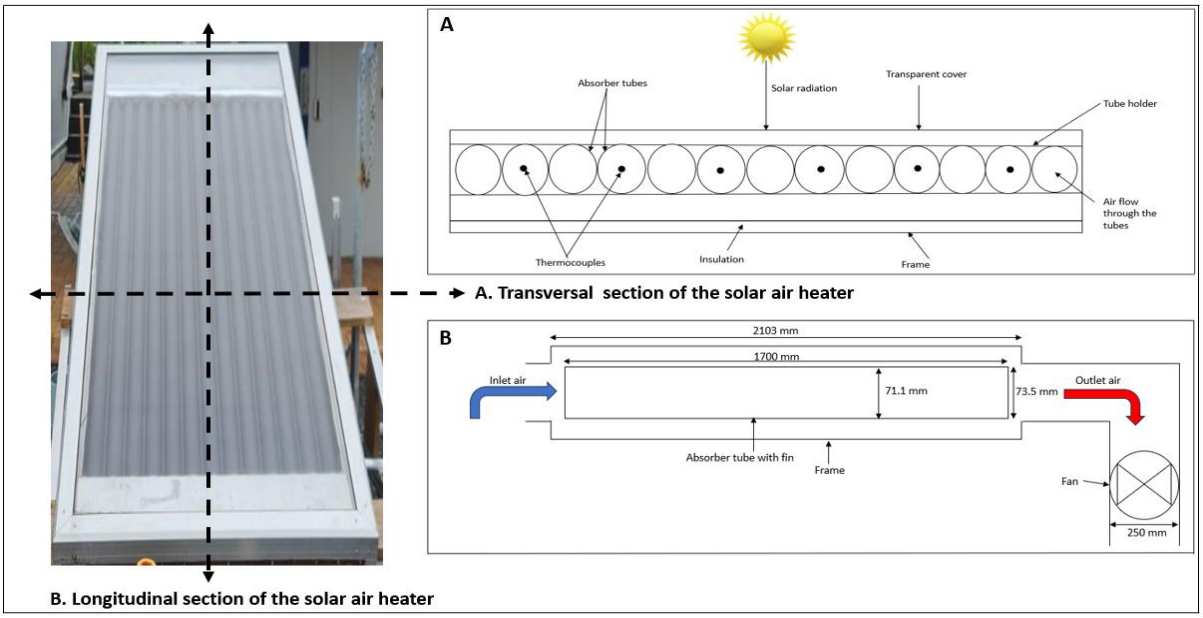

Figure 3-3 Schematic diagram of FT-SAH (A. transversal section) and air circulation through the absorber tube (B. longitudinal section)

The slope was provided for optimizing the angle for solar exposure. To reduce heat losses through the collector frame, the sides and bottom part were insulated with 50.0 mm thick glass wool (thermal conductivity = 0.0343 W/mK, R-value = 1.46 m^2K/W). The FT-SAH frame was made of carbon fiber and aluminium. The FT-SAH top side is covered with a transparent 4.0 mm-thick cover (tempered glass). The height between the underside of the glass and the top of the finned tubes (absorber) was 24.7 mm. FT-SAH consisted of thirteen finned tubes with inner and outer diameters of 71.1 mm and 73.5 mm, respectively, and a length of 1700.0 mm (Figure 3-3). There were thirty fins along the tube's inner periphery; each fin was 2.5 mm high. Figure 3-2 shows that corrugated aluminium ribbons (1700.0 mm x 56.0 mm) were inserted into the finned tubes to increase the heat transfer surface area further. There is a rubber thermal break between the tubes and the frame. A black rubber seal around the aluminium frame is provided to increase the airtightness of the collector.

The solar radiations fall on the collector cover and is then transferred to the interior of the tube by convection/conduction. The energy is transferred to the air flowing through the pipe by forced convection. The air at the outlet was drawn using a 250W variable-speed fan (AM 250, Brespalin, China). The fan can be set at 100% and 50% maximum speed, corresponding to a mass flow rate of 0.056 ± 0.002 kg/s and 0.024 ± 0.001 kg/s, respectively. The schematic diagram of the FT-SAH (transversal section) and the air circulation through the absorber tubes (longitudinal section) are shown in Figure 3.

3.1.2 Experimental setup and test procedure

The FT-SAH thermal efficiency was tested at Massey University's Wellington campus, New Zealand (41.3016° S, 174.7761° E), at 50% and 100% of the ventilator's maximum speed. The FT-SAH was mounted on a custom-made metal frame at a 20° tilt angle. The panel faced true north (at an azimuth angle of 0 °). K-type thermocouples were placed at the inlet and outlet of the alternate tube (6 tubes) to measure the temperature change between the outlet and inlet air temperatures. Figure 3.2 shows the location of the six tubes where the 12 K-type thermocouples were installed. Two data-loggers (TC08, USB, Pico Technology, UK) with eight channels each (16 channels total) were connected to a laptop to process the temperature data. A weather station (WS3085, Wi-Fi weather station, Aercus Instruments, UK) was mounted on the frame to monitor solar irradiance (W/m²), ambient air temperature (°C), and wind speed (m/s). The velocity (m/s) and the temperature of the outlet air (°C) were measured by a hot wire anemometer (AM4214SD, Lutron Electronic Enterprise Co. Ltd., Taipei City, Taiwan). The anemometer was located at the exit of the duct. All the equipment was factory-calibrated and tested both before and after the experiment (as part of the pre- and post-fieldwork colocation process for quality assurance). The characteristics of the equipment used for the experiment are given in Table 3-1.

Table 3-1 The characteristics of the monitoring equipment

Equipment	**Monitoring Parameters**	**Range**	**Accuracy**	**Precision of measurements**
Weather station	Ambient air temperature (°C)	-40.0 °C – 60.0 °C	± 1.0°C	0.1 °C
	Solar radiation (W/m^2)	0–3000.0 W/m^2	± 15.0%	1.0 W/m^2
	Wind speed (m/s)	0 – 50.0 m/s	± 1.0 m/s (speed < 5.0 m/s) ± 10.0% (speed ≥ 5.0 m/s)	0.01 m/s

K type thermocouple	Inlet and Outlet air temperature (° C)	-40.0 ℃+1100.0 ℃	± 1.5℃	0.1 ℃
Hot wire anemometer	Outlet air velocity (m/s)	0.2–25.0 m/s	±5.0% of reading	0.01 m/s
	Minimum air temperature from the duct (° C)	0-50.0 ℃	± 0.8 ℃	0.1 ℃

Experimental data were collected from 9:00 a.m. to 4:00 p.m. NZDT, aligning with New Zealand school timings (9:00 a.m. to 3:00 p.m.), thereby ensuring the testing period was relevant for potential classroom ventilation and heating applications.

Two operational cases were defined for evaluation:

- Case Study 1: Days 1–12 with the fan set at 100% speed during the winter season
- Case Study 2: Days 13–24 with the fan set at 50% speed during the spring season

Winter and Spring seasons were selected due to the practical need for heating and ventilation in buildings during the colder months. Early summer was excluded due to reduced heating demand, and late autumn was avoided due to its transitional, unpredictable weather. A total of 12 test days were selected for each season (winter and spring) to provide realistic weather conditions that reflect the diverse environmental conditions common to each season. The test days included both clear and overcast days, rather than being randomly selected. This method enabled a controlled evaluation of FT-SAH performance across two seasonal climates, with fan speed fixed at 100% (Case Study 1) and 50% (Case Study 2), effectively isolating the influence of fan speed. While the simultaneous variation of seasonal conditions and fan speed limits the ability to isolate the exact effect of airflow rate, the chosen design prioritizes assessing FT-SAH performance under practical, variable environmental conditions.

Environmental conditions (solar irradiance, wind speed, rainfall, and cloud cover), along with ambient and outlet air temperatures and air velocity, were monitored at one-minute intervals using calibrated sensors positioned around the FT-SAH prototype. This sampling frequency is consistent with standard practice in SAH research. It satisfies the Shannon–Nyquist criterion, as variations in solar irradiance, temperature, and airflow occur at much slower timescales than

one minute. To reduce the influence of transient fluctuations caused by sudden changes in cloud cover, wind gusts, or sensor variability, the one-minute data were averaged over one-hour intervals. This approach aligns with standard procedures in solar thermal analysis, ensuring that the results reflect stable, representative performance values rather than short-term fluctuations. Acknowledging that nature is inherently noisy, this study does not assume perfectly smooth behaviour in the system. Instead, the averaging process was applied to highlight overall performance trends across daily and seasonal conditions. To ensure that data variability was still captured, standard deviation analysis was conducted, and results are reported alongside mean values where appropriate. This combination of one-minute sampling, hourly averaging, and statistical evaluation provided both sufficient resolutions to capture system behaviour and comparability with other studies in the field. Due to the space and financial constraints, only one FT-SAH prototype was available. Therefore, both phases were performed progressively with the same setup to maintain consistency across test conditions. A high fan speed was used in winter to enhance airflow under colder conditions. In contrast, a low fan speed was employed in spring to simulate moderate ventilation needs, addressing seasonal ventilation demands. This approach enabled assessment of both environmental and operational influences on FT-SAH performance.

3.1.3 Methodological justification and research philosophy

The methods selected in this study were directly aligned with the thesis objectives of evaluating the thermal efficiency and ventilation capacity of the FT-SAH under classroom-relevant conditions. Data collection was conducted during school hours to ensure that results could be meaningfully applied to New Zealand classrooms. Seasonal selection (winter and spring) reflected periods of practical heating and ventilation demand, and the use of fixed fan speeds in each case study provided a structured way to evaluate the influence of airflow. While this design did not fully isolate seasonal and operational effects, it allowed the system to be assessed under realistic, variable environmental conditions—consistent with the applied nature of the research. The philosophical foundation of this research is pragmatic, emphasizing problem-driven inquiry and real-world applicability. Rather than relying solely on computational fluid dynamics (CFD) or theoretical modelling, an experimental approach was chosen to generate empirical evidence of FT-SAH performance in actual weather conditions. This pragmatic orientation ensured that the findings would be not only scientifically valid but also directly relevant to the practical aim of improving thermal comfort and ventilation in New Zealand classrooms.

3.1.4 Thermal efficiency calculation

The thermal efficiency (η) of the FT-SAH was calculated using Equation 3.1 (John & Beckman, 2013).

$$\eta = \frac{\dot{m}Cp(T_o - T_i)}{I_T A_c} \quad (3.1)$$

With:

$\dot{m} = \rho v A_d$

$A_c = n.\pi.\ D.L$

$T_a = T_i$

Where,

A_c	SAH effective area, (m^2)
Ad	Outlet duct cross-section area, (m^2)
C_P	Specific heat capacity of air, [J/(kg. K)]
I_T	Solar radiation on the tilted SAH surface (W/m^2)
ΔT	Difference between outlet and air temperatures, (K)
Ta	Ambient temperature, (K)
T_i	Inlet air temperature, (K)
T_o	Outlet air temperature, (K)
$\dot{m}$	Air mass flow rate, (kg/s)
η	Efficiency, (%)
ρ	Density of air, (kg/m^3)
v	Air velocity, (m/s)
π	Pi = 3.14
n	Number of tubes
D	Outer tube diameter, (m)
L	Length of the tube, (m)

The inlet temperature (T_i) was assumed to be equal to the ambient air temperature (T_a). The monitored air velocity (v) was assumed to be the mean air velocity across the tube section (D). The specific heat capacity (C_p) was equal to 1007 J/kg. K in the studied temperature range (283.15 K to 343.15K). The effective collector area (A_c) was constant, equalling 4.938 m^2.

Equation 1 demonstrates that the thermal efficiency (η) of the FT-SAH is a function of the air mass flow rate ($\dot{m}$), the temperature difference between outlet and inlet air (T_o-T_i), and the incident solar irradiance on the FT-SAH tilted surface (I_T), which can be written as follows : $\eta_{th} = f(\dot{m}, \Delta T, I_T)$.

The air density (ρ) and dynamic viscosity of air (μ) vary with temperature, and their values at various temperature ranges are given in Table 3-2.

Table 3-2 Air density at different air temperatures (Cengel, 2011)

Air temperature (K)	Air density (kg/m^3)	Air dynamic viscosity $x10^{-5}$ (kg/m*s)
[283.15, 293.15]	1.225	1.797
[293.15, 303.15]	1.184	1.844
[303.15, 313.15]	1.145	1.892
[313.15, 323.15]	1.109	1.938
[323.15, 333.15]	1.076	1.984
[333.15, 343.15]	1.044	2.029

3.1.5 Effective efficiency calculation

Equation 3.2 is used to calculate the effective efficiency of the SAH . (Cortes & Piacentini, 1990; Mittal & Varshney, 2006).

$$m_{\eta_{eff}} = \frac{Q_u - \frac{P_m}{C}}{I_T A_C} \quad \textbf{(3.2)}$$

Where,

$m_{\eta eff}$	Effective efficiency of the SAH (%)
Q_u	Useful thermal energy gained by SAH (W)
P_m	Mechanical power is required to force the air through the SAH
C	The conversion factor = 0.18
I_T	Solar radiation on the tilted SAH surface (W/m^2)
A_c	SAH effective area = 4.938 m^2

Required mechanical power (P_m) can be calculated from Equation 3.3 (Hussien & Farhan, 2019).

$$P_m = \frac{\dot{m}\Delta P}{\rho} \quad \textbf{(3.3)}$$

Where,

ΔP	Pressure drops across the SAH, Pa
ṁ	The mass flow rate of air, kg/s
ρ	Density, kg/m^3

Bernoulli's principle is applied to estimate the pressure drop across the SAH (Dubey, 2014). Assuming a uniform flow and negligible losses, the pressure drop (ΔP) across the SAH can be calculated using Equation 3.4.

$$\Delta P = \rho g(h_2 - h_1) \quad \textbf{(3.4)}$$

Where,

h_1 - Height of SAH (at lower end side) from the base of the metal frame, h_1 = 0m (Figure 2)

h_2 - Height of SAH (at upper-end side) from the base of the metal frame, h_2 = 1.5m (Figure 2)

g - Acceleration due to gravity, 9.81 m/s^2

3.1.6 Uncertainty analysis

In this study, the fractional uncertainty of SAH's thermal efficiency is estimated using equation 3.5 (Abdelkader et al., 2020). The errors in the measurements and the monitoring devices have been analyzed. The inlet and outlet air temperatures, solar radiation, and air velocity are independent measurements. The specific heat of air and air density are considered constants. The equipment used, and its accuracy, are given in Table 3.1.

$$\frac{\omega_\eta}{\eta} = \sqrt{\left(\frac{\omega_{\dot{m}}}{\dot{m}}\right)^2 + \left(\frac{\omega_{I_T}}{I_T}\right)^2 + \frac{\omega_{\Delta T}}{T_o - T_i}} \quad \textbf{(3.5)}$$

Results show the mean values for I_T, $\dot{m}$, ΔT, To, Ti, and η to be 340.9 W/m^2, 0.04 kg/s, 21.4 $^\circ$C, 36.0 $^\circ$C, 14.6 $^\circ$C, and 51.1%, respectively. The fractional uncertainty in the efficiency is 7.8%. This study focuses on experimental test results, and all analyses were conducted using OriginPro software.

3.2 Results and discussion

3.2.1 Wellington weather conditions

Wellington has a temperate maritime climate. Strong winds (31.0 km/h) frequently occur in Wellington due to its proximity to the Cook Strait and its partly cloudy year-round weather. Wellington has 110 wet Days. The southwestern part of Wellington receives 2100 hours of bright sunshine. Cloud cover increases as one approaches the Tararua and Rimutaka Ranges. The bright sunshine hours are less than 1750 hours in the Tararua Ranges. The complex geography of Wellington leads to notable fluctuations in the allocation of solar radiation, airflow characteristics, and cloud coverage (Chappell, 2014). Therefore, it is essential to investigate the thermal performance of the designed FT-SAH under various weather conditions in Wellington, as these conditions are highly variable. The test was conducted from June 2023 to November 2023, during the winter and spring seasons in New Zealand.

The two key parameters that affect the thermal efficiency of FT-SAH and the outlet air temperature are solar radiation and ambient temperature. A study conducted on glazed (transparent glass cover) and unglazed (plastic cover) solar collectors showed that wind speed did not affect the performance of the glazed collector (Burch & Casey, 2009). A similar study

by (Paya-Marin et al., 2015) showed wind speed in the range of 0.3 m/s to 4.0 m/s did not affect the temperature difference between the outlet and inlet air temperature. In this study, the effect of wind and rain on the FT-SAH's temperature difference between the outlet and inlet air temperatures was insignificant. It was therefore not included in the detailed analysis. It would be interesting to expose the FT-SAH to extreme weather conditions and to estimate its thermal performance and temperature differences in future experimental studies.

3.2.2 Ambient temperature, solar radiation, wind speed, and rainfall

The weather data, outlet air temperature, and air velocity were recorded at 1-minute intervals. Case Study 1 was conducted from June 2023 to August 2023 (winter season). Case Study 2 was conducted from September 2023 to November 2023 (spring season). It was noted that the ambient temperature and solar radiation were 1.5 °C to 2.5 °C and 75.4 W/m^2 to 204.6 W/m^2, respectively, lower in winter than in spring. To represent variability in system performance, minimum and maximum values are reported alongside averages. Full distribution plots are not presented because the short-term data contain significant noise from rapid fluctuations in weather conditions (cloud cover, wind, rainfall). Including minimum–maximum values provides a concise yet representative indication of performance variation without obscuring the overall trends.

Case study 1: Fan set at 100% maximum speed of the ventilator

FT-SAH was operated at **100% maximum fan speed** over 12 days. The daily average ambient temperature ranged from 9.9 °C (minimum) to 16.7 °C (maximum), with a mean ± SD of 13.5 ± 2.3 °C. The daily average solar radiation on the tilted SAH surface ranged from 142.9 W/m^2 (minimum) to 476.2 W/m^2 (maximum) with a mean ± SD of 255 ± 120.2 W/m^2. The daily average wind speed ranged from 0.1 m/s (minimum) to 3.2 m/s (maximum) with a mean ± SD of 1.5 ± 1.0 m/s.

The hourly ambient temperature ranged from 6.1°C (minimum, Day 6) to 18.6 °C (maximum, Day 12). The hourly solar radiation on the tilted SAH surface ranged from 73.5 W/m^2 (minimum, Day 6) to 567.2 W/m^2 (maximum, Day 12). The hourly wind speed ranged from 0.1 m/s (minimum, Days 3 and 4) to 3.6 m/s (maximum, Day 10). Rainfall was observed on Days 4, 5, 6, 10, and 11.

Case study 2: Fan set at 50% maximum speed of the ventilator

FT-SAH was operated at 50% of the maximum ventilator speed for 12 days. The daily average ambient temperature ranged from 12.5 °C (minimum) to 18.8 °C (maximum) with a mean ± SD of 15.8 ± 2.2 °C. The daily average solar radiation on the tilted SAH surface ranged from 204.5

W/m^2 (minimum) to 648.4 W/m^2 (maximum) with a mean ± SD of 388.4 ± 148.9 W/m^2. The daily average wind speed ranged from 0.4 m/s (minimum) to 4.8 m/s (maximum) with a mean ± SD of 2.3 ± 1.2 m/s.

The hourly ambient temperature ranged from 8.6 °C (minimum, Day 1) to 20.1 °C (maximum, Day 4). The hourly solar radiation on the tilted SAH surface ranged from 147.9 W/m^2 (minimum, Day 1) to 771.8 W/m^2 (maximum, Day 4). The hourly wind speed ranged from 0.5 m/s (minimum, Day 24) to 5.7 m/s (maximum, Day 17). Rainfall was observed on Days 14, 15, 18, 19, 22, and 23. The mean ± SD values of ambient temperature, wind speed, and rainfall on each test day are given in Table 3-3.

Table 3-3 The daily average ± SD values of ambient temperature (T_a), wind speed, and rainfall on each test day

Maximum speed of the ventilator	Test Day	Ambient temperature (°C)	Minimum ambient temperature (°C)	Maximum ambient temperature (°C)	Wind speed (m/s)	Minimum Wind speed (m/s)	Maximum Wind speed (m/s)	Rainfall (mm)	Minimum rainfall (mm)	Maximum rainfall (mm)
Case study 1	Day 1	12.8 ± 0.9	11.3	13.9	1.2 ± 0.4	0.5	1.6	0.0 ± 0.0	0	0
	Day 2	11.4 ± 2.3	8.0	13.8	1.2 ± 0.4	0.5	1.6	0.0 ± 0.0	0	0
	Day 3	14.2 ± 2.0	11.3	17.0	0.2 ± 0.1	0.1	0.3	0.0 ± 0.0	0	0
	Day 4	15.0 ± 3.0	10.5	18.2	0.4 ± 0.2	0.1	0.7	0.5 ± 0.1	0.09	0.19
	Day 5	12.6 ± 1.1	11.0	14.1	1.3 ± 0.3	0.8	1.7	0.3 ± 0.5	0.4	1.4
	Day 6	9.9 ± 1.9	6.1	11.1	1.8 ± 0.4	1.2	2.5	0.5 ± 0.6	0.04	1.4
	Day 7	12.3 ± 0.8	10.8	13.1	1.8 ± 0.3	1.2	1.9	0.0 ± 0.0	0	0
	Day 8	12.6 ± 0.4	11.9	13.0	2.3 ± 0.4	1.5	2.7	0.0 ± 0.0	0	0
	Day 9	11.8 ± 0.3	11.5	12.3	2.9 ± 0.4	2.0	3.2	0.0 ± 0.0	0	0
	Day 10	15.7 ± 1.2	13.9	17.4	3.0 ± 0.4	2.6	3.6	0.1 ± 0.2	0.06	0.46
	Day 11	16.7 ± 1.2	15.0	18.1	2.0 ± 0.5	1.3	2.5	0.1 ± 0.2	0.06	0.46
	Day 12	16.7 ± 2.2	12.6	18.6	0.7 ± 0.1	0.6	0.9	0.0 ± 0.0	0	0
	Day 13	12.5 ± 2.4	8.2	15.2	0.6 ± 0.4	0.1	1.3	0.0 ± 0.0	0	0
	Day 14	12.7 ± 1.3	10.5	13.9	3.1 ± 0.3	2.7	3.5	0.1 ± 0.3	0	0.7
	Day 15	15.0 ± 0.4	14.2	15.4	2.8 ± 0.4	2.2	3.2	0.1 ± 0.1	0	0.4
	Day 16	17.8 ± 1.6	15.1	20.1	2.3 ± 0.1	2.1	2.4	0.0 ± 0.0	0	0

Case study 2	Day 17	16.7 ± 0.8	15.6	17.5	4.9 ± 0.6	4.1	5.7	0.0 ± 0.0	0	0
	Day 18	13.6 ± 2.7	8.4	15.5	1.7 ± 0.2	1.4	2.2	0.2 ± 0.4	0	1.2
	Day 19	16.3 ± 1.0	14.2	17.1	3.6 ± 0.2	3.2	3.8	0.1 ± 0.3	0	0.9
	Day 20	18.7 ± 1.0	17.0	19.8	2.1 ± 0.6	1.0	2.6	0.0 ± 0.0	0	0
	Day 21	17.9 ± 0.5	16.9	18.5	2.6 ± 0.4	2.1	3.0	0.0 ± 0.0	0	0
	Day 22	15.8 ± 1.3	14.2	17.6	2.9 ± 0.5	2.1	3.6	0.8 ± 0.6	0	1.6
	Day 23	14.2 ± 0.3	13.6	14.5	1.3 ± 0.2	1.1	1.7	0.2 ± 0.2	0	0.6
	Day 24	17.8 ± 1.1	15.8	18.9	0.5 ± 0.2	0.1	0.6	0.0 ± 0.0	0	0

The ambient air temperature, wind speed, solar air temperature, rainfall, air mass flow rate, and FT-SAH operating time all affected the outlet air temperature. However, during the experimental test, the impact of ambient air temperature and solar radiation was dominant.

3.2.3 Temperature difference between outlet and inlet air temperature

Figure 3-4 shows the daily average (±SD) temperature difference values between the outlet and inlet (T_o-T_i) for Case Study 1 and Case Study 2 on each test day. Table 3-4 presents the daily average and standard deviation (±SD) of air mass flow rate, the temperature difference between the outlet and inlet air, and solar radiation for each test day when FT-SAH is operated at different fan speeds.

Case study 1: Fan set at 100% maximum velocity

The daily average temperature difference ranged from 6.0 °C (minimum) to 32.6 °C (maximum) with a mean (±SD) of 18.6 ± 8.7 °C. The hourly temperature difference ranged from 2.0 °C (minimum, Day 2) to 39.5 °C (maximum, Day 12). The hourly air mass flow rate ranged from 0.056 kg/s to 0.059 kg/s, with a mean (± SD) of 0.056 ± 0.0016 kg/s.

Case study 2: Fan set at 50% maximum velocity

The daily average temperature difference ranged from 10.2 °C (minimum) to 41.3 °C (maximum) with a mean (±SD) of 24.1 ± 10.3 °C. The hourly temperature difference ranged from 6.1 °C (minimum, Day 22) to 50.4 °C (maximum, Day 16). The hourly air mass flow ranged from 0.022 kg/s to 0.025 kg/s with a mean (± SD) of 0.024 ± 0.001 kg/s.

Table 3-4 The daily average (± SD) of air mass flow rate ($\dot{m}$), solar radiation incident on the FT-SAH surface (I_T), and temperature difference between the outlet and inlet air ($\Delta T = T_o$-T_i) for Case Study 1 and Case Study 2

Table 3-4 The daily average (± SD) of air mass flow rate ($\dot{m}$), solar radiation incident on the FT-SAH surface (I_T), and temperature difference between the outlet and inlet air ($\Delta T = T_o - T_i$) for Case Study 1 and Case Study 2

Maximum speed of the ventilator	Test Day	Daily Average Air Mass Flow Rate (kg/s)	Minimum Daily Average Air Mass Flow Rate (kg/s)	Maximum Daily Average Air Mass Flow Rate (kg/s)	Daily Average Solar Radiation Incidents On FT-SAH Surface (W/m^2)	Minimum Daily Average Solar Radiation Incidents On FT-SAH Surface (W/m^2)	Maximum Daily Average Solar Radiation Incidents On FT-SAH Surface (W/m^2)	Daily average temperature difference (ΔT) (^oC)	Minimum Daily average temperature difference (ΔT) (^oC)	Maximum Daily average temperature difference (ΔT) (^oC)
Case study 1	Day 1	0.055 ± 0.001	0.053	0.057	248.9 ± 78.4	162.6	367.3	18.6 ± 8.1	10.7	29.6
	Day 2	0.059 ± 0.002	0.057	0.062	142.9 ± 59.9	75.0	237.1	6.0 ± 3.2	2.0	10.2
	Day 3	0.055 ± 0.001	0.054	0.057	290.0 ± 86.4	167.1	396.6	21.4 ± 8.3	10.2	29.8
	Day 4	0.057 ± 0.001	0.056	0.059	198.0 ± 88.9	76.0	336.4	10.8 ± 6.0	2.7	18.8
	Day 5	0.055 ± 0.002	0.052	0.059	188.4 ± 86.2	64.8	283.0	12.9 ± 7.7	3.1	22.5
	Day 6	0.058 ± 0.001	0.056	0.059	201.8 ± 80.6	73.5	276.2	12.3 ± 5.8	3.1	19.9
	Day 7	0.053 ± 0.002	0.051	0.056	395.0 ± 80.2	277.9	479.4	27.3 ± 7.2	15.9	34.1
	Day 8	0.055 ± 0.001	0.054	0.057	336.8 ± 103.4	158.1	420.7	25.1 ± 7.9	11.2	31.5
	Day 9	0.056 ± 0.001	0.054	0.057	372.0 ± 115.0	214.9	514.6	23.6 ± 7.7	14.3	33.0
	Day 10	0.055 ± 0.002	0.052	0.057	199.8 ± 65.2	94.8	267.5	6.3 ± 4.4	1.3	14.0
	Day 11	0.054 ± 0.002	0.052	0.056	468.1 ± 97.8	295.9	559.7	28.3 ± 6.2	18.6	35.0
	Day 12	0.053 ± 0.002	0.052	0.056	476.4 ± 84.7	344.1	567.2	32.6 ± 7.0	22.3	39.5
Case study 2	Day 13	0.024 ± 0.001	0.023	0.026	249.4 ± 81.1	147.9	224.2	17.7 ± 7.3	9.0	27.7
	Day 14	0.024 ± 0.002	0.022	0.026	378.0 ± 110.7	204.6	379.6	24.4 ± 10.8	9.8	38.5
	Day 15	0.025 ± 0.000	0.024	0.025	239.4 ± 36.9	180.6	247.0	11.7 ± 1.9	9.4	15.2
	Day 16	0.022 ± 0.002	0.02	0.024	648.4 ± 118.6	435.7	689.3	41.2 ± 9.2	25.1	50.4
	Day 17	0.024 ± 0.001	0.023	0.025	317.9 ± 74.6	230.0	319.1	21.0 ± 6.0	13.3	28.2
	Day 18	0.023 ± 0.001	0.022	0.025	470.5 ± 107.7	310.5	524.5	31.4 ± 11.5	16.8	42.8
	Day 19	0.023 ± 0.001	0.023	0.025	395.1 ± 68.0	302.9	393.7	24.8 ± 4.4	15.4	29.1

	Day 20	0.023 ± 0.001	0.022	0.024	469.2 ± 127.0	279.1	481.0	31.5 ± 11.3	14.1	44.8
	Day 21	0.023 ± 0.001	0.022	0.024	572.0 ± 79.2	478.3	616.2	38.5 ± 9.7	19.7	49.9
	Day 22	0.025 ± 0.000	0.024	0.025	204.5 ± 28.9	163.8	223.0	11.8 ± 5.1	6.1	19.0
	Day 23	0.025 ± 0.000	0.025	0.025	204.8 ± 44.0	130.6	201.7	10.2 ± 1.9	7.1	12.6
	Day 24	0.023 ± 0.001	0.022	0.025	511.0 ± 225.0	148.9	514.8	24.8 ± 10.9	6.6	36.5

Table 3-4 shows the daily average temperature difference (ΔT) values ranging from 6.0 ± 3.2 ˚C to 41.2 ± 9.2 ˚C. A significant inconsistency in the temperature difference was noted on days 1, 3, 5, 7, 11, 12, 13, 14, 16, 18, 20, and 24 compared to days 2, 4, 6, 10, 19, 21, and 22. External factors, such as rain, cloud cover, solar radiation, and ambient temperature, could influence this. During the test, the hourly average temperature difference was above 18 ˚C for 51.2 % of the time (Case Study 1) and 58.3% of the time (Case Study 2). Figure 3-4 shows the daily average (±SD) temperature differences between the outlet and inlet air on each test day for Case Study 1 and Case Study 2. Results from Figure 3-5 show that the daily average temperature difference throughout the experiment test (Case Study 1 and Case Study 2) ranged from 18.6 ˚C to 24.8 ˚C for 21.9% of the time and above 25.0 ˚C (indicated by red circles) for 33.3% of the time, indicating optimal conditions for FT-SAH performance. The daily average temperature difference was below 18.0 ˚C (indicated by blue circles in Figure 3-5) for 37.5% of the time. However, the system becomes less effective for space heating when the mean temperature difference for SAH drops below 18.0 ˚C, and an external heating system would be required to supplement the indoor air temperature. The study found that a minimum temperature rise of 9.0 ˚C is needed on days when the mean ambient temperature ranges between 9.0 ˚C and 10.0 ˚C to maintain an outlet air temperature of 18.0 ˚C (recommended by the WHO as the minimum indoor comfort standard). Wang et al. (2023) In a two-year NZ classroom study, the researchers found that a minimum 6.0 ˚C temperature rise is needed when the ambient temperature ranges from 12.0 ˚C to 13.0 ˚C for maintaining a temperature of 18.0 ˚C.

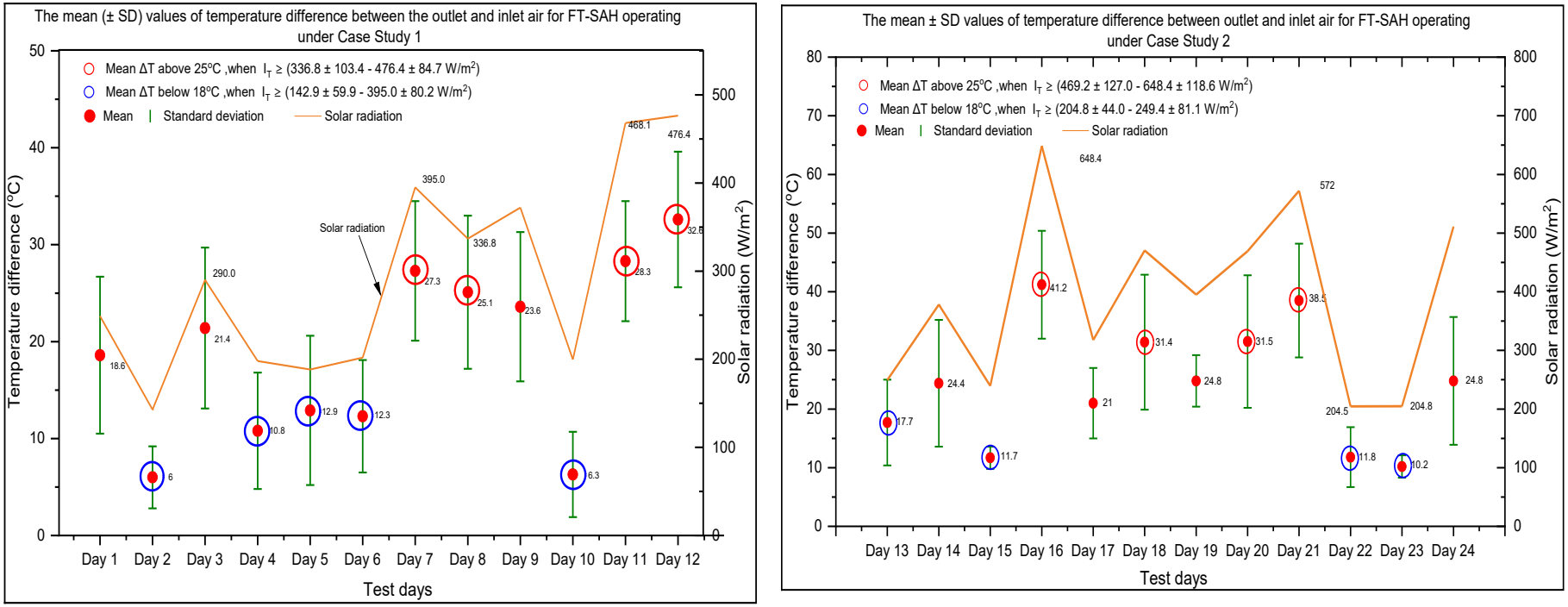

Figure 3-4 The mean (±SD) values of the temperature difference between outlet and inlet air on each test day for FT-SAH operating at 100% (left) and 50% (right) maximum speed of the ventilator

Figure 3-4 shows that $I_T > 400.0$ W/m² is required for Case Study 2 to achieve $\Delta T > 25.0$ ˚C. Case study 2 yielded a better ΔT result at a lower mass flow rate. This result is expected because the air spends more time in the system at a lower mass flow rate, allowing it to absorb more heat from the system.

Figure 3-4 shows a higher temperature difference when the fan is set at a lower mass flow rate (50% set point). A negative relationship was observed between air mass flow rate and temperature difference. These findings are supported by (Jasim Mahmood, 2020). Jasim found that the average temperature difference between the outlet and the ambient air was 38.6 ℃, 36.5 ℃, 33.2 ℃, 26.0 ℃, and 20.3 ℃ at air mass flow rates of 0.003, 0.005, 0.013, 0.016, and 0.018 Kg/s, respectively. The temperature difference obtained for SAH with a net of tubes fitted to an absorber plate was 42.3 ℃, 21.1 ℃, and 17.4 ℃ at 0.019, 0.028, and 0.075 kg/s, respectively (Yassien et al., 2020).

3.2.4 Outlet air temperature and ventilation rate

Figure 3-5 shows the daily average (±SD) outlet air temperatures for each test day in Cases 1 and 2. For Case Study 1, the daily average outlet air temperature ranged from 17.3 ˚C (minimum) to 49.3 ˚C (maximum) with a mean (±SD) of 32.1 ± 9.7 ˚C. The hourly outlet temperature ranged from 9.3 ˚C (minimum, Day 6, 9:00 a.m.) to 57.6 ˚C (maximum, Day 12, 1:30 p.m.), and the air mass flow rate ranged from 0.051 kg/s (minimum) to 0.062 kg/s (maximum).

For Case Study 2, the daily average outlet air temperature ranged from 24.4 ℃ (minimum) to 59.0 ˚C (maximum) with a mean (±SD) of 39.9 ± 11.5 ˚C. The hourly outlet temperature ranged from 17.2 ℃ (minimum, Day 13, 9:00 a.m.) to 68.9 ˚C (maximum, Day 16, 1:30 p.m.), and the air mass flow of 0.020 kg/s (minimum) to 0.026 (maximum) kg/s.

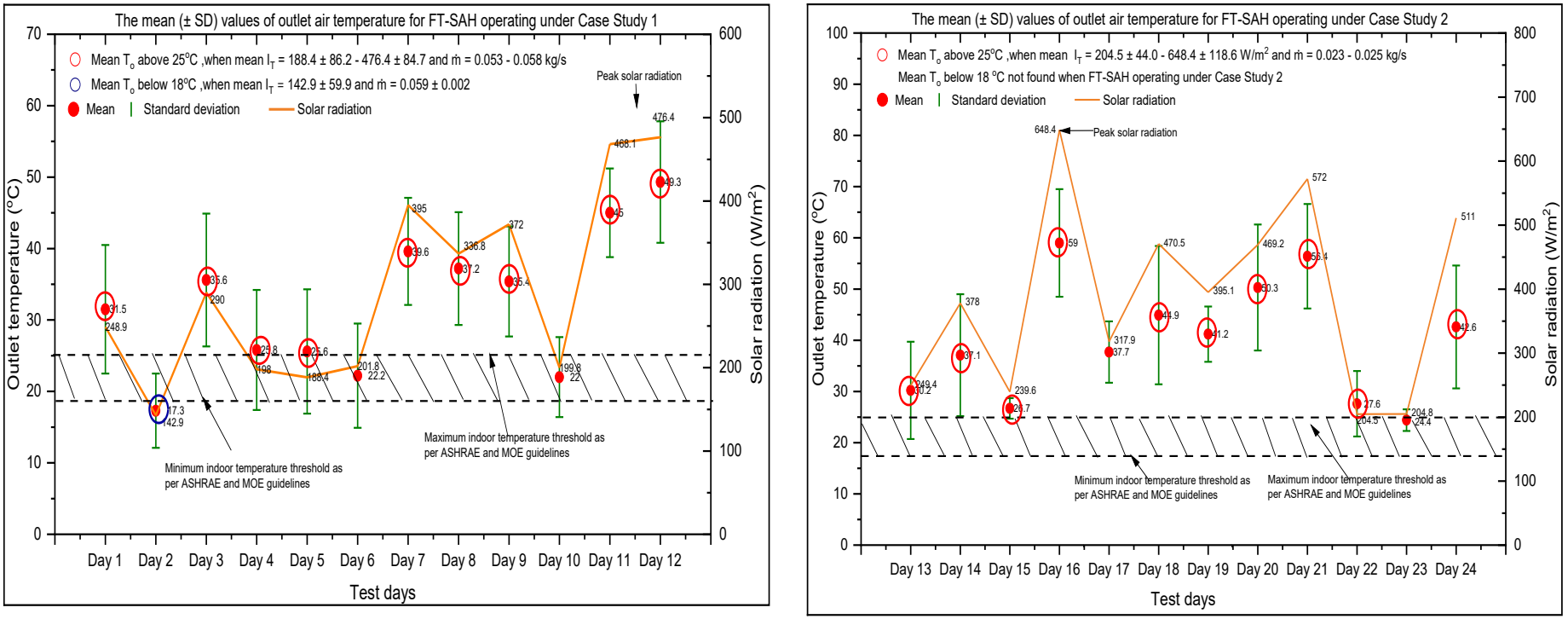

Figure 3-5 Mean (±SD) outlet air temperature and solar radiation for FT-SAH under Case Study 1 (left, winter, 100% fan speed) and Case Study 2 (right, spring, 50% fan speed). Data points are hourly averages; straight-line connections only (no polynomial smoothing). Comfort thresholds (18.0–25.0 ˚C) are shown according to ASHRAE and MOE guidelines

A positive relationship was found between the outlet air temperature and the solar radiation, whereas a negative relationship was found between the outlet air temperature and the air mass flow rate. The daily average outlet temperature was highest on Day 16 (59.0 ± 10.5 ℃ at 0.022 ± 0.002 kg/s) compared to the other days due to the higher mean solar radiation (648.4 ± 118.6 W/m^2) on that day. The daily average solar radiation value was lowest on Day 2 (142.9 ± 59.9 W/m^2), and hence, the outlet temperature was lowest on Day 2 (17.3 ± 5.2 ℃ at 0.059 ± 0.002 kg/s). Studies conducted by (Hassan et al., 2020; Singh & Vardhan, 2021). They found similar results, where the outlet air temperature increases with increasing solar radiation and decreases with increasing air mass flow rate. Research conducted by (Hassan et al., 2020) found that the outlet air temperature of TSAH and FSAH were 56.1 ℃, 47.2 ℃, 44.1 ℃, and 42.1 ℃, 41.1 ℃, 40.9 ℃ at air mass flow rates of 0.025 kg/s, 0.050 kg/s, and 0.075 kg/s, respectively. The study revealed that the outlet air temperature of TSAH was higher than that of FSAH, attributed to the larger contact area of TSAH. The contact area of TSAH was 3.141 times that of flat plate SAH due to the peripheral region of all tubes. Moreover, internal reflections between the absorber surfaces reduced the amount of reflected solar radiation reaching the atmosphere. Thus, reducing the top heat loss indicates higher heat transfer in TSAH (Hassan et al., 2020). A study conducted by (Wang et al., 2023) found the mean outlet air temperature to be 28.9 ± 10.6 ℃ across the two-year study, and it was affected by ambient temperature, solar radiation, wind speed, rainfall, and operation time.

During the test, it was found that solar radiation rises until 12:30 pm and then decreases over time. It was found that the outlet air temperature exhibits a similar pattern to solar radiation, increasing until 1:30 pm and subsequently decreasing over time for all test days, except for Days 5, 6, 15, and 22. It could be due to the cooling effect of wind and rain because the wind and rain were measured at 1-minute intervals. The time lag between the optimum temperature and the optimum solar radiation could be due to the time required to heat the air and the FT-SAH. The time lag is shown in Figure 3-6, considering the day with the highest efficiency (Day 3 and Day 13) for Case Studies 1 and 2.

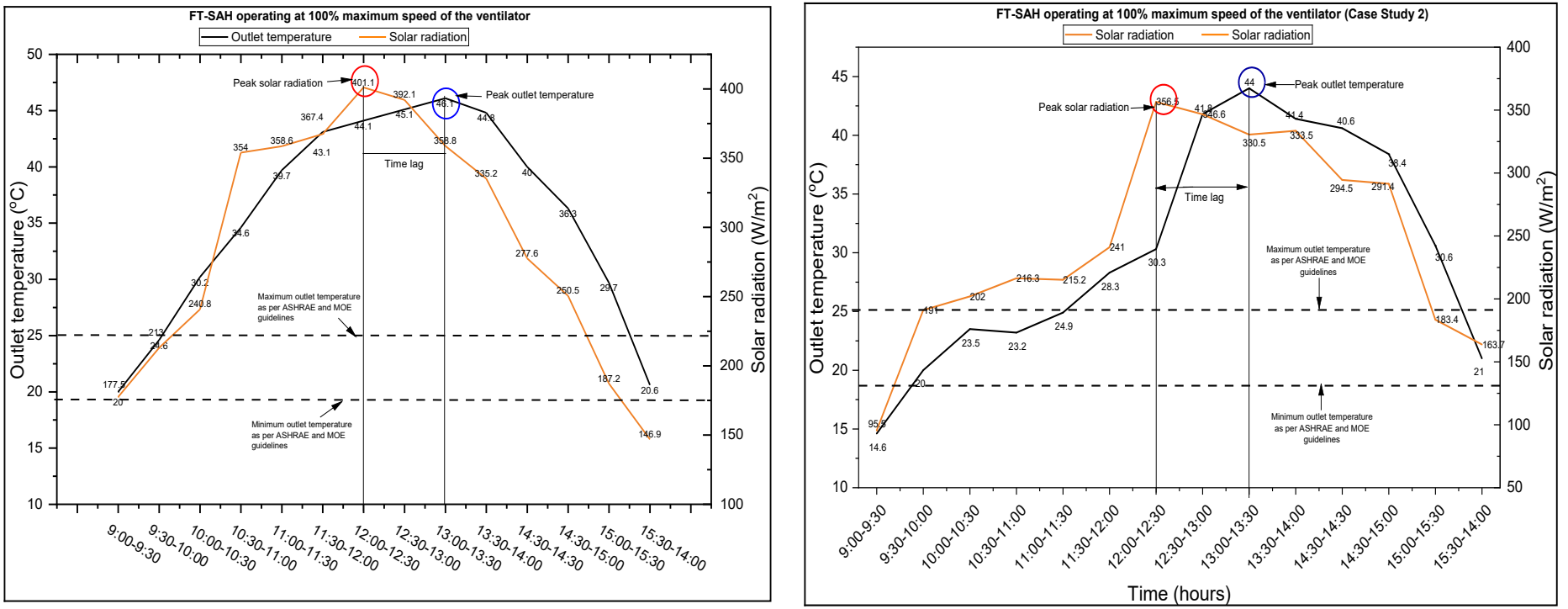

Figure 3-6 The time lag between the optimum temperature and the optimum solar radiation for FT-SAH operating at 100% (Case Study 1) and 50% (Case Study 2) maximum speed of the ventilator

The hourly outlet air temperature was above 18.0 ˚C for 86.9% and 98.8% of the time for Case Studies 1 and 2, respectively. As per MOE guidelines, the recommended temperature levels in NZ classrooms are to be maintained between 18.0 ˚C and 25.0 ˚C (N. Z. Ministry of Education, 2014).

At higher temperatures, it is essential to ventilate to maintain a healthy and comfortable indoor environment. Ventilation is the movement or circulation of air to remove pollutants, odours, moisture, and excess heat, and to maintain CO_2 levels. In this study, the ventilation rate of outlet air was calculated by dividing the air mass flow rate by air density. One input parameter for calculating the air mass flow rate is air velocity, which is linked to the fan speed regulator setting. The daily average ± SD values of ventilation correspond to the outlet air temperature for Case Studies 1 and 2 in Table 3-5. For Case Study 1, the calculated daily average ventilation rate ranged from 164.2 m^3/h (minimum) to 176.1 m^3/h (maximum) with a mean ± SD of 173.1 ± 3.5 m^3/h. The hourly ventilation rate ranged from 163.5 m^3/h (minimum, Days 5 and 10) to 176.1 m^3/h (maximum, Days 3, 4, 6, 8, 9, 11, and 12).

The daily average ventilation rate for Case Study 2 ranged from 69.9 m^3/h to 77.0 m^3/h, with a mean ± SD of 74.8 ± 1.9 m^3/h. The hourly ventilation rate ranged from 71.4 m^3/h (minimum, Day 12) to 77.9 m^3/h (maximum, Day 4).

Table 3-5 The daily average ± SD values of ventilation correspond to the outlet air temperature values when FT-SAH operates at 100% and 50% maximum ventilator speed in good weather conditions

Case Study	Test Day	Daily average air mass flow rate (kg/s)	Daily average outlet temperature (°C)	Minimum daily average outlet temperature (°C)	Maximum daily average outlet temperature (°C)	Daily average ventilation rate (m^3/h)	Minimum daily average ventilation rate (m3/h)	Maximum daily average ventilation rate (m^3/h)
Case Study 1	Day 1	0.055 ± 0.001	31.5 ± 9.0	22.1	43.2	170.7 ± 3.0	167.2	175.3
	Day 2	0.059 ± 0.002	17.3 ± 5.2	10.0	23.3	173.7 ± 1.0	173.3	175.9
	Day 3	0.055 ± 0.001	35.6 ± 9.3	22.3	45.4	175.0 ± 1.2	173.3	176.1
	Day 4	0.057 ± 0.001	25.8 ± 8.4	13.2	36.6	174.1 ± 1.3	173.3	176.1
	Day 5	0.055 ± 0.002	25.6 ± 8.7	15.0	36.5	165.8 ± 3.6	163.5	173.4
	Day 6	0.058 ± 0.001	22.2 ± 7.3	9.3	30.8	173.7 ± 1.0	173.3	176.1
	Day 7	0.053 ± 0.002	39.6 ± 7.5	28.7	46.6	168.9 ± 3.2	165.6	172.9
	Day 8	0.055 ± 0.001	37.2 ± 7.9	23.6	44.4	175.2 ± 0.9	173.3	176.1
	Day 9	0.056 ± 0.001	35.4 ± 7.7	25.8	44.7	175.1 ± 1.3	173.3	176.1
	Day 10	0.055 ± 0.002	22.0 ± 5.6	15.2	31.5	165.1 ± 1.6	163.5	167.5
	Day 11	0.054 ± 0.002	45.0 ± 6.2	36.6	51.6	175.0 ± 1.0	174.0	176.1
	Day 12	0.053 ± 0.002	49.3 ± 8.5	34.9	57.6	174.7 ± 0.9	174.0	176.1
Case Study 2	Day 13	0.024 ± 0.001	30.2 ± 9.5	17.2	42.9	75.6 ± 0.7	74.7	76.4
	Day 14	0.024 ± 0.002	37.1 ± 11.9	20.3	52.2	74.7 ± 1.3	73.0	76.4
	Day 15	0.025 ± 0.000	26.7 ± 2.0	24.8	30.4	75.9 ± 0.2	75.5	76.0
	Day 16	0.022 ± 0.002	59.0 ± 10.5	40.2	68.9	72.7 ± 4.0	69.0	77.9
	Day 17	0.024 ± 0.001	37.7 ± 6.0	30.3	44.3	75.2 ± 0.5	74.7	76.0
	Day 18	0.023 ± 0.001	44.9 ± 13.5	25.8	58.2	74.2 ± 1.3	72.3	76.0
	Day 19	0.023 ± 0.001	41.2 ± 5.4	29.6	45.8	74.9 ± 0.5	74.7	76.0
	Day 20	0.023 ± 0.001	50.3 ± 12.3	31.1	64.5	75.9 ± 0.8	74.7	77.0
	Day 21	0.023 ± 0.001	56.4 ± 10.2	36.6	68.4	76.3 ± 0.7	75.5	77.0

	Day 22	0.025 ± 0.000	27.6 ± 6.4	20.3	36.0	75.9 ± 0.2	75.5	76.0
	Day 23	0.025 ± 0.000	24.4 ± 2.1	20.7	27.1	76.0 ± 0.0	76.0	76.0
	Day 24	0.023 ± 0.001	42.6 ± 12.0	22.4	55.2	74.3 ± 1.6	71.4	76.0

The maximum hourly ventilation rates for FT-SAH in Case Studies 1 and 2 were 176.1 m³/h (at 0.056 kg/s) and 77.9 m³/h (0.024 kg/s), respectively. This indicates that operating FT-SAH under Case Study 1 is recommended. However, the obtained ventilation rate was five times lower than the recommended ventilation rate as per the compliance document G4 (NZ Building Code compliance document for ventilation) and the cited New Zealand Standard (NZS) 4303:1990, which recommends a flow rate of 8 liters per second, per child to maintain a CO_2 level below 1000 ppm. This recommended flow rate is equivalent to 864 m^3 /h for an average classroom of 30 children (MBIE, 2017). For Case Study 1, the time required for a complete air change in a classroom of 220.0 m³ will be 1.2 hours if the SAH is the only means of ventilation. Little research is available on estimating ventilation rates in SAHs. However, a study conducted by (Wang et al., 2023) In NZ classrooms, it was found that the ventilation rate for the flat plate SAH with a perforated back plate was twenty five times lower than the compliance document G4 and cited NZ standards (NZS) 4303:1990, and that the time taken for one complete air change was 6.5 hours.

Therefore, FT-SAH can be used as a supplemental solution to increase ventilation rates, as it cannot provide adequate ventilation on its own.

3.2.5 Application of FT-SAH

Thermal comfort and ventilation could impact indoor environmental quality and affect cognitive performance (Ahmed et al., 2022; Fang et al., 2004). A study conducted in the building found that the optimal temperature range for cognitive performance was 22.0 °C – 24.0 °C. The Same study showed that elevated (above 26.0 °C) and low (below 18.0 °C) temperatures can cause respiratory and cardiovascular diseases, whereas low humidity (below 40.0%) can cause dry eyes (Wolkoff et al., 2021). There are several studies indicating that poor classroom ventilation affects student's learning, health, and school attendance (Ferreira & Cardoso, 2014; Forns et al., 2016) . Children are more vulnerable to contaminants than adults, as they have larger lungs and breathe faster. Therefore, contaminants get concentrated in their bodies. (Bennett et al., 2019). Henceforth, it is imperative to provide students with a healthy environment in the classroom, for it is in this space that students acquire knowledge and spend most of their time (M. Ministry of Education, 2014).

A practical application of FT-SAH could be in the school environment, as school hours are well-aligned with optimal solar radiation (9:00 am to 3:00 pm). The school environment is high-density, and a high ventilation rate is needed to remove potential pollutants (Sadrizadeh et al., 2022). Table 3-6 shows the hourly average percentage of time when the outlet air temperature

was above 18.0 ˚C. Between 11:00 a.m. and 4:00 p.m., the outlet air temperature exceeded 18.0 ˚C for 97.3% and 100.0% of the time in Case studies 1 and 2, respectively.

Table 3-6 Percentage of the time when the hourly average outlet temperature is above 18.0 ˚C for Case Studies 1 and 2

Case Study	Parameter	9:30 am	10:30 am	11:30 am	12:30 pm	1:30 pm	2:30 pm	3:30 pm
Case study 1	T_o>18.0 ˚C	58.3%	75.0%	91.7%	100.0%	100.0%	100.0%	83.3%
	T_o>18.0 ˚C assuming 30% heat loss	25.0%	50.0%	66.7%	83.3%	75%	66.7%	33.3%
Case study 2	To>18.0 ˚C	91.6%	100.0%	100.0%	100.0%	100.0%	100.0%	100.0%
	To>18.0 ˚C assuming 30% heat loss	50.0%	75.0%	83.3%	91.7%	100.0%	100.0%	100.0%

Heinrich (2007) reported that increasing duct length from 0.5 m to 2.2 m reduced both efficiency and outlet temperature by 39%. Similarly, Wang et al. (2023) observed a 30.0% drop in efficiency when the duct length increased from 0.5 m to 5.0 m, with sensors placed 5 m downstream of the SAH. Based on these findings, this study assumed a 30.0% heat loss when the duct length was increased from 1.0 m to 2.5 m, even with insulation. Under these conditions, the hourly average outlet air temperature exceeded 18.0 ˚C for 57.1% of the time in Case Study 1 and 85.7% of the time in Case Study 2. However, outlet air temperatures above 25.0 ˚C would require cooling before being supplied indoors, as the recommended classroom range is 18.0–25.0 ˚C. A plenum (fluid mixing box) could be used to blend outlet and ambient air, achieving both the target temperature and the required airflow rate.

Table 3-7 presents the hourly average airflow rates at a reference temperature of 20.0 ˚C. At 32.2 ˚C, the hourly average volumetric flow rate was 172.1 m³/kg, while the required average volumetric flow rate at 20.0 ˚C to meet the target 864.0 m³/h was 668.4 m³/h and 589.0 m³/h in Case Studies 1 and 2, respectively.

Table 3-7 Hourly average airflow rates at 20 ˚C and percentage of time when volume flow rate ≥ 864 m³/h

Case Study	Parameter	9:30 am	10:30 am	11:30 am	12:30 pm	1:30 pm	2:30 pm	3:30 pm
Case study 1	Volume flow rate at 20 ˚C (m^3/h)	255.5	421.8	649.3	955.2	1018.7	870.1	508.2

Case study 2	Volume flow rate at 20 ̊C (m^3/h)	208.2	402.9	597.9	992.4	980.0	733.0	208.0

When accounting for a 30.0% energy loss, 1234.3 m³/h of supply air is required to achieve the target 864.0 m³/h at 20.0 ˚C. This indicates that at least two collectors are necessary to maintain the recommended classroom ventilation rate.

A further operational recommendation is to regulate fan speed: operate at 50% when the outlet temperature is below 18.0 ˚C, and increase to 100% when the outlet temperature exceeds 25.0 ˚C.

3.2.6 Thermal efficiency of FT-SAH

The thermal efficiency of the FT-SAH was evaluated using Equation 3.1 and was tested in two case studies. In Case Study 1, the thermal efficiency ranged from 38.6% to 83.8%, with an average of 69.5 ± 13.4%. The ratio of the temperature difference to solar radiation (ΔT/IT) for this case study ranged from 0.035 Km²/W to 0.075 Km²/W, with a mean of 0.061 ± 0.012 Km²/W. Hourly efficiency ranged from 15.9% (on Day 10) to a peak of 95.7% (on Day 1), corresponding to $\Delta T/I_T$ values of 0.014 Km²/W (minimum) to 0.089 Km²/W (maximum).

For Case Study 2, thermal efficiency showed a narrower range, from 23.8% to 34.7%, with a mean of 29.4 ± 3.5%. In this case, the $\Delta T/I_T$ values ranged between 0.049 Km²/W and 0.071 Km²/W, with a mean of 0.062 ± 0.008 Km²/W. Hourly efficiency was observed between 17.9% (Day 18) and 43.6% (Day 17), while $\Delta T/I_T$ values ranged from 0.037 Km²/W to 0.085 Km²/W. The overall efficiency of the FT-SAH, including the mechanical power consumed by the fan, was analysed. The mean effective efficiency increased by only 2.8% as the air mass flow rate increased from 0.024 kg/s to 0.056 kg/s. The mean effective efficiency ranged from 65.0 ± 14.6% at higher airflow rates (0.054–0.059 kg/s) to 28.0 ± 3.6% at lower airflow rates (0.022–0.025 kg/s).

Figure 3-7, which illustrates daily thermal efficiency as a function of the temperature difference ratio to solar radiation (ΔT/IT), shows a linear relationship between thermal efficiency and $\Delta T/I_T$. At a $\Delta T/I_T$ of 0.05 Km²/W, the thermal efficiency was 25.5% at an air mass flow rate of 0.025 kg/s and 56.5% at a flow rate of 0.056 kg/s. Additionally, the study found that the maximum hourly efficiency reached 95.7% at an air mass flow rate of 0.053 kg/s, with a daily average efficiency of 83.9% at full fan speed.

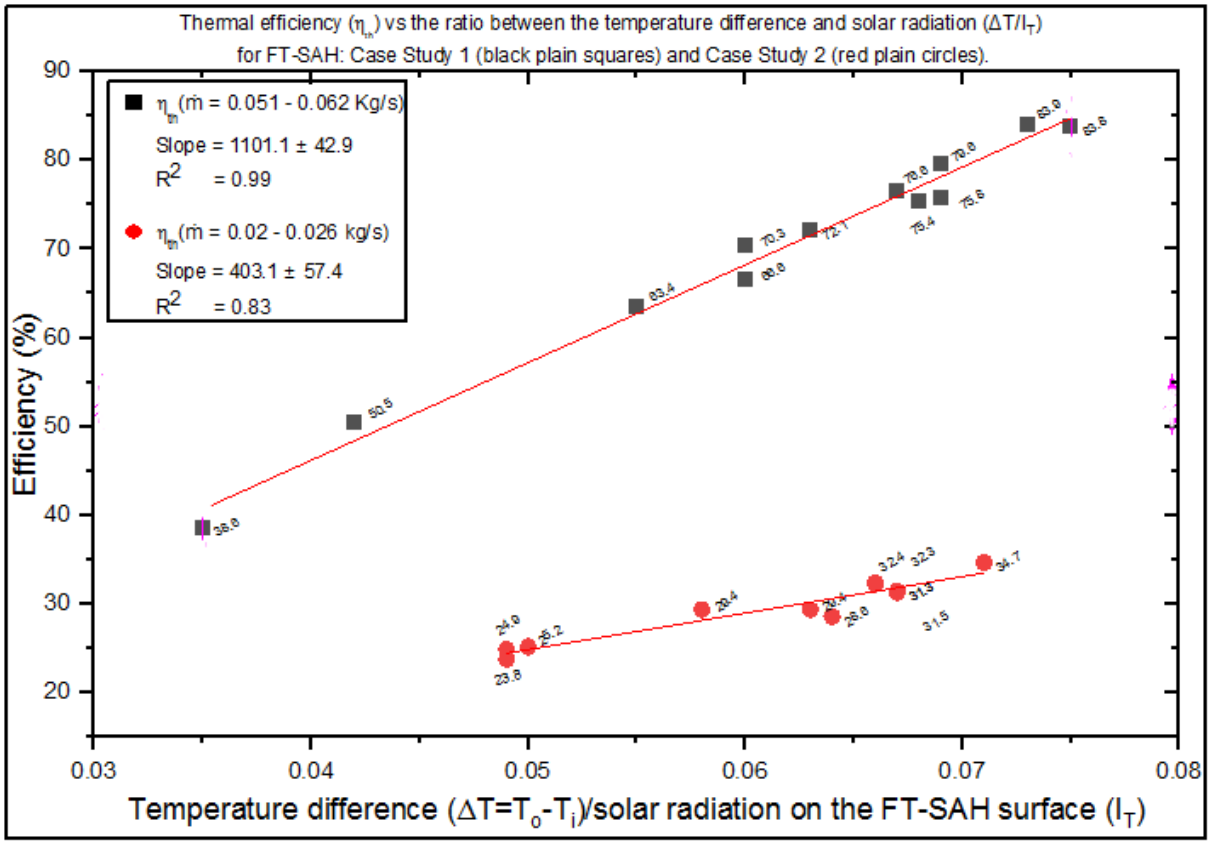

Figure 3-7 Relationship between thermal efficiency and the temperature difference ratio ($\Delta T/I_T$) for FT-SAH at two mass flow rate ranges: 0.051–0.062 kg/s (Case Study 1, black plain squares) and 0.020–0.026 kg/s (Case Study 2, red plain circles). Data points represent hourly averages calculated from one-minute sampling intervals.

The results from both case studies indicate a clear relationship between thermal efficiency and the $\Delta T/I_T$. Case Study 1 consistently outperformed Case Study 2, which can be attributed to the higher mass flow rates in the former. This outcome aligns with the expected performance of SAHs: increased airflow enhances heat transfer, reducing temperature losses and boosting overall system efficiency. The strong positive correlation between $\Delta T/I_T$ and thermal efficiency ($R^2 = 0.99$ for higher mass flow rates) further supports this observation.

In contrast, the lower mass flow rates in Case Study 2 resulted in less efficient heat transfer, as evidenced by the shallower slope (403.1) and weaker correlation ($R^2 = 0.83$). This suggests that lower airflow is more sensitive to environmental conditions, such as rain, wind, and cloud cover, thereby introducing variability in system performance.

From the experiment's results, it can be concluded that the thermal efficiency of the FT-SAH is directly proportional to the temperature difference between the outlet and inlet air (ΔT) and inversely proportional to the solar radiation level (I_T). In Case Study 1, with the system operating at full fan speed, the maximum hourly thermal efficiency reached 95.7% at an air

mass flow rate of 0.053 kg/s, and the daily average efficiency was 83.9%. At a lower mass flow rate of 0.024 kg/s, the maximum hourly efficiency decreased to 43.6%, indicating the impact of airflow on system performance. These high-efficiency levels are attributed to the finned tube design and corrugated fins, which enhance heat transfer.

Weather conditions strongly influenced performance variability. Overall, the results confirm that both operational settings (mass flow rate) and environmental factors play critical roles in determining the thermal performance of the FT-SAH, with higher mass flow rates providing more reliable and efficient operation.

Comparisons with other studies highlighted the FT-SAH's superior performance, as shown in Table 3-8. Its maximum thermal efficiency was 95.7%, which surpassed that of other SAHs. Singh and Vardhan (2021) found that an evacuated tube SAH with helical fin inserts achieved a maximum thermal efficiency of 70.9% at a mass flow rate of 0.015 kg/s, while (Yassien et al., 2020) reported a peak efficiency of 80.2% for a triple-pass SAH with a net of tubes at a mass flow rate of 0.028 kg/s. In another study, Elbrashy et al. (2023) recorded a maximum thermal efficiency of 64.2% for an evacuated tube SAH with thermal storage at a mass flow rate of 0.05 kg/s. Additionally, SAHs with V corrugated absorbers reached a maximum thermal efficiency of 57.0% at a mass flow rate of 0.02 kg/s, and double-pass SAHs with V corrugated plates had an average thermal efficiency of 65.3% at a flow rate of 0.04 kg/s (El-Sebaii et al., 2011a). These comparisons indicate that the FT-SAH used in the present study achieved higher thermal efficiency than the systems in these other studies.

Table 3-8 Thermal efficiency comparison of the present work with work conducted by other researchers

SAH design	**Air mass flow rate (kg/s)**	**Peak thermal efficiency (%)**	**Daily average thermal efficiency**
FT-SAH (present work)	0.053	95.7	83.9
	0.024	43.6	32.3
Evacuated tube with helical inserts (Singh & Vardhan, 2021)	0.015	70.9	58.1
Triple pass SAH with double glass and net of tubes (Yassien et al., 2020)	0.0075 0.0188 0.0282	54.4 64.9 80.2	- - -

Evacuated tube SAH with thermal storage (Elbrashy et al., 2022)	0.05	64.2	57.0
SAH with corrugated plates (Poongavanam et al., 2018)	0.015 0.02	36.0 57.0	34.2 56.0
Double pass SAH with v corrugated plate (El-Sebaii et al., 2011a)	0.02	-	57.4
	0.04	-	65.3

Figure 3-8 illustrates the overall (effective) efficiency of the FT-SAH for two case studies, considering the mechanical power consumed by the fan. In Case Study 1, where the system operated at full ventilator speed, both thermal and effective efficiencies were strongly correlated with the ratio of the temperature difference to incident solar radiation (ΔT/IT), with an R^2 of 0.99. The thermal efficiency had a slope of 1101.2, indicating a predictable increase in efficiency with increasing temperature difference. With a slightly lower slope, the effective efficiency still followed a similar trend.

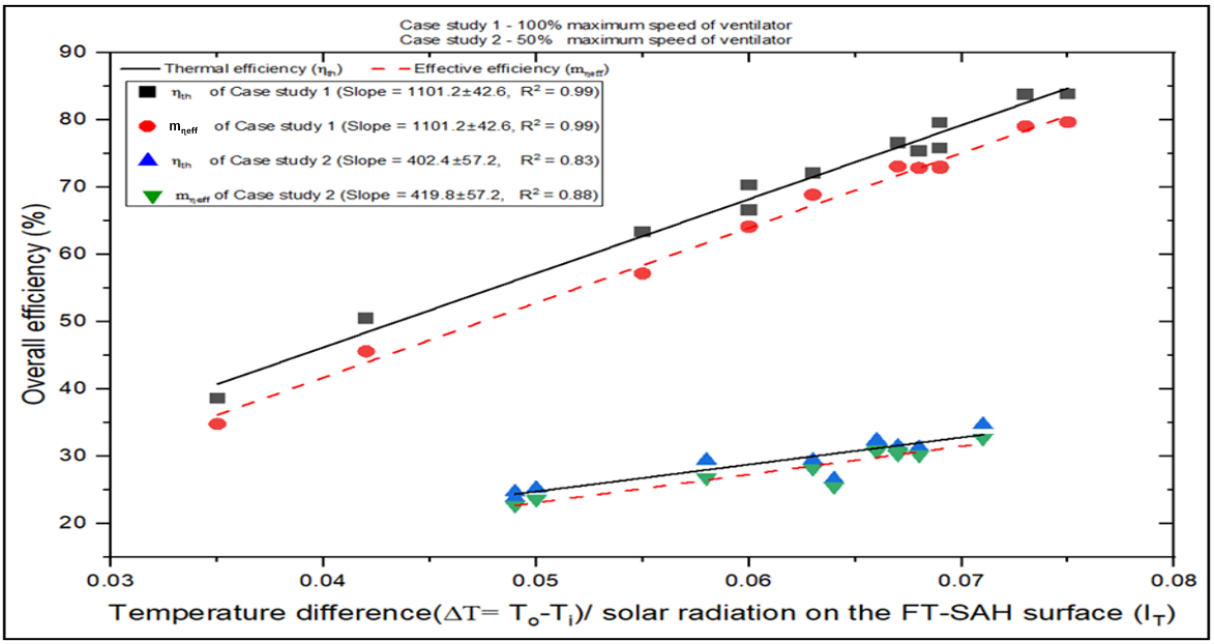

Figure 3-8 The overall efficiency of FT-SAH for Case Studies 1 and 2

In contrast, Case Study 2, which ran at 50% ventilator speed, showed a weaker correlation between thermal efficiency and ΔT/IT, with an R^2 of 0.83. The effective efficiency, although slightly stronger (R^2 = 0.88), also exhibited more variability in performance. The system in Case Study 1 consistently achieved higher thermal and effective efficiencies due to enhanced heat transfer enabled by the higher airflow.

The comparison between the two case studies highlights the impact of ventilator speed on performance. Higher airflow yields more efficient heat transfer and improved predictability in the relationship between $\Delta T/I_T$ and efficiency, as observed in Case Study 1. The difference between thermal and effective efficiency in both studies reflects the gap between theoretical heat transfer and actual energy utilization under practical conditions. Overall, the study emphasizes the importance of adequate airflow in maximizing system efficiency.

3.3 Conclusion

The thermal efficiency of SAHs is relatively low, limiting their use to low-temperature applications such as space heating, drying, and ventilation. Researchers have found that applying artificial roughness to the collector's surface can significantly enhance heat transfer, improving thermal efficiency and making SAHs more viable for these specific applications. In this study, SAH was experimented with using finned tubes (absorbers). Corrugated fins were inserted into the tubes to increase the surface area and heat transfer. Data collected from June 2023 to November 2023 have been presented, including SAH outlet air temperature and air volumetric flow rate. The temperature difference between the outlet and inlet air, as well as the thermal efficiency, was calculated. The following conclusions are drawn from the study:

1) The ratio of the temperature difference between the outlet and inlet air temperature to the solar radiation incident on the tilted surface of the FT-SAH and the air mass flow rate positively impacted the thermal efficiency of FT-SAH. The FT-SAH achieved its highest thermal efficiency in Case Study 1, with a mean efficiency of 69.6 ± 13.4% at a $\Delta T/I_T$ of 0.069 ± 0.004 Km^2/W. In comparison, Case Study 2 recorded a lower mean efficiency of 29.4 ± 3.5% at a $\Delta T/IT$ of 0.062 ± 0.008 Km^2/W.
2) Solar radiation and air mass flow rate dominated the outlet air temperature. The maximum outlet air temperature was 68.9 °C when the solar radiation was 771.8 W/m^2, and the air mass flow rate was 0.020 kg/s. The minimum outlet air temperature was 9.3 °C when the solar radiation was 73.5 W/m^2, and the air mass flow rate was 0.059 kg/s. Based on the results of this study, it can be concluded that weather conditions had some impact on the performance of FT-SAH. However, the overall effect was not significant enough to drastically reduce its efficiency.
3) The outlet air temperature (mean) was above 18.0 °C for at least 95.8% of the test time. The ability to consistently provide outlet air temperatures above 18.0 °C more than 95% of the time highlights its value in improving thermal comfort in low-energy settings, particularly in temperate climates such as New Zealand.

4) The outlet air temperature follows the same trend as solar radiation. It increases from 9 a.m. to 1:30 p.m. and then decrease later in the afternoon. The time lag between peak solar radiation and peak outlet air temperature may be due to the time taken to heat the SAH and the air.
5) To enhance space heating efficiency, it is crucial to reduce the elevated outlet air temperatures (exceeding 25.0 ˚C) before distributing them into the living space. Therefore, it is recommended to incorporate a plenum box with the SAH. The plenum box functions as a compartment where incoming air is mixed with warm air to lower its temperature.
6) The mean volumetric flow rate of FT-SAH operating under Case Study 1 was 172 ± 3.0 m^3/h, at a mean outlet air temperature of 29.4± 9.9 ˚C. The mean volumetric flow rate of FT-SAH operating under Case Study 2 was 74.8 ± 1.9 m^3/h, at a mean outlet air temperature of 39.9 ± 11.5 ˚C m/s. The time required for a complete air change was 1.2 hours and 2.8 hours at mass flow rates of 0.056 kg/s and 0.024 kg/s, respectively, for a classroom of 220.0 m^3, if operating the FT-SAH is the only means of ventilating the classroom. However, it was not sufficient to provide adequate ventilation on its own.

3.4 Limitations and Future Scope

The experiment conducted in Massey University's car park presents several limitations that should be addressed in future studies. First, the testing environment does not replicate the operating conditions of SAH installed on a rooftop, as would be the case in a real-world application, such as on top of a classroom. This research did not consider factors such as duct length, which can significantly affect both thermal efficiency and outlet air temperature. These variables could lead to different performance outcomes in practice.

Additionally, to meet the ventilation requirements specified by the Ministry of Education (MOE) and the American Society of Heating, Refrigerating, and Air-Conditioning Engineers (ASHRAE), multiple SAHs would be required. This increases the roof space needed and adds to the overall installation cost. Although the FT-SAH demonstrates potential as a supplementary heating and ventilation source, the scalability and economic feasibility of installing multiple units remain challenges.

Moreover, this study did not compare the FT-SAH's performance with and without fins, which is essential for optimising design and cost. Although the FT-SAH showed promising thermal performance at higher mass flow rates, further investigation is needed to determine whether fin structures provide sufficient benefits to justify their additional cost and complexity.

To address this gap, the next chapter will present a comparative analysis of finned and unfinned designs, providing deeper insights into the influence of fins on heat transfer performance and practical viability.

4 Effect of fin inserts on the thermal efficiency of the tube-type solar air heater

Chapter 3 discussed the thermal performance of FT-SAH with corrugated fin inserts. The study found that the mass flow rate and the temperature difference ($\Delta T/I_T$) ratio between the outlet and inlet air significantly influenced the thermal efficiency of the FT-SAH. The results indicated that while FT-SAH could serve as a supplemental solution to increase ventilation rates, it could not provide adequate ventilation independently. The FT-SAH study achieved an efficiency of 83.9% at a mass flow rate of 0.056 kg/s**,** which surpasses the maximum efficiency reported for triple-pass SAHs (80.2%) in (Yassien et al., 2020) and evacuated tube SAHs (70.9%) in (Singh & Vardhan, 2021).This suggests that incorporating corrugated fins effectively enhances the surface area for heat transfer, improving system efficiency. Given these findings, it is crucial to investigate further the effect of fin inserts on FT-SAH's thermal performance.

The literature review indicated that various enhancement techniques could potentially be integrated into the SAH design (Foued Chabane, Nesrine Hatraf, et al., 2014; El-Sebaii et al., 2011a; Saxena et al., 2015) ; however, this aspect was not tested in the experiment. The solar air heater used in this study was a prototype developed by Sojol Pvt. Ltd., which limited our ability to modify its design. Consequently, the research was constrained by these design limitations. Additionally, time constraints prevented us from developing a complete system for the PhD project. The PhD focused primarily on prototype environmental testing rather than product design.

Chapter 4 investigates the thermal performance of a TSAH equipped with fin inserts (treatment SAH) and compares it to a control system without fin inserts. The results indicate that the treatment SAH significantly improves thermal efficiency, particularly at higher mass flow rates. At a mass flow rate of 0.07 kg/s, the treatment SAH achieved a peak thermal efficiency of 75.3%, outperforming the control SAH's 46.4%. At a lower mass flow rate of 0.04 kg/s, the treatment system maintained an efficiency of 62.3%, compared to 32.9% for the control. Additionally, the temperature difference between the inlet and outlet air was consistently higher in the treatment SAH due to enhanced heat transfer provided by the fin inserts. At high-speed operation, the temperature difference in the treatment SAH reached 7.0 $^{\circ}$C, compared to 4.4 $^{\circ}$C in the control SAH, with the difference increasing to 10.4 $^{\circ}$C and 6.3 $^{\circ}$C, respectively, at lower speeds. The study also demonstrates that fin inserts increase the system's thermal mass, enabling better heat retention and capture. Despite these improvements, the system could not meet

standalone ventilation requirements based on the Ministry of Education (MOE) guidelines, suggesting that multiple SAH units would be necessary for adequate ventilation, which could increase installation costs and required roof space.

The chapter is divided into four sections, as outlined in Figure 4.1. It begins with an introduction (Section 4.1) and proceeds to the materials and methods section (Section 4.2), which details the experimental setup for the control and treatment SAH. Data collection, including ambient temperature, solar radiation, outlet temperature, ventilation rate, and thermal efficiency, follows. The results and discussion section (Section 4.3) compares the parameters influencing the system's performance. Finally, the chapter concludes with a summary of the findings and suggestions for future research and improvements (Section 4.4).

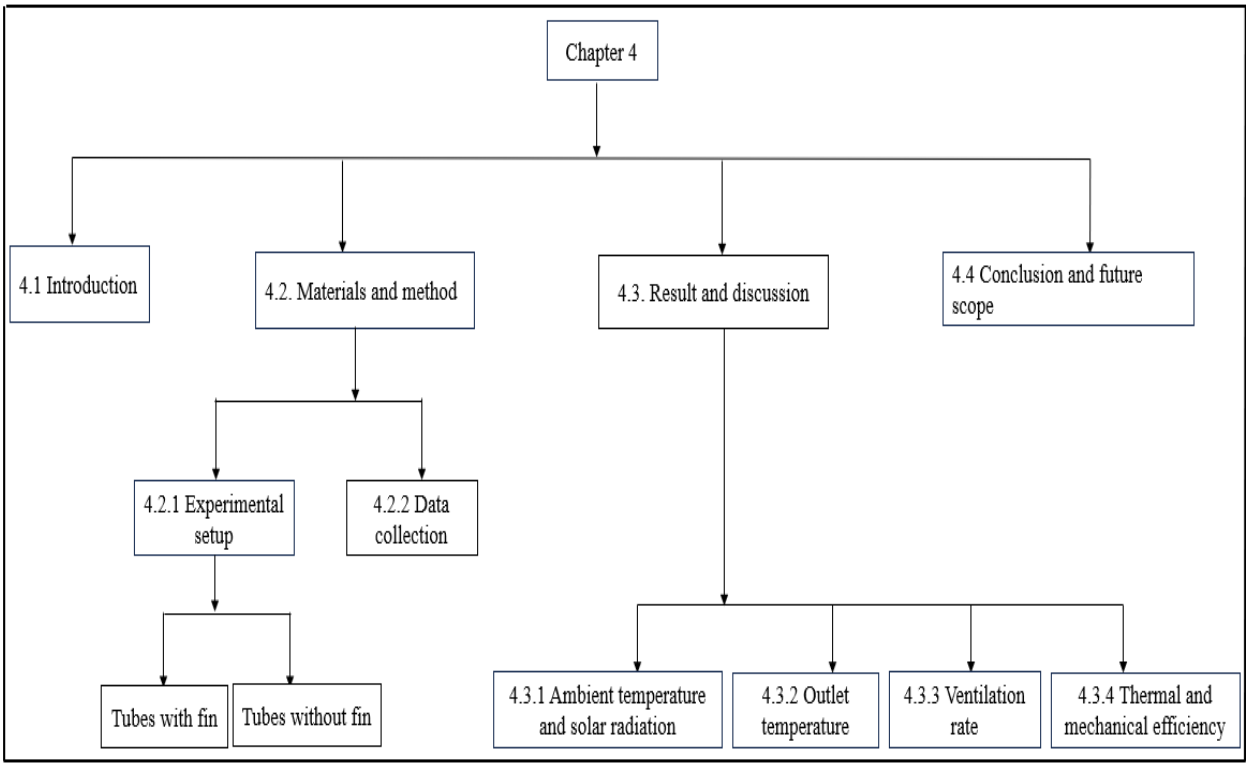

Figure 4-1 Sections discussed in the chapter

4.1 Introduction

As discussed in Chapter 2, the application of artificial roughness (Saxena et al., 2023), integrating solar thermal energy systems (Tyagi et al., 2012), application of nanofluid coatings (Kumar et al., 2020), reflectors (Abdullah, Amro, et al., 2020) inside the SAHs, using evacuated tubes (Abi Mathew & Thangavel, 2021) and micro heat pipe array systems (Zhu & Zhang, 2021) are techniques investigated to improve the thermal efficiency of SAHs. These techniques are discussed in detail in the literature review of Chapter 2. Therefore, only relevant literature studies on SAHs with and without artificial roughness are briefly discussed in this chapter to show the effect on efficiency when fins are added. The following section briefly discusses the

improvements achieved in SAH applications utilizing fin inserts, and Table 4-1 summarizes the relevant literature studies.

Table 4-1 Literature studies on improving the thermal efficiency of SAHs integrated with artificial roughness

Study	Author name and year	Solar air heater type	Mass flow rate (kg/s)	Efficiency (%)	Change in efficiency (%)
1.	Kumar and Rosen (2011)	SAH with fins	0.060	55.0	10.0
		SAH without fins		45.0	
2.	Sivakumar et al. (2019)	Pin finned SAH	-	13.0 to 38.0	3.0-12.0
		Flat plate SAH	-	10.0 to 26.0	
3.	F. Chabane et al. (2014)	SAH with longitudinal fin	0.012 0.016	51.5 40.0	7.6 and 5.1 at 0.012 kg/s and 0.016 kg/s respectively
		SAH without longitudinal fin	0.012 0.016	43.9 34.9	
4.	Fan et al. (2019)	SAH with longitudinal fins	0.021	69.2	7.5
		SAH without longitudinal fins		61.7	
5.	Sivarathinamoorthy and Sureshkannan (2021)	Double pass SAH with longitudinal fin inserts and heat storage	0.016	54.0	8.0
		Double pass SAH without longitudinal fin inserts and heat storage		46.0	
6.	Kumar and Chand (2017)	SAH with herringbone corrugated fin	0.026	56.6	20.4
		SAH without herringbone corrugated fin	0.026	36.2	
7.	Hussien and Farhan (2019)	SAH with corrugated fin inserts	0.050	86.0	33.0
		SAH with longitudinal fin inserts		53.0	

8.	El-Sebaii et al. (2011b)	Double pass V corrugated plate SAH	0.023	67.9	11.9
		Double pass finned plate SAH		56.0	
9.	Daliran and Ajabshirchi (2018)	SAH with rectangular fin inserts	0.033	55.0	22.0
		SAH with rectangular fin inserts		33.0	
10.	Abu Hamed and Alkharabsheh (2020)	SAH with aluminium fins	0.013	37.0	13.0 and 5.0 higher compared to SAH with copper coils and smooth plate
		SAH with copper coils	0.013	29.0	
		Smooth plate SAH	0.013	24.0	
11.	Singh and Vardhan (2021)	SAH with helical coil inserts	0.015	70.9	6.1
		SAH without helical coil inserts		64.8	
12.	Afshari et al. (2020)	SAH with full finned turbulator	0.015	72.0	11.3
		SAH with smooth tube		60.7	
13.	Karim and Hawlader (2006)	SAH with v grooved fins	0.056	82.0	5.0
		Flat plate SAH		77.0	

Table 4-1, Study 1, estimates the thermal and electrical efficiencies of photovoltaic thermal SAHs (PV/T SAH) with and without fins. It was found that the thermal and electrical efficiency of PV/T SAH was increased to 15.5% and 10.5%, respectively (Kumar & Rosen, 2011). Table 4-1, Study 2, found that the efficiency of SAH using a pin fin absorber was 3.0-12.0% higher compared to the flat plate SAH (Sivakumar et al., 2019). Table 4-1, Study 3, found that the addition of longitudinal fins increased the thermal efficiency of the SAH by 10.5% and 9.0% compared to the SAH without fins at a mass flow rate of 0.012 kg/s and 0.016 kg/s, respectively (F. Chabane et al., 2014). Table 4.1, Study 4, SAH fitted with a longitudinal fin had 7.5% higher thermal efficiency compared to SAH without fins (Fan et al., 2019).

Table 4-1, Study 5, evaluated the thermal efficiency of a double-pass SAH with longitudinal fins and heat storage compared to a double-pass SAH without fins and heat storage. The results

showed that the thermal efficiency of SAH with a longitudinal fin and heat storage was 8.0% higher compared to SAH without a fin and heat storage (Sivarathinamoorthy & Sureshkannan, 2021). Table 4-1, Study 6, evaluated the thermal efficiency of an SAH with herringbone corrugated fins. Results showed that the thermal efficiency increased by 20.4% when the herringbone corrugated fins were attached to the SAH absorber surface (Kumar & Chand, 2017). Table 4-1, Study 7, found that the maximum thermal efficiency of SAH with corrugated fin inserts was 33.0% higher than that of SAH with solid longitudinal fin inserts at a mass flow rate of 0.05 kg/s (Hussien & Farhan, 2019). Table 4-1, Study 8, found that the thermal efficiency of double-pass V corrugated plate SAH was 9.0 -11.9% higher than double-pass finned plate SAH for air mass flow rate ranging from 0.013-0.023 kg/s (El-Sebaii et al., 2011b).

Table 4-1, Study 9, found that the thermal efficiency of SAH with rectangular fin inserts was 18.0% higher compared to SAH without fins (Daliran & Ajabshirchi, 2018). Table 4-1, Study 10, tested a SAH with copper coil and aluminium fins. The thermal efficiency of SAH with copper coil and aluminium fins was 5.0% and 13.0% higher compared to smooth plate SAH (Abu Hamed & Alkharabsheh, 2020). Table 4-1, Study 11, showed that the addition of helical coil inserts to the evacuated tube increased its efficiency by 6.1% (Singh & Vardhan, 2021).

Table 4-1, Study 12, found that the thermal efficiency of SAH with a full-finned turbulator (like fins) was 11.7% higher compared to smooth SAH (Afshari et al., 2020). Table 4-1, Study 13, found that double-pass SAH with V-grooved fins performed 5.0% better than the flat plate SAH (Karim & Hawlader, 2006).

From studies 1-13, it can be concluded that the application of fins improved the thermal efficiency of SAHs. A study by (Hussien & Farhan, 2019). SAH with corrugated fin inserts had higher thermal efficiency (86.0%) than the other studied SAH. SAH with corrugated fin inserts performed better compared to v-groove fins. SAH with aluminium fins performed better than copper coils. It can be concluded that the fin design and material affected the thermal efficiency of SAH. Literature studies show that no study on SAHs having finned tubes integrated with corrugated fin inserts is available. Therefore, an attempt is made to estimate the thermal efficiency of SAHs with finned tubes and integrated fin inserts (treatment SAH) and compare their thermal performance with that of SAHs without fin inserts (control SAH).

4.2 Materials and methods

4.2.1 Structure of the tested FT-SAH with and without fin inserts

Sojol Pvt Ltd (NZ) developed the prototype of FT-SAH. The studied FT-SAH's length and width are 2103.0 mm and 985.8 mm, respectively. The collector height at the lower end was 211.6 mm, and the upper end was 333.8 mm, as shown in Figure 4-2.

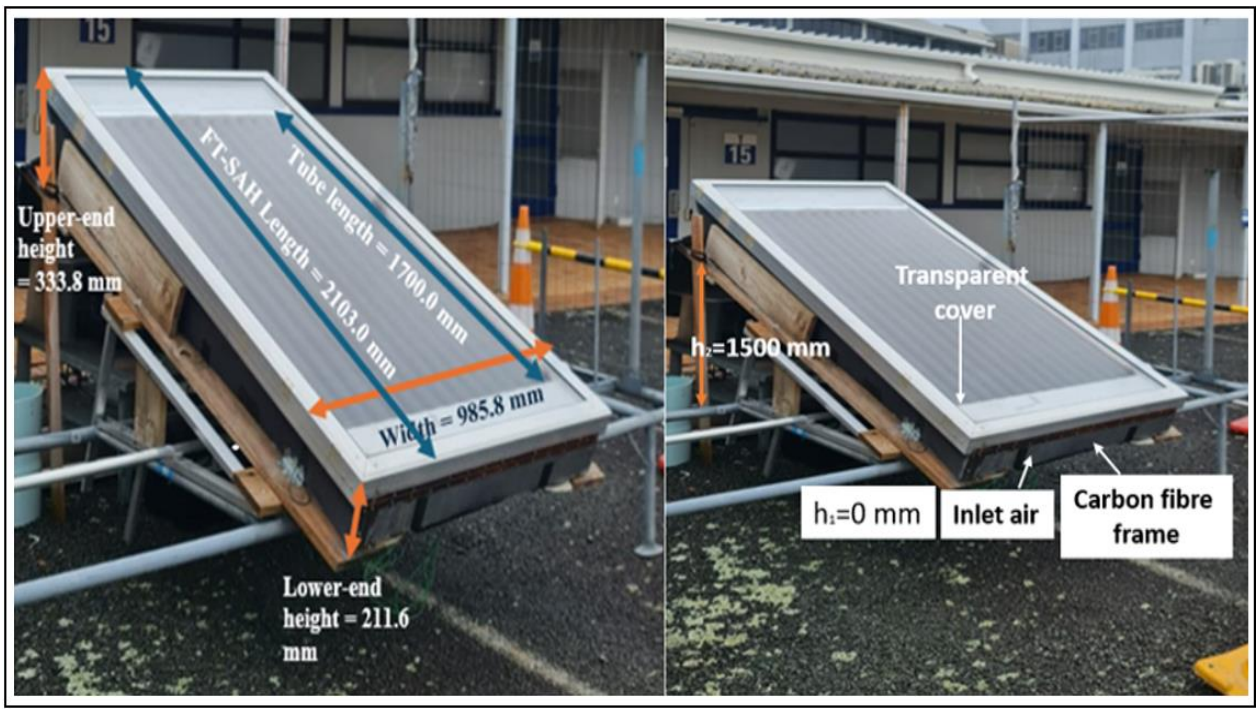

Figure 4-2 The experimental set of FT-SAH

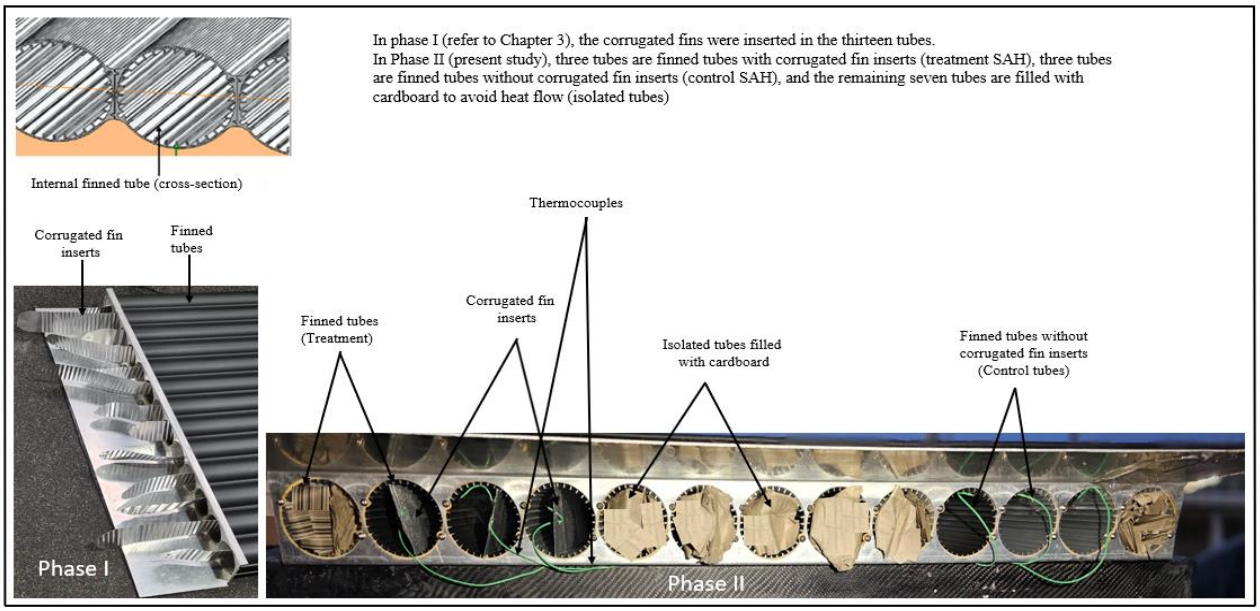

Figure 4-3 Tube setting for treatment and control SAH

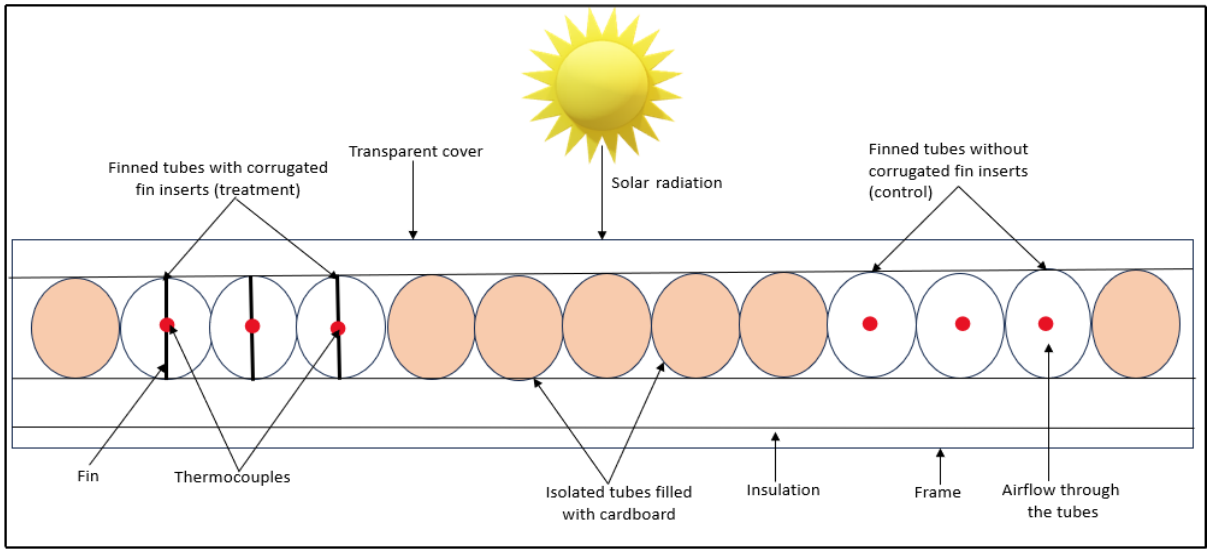

Figure 4-4 Schematic diagram of the FT-SAH

The slope was provided for optimizing the angle for solar exposure. The sides and bottom part were insulated with 50.0 mm thick glass wool (thermal conductivity = 0.0343 W/mK, R-value = 1.46 m²K/W). The insulation is provided to reduce the heat losses through the collector frame. The FT-SAH frame was made of carbon fiber and aluminium. The FT-SAH top side is covered with a 4.0 mm-thick transparent cover (tempered glass). The height between the underside of the glass and the top of the finned tubes (absorber) was 24.7 mm. The FT-SAH consisted of thirteen finned tubes with inner and outer diameters of 71.1 mm and 73.5 mm, respectively, and a length of 1700.0 mm (Figures 4-2 and 4-3). There were thirty fins along the inner periphery of the tube, and each fin's height was 2.5 mm.

The solar radiations fall on the collector cover and is then transferred to the interior of the tube by convection/conduction. The energy is transferred to the air flowing through the pipe by forced convection. The air at the outlet was drawn using a 250W variable-speed fan (AM 250, Brespalin, China). The fan can be set at 100% (high speed) and 50% maximum speed (low speed), which corresponds to a mass flow rate of 0.07 kg/s (at 100% maximum speed) and 0.019 ± 0.000 kg/s (at 50% maximum speed). The schematic diagram of the FT-SAH is shown in Figure 4-4.

4.2.2 Tube setting

This experiment aims to investigate the change in temperature increase (outlet vs. inlet) and SAH efficiency when the inserts were added to the airflow path. Due to constraints, including having only one SAH and needing to perform tests under identical outdoor conditions, the system was split into two parts: one section with fins (treatment) and another without fins (control). An insulated zone separated these two sections to reduce thermal transmittance

between them. Three of thirteen tubes were equipped with fins (treatment), three tubes had no fins (control), and the remaining seven were isolated using cardboard to avoid heat flow. Figure 4-3 shows the tube arrangement for treating and controlling SAH. There is a rubber thermal break between the tubes and the frame. A black rubber seal around the aluminium frame is provided to increase the collector's airtightness.

4.2.3 Experimental setup and test procedure

The FT-SAH thermal efficiency was tested at Massey University's Wellington campus, New Zealand (41.3016° S, 174.7761° E), from 21 December 2023 to 24 December 2023 at 50% and 100% maximum ventilator speed. The FT-SAH was mounted on a custom-made metal frame at a 20° tilt angle. The panel faced true north (at an azimuth angle of 0°). K-type thermocouples were placed at the inlet and outlet of tubes with and without fins (six tubes) to measure the change in temperature between the outlet and inlet air temperatures. Figure 4-4 shows the location of the six tubes where the 12 K-type thermocouples were installed. Two data-loggers (TC08, USB, Pico Technology, UK) with eight channels each (a total of 16 channels) were connected to a laptop to process the temperature data. A weather station (WS3085, Wi-Fi weather station, Aercus Instruments, UK) was mounted on the frame to monitor the solar irradiance (W/m^2), ambient air temperature (°C), and wind speed (m/s). The velocity (m/s) and temperature of the outlet air (°C) were measured using a hot wire anemometer (AM4214SD, Lutron Electronic Enterprise Co., Ltd., Taipei City, Taiwan). The anemometer was located at the exit of the duct. All the equipment was factory-calibrated and tested both before and after the experiment (as part of the pre- and post-fieldwork colocation process for quality assurance). The characteristics of the equipment used for the experiment are given in Table 4-2.

Table 4-2 The characteristics of the monitoring equipment

Equipment	Monitoring Parameters	Range	Accuracy
Weather station (WS3085)	Ambient air temperature (°C)	-40.0°C – 60.0°C	± 1.0°C
	Solar radiation (W/m^2)	0–3000.0 W/m^2	± 15.0%
	Wind speed (m/s)	0 – 50.0 m/s	± 1.0 m/s (speed < 5.0 m/s) ± 10.0% (speed ≥ 5.0 m/s)
K type thermocouple	Inlet and Outlet air temperature (°C)	-40.0°C+1100.0°C	± 1.0°C

hot wire anemometer AM4214SD	Outlet air velocity (m/s) Incoming air temperature from the duct (°C)	0.2–25.0 m/s	±5.0% of reading

The experiment began at 9:00 a.m. and concluded at 4:00 p.m. (New Zealand Daylight Time) each day. The rationale for selecting this time is that the solar collector could complement the ventilation in New Zealand schools (operating between 9:00 a.m. and 3:00 p.m.).

The fan was set to 100% (high speed) on 21/12/2023 and 22/12/2023, and to 50% (low speed) on 23/12/2023 and 24/12/2023. The parameters affecting the FT-SAH performance, namely solar radiation, ambient temperature, outlet temperature, and air velocity, were monitored at one-minute intervals. The average values of the monitored parameters for every 60-minute interval were calculated and used to estimate the thermal efficiency of the FT-SAH operating under high and low fan speeds.

4.2.4 Thermal efficiency calculation

The FT-SAH's thermal efficiency (η) was calculated using Equation 3.1. The effective collector area (A_c) was constant and equal to 1.18 m^2. Equation 3.1 demonstrates that the thermal efficiency (η) of the FT-SAH is a function of the air mass flow rate ($\dot{m}$), the temperature difference between outlet and inlet air (T_o-T_i), and the incident solar irradiance on the FT-SAH tilted surface (I_T), which can be written as follows as $\eta_{th} = f(\dot{m}, \Delta T, I_T)$.

The air density (ρ) and dynamic viscosity of air (μ) vary with temperature, and their values at various temperature ranges are given in Table 4-3.

Table 4-3 Air density at different air temperatures (Cengel, 2011)

Air temperature (K)	Air density (kg/m^3)	Air dynamic viscosity $x10^{-5}$ (kg/m*s)
[283.15, 293.15]	1.225	1.797
[293.15, 303.15]	1.184	1.844
[303.15, 313.15]	1.145	1.892
[313.15, 323.15]	1.109	1.938
[323.15, 333.15]	1.076	1.984
[333.15, 343.15]	1.044	2.029

4.3 Results and discussion

FT-SAH was tested in the Massey University, Wellington campus car park. The test was conducted on clear-sky days from December 21, 2023, to December 24, 2023. Due to time constraints, equipment availability, and the single-prototype design, it was not possible to repeat the experiments with individual airflow measurements during the study period. The experimental schedule was already compressed, as two sequential sets of tests (with and without fins) were conducted over a limited timeframe during which stable weather conditions were required. Additionally, only one calibrated hot-wire anemometer was available, which was used to measure the combined outlet velocity. To mitigate this limitation, airflow was carefully regulated by maintaining a constant fan setting throughout all tubes, and comparisons were made between treatment and control tubes tested under the same environmental and operational conditions. While this approach ensured consistent operating conditions, future studies should include repeated measurements of individual airflows to enhance the reliability and repeatability of efficiency calculations.

4.3.1 Ambient temperature, solar radiation, wind speed

The mean ± standard deviation (SD) values of ambient temperature and windspeed on each test day for high and low fan speed are given in Table 4-4.

At high fan speed, the daily average ambient temperature ranged from 18.0 °C to 18.9 °C, with a mean ± SD of 18.5 ± 0.6 °C. The daily average solar radiation on the tilted SAH surface ranged from 505.5 W/m^2 (minimum) to 624.7 W/m^2 (maximum) with a mean ± SD of 565.1 ± 84.3 W/m^2.

At low fan speed, the daily average ambient temperature ranged from 18.3 °C (minimum) to 19.7 °C (maximum), with a mean ± SD of 19.0 ± 1.0 °C. The daily average solar radiation on the tilted FT-SAH surface ranged from 540.6 W/m^2 (minimum) to 733.9 W/m^2 (maximum), with a mean ± SD of 637.3 ± 136.7 W/m^2.

Table 4-4: The daily average ± SD values of ambient temperature and solar radiation on each test day

Maximum speed of the ventilator	Test Day	Ambient temperature (°C)	Solar radiation on the tilted surface (W/m^2)
High speed	21/12 to 22/12/2023	18.5 ± 0.6°C	565.1 ± 84.3

Low speed	23/12 to 24/12/2023	19.0 ± 1.0 ℃	637.3 ± 136.7

4.3.2 Investigating the change in Temperature difference (outlet temperature minimum inlet temperature) between the control case (no insert) and the treatment case (insert)

Figure 4-5 shows the daily average temperature rise in control and treatment SAH at different times. Table 4.5 presents the daily average values of outlet temperature, temperature difference, and change in temperature difference between control and treatment (ΔT_1).

Figure 4-5 compares the performance of control and treatment SAH and the notable time lag in temperature response. In the case of the treatment SAH, the outlet temperature continued to increase slightly after peak solar radiation before gradually declining. This apparent delay is likely influenced by the one-hour averaging interval, which can smooth out short-term variations and shift the temperature peak relative to solar input. Nevertheless, the trend suggests that the treatment SAH retains heat for longer than the control, consistent with the enhanced heat-transfer area and greater thermal mass provided by the fin inserts. By contrast, the control SAH showed a more direct relationship between outlet temperature and solar radiation, suggesting a lower heat retention capacity. The fin inserts increase the system's thermal mass and heat retention, causing a lag between solar radiation and temperature peaks, ultimately resulting in better overall heat capture and transfer. These results strongly agree with the results of (Reardon et al., 2020) and (Mostafavi, 2022).

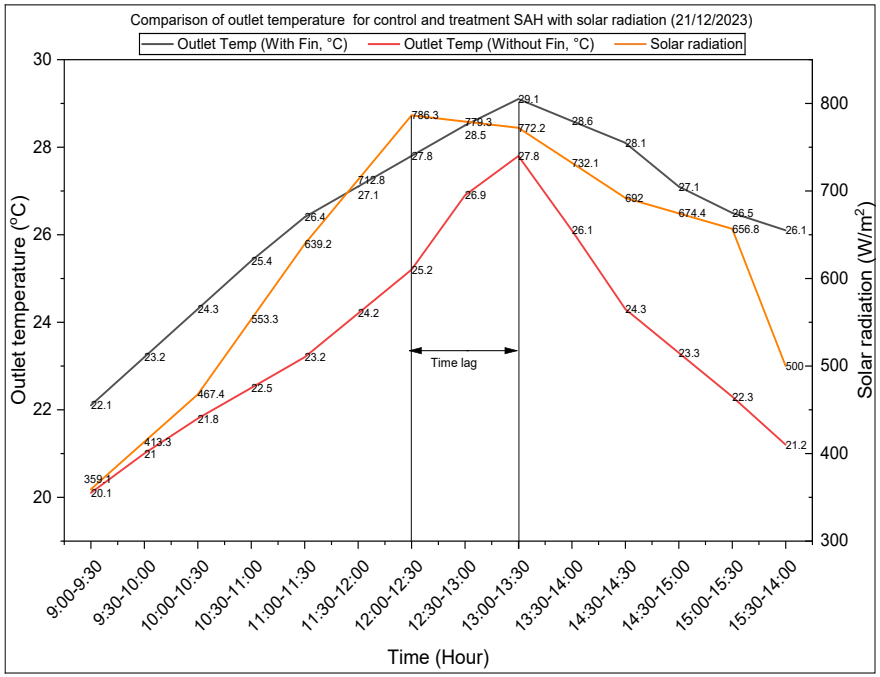

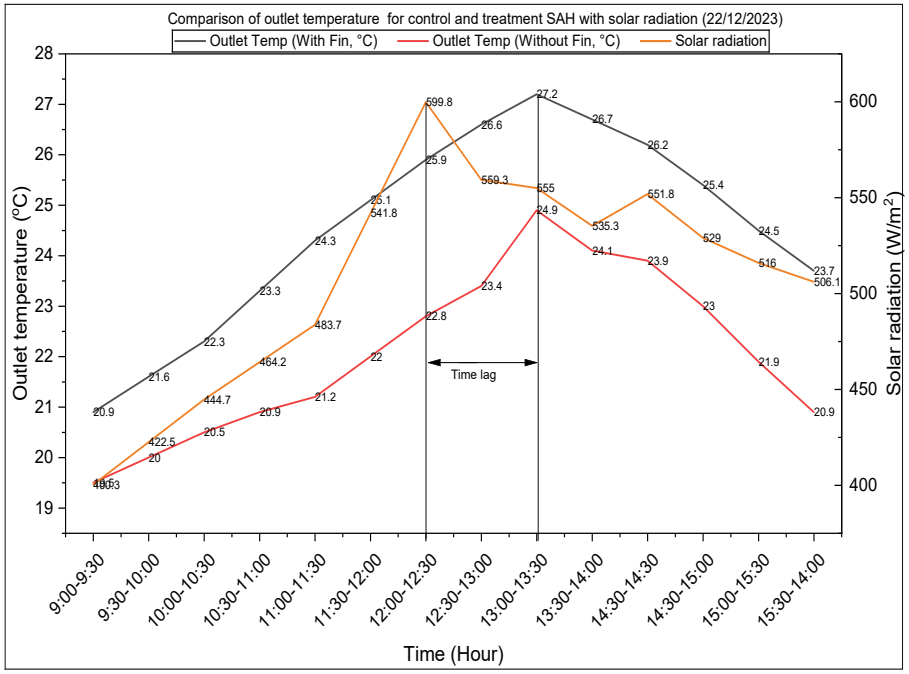

Figure 4-5 Comparison of outlet temperature for control and treatment SAH with solar radiation operating at high fan speed (21/12/2023 and 22/12/2023)

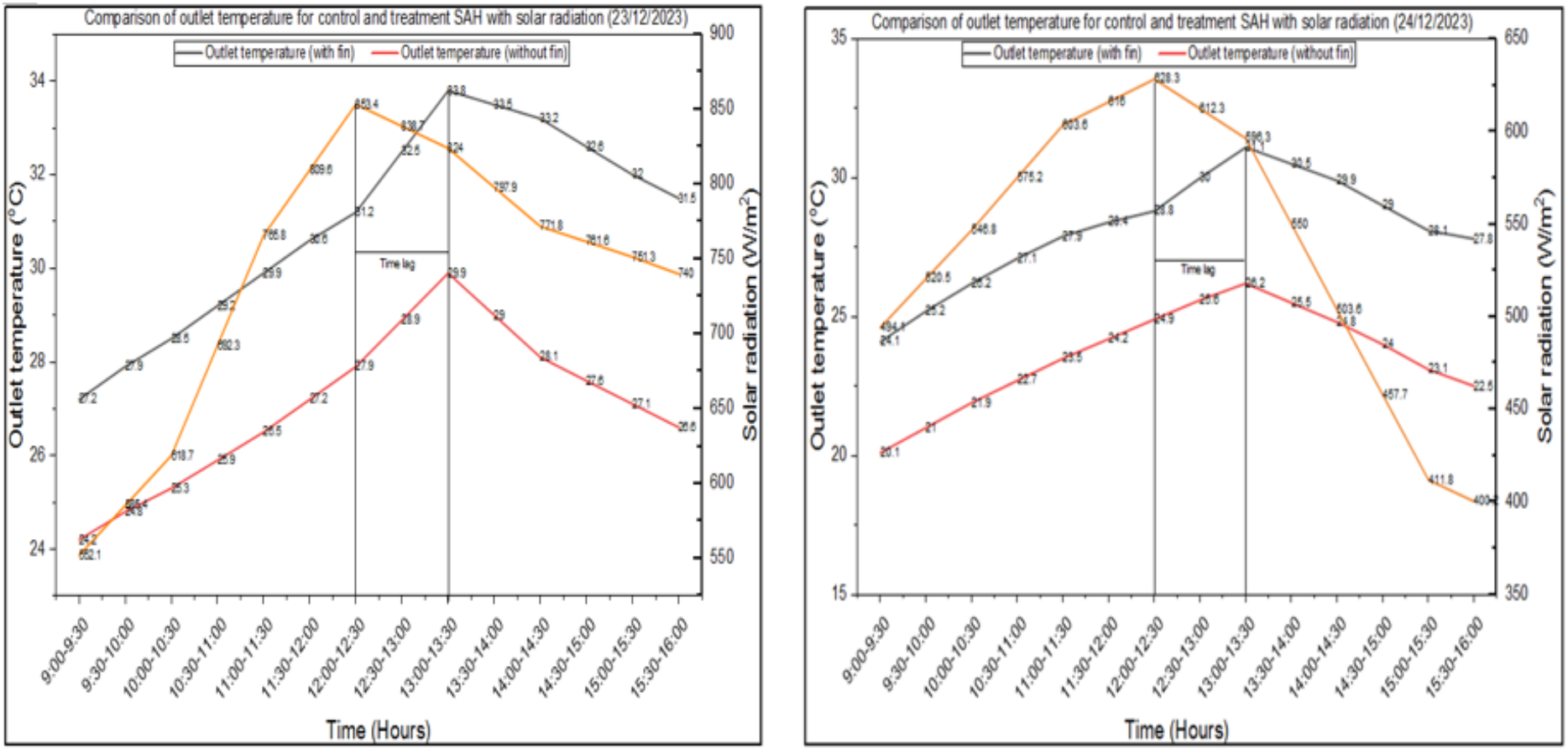

Figure 4-6 Comparison of outlet temperature for control and treatment SAH with solar radiation operating at low fan speed (23/12/2023 and 24/12/2023)

Tables 4-5 and 4-6 compare the thermal performance of control and treatment SAH under high and low fan speeds. The treatment SAH performs better in both cases, with higher outlet temperatures (T_o) and more significant temperature differences (ΔT) than the control system.

Table 4-5 The daily average values of T_o, T_a, ΔT, and ΔT_1 for control SAH operating at high speed

Fan speed	SAH type	T_o (°C)	$T_a=T_i$ (°C)	$\Delta T= T_o - T_a$ (°C)	$\Delta T_1 = \Delta T_{treatment} - \Delta T_{control}$ (°C)
High speed ($\dot{m}$ = 0.07 kg/s)	Control	22.3	18.5	4.4	NA
	Treatment	25.4	18.5	7.0	2.6

Under high-speed operation, the control SAH has an outlet air temperature of 22.3°C and a temperature difference of 4.4°C between the inlet and outlet air. In contrast, the treatment SAH shows a higher outlet temperature of 25.4°C and a temperature difference of 7.0°C. The improvement due to the treatment is reflected in the value of ΔT_1, which indicates a 2.6 °C increase in temperature compared to the control system.

Table 4-6 The daily average values of T_o, T_a, ΔT, and $\Delta T1$ for control SAH operating at low speed

Fan speed	SAH type	T_o (°C)	$T_a=T_i$ (°C)	$\Delta T= T_o - T_a$ (°C)	$\Delta T_1 = \Delta T_{treatment} - \Delta T_{control}$ (°C)
Low ($\dot{m}$ = 0.04 kg/s)	Control	25.3	19.0	6.3	NA
	Treatment	29.4	19.0	10.4	4.1

At low fan speeds, the differences are even more pronounced. The control SAH exhibits a daily average outlet temperature of 25.3°C and a daily average temperature difference of 6.3°C. However, the treatment SAH achieves a higher daily average outlet temperature of 29.4°C, resulting in a significant daily average temperature difference of 10.4°C. The ΔT_1 for low-speed operation is 4.1°C, indicating a greater performance improvement than for high-speed operation.

The observed improvement in the treatment SAH's performance was likely due to enhanced heat transfer mechanisms, possibly due to modifications or artificial roughness applied to the system. These modifications could increase turbulence in the airflow, improving the heat exchange between the air and the heated surfaces of the SAH. The effect is more pronounced at lower fan speeds, where slower air movement allows for more efficient heat absorption, leading to a more significant temperature increase. At higher fan speeds, while the system still performs better than the control, the reduced residence time of air in the system may limit the extent of heat transfer, resulting in a marginal relative improvement.

4.3.3 Ventilation rate

The air velocity through the ducts was measured as a combined value rather than separately for control and treatment SAH. This limits the ability to fully understand how the control and treatment systems differ in thermal performance, making it challenging to attribute the observed ventilation rates (211.7 m^3/h for control and 123.5 m^3/h for treatment) directly to the structural differences between the SAHs. The daily average ventilation rates for control and treatment SAH operating at high fan speed were 211.7 m^3/h and 123.5 m^3/h, respectively. The restricted airflow (in seven tubes) generated turbulence. This turbulence can create vibrations and acoustic disturbances, leading to a noisy fan. However, the results show that the SAH alone is insufficient to ventilate the classroom; therefore, multiple SAHs would be needed.

4.3.4 Thermal efficiency of FT-SAH

The thermal efficiency of the SAH is calculated using Equation 3.1 (Section 3). The average mean (± SD) values of thermal efficiency for the control and treatment SAH were 44.5 ± 2.8% and 72.6 ± 3.9%, respectively. The average mean (± SD) values of thermal efficiency for the control and treatment SAH were 33.4 ± 0.6% and 57.0 ± 7.6%, respectively.

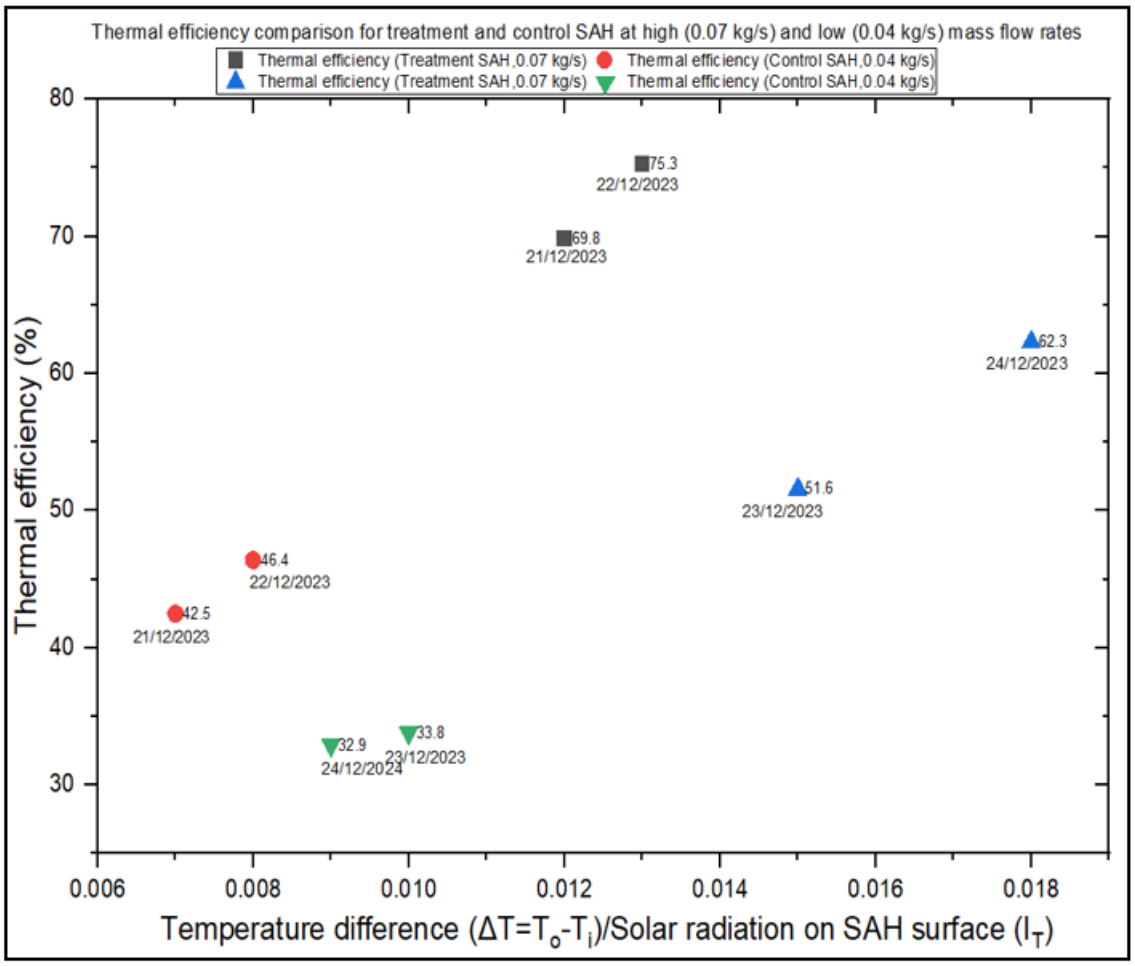

Figure 4-7 Thermal efficiency comparison for treatment and control SAH at high (0.07 kg/s) and low (0.04 kg/s) mass flow rates

Figure 4-7 compares the thermal efficiency of the treatment and control SAHs at two representative mass flow rates (0.07 kg/s and 0.04 kg/s), plotted against the ratio of temperature difference to solar radiation on the collector surface ($\Delta T/I_T$). The results demonstrate that thermal efficiency increases with the $\Delta T/I_T$ ratio, and that the treatment SAH consistently outperformed the control at both tested flow rates. At the higher mass flow rate of 0.07 kg/s, the treatment SAH achieved a maximum thermal efficiency of 75.3% (22 December 2023), compared to 46.4% for the control on the same day. This substantial difference highlights the positive effect of fins and surface modifications, which improve the effective heat transfer area. Increased airflow at higher flow rates also enhances the convective heat transfer coefficient, enabling more effective heat exchange. This observation aligns with previous studies by Karwa (2023) and Ghritlahre et al. (2020).

At the lower mass flow rate of 0.04 kg/s, both systems showed reduced efficiency. On 24 December 2023, the treatment SAH reached 62.3%, while the control peaked at 32.9%. The lower efficiencies reflect reduced convective heat transfer at slower air velocities, consistent

with observations by Saleh Abo-Elfadl et al. (2021), who noted that lower flow rates increase residence time but reduce the rate of heat removal, allowing losses to dominate. Figure 4-7 shows thermal efficiency increases with the $\Delta T/I_T$ ratio, regardless of flow rate. This relationship occurs because, as the $\Delta T/I_T$ ratio increases, the system can harness more of the available thermal energy. Systems that maximize this ratio show greater efficiency in converting solar energy into proper heat. The treatment SAH's superior performance at both flow rates can be attributed to design modifications, possibly involving surface roughness or fin enhancements, which increase the effective surface area for heat exchange. Studies such as those by Singh et al. (2022) and Rajendran et al. (2022) have demonstrated that incorporating artificial roughness into SAHs can significantly enhance heat transfer by disrupting the boundary layer and promoting turbulence, thereby improving convective heat transfer. The maximum thermal efficiency of evacuated tube SAH with helical fin inserts was 70.9% at a mass flow rate of 0.015 kg/s (Singh & Vardhan, 2021). The maximum thermal efficiency of rectangular duct SAH integrated with a wavy fin was 85.0% (CJ Thomas Renald et al., 2022). The SAH with V corrugated absorber had a maximum thermal efficiency of 57% at a mass flow rate of 0.02 kg/s (El-Sebaii et al., 2011a). The highest thermal efficiency of SAH with corrugated metal foam fins was 86.0% (Hussien & Farhan, 2019). The studies show that the thermal efficiency of SAHs with fin inserts is higher than that of SAHs without them. The present study's thermal efficiency was higher than that of other researchers.

In summary, Figure 4-7 shows that both airflow rate and system modifications significantly affect thermal efficiency. Higher flow rates improved efficiency in both systems, but the treatment SAH consistently achieved higher values due to its enhanced heat transfer area and thermal mass. The findings are consistent with prior literature on fin-enhanced SAHs, confirming the effectiveness of the treatment design in improving thermal performance.

4.4 Conclusion and future scope

The FT-SAH underwent testing at the Massey University, Wellington Campus car park, from December 21, 2023, to December 24, 2023, under clear-sky conditions. Through experimentation, researchers observed that integrating artificial roughness can enhance the collector's thermal performance. The study involved the use of a finned tube (FT-SAH) equipped with corrugated fins, comprising thirteen such tubes. Among these, three tubes were outfitted with corrugated fin inserts (treatment SAH), while another three lacked fin inserts (control). The rest were segregated by cardboard filling. The incorporation of fin inserts increased surface area and facilitated heat transfer. Subsequent calculations involved

determining the temperature differential between the outlet and inlet air and assessing thermal efficiency. The primary objective of the research was to investigate the impact of fin addition on the thermal performance of the mentioned SAHs. The findings from the study are as follows:

1) The treatment SAH with fin inserts significantly improved thermal efficiency compared to the control system. At high mass flow rates (0.07 kg/s), the treatment SAH achieved a peak thermal efficiency of 75.3%, compared to the control SAH's maximum of 46.4%. At low mass flow rates (0.04 kg/s), the treatment SAH outperformed the control with 62.3% efficiency, compared to 32.9% for the control system. These results show that efficiency increases positively with increasing mass flow rate.
2) The temperature difference between the inlet and outlet air was consistently lower for the control SAH, which did not have fin inserts. It showed a temperature difference of 4.4 °C during high-speed operation, and at lower speeds, this difference increased slightly to 6.3 °C. The treatment SAH, equipped with fin inserts, exhibited a much higher temperature difference due to improved heat transfer. The treatment SAH achieved a temperature difference of 7.0°C at high-speed operation, which increased significantly to 10.4°C during low-speed operation. These results demonstrate the effectiveness of fin inserts in enhancing heat transfer and improving system performance.
3) The fin inserts increase the system's thermal mass and heat retention capacity, causing a lag between solar radiation and temperature peaks, ultimately resulting in better heat capture and transfer.
4) While both control and treatment SAH demonstrated improved thermal performance, it was insufficient for standalone ventilation based on the Ministry of Education (MOE) guidelines. To meet adequate ventilation standards, multiple SAH units would be required, increasing the cost and the roof space needed for installation.

4.5 Limitation

The experiment took place on Massey University's campus car park. It is necessary to perform on-site testing of the FT-SAH installed on the rooftop of a building. The length of the duct adversely affects the thermal efficiency and the temperature of the air expelled from the SAH. However, these factors have not been considered in the scope of this research. A study by (Wang, 2020) reported a 30.0% drop in the efficiency of SAH when the duct length was increased from 0.5 m to 5.0 m, and sensors were placed 5.0 m away from the SAH.

The isolated tubes were filled with cardboard to avoid heat transfer between them. Monitoring the temperature of the isolated tubes to ensure no heat transfer is occurring is essential, but this study has not considered it.

While experimenting, the air velocity through the ducts was measured as a single value, meaning airflow in the finned and non-finned sections was combined rather than assessed separately for each zone. This presents a limitation, as it is challenging to determine the exact airflow behaviour and its direct influence on thermal performance within the finned and non-finned sections.

In conclusion, the treatment SAH with fin inserts significantly outperformed the control SAH (without fins), demonstrating enhanced thermal efficiency and improved heat transfer. However, to meet the Ministry of Education's ventilation standards, multiple SAH units would need to be installed, increasing roof space requirements and overall costs. Despite this, the studied SAH can serve as a valuable supplementary source of heating and ventilation for classrooms.

The next chapter will focus on the thermal performance of nanocoated tubes, a technique with great potential to improve SAH performance. Nanocoating can enhance the system's heat absorption and transfer, making it an important area for future improvements.

5 Experimental investigation of the thermal performance of uncoated and nanocoated tubes

Preamble:

Chapter 4 demonstrated that SAH performance is highly sensitive to weather variability, particularly solar irradiance, ambient air temperature, and their interactions with the air mass flow rate supplied to the tubes. The analysis revealed that outlet temperature and ΔT fluctuated substantially even within a single day, with strong dependence on passing clouds, irradiance peaks, and diurnal temperature changes. These findings make it clear that outdoor SAH performance cannot be fully controlled and will always reflect short-term atmospheric variability.

These observations directly inform the interpretation of the experimental results presented in Chapter 5. Because the prototype was tested under real outdoor conditions, variations in solar irradiance and ambient temperature inevitably influenced the observed thermal response. Consequently, differences between experimental runs may partly reflect environmental fluctuations rather than coating or fin effects alone. While Chapter 5 focuses on isolating coating and fin influences through a simplified experimental rig, these experiments still inherit the natural variability highlighted in Chapter 4.

The implications are two-fold:

1. Limitations in Repeatability:
   The experiments cannot be repeated under identical atmospheric conditions, meaning absolute values (e.g., outlet temperature in °C) are subject to weather-driven variability. Measurement uncertainties combined with irradiance variability add further complexity.
2. Confidence in Trends Rather Than Exact Values:
   Although the experiment cannot provide laboratory-grade repeatability, it can provide reliable comparative trends. Consistent directional patterns (coated vs. uncoated, finned vs. unfinned) across multiple days support the validity of performance differences despite environmental variability.

By acknowledging these limitations upfront, Chapter 5 positions its findings appropriately: as trend-based comparative insights into how nanofluid coatings and fin inserts influence tube-level thermal behaviour, rather than as exact reproducible results expected from controlled indoor laboratory conditions.

Recent advancements in nanotechnology have opened up new possibilities for enhancing the efficiency of SAHs. Nanofluids—suspensions of nanoparticles in base fluids have shown great promise in improving the thermal performance of SAHs due to their superior thermophysical properties (Said et al., 2015). One approach that has gained attention is the application of nanocoatings on the absorber surfaces of SAHs, which can significantly improve thermal conductivity and heat transfer rates. In particular, aluminium oxide (Al_2O_3) and copper oxide (CuO) have emerged as effective nanomaterials for this purpose due to their favourable thermal and mechanical properties (Mazzei & Rodrigues, 2000; Zhang et al., 2014).

Chapter 2 explored the potential applications of Al_2O_3 and CuO in solar thermal systems, highlighting their widespread availability, cost-effectiveness, and properties that enhance efficiency. Al_2O_3 offers high thermal stability and resistance to oxidation, while CuO's high absorption coefficient makes it ideal for solar energy conversion. Recent studies have shown that nanocoating solar absorbers with these materials can significantly improve their performance (Khanlari et al., 2022; Robert et al., 2018).

This chapter expands on this concept by incorporating fin inserts into nanocoated aluminium tubes. As highlighted by Al-Kayiem et al. (2021), fin inserts increase the heat transfer area, and when combined with nanocoatings, they are expected to provide synergistic improvements in thermal efficiency. Compared to control and black paint-coated tubes, the study presents experimental results that quantify the thermal efficiency and outlet temperature of tubes coated with Al_2O_3 and CuO nanoparticles. The added effect of fin inserts is also examined to assess their impact on overall thermal performance.

The experimental results of this chapter revealed that tubes coated with 4% Al_2O_3/black paint achieved the highest thermal efficiency and outlet air temperature. The daily average thermal efficiency of Al_2O_3-coated tubes ranged from 35.2% to 79.1%, outperforming the CuO-coated tubes, which ranged from 25.2% to 63.2%. Furthermore, the outlet temperature of the 4% Al_2O_3-coated tubes reached 65.0 $^{\circ}$C, significantly higher than that of the other configurations. However, the ventilation rate in this study remained lower than the recommended standards, highlighting the need for further optimization.

This chapter is organized into five sections. Section 5.1 provides an overview of the chapter's objectives, while Section 5.2 outlines the experimental methods. Section 5.3 discusses the materials and procedures used in the study. In Section 5.4, the results are analyzed, and the thermal performance of the different tube configurations is compared. Finally, Section 5.5 concludes the chapter, summarizing the key findings and proposing directions for future research. The results of this study will contribute to the broader field of solar thermal

technology, offering valuable insights into the practical applications of nanocoatings and fin inserts in enhancing SAH efficiency.

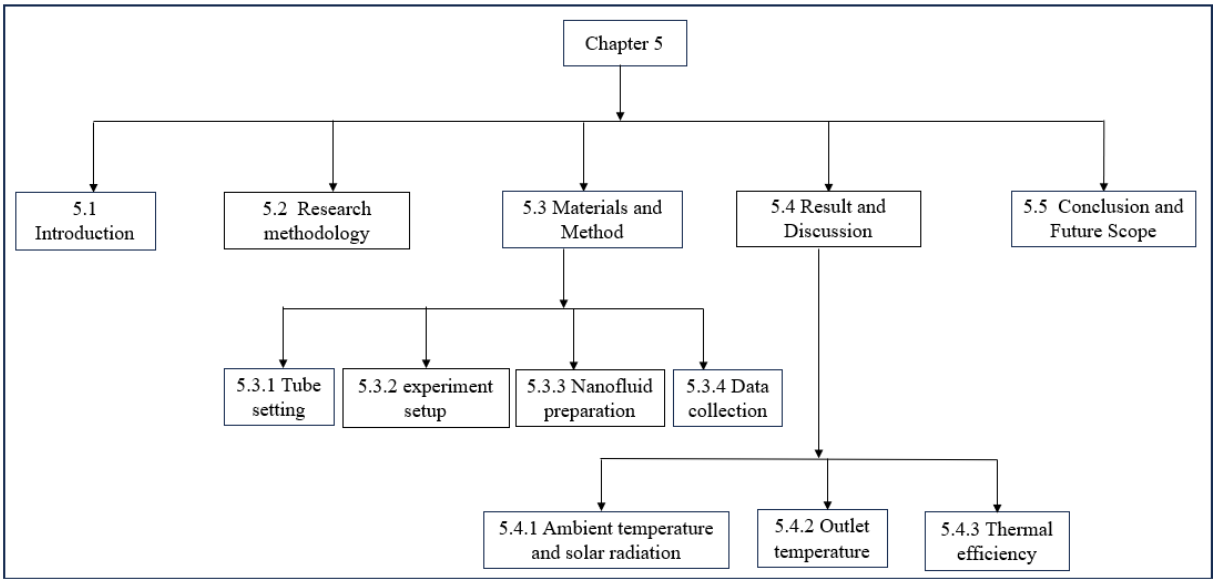

Figure 5-1 chapter 4 framework

5.1 Introduction

Nanocoating the absorber surface is one of the most effective methods for enhancing the thermal efficiency of SAHs (Kabeel, Omara, et al., 2017). Studies discussed in Chapter 2 have demonstrated that Al_2O_3 and CuO can effectively coat the absorber surfaces of SAHs, thereby enhancing their thermal performance. This section provides a brief overview of research conducted on nanocoated SAHs.

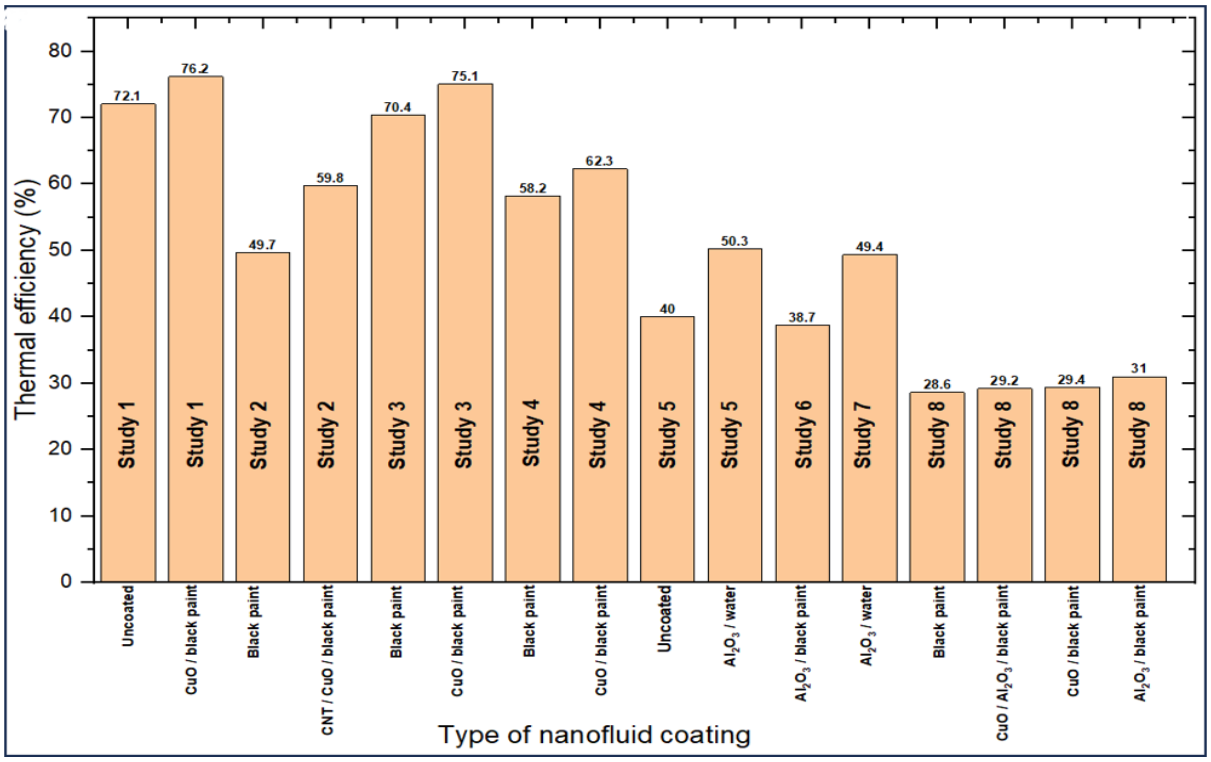

Figure 5-2 Studies on nanofluid-coated solar collectors

A vertical SAH, both with and without a nanocoated absorber surface, was tested to evaluate its thermal efficiency (Figure 5-2, Study 1). The results demonstrated that the thermal efficiency of an SAH with CuO/black paint coating was 3.1% to 4.1% higher than that of an uncoated SAH, with a mass flow rate varying between 0.012 kg/s and 0.020 kg/s (Khanlari et al., 2022). In a separate study (Figure 5-2, Study 2), an SAH coated with a mixture of 4% carbon nanotubes and copper oxide (CuO) dispersed in black paint showed a 10.1% improvement in thermal efficiency compared to an SAH coated only with black paint (Abdelkader et al., 2020). Additionally, a triple-flow solar air collector with a CuO/black paint coating (Figure 5-2, Study 3) exhibited 4.7% greater thermal efficiency than a collector coated only with black paint (Selimefendigil et al., 2022).

The effect of increasing the CuO concentration on the efficiency of a solar dryer has also been explored. Sivakumar et al. (2020) found that the solar dryer's efficiency improved by 7.3% when using a 0.04% CuO/black paint nanocoating compared to a 0.02% CuO/black paint coating and by 4.1% compared to conventional black paint (Figure 5-2, Study 4). The CuO nanocoated collector absorbed 5.3% more solar energy than a black paint-coated collector.

Studies have also explored the use of Al_2O_3 nanofluid in enhancing the thermal conductivity and heat transfer properties of base fluids (Robert et al., 2018; Tyagi et al., 2012). In one experiment (Figure 5-2, Study 5), applying a 0.02% Al_2O_3 nanofluid coating on a solar collector

increased its efficiency by 3.6% compared to an uncoated collector (Gupta et al., 2021). Another study (Figure 5-2, Study 6) demonstrated that coating the bottom part of a solar still with Al_2O_3 in black paint increased its thermal efficiency by 38.7% (Manoj Kumar Sain & Kumawat, 2015).

(Figure 5.2, Study 7) showed that adding Al_2O_3 to water as a base fluid in a solar water heater increased the collector's efficiency from 49.0% to 56.0%, a result attributed to the improved heat transfer properties of the nanofluid (El-Said et al., 2016). Another experiment (Figure 5.2, Study 8) demonstrated that using Al_2O_3/acetone as the working fluid boosted the solar collector's thermal efficiency by 11.1% (Eidan et al., 2023).

In addition to these individual nanoparticle applications, hybrid nanofluids, mixtures of two or more nanoparticles, have also been studied for their potential to enhance the thermal properties of the base fluid. However, a study by (Al-Kayiem et al., 2021) found that the resulting thermal conductivity decreased when CuO and Al_2O_3 were combined in black paint. This study tested five different absorbing tubes: one uncoated and four coated with black paint, CuO/black paint, Al_2O_3/black paint, and a mixture of CuO and Al_2O_3 in black paint. The results (Figure 5.2, Study 9) showed an average efficiency improvement of 44.9% for black paint, 51.0% for Al_2O_3-black paint, 42.2% for CuO-black paint, and 39.8% for the CuO/Al_2O_3/black paint hybrid.

The literature consistently reports that Al_2O_3-based nanofluid coatings exhibit higher thermal conductivity than CuO when combined with plain black paint, thereby enhancing the thermal performance of solar collectors. Building on these insights, Chapters 2 and 3 demonstrated that the addition of fins to absorber tubes further enhances the thermal efficiency of SAHs by increasing the heat transfer surface area. In this chapter, the combined effect of Al_2O_3 nanofluid coatings and corrugated fin inserts is evaluated for aluminium tubes used in SAHs. This assessment aims to determine whether the integration of nanofluid-based coatings with finned-tube configurations can deliver synergistic improvements in thermal efficiency and overall system performance.

5.2 Research Methodology

The first step was a literature study identifying the nanocoating material and the nanofluid preparation process. The second step was preparing and applying the nanofluid coating to the tube surface. The third step was experimental setup and data collection. The last step was data interpretation, estimating the thermal efficiency, and recommending the best suitable nanocoating material for designing SAHs. The research process is illustrated in Figure 5-3.

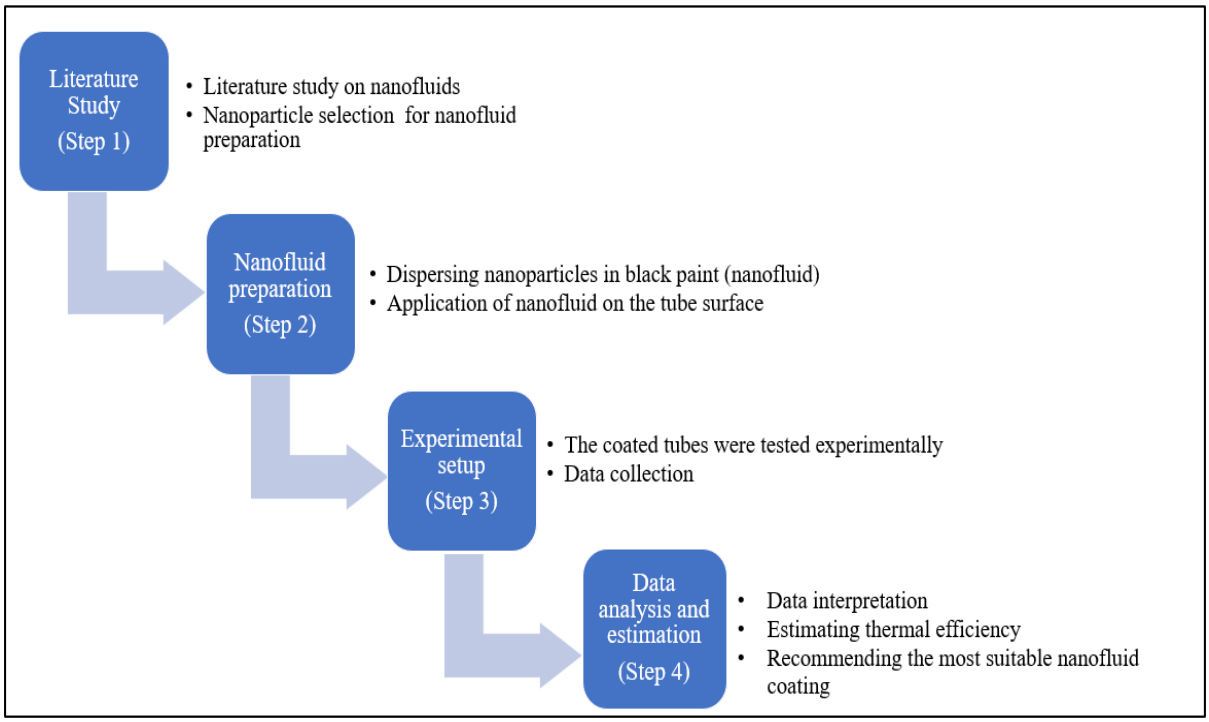

Figure 5-3 Research process for experimental test results of nanocoated tube

In step 3 (experimental setup), four experimental tests were conducted, and the overview of the experimental tests is presented in Table 5-1.

- Test 1: experimental test on control (uncoated) tubes, black paint-coated tubes, and tubes coated with 1%, 2%, 3%, and 4% Al_2O_3 in plain black paint.
- Test 2: experimental test on control tubes, black paint-coated tubes, and tubes coated with 1%, 2%, 3%, and 4% CuO/ black paint.
- Test 3: Experiment test on control tube with fin, black paint-coated tube with fin, 1%, 2%, 3%, and 4% Al_2O_3/black paint-coated tube with fin.
- Test 4: Experiment test on control tube with fin, black paint-coated tube with fin, 1%, 2%, 3%, and 4% CuO/black paint-coated tube with fin.

Table 5-1 Overview of experimental tests for control, black paint coating, and nanocoated tubes with and without fins

Test	Control Tube	Black Paint Coated Tube	1% Al2O3 in Black Paint	2% Al2O3 in Black Paint	3% Al2O3 in Black Paint	4% Al2O3 in Black Paint	1% CuO in Black Paint	2% CuO in Black Paint	3% CuO in Black Paint	4% CuO in Black Paint
Test 1 (14/11/2023 to 21/11/2023)	Y	Y	Y	Y	Y	Y	-	-	-	-
Test 2 (22/11/2023 to (24/11/2023)	Y	Y	-	-	-	-	Y	Y	Y	Y
Test 3 (27/11/2023)	Y (with fin)	Y (with fin)	Y (with fin)	Y (with fin)	Y (with fin)	Y (with fin)	-	-	-	-
Test 4 (29/11/2023)	Y (with fin)	Y (with fin)	-	-	-	-	Y (with fin)	Y (with fin))	Y (with fin))	Y (with fin)

Note:

- Y indicates that the tube was tested in the given configuration (e.g., control tube, black paint, or specific nano coating).
- (-) indicates that the tube was not tested in this configuratio

5.3 Materials and Methods

The experimental setup in Chapter 5 was designed as a practical, low-cost platform to investigate the effect of Al_2O_3 and CuO nanofluid coatings on the thermal performance of aluminium tubes, both with and without fin inserts.

5.3.1 Tubes setting

We used ten aluminium tubes of length 1700 mm with an inner diameter and outer diameter of 72 mm and 75 mm, respectively. One tube was an uncoated smooth tube (control tube), and the other nine aluminium tubes were coated with lumbersider matt black paint (Resene paints, NZ)), 1%, 2%, 3%, and 4% Al_2O_3/black paint, 1%, 2%, 3%, and 4% CuO/black paint. The experiment was conducted in four sets, as shown in Table 5-1 The details of the paint and nanoparticles are presented in Table 5-2.

5.3.2 Experimental setup

The tubes were mounted on a custom-made galvanized metal frame at an angle of 20° as shown in Figure 5-4. The spacing of 500 mm between tubes was chosen to avoid cross-contamination of thermal fields, allowing each tube to be studied as an independent unit. The collector frame was deliberately designed without glazing, insulation, or ducting to isolate the effect of surface coatings on heat absorption and transfer. While this configuration allowed direct evaluation of the influence of nanocoatings on thermal performance, the absence of glazing and insulation means the results represent an idealized tube-level response rather than the behavior of a complete, commercially viable SAH.

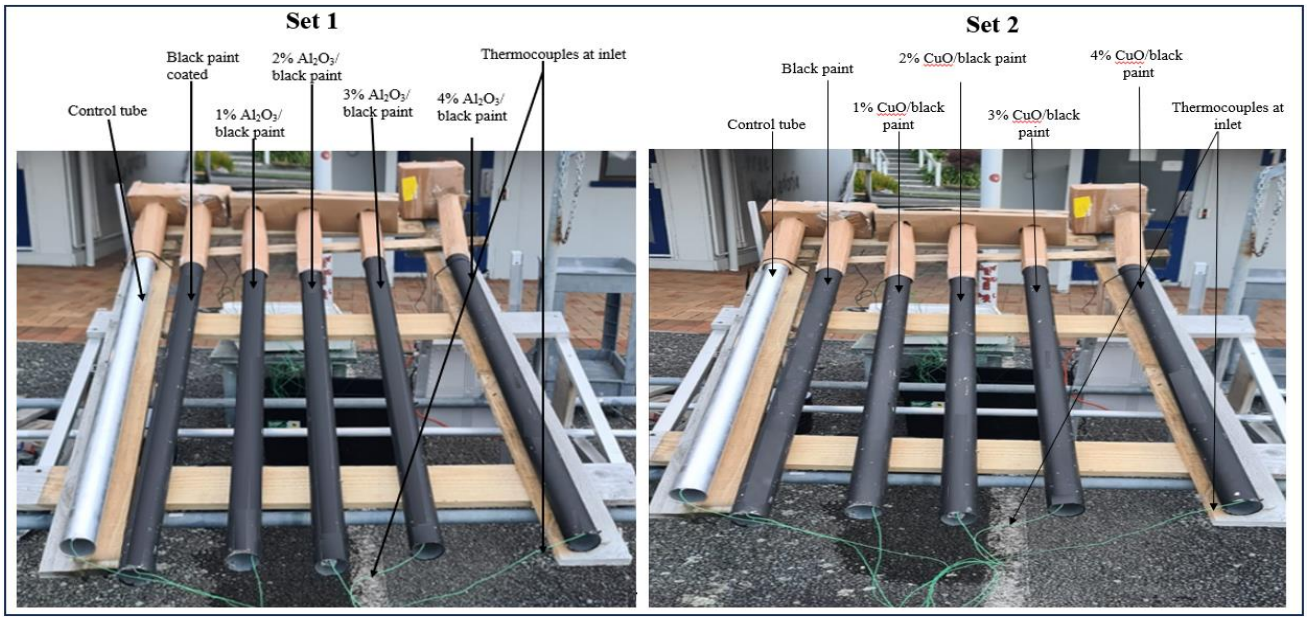

Figure 5-4 Experimental set of control and modified tubes

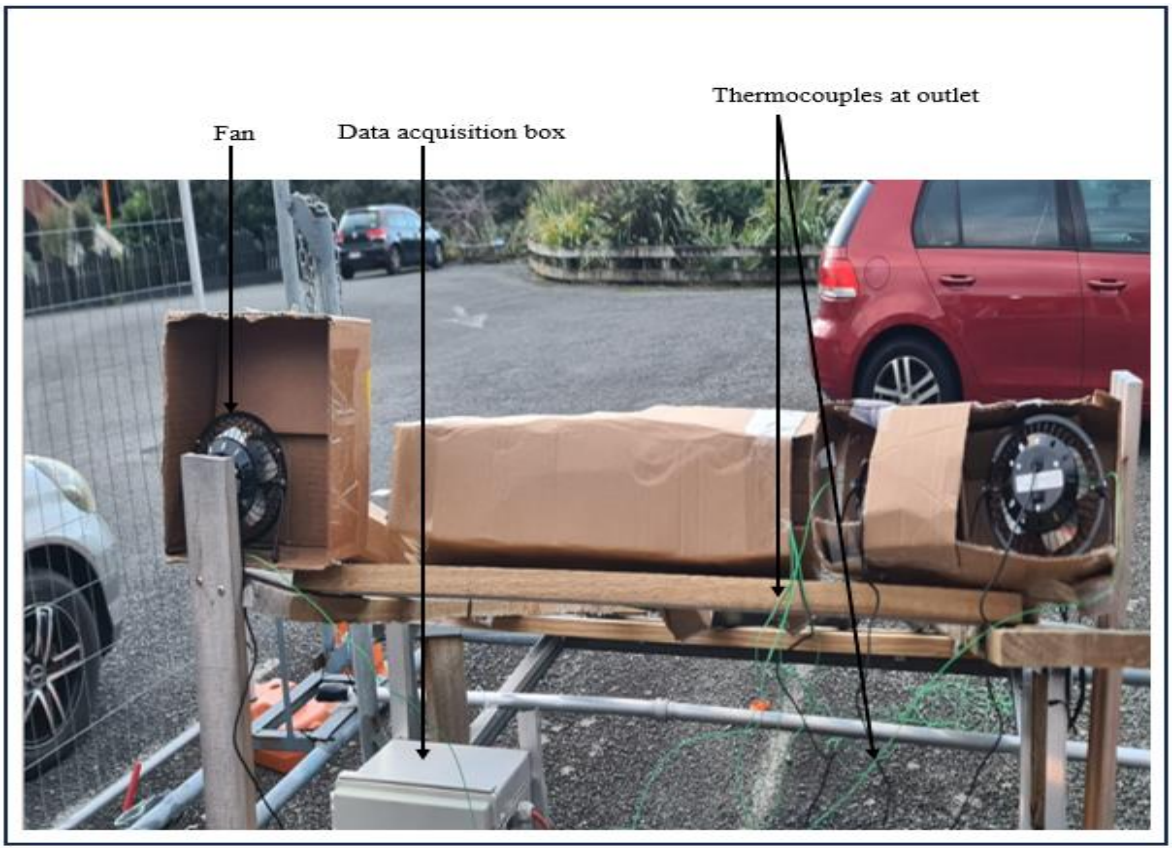

Figure 5-5 Experimental setup of data acquisition and outlet system

The experiment was conducted at the car park of Massey University's Wellington campus, New Zealand (41.3016° S, 174.7761° E), from 9:00 am to 4:00 pm (New Zealand Daylight Time) over six days. The tube's surface absorbs solar energy, which is then transferred to the interior of the tube by conduction. The energy is transferred to the air flowing through the pipe by forced convection. A minimum USB cable connected a table fan (100 mm diameter) with a rated power of 2W (Living & Co, China) to pull air out from the tube exit. The airflow rate throughout the experiment was maintained at 0.003 kg/s to ensure that all tubes were tested under identical flow conditions, allowing for relative comparisons. The fan setting and data acquisition box are shown in Figure 5-5.

5.3.3 Nanofluid preparation

Figure 5-6 and Table 5-2 shows the materials and equipment used to prepare Al_2O_3/black paint and CuO/black paint.

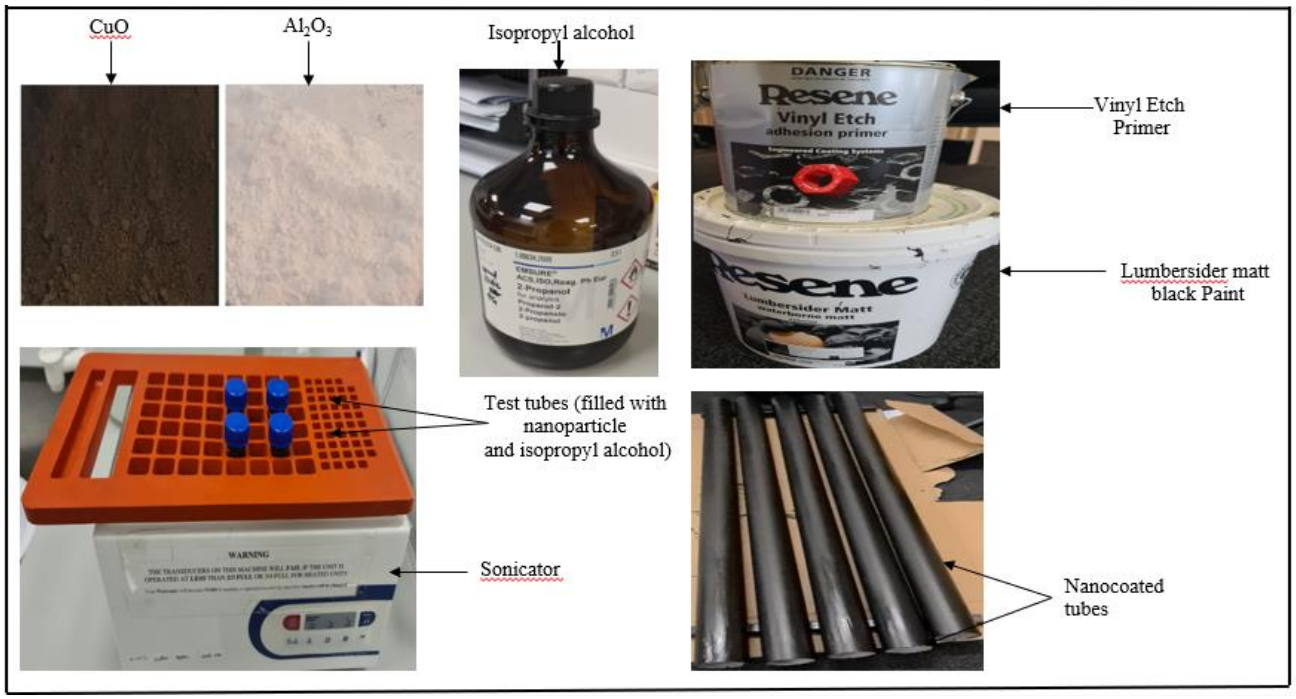

Figure 5-6 The materials used and setup of the test tube and sonicator bath

Al_2O_3 and CuO nanoparticles (SkySpring Nanomaterials, Inc, USA) cannot be dispersed directly into the paint as they form lumps. Therefore, the nanoparticles were first dispersed in isopropyl alcohol (IPA) and mixed in black paint. The nanofluid preparation process is given in Figure 5-8. In this experiment, the nanofluid was prepared in two batches (i.e., in the first batch, Al_2O_3/black paint, and in the second batch, CuO/black paint was prepared). This nanofluid was then coated on the tubes to perform Tests 1 through 4.

Table 5-2 shows the properties of Al_2O_3, CuO nanoparticles, and Lumberside matt black paint

Property	**Al_2O_3 nanoparticle**	**CuO Nanoparticle**	**Lumbersider matt black paint**
Material provider	(SkySpring Nanomaterials, Inc, USA)	(SkySpring Nanomaterials, Inc, USA)	(Sponsored by Resene Paints, NZ)
Purity (%)	99.0%	99.0+%	Not available
Particle size (Nm)	40.0	<100.0	Not available
Colour	White	Metallic brown	Matt black
Thermal conductivity (W/m.K)	30.0	13.0	Not available

Viscosity	Not available	Not available	1000.0-2000.0 Centistokes
Relative density	Not available	Not available	1.2-1.4

5.3.4 Nanofluid preparation process

In the first step, the nanoparticles (Al_2O_3 and CuO) were weighed (g) and added to isopropyl alcohol (IPA, ml) in a test tube. Following equation 5.1, the weight % (wt %) was calculated for 1%, 2%, 3%, and 4% nanofluid concentration. A magnetic stirrer was used to mix the nanoparticle and IPA for 30 minutes. This mixture was sonicated for 2 hours using a water bath sonicator to disperse the nanoparticles uniformly. In step two, the uniformly dispersed nanoparticles were added to 60 ml of lumbersider matt black paint (Resene Paints, New Zealand) and stirred manually. In step three, the aluminium tubes were coated manually with a brush and left to dry overnight in the laboratory. The nanofluid process is demonstrated in Figure 5-7.

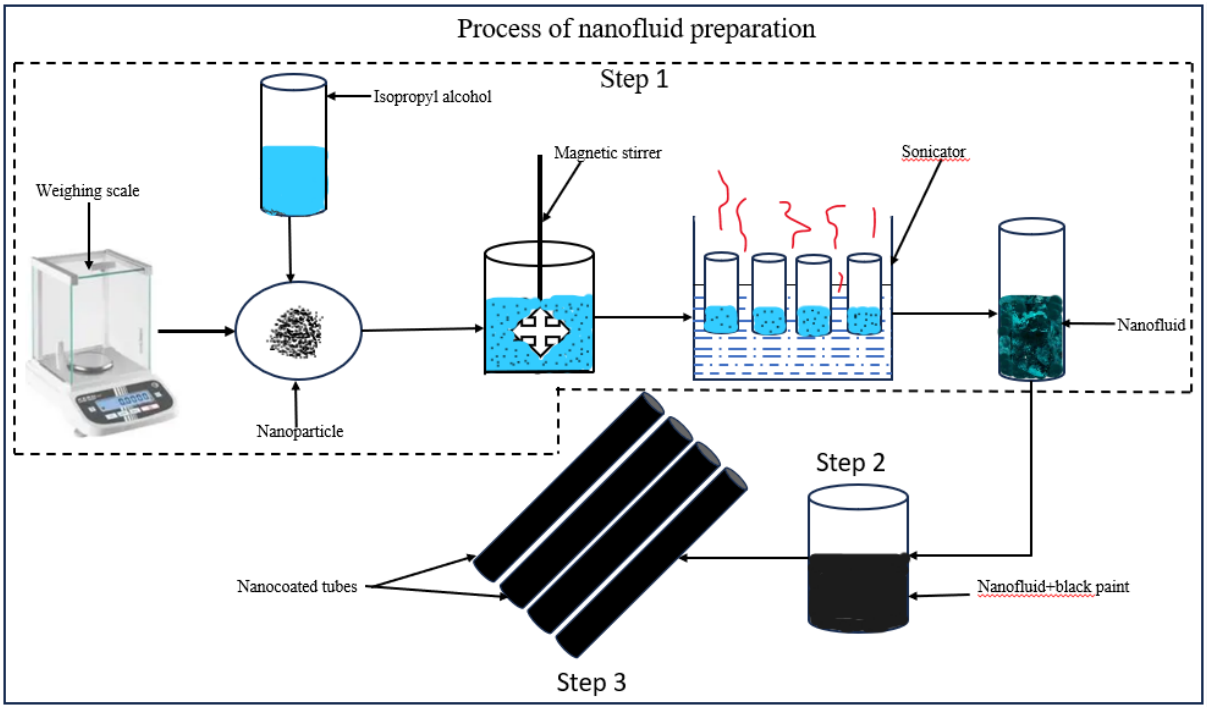

Figure 5-7 The nanofluid preparation process

The equation used to calculate the nanofluid concentration, as presented in Che Sidik et al. (2017), is given as:

$$concentration\ (wt\%) = \left(\frac{weight\ of\ nanoparticles}{weight\ of\ IPA + weight\ of\ black\ paint}\right) * 100 \qquad (5.1)$$

where,

Weight of Paint=Relative Density of Paint×Volume of Paint

Weight of IPA=Relative Density of IPA×Volume of IPA

5.4 Data collection

K-type thermocouples measured the inlet and outlet air temperatures of each tube. The thermocouples were connected to the datalogger (TC08, USB, Pico Technology, UK). The data loggers were connected to the laptop to monitor the temperature. The solar radiation, wind speed, and ambient temperature were recorded by an on-site weather station (WS3085, Wi-Fi weather station, Aercus Instruments, UK) mounted on the frame. A hot wire anemometer (AM4214SD, Lutron Electronic Enterprise Co. Ltd., Taipei City, Taiwan) measured the air velocity and the outlet air temperature. All the equipment was factory-calibrated. The characteristics of the equipment used for the experiment are given in Table 5-3.

Table 5-3 The characteristics of the monitoring equipment used for the experiment

Equipment	Monitoring Parameters	Range	Accuracy
Weather station (WS308)	Ambient air temperature (° C)	-40.0℃ – 60.0 ℃	± 1.0℃
	Solar radiation (W/m^2)	0–3000.0 W/m^2	± 15.0%
	Wind speed (m/s)	0 – 50.0 m/s	± 1.0 m/s (speed < 5.0 m/s) ± 10.0% (speed ≥ 5.0 m/s)
K type thermcouple	Inlet and Outlet air temperature (℃)	-40.0℃+1100.0 ℃	± 1.0℃
Hot wire anemometer AM4214SD	Outlet air velocity (m/s) Incoming air temperature from the duct (℃)	0.2–25.0 m/s 0-50.0 ℃	±5.0% of reading ± 0.8 ℃

The experimental setup in Chapter 5 was deliberately simplified to isolate the influence of nanofluid coatings and fin inserts on aluminium tubes. The absence of glazing, insulation, or ducting ensured that observed differences were attributable to coating and geometry effects rather than secondary system components. Critical parameters identified in earlier chapters—solar irradiance, air mass flow rate, and ambient air temperature—were monitored using calibrated instruments. However, the setup had inherent limitations: it relied on a single prototype, natural weather variability, and instruments with finite accuracy (±1.0℃ for thermocouples, ±15.0% for solar irradiance, ±5.0% for airflow velocity). While these

constraints limited strict repeatability, this was addressed by recording data at one-minute intervals,

averaging over hourly periods, and reporting mean ± SD values to capture variability.

The setup, therefore, provided comparative insights into coating and fin performance

under realistic outdoor conditions, though it cannot replace a laboratory-grade research rig designed for full repeatability.

5.4.1 Thermal efficiency calculation

The thermal efficiency (η) of the tubes was calculated using Equation 3.1. The SAHs effective area (m^2), was calculated to be 0.389 m^2

The ambient air temperature was considered the inlet temperature (T_a=T_i) The monitored air velocity was assumed to be the mean air velocity. The heat of the air (C_p) and effective collector area (A_c) were constant. Equation 3.1 demonstrates that the thermal efficiency of SAH relies on factors such as the air mass flow rate (m), the temperature difference between outlet and inlet air (T_o-T_i), and the incident solar radiation on the SAH surface (I_T), which can be written as following as η_{th} = f(m^o, ΔT, I_T). The air-specific capacity and density at different air temperatures are given in Table 5-4.

Table 5-4 Air-specific capacity and air density at different air temperatures (Cengel, 2011)

Air temperature (K)	Air-specific heat capacity (J/(kg*K)	Air density (kg/m^3)
[283.15, 293.15]	1007	1.225
[293.15, 303.15]	1007	1.184
[303.15, 313.15]	1007	1.145
[313.15, 323.15]	1007	1.109
[323.15, 333.15]	1007	1.076
[333.15, 343.15]	1007	1.044

5.5 Results

5.5.1 Ambient temperature and solar radiation

The weather data (ambient temperature and solar radiation), outlet air temperature, and air velocity were recorded at 1-minute intervals for eight days in November 2023 (November 14, 16, 21, 22, 23, 24, 27, and 29). The daily average ambient temperature and solar radiation on

the tilted surface are given in Table 5-5. During the test, the average daily ambient temperature (T_a) ranged from 15.8 °C (minimum) to 21.6 °C (maximum) with a mean ± SD of 17.8 ± 1.8 °C. The average daily solar radiation (I_T) on the absorber (tube) surface ranged from 411.2 W/m^2 (minimum) to 796.9 W/m^2 (maximum) with a mean ± SD of 569.8 ± 128.2 W/m^2.

The hourly average ambient temperature ranged from 14.8 °C (minimum) to 22.8 °C (maximum). The hourly solar radiation on the absorber surface ranged from 275.1 W/m^2 (minimum) to 892.2 W/m^2 (maximum).

Figures 5-8 to 5-11 show that solar radiation increased from 9:00 to 12:30 p.m. and then decreased later in the afternoon.

Table 5-5 The daily average ambient temperature (T_a) and solar radiation on the tilted surface (I_T)

Phase	Test Day	Ambient temperature (°C)	Daily mean solar radiation on the tilted surface (W/m^2)
Test 1	14/11/2023	16.7 ± 0.4	437.7 ± 86.4
	16/11/2023	18.1 ± 0.3	666.7 ± 57.5
	21/11/2023	21.6 ± 1.6	796.9 ± 79.1
Test 2	22/11/2023	15.8 ± 0.6	411.2 ± 99.2
	23/11/2023	16.3 ± 0.5	525.5 ± 75.0
	24/11/2023	17.7 ± 1.4	648.4 ± 118.6
Test 3	27/11/2023	18.0 ± 0.5	559.4 ± 72.9
Test 4	29/11/2023	17.8 ± 0.6	512.2± 70.0

5.5.2 Outlet air temperature and temperature difference (T_o-T_i)

During the test, the temperature difference and the outlet temperature followed a similar trend to solar radiation. The air temperature increased from 9:00 am to 1:30 pm and decreased later in the afternoon. Figures 5-8, 5-9, 5-10, and 5-11 show the variation in mean outlet temperature and solar radiation with time for different absorber tubes from 14/11/2023 to 29/11/2023. The time lag between the peak solar radiation and peak outlet temperature was observed on each test day, as shown in Figures 5-8 to 5-11. This could be due to the time it takes to heat the absorber and the air.

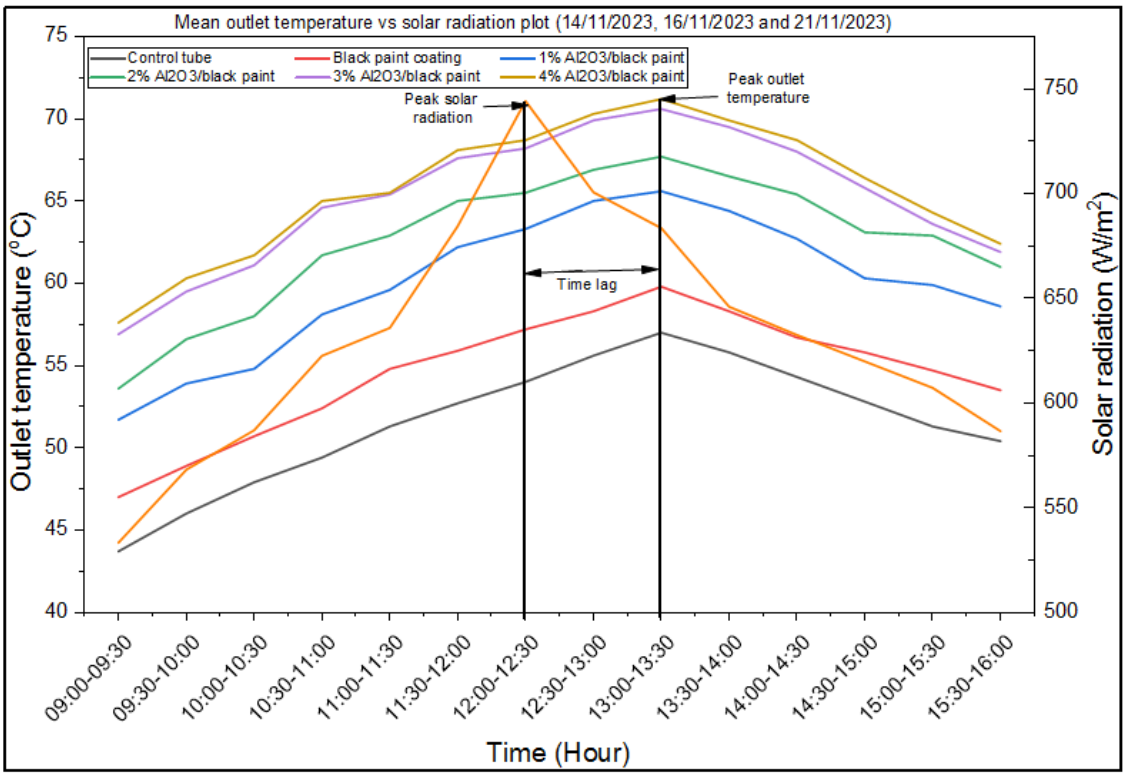

Figure 5-8 Mean outlet temperature vs Solar radiation plot on a tilted surface for Test 1 (14/11/2023, 16/11/2023 and 21/11/2023)

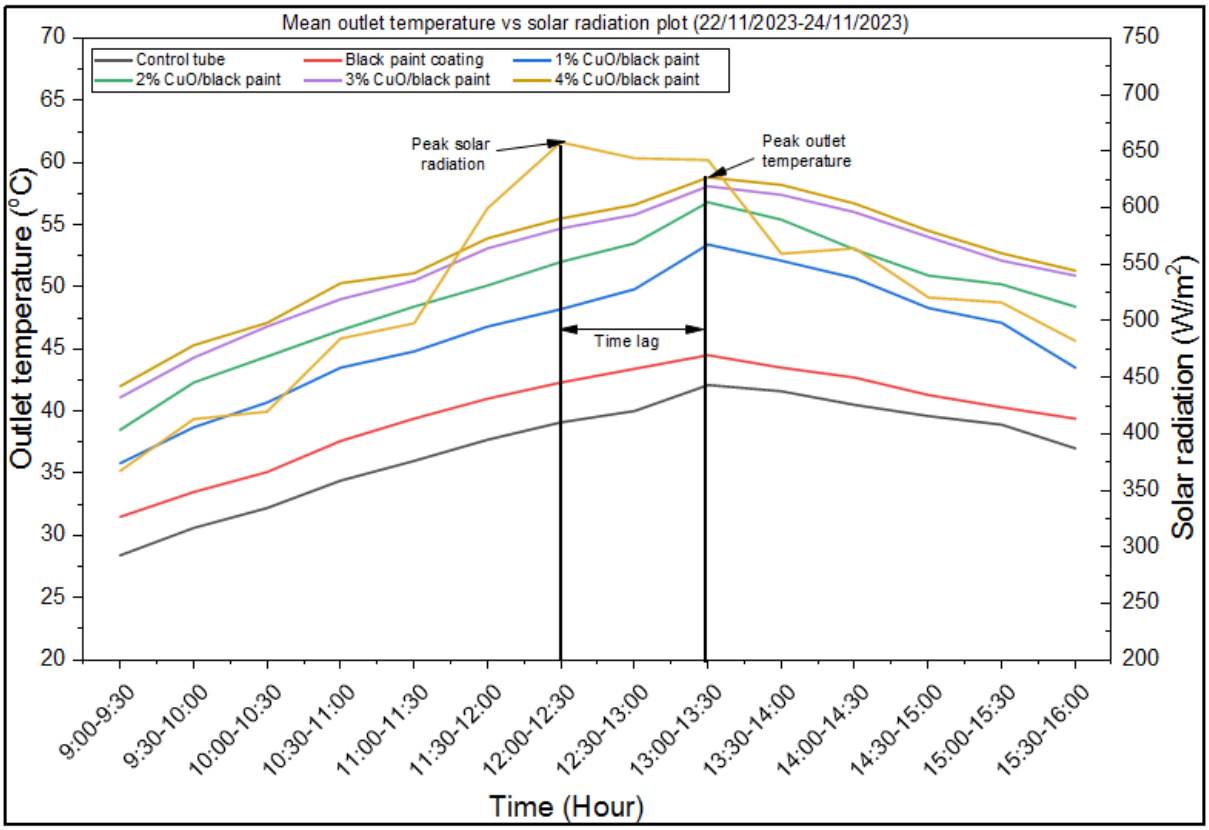

Figure 5-9 Mean outlet temperature vs Solar radiation plot on a tilted surface for Test 2 (22/11/2023, 23/11/2023 and 24/11/2023)

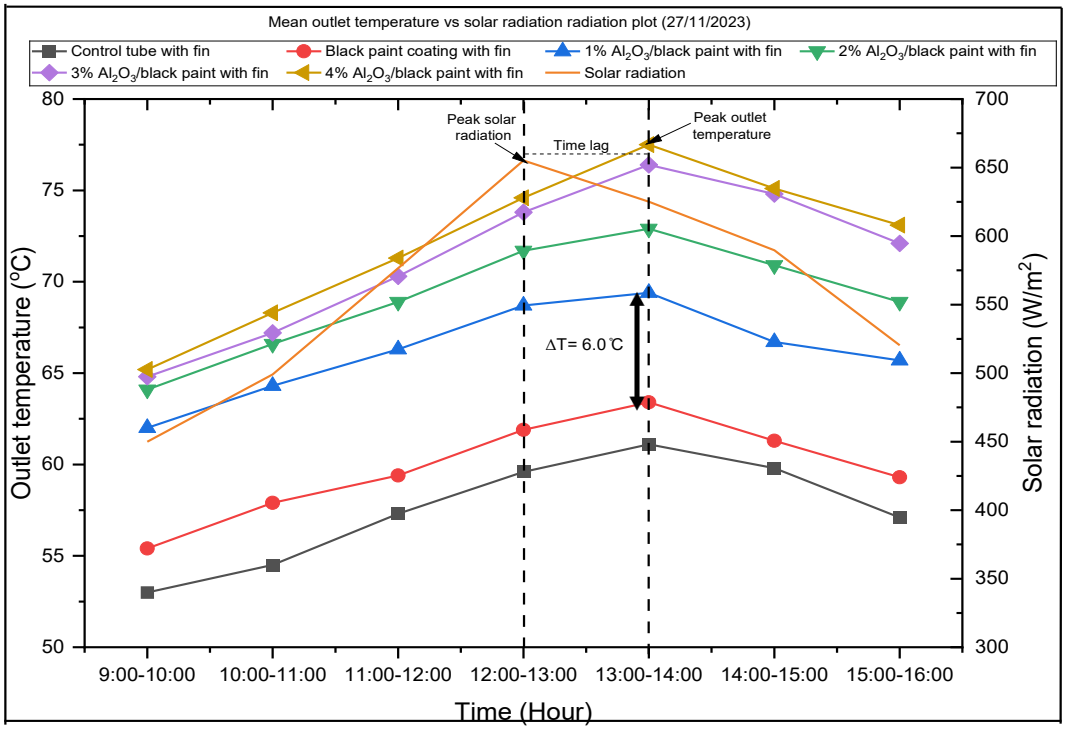

Figure 5-10 Mean outlet temperature vs Solar radiation plot on a tilted surface for Test 3 (27/11/2023)

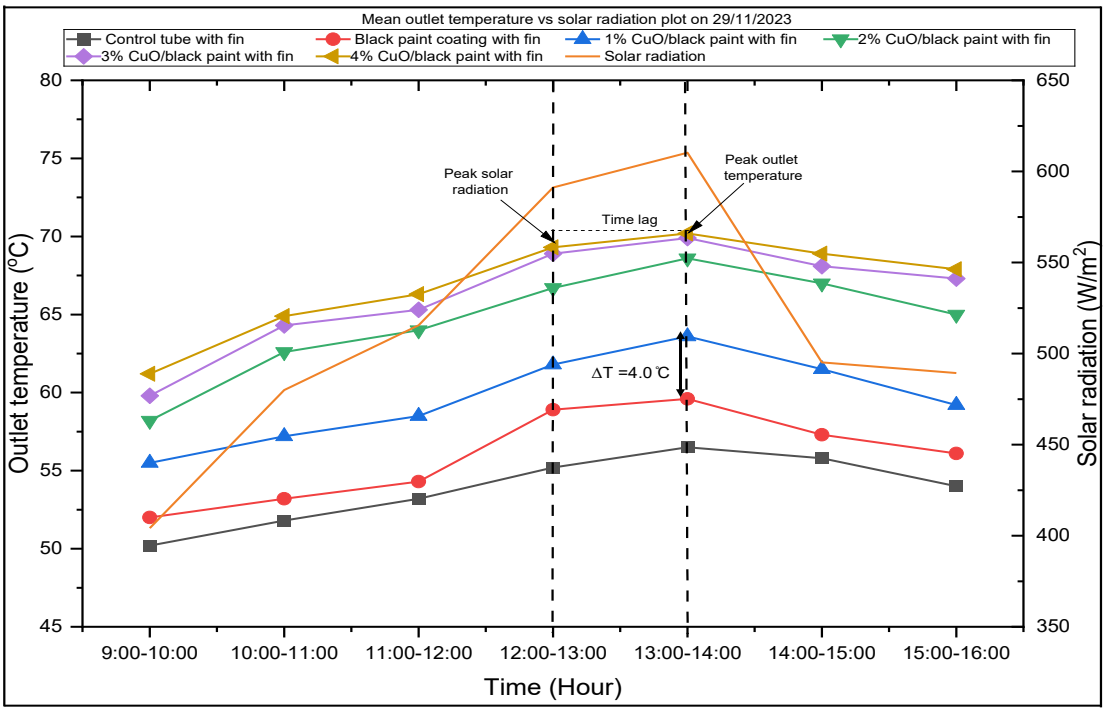

Figure 5-11 Mean outlet temperature vs Solar radiation plot on a tilted surface for Test 4 (29/11/2023)

Test 1 was conducted on 14/11/2023, 16/11/2023 and 21/11/2023. During Test 1, the mean ± SD values of ambient temperature was18.8 ± 0.8 ˚C and for solar radiation was 637.8 ± 74.3 W/m^2. During test 1, the temperature difference (ΔT) between the outlet and inlet air ranged from 32.8 ˚C to 46.8 ˚C, and the outlet temperature ranged from 51.5 ˚C– 65.4 ˚C. Table 5.6 shows the effect of adding varying concentrations of Al_2O_3 nanoparticles to black paint on heat absorption on the outlet air temperature (T_o), ambient temperature (T_a), and ΔT values measured during Test 1.

Table 5-6 The daily average outlet temperature (T_o), ambient temperature (T_a), and temperature difference (ΔT) and change in temp difference between treatment and control tubes (ΔT_1) values for Test 1

Treatment	Tube type	T_o (˚C)	$T_a=T_i$ (˚C)	$\Delta T= T_o - T_a$ (˚C)	$\Delta T_1 = \Delta T_{treatment} - \Delta T_{control}$ (˚C)
Without treatment	Control tube	51.5	18.8	32.8	NA
With treatment	Black paint	55.0	18.8	36.3	3.5
	1% Al_2O_3/black paint	59.9	18.8	41.4	8.6
	2% Al_2O_3/black paint	62.5	18.8	43.7	10.9
	3% Al_2O_3/black paint	64.9	18.8	45.7	12.9
	4 Al_2O_3/black paint	65.4	18.8	46.8	14.0

In the first set of tests, tubes coated with black paint and Al_2O_3 nanoparticles showed greater heat absorption at higher nanoparticle concentrations. Table 5-6 shows the control tube exhibited a ΔT of 32.8 ˚C. When black paint was applied, the ΔT increased by 3.5 ˚C, indicating enhanced heat absorption due to the paint's properties. Adding 1% Al_2O_3 to black paint increased the temperature difference (ΔT_1) by 8.6 ˚C compared to the control, showing that nanoparticles enhance heat absorption. As the concentration of Al_2O_3 increased to 2%, 3%, and 4%, the ΔT continued to rise, reaching a maximum of 46.8 ˚C with 4% Al_2O_3, which was 14.0 ˚C higher than the control. Similarly, the second set of CuO nanoparticle tests followed the same trend.

Test 2 was conducted on 22/11/2023, 23/11/2023 and 24/11/2023. Table 5-7 presents the values of T_o, T_a, ΔT, and ΔT_1. The experiment investigates the effect of adding CuO nanoparticles at different concentrations to black paint on heat absorption. During Test 2, the mean ± SD values of ambient temperature was16.6 ± 0.8 ˚C and for solar radiation was 528.4 ± 97.6 W/m^2. During Test 2, ΔT ranged from 20.2 ˚C to 35.4 ˚C. Table 5.5 presents the values of T_o, T_a, ΔT, and ΔT_1.

Table 5-7 The daily average outlet temperature (T_o), ambient temperature (T_a), and temperature difference (ΔT) and change in temp difference between treatment and control tubes (ΔT_1) values for Test 2

Treatment	Tube type	T_o (˚C)	$T_a=T_i$ (˚C)	$\Delta T= T_o - T_a$ (˚C)	$\Delta T_1 = \Delta T_{treatment} - \Delta T_{control}$ (˚C)
Without treatment	Control tube	36.8	16.6	20.2	NA
With treatment	Black paint	39.7	16.6	23.1	2.9
	1% CuO/black paint	45.9	16.6	29.3	9.1
	2% CuO /black paint	49.2	16.6	32.7	12.4
	3% CuO /black paint	51.7	16.6	35.1	14.9
	4 CuO /black paint	52.0	16.6	35.4	15.2

Table 5-7 shows a temperature difference (ΔT) of 20.2 ˚C for the control tube. When black paint was applied, the ΔT increased by 2.9 ˚C, indicating an improvement in heat absorption due to the paint's properties. Adding 1% CuO to the black paint increased the ΔT by 9.1°C compared to the control, demonstrating a significant enhancement in heat absorption. As the concentration of CuO increased to 2%, 3%, and 4%, the ΔT continued to rise, reaching a maximum of 52.0 ˚C with 4% CuO, which was 15.2 ˚C higher than the control. However, the increase in ΔT between 3% and 4% CuO is minimal (only 0.3 ˚C), suggesting diminishing returns in heat absorption beyond 3%. This indicates that the optimal concentration for maximizing heat absorption with minimal additional material is around 3% CuO in black paint, like the trend observed with Al_2O_3.

Based on the results of Test 1 and Test 2, further modifications were made to the tube. The tubes were integrated with the fin inserts and tested for the outlet temperature and thermal efficiency during Tests 3 and 4.

Test 3 was conducted on 27/11/2023. The experiment investigates the effect of coating the tubes with Al_2O_3/black paint at varying concentrations and integrating the tubes with fin inserts. Table 5-8 presents the values of T_o, T_a, and ΔT. During Test 3, the mean ± SD values of ambient temperature were 18.0 ± 0.5 ˚C, and for solar radiation were 559.4 ± 72.9 W/m^2. During Test 3, ΔT ranged from 39.5 ˚C to 54.1 ˚C.

Table 5-8 The daily average outlet temperature (T_o), ambient temperature (T_a), and temperature difference (ΔT) and change in temp difference between treatment and control tubes (ΔT_1) values for Test 3

Treatment	Tube type	T_o (˚C)	$T_a=T_i$ (˚C)	$\Delta T= T_o - T_a$ (˚C)	$\Delta T_1 = \Delta T_{treatment} - \Delta T_{control}$ (˚C)
Without treatment	Control tube + fin	57.5	18.0	39.5	NA
With treatment	Black paint + fin	59.8	18.0	41.8	2.3
	1% Al_2O_3/black paint + fin	65.2	18.0	48.2	8.7
	2% Al_2O_3/black paint + fin	69.1	18.0	51.1	11.6
	3% Al_2O_3/black paint + fin	71.3	18.0	53.3	13.8
	4 Al_2O_3/black paint + fin	72.2	18.0	54.1	14.6

In the case of Al_2O_3 with fins, the control tube had a ΔT of 39.5°C. With black paint and fins, ΔT improved to 41.8 ˚C, showing a 2.3 ˚C increase. The introduction of 1% Al_2O_3 raised ΔT to 48.2˚C, and as concentrations increased to 3% and 4%, ΔT reached 54.1 ˚C, with the highest improvement of 14.6 ˚C at 4% concentration.

Test 4 was conducted on 29/11/2023. The experiment investigates the effect of coating the tubes with Al_2O_3/black paint at varying concentrations and integrating the tubes with fin inserts. Table 5-9 presents the values of T_o, T_a, and ΔT. During Test 3, the mean ± SD values of ambient temperature were 17.8 ± 0.6 °C, and for solar radiation, 512.2 ± 70.0 W/m². During Test 3, ΔT ranged from 36.0 ˚C to 49.1 ˚C.

Table 5-9 The daily average outlet temperature (T_o), ambient temperature (T_a), and temperature difference (ΔT), and change in temp difference between treatment and control tubes (ΔT_1) values for Test 4

Treatment	Tube type	T_o (˚C)	$T_a=T_i$ (˚C)	$\Delta T= T_o - T_a$ (˚C)	$\Delta T_1 = \Delta T_{treatment} - \Delta T_{control}$ (˚C)
Without treatment	Control tube + fins	53.8	17.8	36.0	NA
With treatment	Black paint	55.9	17.8	38.1	2.1
	1% CuO/black paint + fins	59.6	17.8	41.8	5.8

	2% CuO /black paint + fins	65.6	17.8	46.8	10.8
	3% CuO /black paint+ fins	65.2	17.8	48.4	12.4
	4% CuO /black paint+ fins	67.0	17.8	49.1	13.1

In the Test 4, the control tube with fins had a T_o of 53.8˚C and a ΔT of 36.0˚C. Coating the tube with black paint and fins increased the T_o to 55.9 ˚C (ΔT = 38.1 ˚C), showing a small 2.1˚C improvement. When 1% CuO was added to the black paint, the T_o increased to 59.6 ˚C (ΔT = 41.8˚C), an improvement of 5.8˚C. With 2% CuO, the T_o rose to 65.6˚C (ΔT = 46.8˚C), a notable increase of 10.8˚C over the control. At 3% CuO, the T_o reached 65.2 ˚C (ΔT = 48.4˚C), with a 12.4˚C increase, and at 4% CuO, the T_o was 67.0˚C (ΔT = 49.1˚C), with only a marginal 13.1˚C improvement over the control. Like Al_2O_3, CuO-enhanced tubes reached optimal performance at 3% concentration, with diminishing returns at higher levels.

Comparing the thermal performance of tubes coated with Al_2O_3 and CuO nanoparticles shows that both materials significantly enhance heat absorption, particularly when combined with fins. However, tubes coated with Al_2O_3 appear to achieve slightly higher ΔT values than those with CuO, especially at higher nanoparticle concentrations. For example, at 3% concentration, tubes with Al_2O_3 and fins reached a ΔT of 53.3 ˚C, whereas tubes with CuO and fins reached 48.4˚C. This suggests that Al_2O_3 may offer a marginally better thermal performance improvement than CuO in this setup. Table 5.9 compares the outlet temperature from the present study with that reported by various researchers.

5.5.3 Ventilation rate of tubes

The average ventilation rate through each tube ranged between 9.0 m^3/h (minimum) – 10.5 m^3/h (maximum). However, the obtained ventilation rate was eighty times lower than the recommended ventilation rate as per the compliance document G4 (NZ Building Code compliance document for ventilation) and the New Zealand Standard (NZS) 4303:1990, which recommends a flow rate of 8.0 litres per second, and per child (28.8 m^3/h/child) to maintain a CO_2 level below 1000.0 ppm. This recommended flow rate is equivalent to 864.0 m^3 /h for an average classroom of 30 children (MBIE, 2017). A similar study was conducted by (Wang et al., 2023) in NZ classrooms. They found that the ventilation rate for the flat plate SAH with a perforated back plate was twenty-five times lower compared to the compliance document G4 and NZ standards (NZS) 4303:1990. The ventilation rate could be increased by installing multiple tubes in a well-insulated box and increasing the fan capacity.

5.5.4 Comparison of thermal efficiency of control vs treatment tubes

5.5.4.1 Thermal efficiency trend

Figures 5-12 to 5-14 show plots of thermal efficiency versus the ratio of the temperature difference between the outlet and inlet temperatures to the solar radiation on a tilted surface ($\Delta T/I_T$). It was noted that the thermal efficiency of tubes was directly proportional to the $\Delta T/I_T$ values. Figures 5-12 to 5-14 show the daily average efficiency of nanocoated tubes. There was no significant difference in thermal efficiency between the 4% and 3% nanocoated tubes.

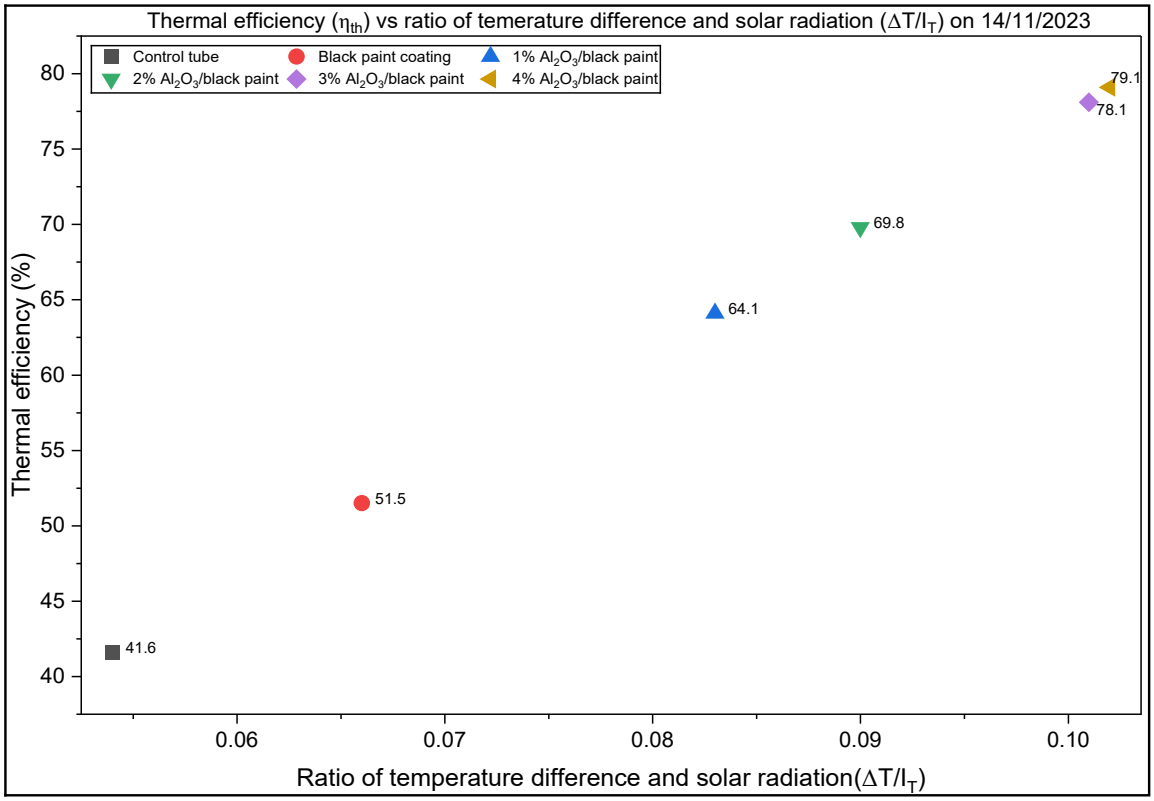

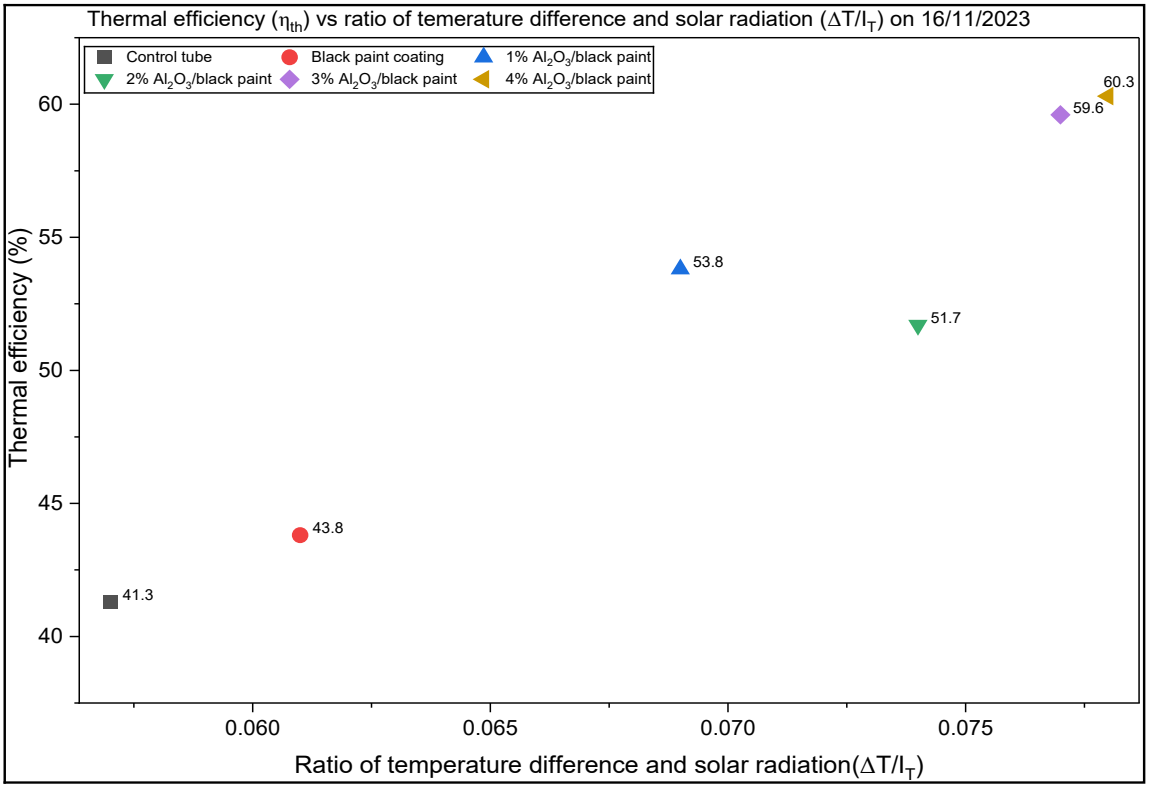

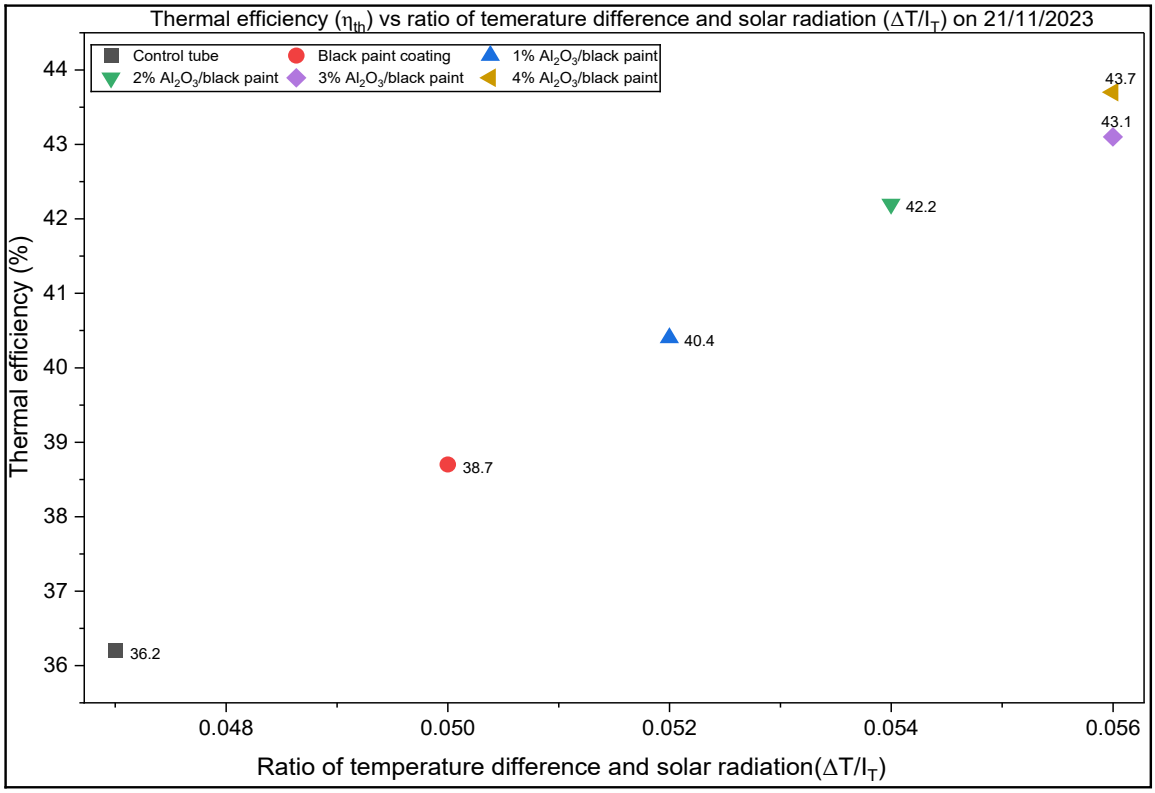

Figure 5-12 Test 1 ηth vs. ΔT/IT plot over three days (14/11, 16/11, and 21/11/2023)

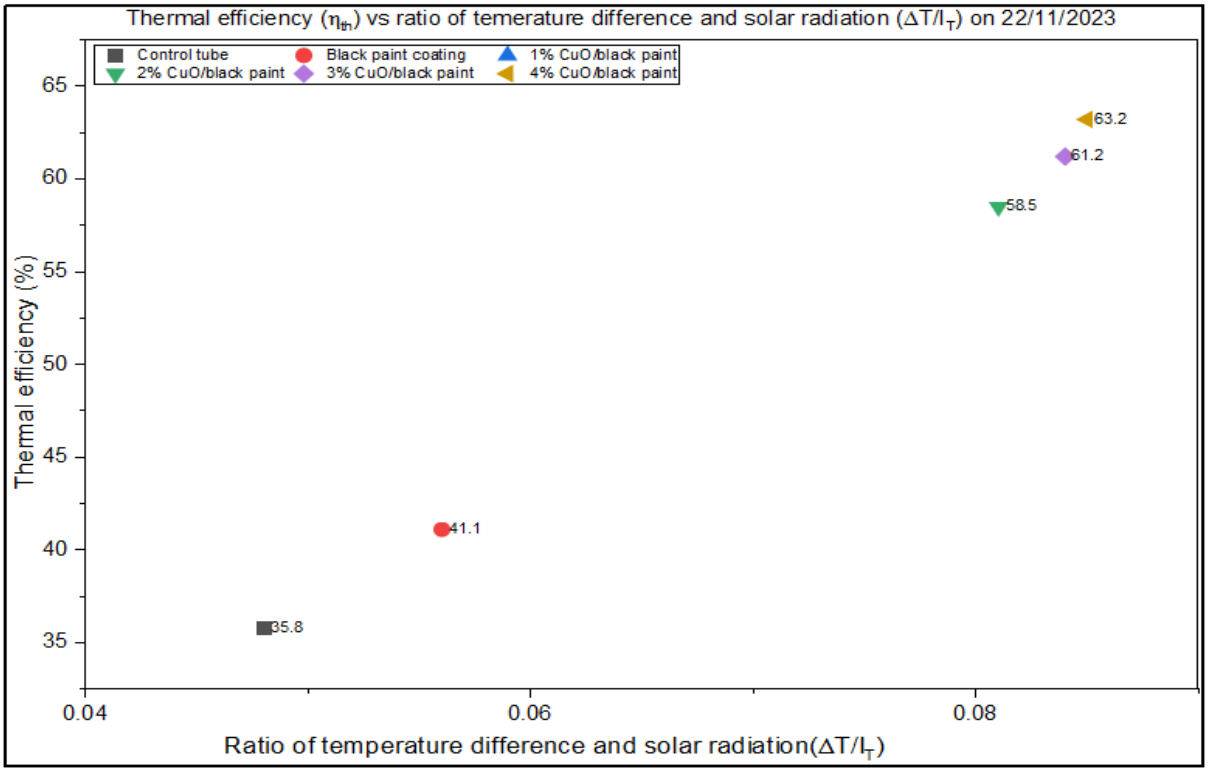
Thermal efficiency (η_{th}) vs ratio of temerature difference and solar radiation ($\Delta T/I_T$) on 22/11/2023
Control tube
Black paint coating
1% CuO/black paint
2% CuO/black paint
3% CuO/black paint
4% CuO/black paint
63.2
61.2
58.5
41.1
35.8
Thermal efficiency (%)
Ratio of temperature difference and solar radiation($\Delta T/I_T$)

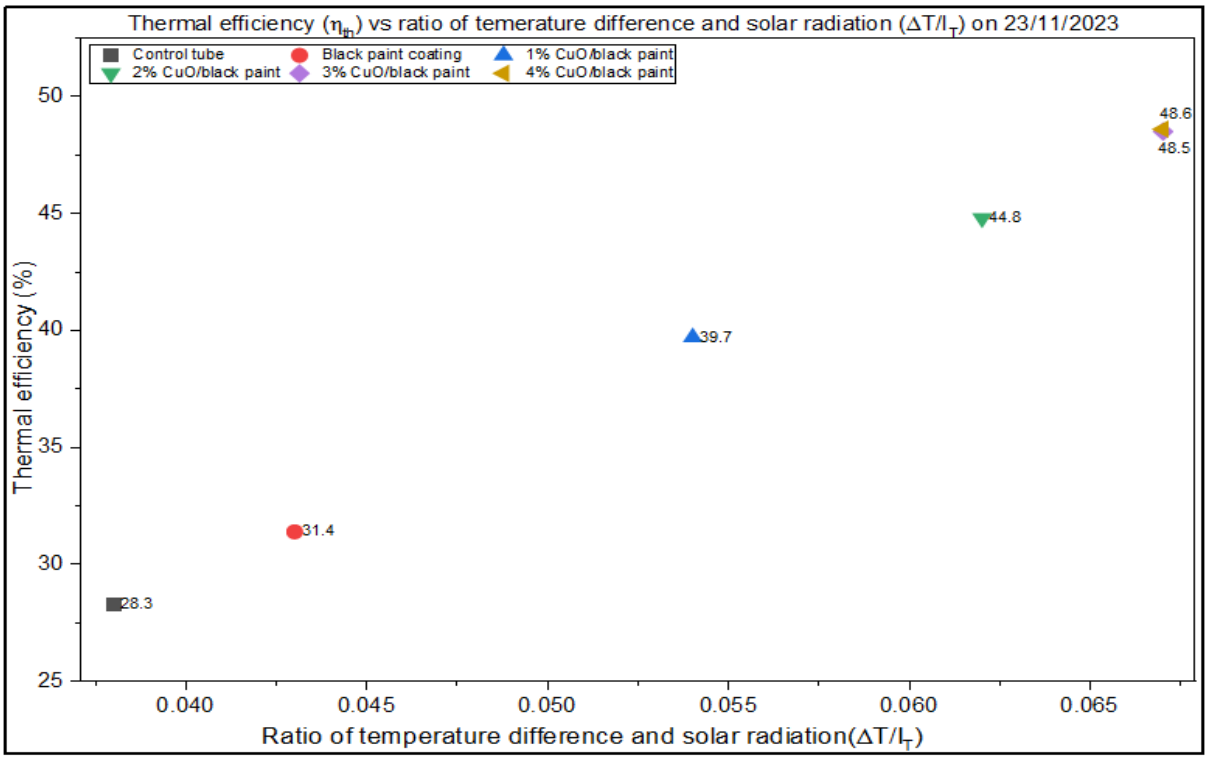
Thermal efficiency (η_{th}) vs ratio of temerature difference and solar radiation ($\Delta T/I_T$) on 23/11/2023
Control tube
Black paint coating
1% CuO/black paint
2% CuO/black paint
3% CuO/black paint
4% CuO/black paint
48.6
48.5
44.8
39.7
31.4
28.3
Thermal efficiency (%)
Ratio of temperature difference and solar radiation($\Delta T/I_T$)

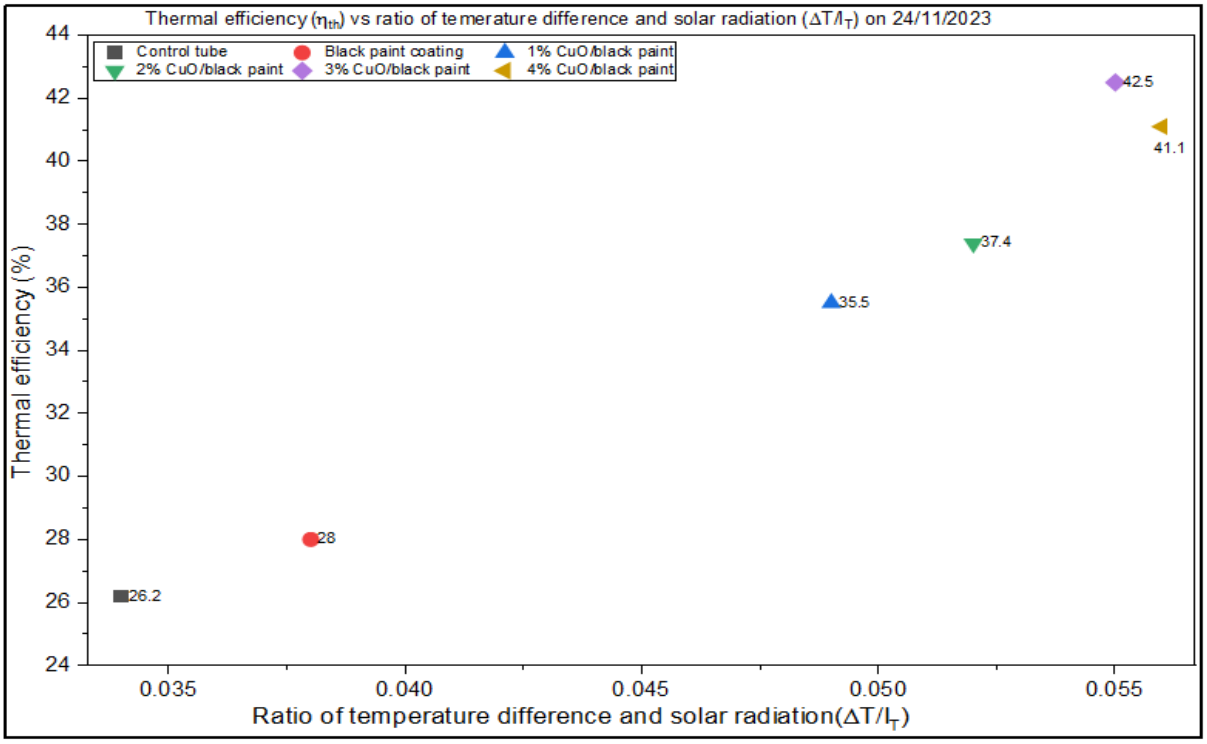

Figure 5-13 Test 2 ηth vs. ΔT/IT plot over three days (22/11, 23/11 and 24/11/2023)

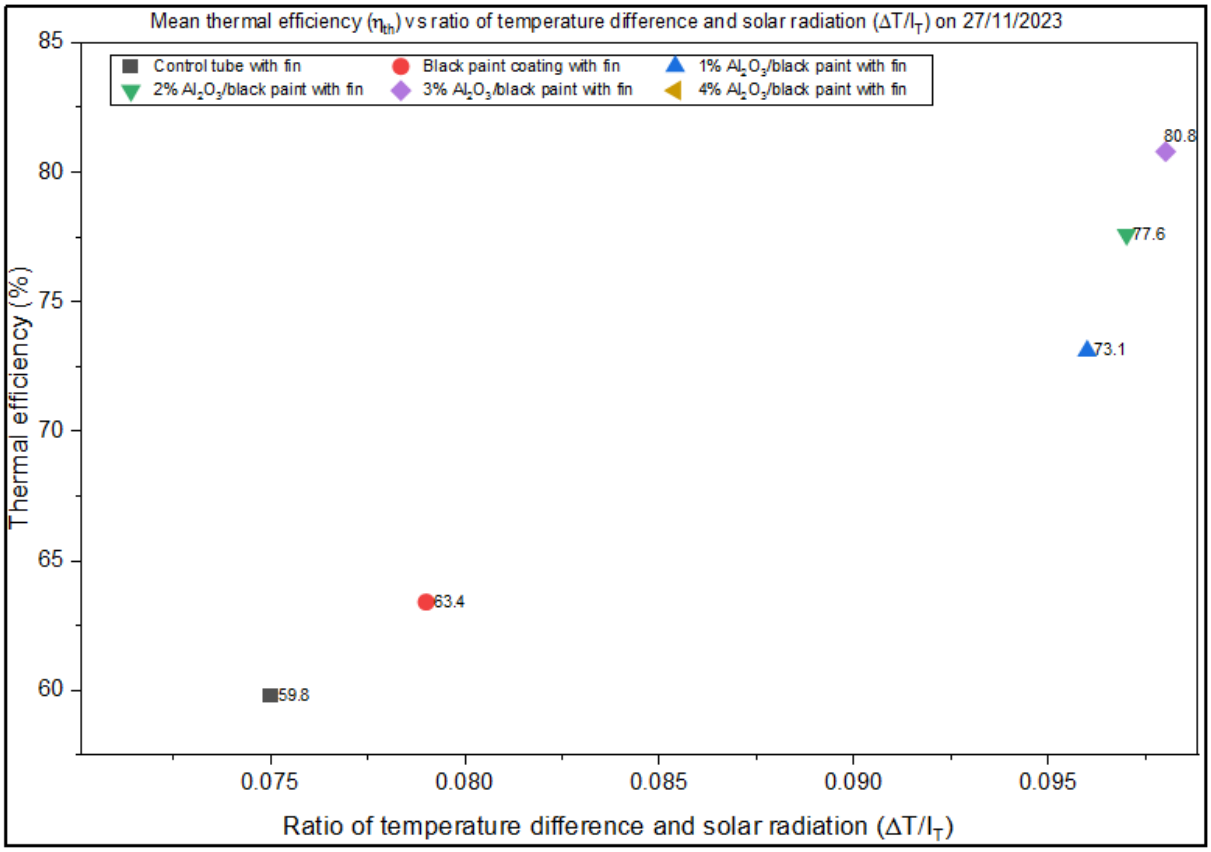

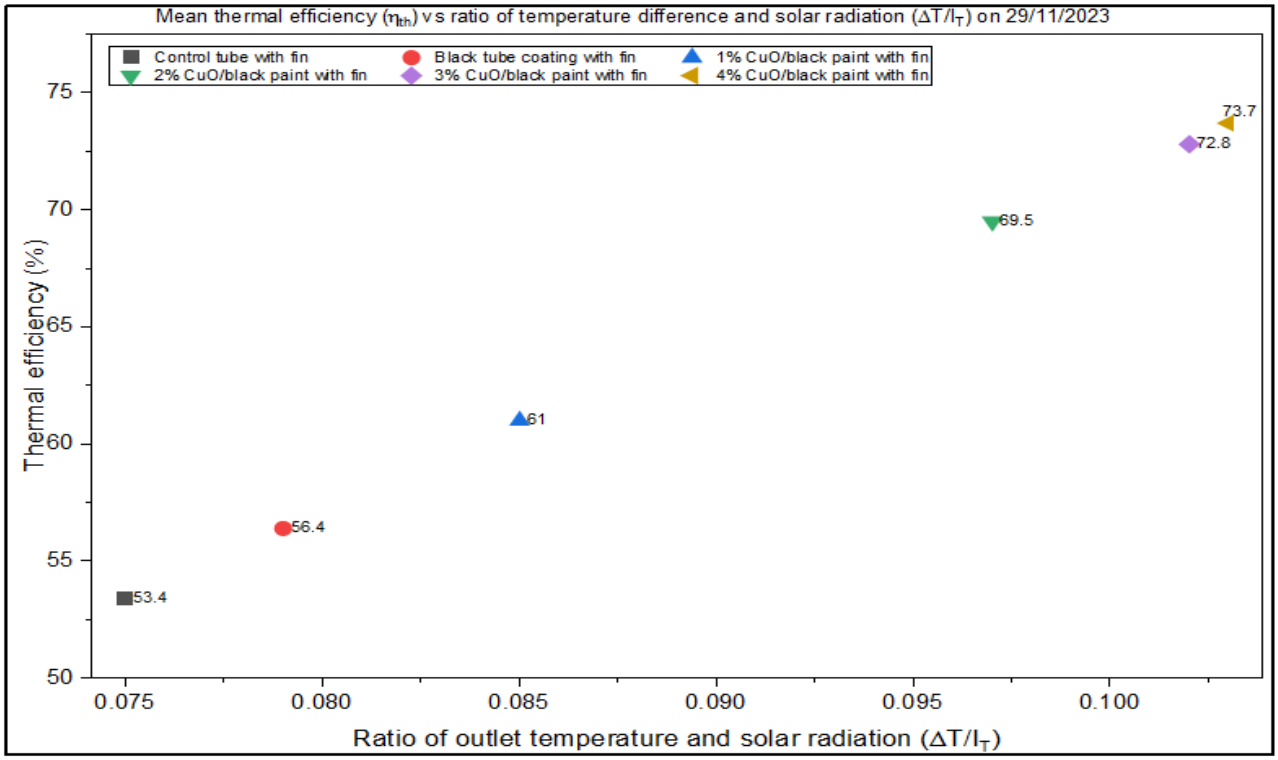

Figure 5-14 Test 3 and Test 4 ηth vs. ΔT/IT plot (27/11 and 29/11/2023)

In each of the graphs, the general trend of thermal efficiency increases with the rise in the ratio of ΔT/IT. Across different dates, the data points represented by black, red, and other colors follow a similar pattern of behaviour:

1. **Initial Increase in Efficiency:** At the beginning of each test day, as the ΔT/IT ratio increases (indicating a higher temperature difference between the inlet and outlet than solar radiation), the thermal efficiency for all datasets represented by black and red markers rises. This shows that as the system absorbs more heat, the overall efficiency improves predictably.
2. **Plateau in Efficiency:** After a certain point, the graphs show a visible plateau in thermal efficiency, where the increase in ΔT/IT results in smaller incremental gains in efficiency. The black and red markers exhibit this pattern, indicating that once the system reaches a certain temperature difference relative to the solar radiation, further increases in ΔT/IT yield diminishing returns in terms of efficiency. This suggests a saturation point where the system's thermal absorption capability is maximized.

3. **Consistency Across Multiple Test Days**: Despite slight variations in the absolute values of efficiency on different test days (Figure 5-12 and Figure 5-14), the overall trend remains consistent across the black and red markers. This consistency supports the notion that the system's thermal behaviour is robust and follows a predictable trend, regardless of the specific day-to-day environmental factors.
4. **Minimum Deviations**: While the overall trend is similar, slight deviations between black and red markers can be observed in the form of small differences in absolute efficiency values. These deviations are likely due to the differences in coating materials or nanoparticle concentrations. However, the overall pattern of increasing efficiency with rising $\Delta T/I_T$, followed by a plateau, is consistently observed across both marker sets.

5.5.4.2 Impact of adding fins to the tubes

The impact of adding fins to uncoated and nanocoated tubes on thermal efficiency was studied. Table 5-10 summarizes the results of Test 1, which demonstrates the thermal efficiency performance of various tubes with and without fins. The data clearly show that the Al_2O_3/black paint-coated tubes with fins outperformed the other tubes in terms of thermal efficiency.

Table 5-10: Thermal efficiency of tubes with and without fins when coated with black paint and Al_2O_3

Tube tested	Thermal efficiency without fins (%)	Thermal efficiency with fins (%)	The thermal efficiency difference between with fins and without fins (%)
Control	39.7	59.8	20.1
Black paint	44.7	63.4	18.7
1% Al_2O_3/black paint	52.8	73.1	20.3
2% Al_2O_3/black paint	54.6	77.6	23.0
3% Al_2O_3/black paint	60.2	80.8	20.6
4% Al_2O_3/black paint	61.0	82.0	21.0

For the control tube, the thermal efficiency without fins was 39.7%, increasing to 59.8% with fins, yielding an improvement of 20.1%. Introducing 1% Al_2O_3 into the black paint significantly increased efficiency, achieving 52.8% without fins and 73.1% with fins, resulting in a 20.3%

improvement. As the concentration of Al_2O_3 nanoparticles increased, the thermal efficiency followed a similar upward trend, reaching 61.0% without fins and 82.0% with fins at a 4% Al_2O_3 concentration, representing a 21.0% improvement with fins. This substantial increase in efficiency with Al_2O_3 coatings can be attributed to nanoparticles' ability to increase surface area and improve heat transfer rates, thereby enhancing energy absorption and conversion efficiency. The data reveal that fins consistently enhance thermal performance across all concentrations, further improving heat dissipation by increasing the surface area.

A similar pattern was observed for CuO nanofluid coatings. The results, summarized in Table 5-11, show that CuO coatings also improved the thermal efficiency of the tubes, though to a slightly lesser extent than Al_2O_3.

Table 5-11 Thermal efficiency of tubes with and without fins when coated with black paint and CuO

Tube tested	Thermal efficiency without fins (%)	Thermal efficiency with fins (%)	The thermal efficiency difference between with fins and without fins (%)
Control	30.1	53.4	23.3
Black paint	33.5	56.4	22.9
1% CuO/black paint	42.1	61.0	18.9
2% CuO/black paint	46.9	69.5	22.6
3% CuO/black paint	50.7	72.8	22.1
4% CuO/black paint	51.0	73.7	22.7

For the control tube, the thermal efficiency without fins was 30.1%, increasing to 53.4% with fins, representing a 23.3% improvement. When 1% CuO was added to black paint, the efficiency increased to 42.1% without fins and 61.0% with fins, representing an 18.9% improvement. As the CuO concentration increased, the thermal efficiency continued to improve, with the tube coated with 4% CuO/black paint achieving 51.0% without fins and 73.7% with fins, resulting in a 22.7% improvement. This improvement can be attributed to the enhanced thermal conductivity and heat-absorption properties of CuO nanoparticles, thereby improving the coating's heat transfer efficiency.

When comparing the performance of Al2O3 and CuO nanoparticle coatings, both significantly improve the thermal efficiency of the tubes. However, the Al_2O_3-coated tubes consistently demonstrate slightly higher thermal efficiency, especially at higher nanoparticle concentrations. For example, the 4% Al_2O_3/black paint-coated tube reached a thermal efficiency of 61.0% without fins and 82.0% with fins, whereas the 4% CuO/black paint-coated tube achieved 51.0% without fins and 73.7% with fins. This performance difference could be attributed to the inherent thermal properties of Al_2O_3 and CuO. Al_2O_3, while a better insulator, still enhances heat transfer when incorporated into nanocoatings, whereas CuO primarily improves the coating's thermal conductivity. Despite this, both nanoparticle coatings provide substantial improvements over the control and black paint-coated tubes.

The fins in both tests consistently improved thermal efficiency across all coating types, as they significantly increased the surface area available for heat exchange, leading to more efficient heat dissipation. This effect is especially notable in tubes coated with higher concentrations of nanoparticles, where the synergy between increased surface area and improved thermal conductivity yields the greatest efficiency gains.

In conclusion, the results from both tests demonstrate that adding nanoparticles to black paint coatings significantly enhances thermal efficiency, particularly when coupled with fin inserts. These results are illustrated in Figure 5-15. Al_2O_3/black paint coatings offer slightly better efficiency improvements than CuO/black paint coatings, particularly at higher concentrations. This improvement in thermal performance can be attributed to better heat absorption, improved thermal conductivity, and increased surface area for heat transfer, all of which are enhanced by

the presence of fin

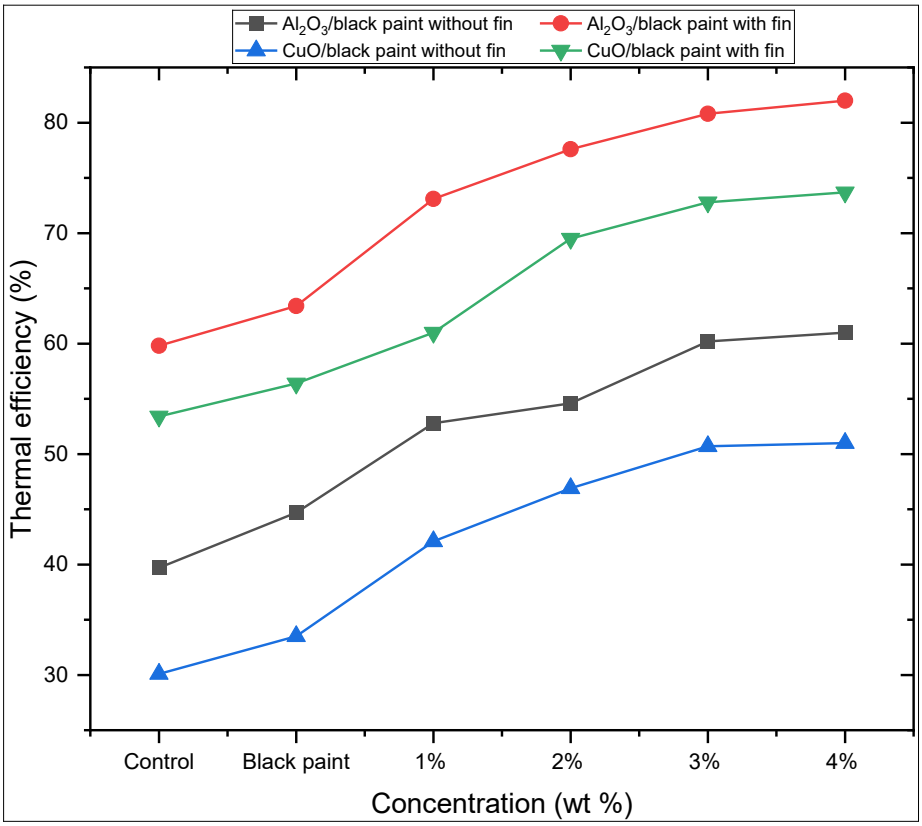

Figure 5-15 Comparison of thermal efficiency of tubes with 4% nanofluid coating (present study)

5.5.5 Discussion

The finding showed that tubes coated with 4% Al_2O_3/black paint yielded an outlet air temperature 21.3℃ higher than the control and 18.0℃ higher than tubes coated with black paint, consistent with studies highlighting Al_2O_3's high thermal conductivity. Caturwat et al. (2023) also reported an increase of 4.6℃ when Al_2O_3/black paint was used in solar collectors compared to uncoated ones, affirming the superior heat absorption capacity of Al_2O_3 over black paint. Furthermore, Al-Kayiem et al. (2021) found that Al_2O_3/black paint increased outlet temperatures by 2.0℃, 1.6℃, and 2.8℃ compared to black paint, CuO/black paint, and a mixture of CuO/Al_2O_3, respectively. This corresponds with our findings that tubes coated with 4% Al_2O_3/black paint exhibit better thermal performance than those coated with 4% CuO/black paint by a margin of 13.4℃. This difference is also in line with Abdelkader et al. (2020), who noted that a combination of carbon nanotubes and CuO dispersed in black paint only resulted in a 3.6 ℃ increase in outlet temperature compared to a black paint-coated collector, emphasizing the effectiveness of Al_2O_3 over CuO-based coatings.

The addition of fin inserts to tubes coated with 4% Al_2O_3/black paint resulted in outlet temperatures 16.4 °C higher than the control and 5.1°C higher than those of 4% CuO/black paint-coated tubes with fin inserts, further supporting the enhanced thermal conductivity of Al_2O_3. The effect of fin inserts combined with nanoparticle coatings amplifies heat transfer, which is supported by the findings of Al-Kayiem et al. (2021) and Caturwat et al. (2023). Both emphasized the importance of nanoparticle integration in improving thermal performance.

The recommendation to use 3% nanoparticle concentrations for optimal thermal performance aligns with literature findings. Increasing the nanoparticle concentration from 1% to 3% resulted in notable improvements in both outlet temperature and efficiency; however, further increasing it to 4% offered diminishing returns. This result is consistent with the findings of Kim et al. (2017), who reported that higher concentrations of nanoparticles can lead to agglomeration, reducing nanofluid stability and impairing thermal efficiency due to poor heat transfer between nanoparticles. The study by Khanlari et al. (2022) Additionally, this supports the observation that increasing the concentration of CuO/black paint coatings provided only marginal gains, with outlet temperatures rising by only 1.7 °C to 1.3 °C at different mass flow rates compared to uncoated solar collectors.

Overall, the results strongly align with existing literature, demonstrating that coatings containing Al_2O_3/black paint significantly improve outlet temperature compared to those containing CuO/black paint, and that increasing nanoparticle concentration beyond 3% is not advantageous due to agglomeration effects.

5.6 Limitations of the experimental setup

The setup's limitations must also be acknowledged. The use of a single prototype system and short test durations (due to time constraints) meant that repeatability under identical conditions was not possible. Instead, each tube was tested once under naturally varying environmental conditions. This limits the ability to control for weather fluctuations fully, even though the data were averaged and compared across multiple days. Furthermore, the accuracy and precision of the instruments introduce additional uncertainty: ±1 °C for thermocouples, ±15% for solar radiation from the weather station, and ±5% for airflow velocity from the anemometer. While these are within acceptable limits for field experiments, they contribute to data scatter and reduce the precision of calculated efficiency values, especially at low ΔT.

Although the setup did not achieve laboratory-grade repeatability, it was adequate for identifying relative trends among coatings, concentrations, and fin configurations. The insights

gained, therefore, represent comparative performance outcomes under realistic outdoor conditions rather than absolute values that can be generalised.

It should be noted that the control tubes tested on different days showed varying performance. This reflects the influence of changing environmental conditions rather than inconsistencies in the experimental method. While relative comparisons within each test set (control vs. coated tubes) remain valid, absolute control values across different days cannot be treated as identical benchmarks. This limitation highlights the importance of simultaneous control testing under identical conditions, which should be considered in future studies to strengthen repeatability.

5.7 Conclusion and future scope

The test was conducted at Massey University's Wellington Campus from June 14, 2023, to November 29, 2023. The following conclusions are drawn from the experimental study:

1) The thermal efficiency of tubes was directly proportional to the temperature difference and inversely proportional to the solar radiation level. A nanoparticle-embedded black paint tube with fins enhanced thermal efficiency and reduced outlet air temperature.
2) During Test 1 (14/11/2023 – 21/11/2023), the daily average thermal efficiency ranged from 35.2% - 41.6%, 38.7% - 51.5%, 40.4% - 64.1%, 42.2% – 69.8%, 43.1% - 78.1%, and 43.7% - 79.1% for control tube, black paint coated, 1% Al_2O_3/black pain, 2% Al_2O_3/black paint, 3% Al_2O_3/black paint and 4% Al_2O_3 / black paint respectively.
3) During Test 2 (22/11/2023 – 24/11/2023), the daily average thermal efficiency ranged from 25.2.0% - 35.8%, 28.0% - 41.1%, 35.5% - 51.0%, 37.4% - 58.5%, 42.5% - 61.2%, and 41.1% - 63.2% for control tube, black paint coated, 1% CuO/ black paint, 2% CuO/ black paint, 3% CuO/ black paint and 4% CuO/ black paint respectively.
4) During Test 3, the daily average thermal efficiency was 59.8%, 63.4%, 73.1%, 77.6%, 80.8%, and 82% for control tube with fin, black paint with fin, 1% Al_2O_3/black paint with fin, 2% Al_2O_3/black paint with fin, 3% Al_2O_3/black paint with fin and 4% Al_2O_3/ black paint with fin respectively.
5) During Test 4 (29/11/2023), the daily average thermal efficiency was 53.4%, 56.4%, 61.0%, 69.5%, 72.8%, and 73.7% for control tube with fin, black paint coated with fin, 1% CuO/black paint with fin, 2% CuO/black paint with fin, 3% CuO/black paint with fin and 4% CuO/ black paint with fin respectively.
6) The average outlet temperature for the control tube, black paint coating, 1% Al_2O_3/black paint and 2% Al_2O_3/black paint, 3% Al_2O_3/black paint and 4% Al_2O_3/black paint was 51.1 ℃, 54.6 ℃, 59.4 ℃, 62 ℃, 64.3 ℃, and 65.0 ℃, respectively.

7) The average outlet temperature for the control tube, black paint coating, 1% CuO/black paint and 2% CuO /black paint, 3% CuO/black paint, and 4% CuO/black paint was 36.8 ℃, 39.0 ℃, 45.3 ℃, 49.0 ℃, 53.7 ℃, and 54.1 ℃ respectively.
8) The outlet air temperature of tubes coated with 4% Al_2O_3/black paint was 21.3 ℃,18.0 ℃, and 13.4 ℃ higher than that of control, black paint, and 4% CuO/black paint-coated tubes, respectively.
9) Tubes coated with 4% Al2O3/ black paint with fin inserts were 16.4 ℃, 14.2 ℃, and 5.1 ℃ higher than control and black paint, 4% CuO/black paint coated tubes with fin inserts, respectively.
10) The obtained ventilation rate was eighty times lower than the recommended rate as per the compliance document G4 (NZ Building Code compliance document for ventilation) and the New Zealand Standard (NZS) 4303:1990, which recommends a flow rate of 8 litres per second and per child (28.8 m^3/h/child) to maintain a CO_2 level below 1000 ppm.

The present study concludes that applying Al_2O_3/black paint to the absorber surface improved the thermal efficiency and outlet air temperature of the tube. However, in the present study, the tubes are exposed to ambient conditions as they are not enclosed in an insulated box. This leads to significant heat loss. Future work would involve inserting the nanocoated tubes into an insulated box and monitoring changes in temperature difference (outlet–inlet) and thermal efficiency. It would be interesting to coat the absorber tubes with different nanoparticles embedded in black paint at varying concentrations and test their efficiency. The ventilation rate is to be investigated for a well-insulated tube-type collector. The effect of wind was neglected in this study. In future work, a more rigorous approach would involve simultaneous parallel testing of multiple controls under identical conditions or implementing a laboratory-grade setup with artificial solar simulation to eliminate environmental fluctuations.

6 General Discussion

Research from Australia and New Zealand has shown that poor indoor environments, such as cold, damp, mouldy, crowded, or smoke-exposed environments, are linked to increased hospital admissions for children and older adults (Ingham et al., 2019). Children's immune system is not yet mature (Simon et al., 2015). This lack of maturity makes children more susceptible to unhealthy conditions (airborne contaminants, lack of thermal comfort). Specifically, conditions like pneumonia (Musolino et al., 2020), acute bronchitis in children under four (Bai et al., 2018), respiratory issues in children under fourteen, and asthma in children aged five to fourteen have been connected to these unhealthy conditions (Kulkarni & Grigg, 2008; McNamara et al., 2020)). Poor indoor air quality further impacts the cognitive performance and absenteeism in classrooms (Calderon-Garciduenas et al., 2016; Doe, 2023; Kabirikopaei et al., 2021; Sunyer et al., 2015; Wargocki et al., 2020).

Classrooms are densely occupied spaces; ventilation is critical to improving and maintaining a healthy indoor environment (Sadrizadeh et al., 2022). Suitable airflow is challenging, especially when relying on natural ventilation (Hama et al., 2023). Studies show that many New Zealand schools fail to meet the required ventilation standards during winter, as set by the MOE and ASHRAE standards (Bassett & Gibson, 1999; Cutler-Welsh, 2006b; McIntosh, 2011b). As cited in NS 4303. The New Zealand Standard 4303, “Ventilation for Acceptable Indoor Air Quality,” recommends a ventilation rate of 8.0 liters of fresh air per second per person (NZS4303, 1990). Implementing mechanical ventilation systems frequently incurs prohibitive costs, particularly in light of the financial constraints educational institutions face. Furthermore, the academic schedule coincides with the periods of maximum solar irradiance, thereby positioning solar energy as a viable option for heating and ventilation of classroom settings.

A study in New Zealand found that SAH (insulated boxes placed on classroom roofs) can help improve ventilation rates (N. Z. Ministry of Education, 2014; Y. Wang et al., 2019; Wang et al., 2023). SAHs are an ideal solution because the school day aligns well with the availability of sunlight, allowing solar energy to heat and circulate air in classrooms (Ravi & Saini, 2016b). Nevertheless, owing to inherent thermal losses, SAHs typically exhibit suboptimal thermal efficiency, ranging from 38.0% to 45.0%. Furthermore, there is a paucity of scholarly research on the efficacy of SAHs in facilitating adequate ventilation, underscoring the need to enhance both their thermal and ventilation performance.

To enhance the thermal conductivity and ventilation efficiency of TSAHs, a series of experimental analyses was conducted to compare different enhancement strategies, including design modifications and nanofluid coatings, against baseline control configurations. This

discussion chapter critically compares the outcomes of the present experiments with findings reported by other researchers in the field, highlighting similarities, differences, and the relative performance of the proposed enhancements.

6.1 Finned tube solar air heater with corrugated fin inserts

The thermal performance of FT-SAH integrated with corrugated fin inserts was tested under New Zealand conditions. The study's results showed a wide range of thermal efficiencies, influenced primarily by the mass flow rate and the ratio of the temperature difference between the inlet and outlet air (ΔT) to the solar radiation (I_T) incident on the system. The maximum daily average thermal efficiencies achieved were 83.9% and 43.6% at mass flow rates of 0.053 kg/s and 0.024 kg/s, respectively. The results obtained from the FT-SAH strongly agree with those of other researchers, and they are as follows:

1) **Thermal Efficiency**: The FT-SAH in this study achieved an efficiency of 83.9% at a mass flow rate of 0.056 kg/s, which surpasses the maximum efficiency reported for triple-pass SAHs (80.2%) in (Yassien et al., 2020) and evacuated tube SAHs (70.9%) in (Singh & Vardhan, 2021). This indicates that the FT-SAH's design, incorporating corrugated fins, effectively increases the surface area for heat transfer, which boosts the system's efficiency. The maximum thermal efficiency of the evacuated tube SAH with thermal storage was 64.2% at a mass flow rate of 0.05 kg/s (Elbrashy et al., 2023). The SAHs with V corrugated absorber had a maximum thermal efficiency of 57.0% at a mass flow rate of 0.02 kg/s, and the average thermal efficiency of double pass SAH with V corrugated plates was 65.3% at a mass flow rate of 0.04 kg/s (El-Sebaii et al., 2011a). The studies show that FT-SAH's thermal efficiency is the highest compared to the other types of SAHs.
2) **Temperature Difference (ΔT)**: A key finding was that the FT-SAH produced a higher temperature difference when the air moved more slowly through the system. The average temperature difference at average mass flow rates of 0.055 kg/s and 0.024 kg/s was 18.8 °C and 24.1 °C. These findings are supported by (Jasim Mahmood, 2020), who found that the average temperature difference between the outlet and the ambient air was 38.6°C, 36.5 °C, 33.2 °C, 26.0 °C, 20.3 °C at an air mass flow rate of 0.003, 0.005, 0.013, 0.016, and 0.018 Kg/s , respectively. The temperature difference obtained for SAH with a net of tubes fitted to an absorber plate was 42.3 °C, 21.1 °C, and 17.4 °C at 0.019, 0.028 and 0.075 kg/s respectively (Yassien et al., 2020). The FT-SAH's ability to raise the temperature more at lower airflow rates makes it well-suited for heating spaces where low or moderate heating

is required. FT-SAH is less effective when higher temperatures are needed for applications like industrial heating or drying processes.

3) **Ventilation Rate**: The ventilation performance did not meet the recommended rates for classroom environments in New Zealand. The maximum ventilation rate achieved by the FT-SAH was 176.1 m^3/h at 100% fan speed, but this was five times lower than the recommended rate of 864 m^3/h for a typical classroom. At 100% maximum ventilator speed, the time taken for one complete air change will be 1.2 h for a classroom of 220 m^3 if operating the SAH is the only means of ventilating the classroom. Not many studies are available on estimating the ventilation rate of SAHs. This suggests that while the FT-SAH can significantly enhance ventilation, it should be seen as a supplementary system rather than a primary ventilation solution. Similar issues were noted in other studies, such as the research conducted by Wang et al. (2023) on classroom ventilation highlighted the limitations of SAHs in achieving the required ventilation rates. Visagavel and Srinivasan (2010) found a similar result, with an air change per hour (ACH) ranging from 1.5 to 3.9, depending on the solar radiation intensity and airflow rate.

4) **Effect of Weather Conditions**: Solar radiation and ambient temperature were key factors influencing the performance of the FT-SAH. The results revealed a time delay between the peak solar radiation and the highest outlet air temperature, typically around 1:30 p.m. This delay is likely due to the time required for the air inside the system to absorb and retain heat. Similar results were reported by (Rajendran et al., 2022) and (Hassan et al., 2020). Additionally, the study found that wind and rain had little to no significant impact on the system's efficiency. These findings align with the results of (Paya-Marin et al., 2015), who conducted a large-scale test on a novel back-pass non-perforated unglazed solar air collector. Their study also showed that wind speed, ranging from 0.3 to 4 m/s, did not notably affect the performance of their solar air heater, particularly in terms of the temperature difference between the inlet and outlet air. This supports the conclusion that wind, and rain have a minimal effect on glazed solar air heaters like the FT-SAH. However, these results do not agree with the study conducted by (Wang et al., 2023). Their study shows that for every 10.0 km/h increase in wind speed, the outlet temperature drops by about 2.0 ℃, and for every 100.0 W/m^2 increase in solar radiation, the temperature rises by roughly 5.0 ℃. The disagreement between the results could be due to different designs, weather conditions, or testing equipment. Compared to other SAH designs, the FT-SAH system exhibits high thermal efficiency with its corrugated fin design. However, its application in classroom settings as a sole ventilation system is limited due to the ventilation

rates achieved. Future studies should focus on optimizing the system for specific use cases, such as classrooms, or exploring its potential as part of a hybrid system or increasing the area of the collector (the tested collector was 4.9 m^2). The ability to consistently provide outlet air temperatures above 18.0 °C more than 95.0% of the time highlights its value in improving thermal comfort in low-energy settings, particularly in temperate climates such as New Zealand. However, its ventilation rate (176.1 m^3/h) is lower than recommended, indicating it works best as a supplementary system.

6.2 Finned tube SAH with and without fin inserts

An experimental study was conducted to evaluate the thermal performance of a finned-tube solar air heater (FT-SAH) with fin inserts (treatment) and without (control). The test was conducted on the same FT-SAH, as discussed in Chapter 3. Initially, the experiment was not designed to compare these two setups. However, after analysing the test results of the FT-SAH with fin inserts, it became essential to examine the system without fins to clarify the fins' impact on thermal performance. Due to constraints, including having only one SAH and the need to perform tests under identical outdoor conditions, the system was divided into two parts: one section with fins (treatment) and another without fins (control). An insulated zone separated these two sections to reduce thermal transmittance between them. Three of the thirteen tubes were equipped with fins (treatment), three had no fins (control), and the remaining seven were isolated with cardboard to prevent heat transfer.

While experimenting, the air velocity through the ducts was measured as a single value, meaning the airflow in both the treatment and control sections was combined rather than assessed separately for each zone. This presents a limitation, as it is challenging to find the exact airflow pattern and its direct influence on thermal performance within the treatment and control sections individually. The experimental test results are as follows:

The test results demonstrate that using treatment and control significantly enhances thermal efficiency. The average thermal efficiency of the treatment SAH was 72.6%, while for the control it was 44.5%. The outlet air temperature for the treatment SAH averaged 25.4 ℃ compared to 22.8 ℃ for the control SAH. The temperature difference between the treatment SAH and ambient air (ΔT_1) averaged 7.0 ℃, whereas for controlled SAH, the average difference (ΔT_1) was 4.4 ℃. This data confirms that the finned SAH exhibits improved heat transfer performance due to its increased surface area and enhanced turbulence, resulting in higher outlet temperatures and higher thermal efficiency.

These findings are consistent with previous studies, which have shown that finned systems outperform non-finned configurations. For example, studies by (Singh & Vardhan, 2021) and (Rajendran et al., 2022) reported efficiency improvements ranging from 7.5% to 20.4% when fins were used, further validating the test results observed in this analysis. The maximum thermal efficiency of the evacuated tube SAH with helical fin inserts was 70.9% at a mass flow rate of 0.015 kg/s (Singh & Vardhan, 2021). The maximum thermal efficiency of the rectangular duct SAH integrated with a wavy fin was 85% (CJ Thomas Renald et al., 2022). The SAH with V corrugated absorber had a maximum thermal efficiency of 57% at a mass flow rate of 0.02 kg/s (El-Sebaii et al., 2011a). The highest thermal efficiency of SAH with corrugated metal foam fins was 86% (Hussien & Farhan, 2019). The studies show that the thermal efficiency of SAHs with fin inserts is higher than that of SAHs without them. The present study's thermal efficiency was higher than that reported by the other researcher.

6.3 Nanocoated tubes.

The research consisted of four sets of tests to assess the thermal efficiency of nanocoated aluminium tubes. Test 1 evaluated uncoated (control) tubes, black-painted tubes, and Al_2O_3-black-painted tubes (1% to 4%) without fins. Test 2 examined control tubes, black paint-coated, and CuO/black paint-coated tubes (1% to 4%) without fins. In Test 3, control tubes, black paint coating tubes, and tubes with Al_2O_3/black paint (1% to 4%) were tested with fins, while Test 4 tested control tubes, black paint coating, and CuO/black paint-coated tubes (1% to 4%) with fins. These tests measured outlet temperature and thermal efficiency to determine the effectiveness of nanocoating and fins in enhancing heat transfer. The results obtained from the FT-SAH strongly agree with those of other researchers, and they are as follows:

1. **Temperature difference (ΔT):** The temperature difference (ΔT) data from the nanocoated tubes show a clear improvement in heat absorption as nanoparticle concentration increases. In Test 1 (Al_2O_3/black paint), the ΔT increased from 32.8 ℃ for the control to 46.8 ℃ for the 4% Al_2O_3 coating, reflecting a 14.0 ℃ increase. Similarly, in Test 2 (CuO/black paint), ΔT increased from 20.2 ℃ to 35.4 ℃. These results align with the findings of (Caturwat et al., 2023), who reported enhanced heat absorption with Al_2O_3 coatings due to improved thermal conductivity and surface properties. With the addition of fins, the temperature difference (ΔT) increased further in both Al_2O_3 and CuO-coated tubes. For the 4% Al_2O_3-coated tube, ΔT increased to 54.1 ℃ with fins, an improvement of 14.6 ℃, over the control tubes with fins. Similarly, for the 4% CuO-coated tube, ΔT increased to 49.1 ℃ with fins, showing an improvement of 13.1 ℃. These results align with (Al-Kayiem et al., 2021), who found that

fins significantly boost thermal efficiency by enhancing surface area and heat transfer. The impact is slightly higher for Al_2O_3-coated tubes.

2. **Thermal efficiency:** The combination of fins improved the thermal performance of tubes. The thermal efficiency of the tube coated with 4% Al_2O_3/black paint increased from 61.0% (without fins) to 82.0% with fins, as supported by studies such as those by Kabeel, Omara, et al. (2017), which highlighted the role of fins in enhancing surface area for heat transfer. Additionally, (Al-Kayiem et al., 2021) observed that Al_2O_3 coatings provided a thermal efficiency increase of 51.0%**,** comparable to the 61.0% thermal efficiency observed in the present study for 4% Al_2O_3 without fins. In comparison, tubes coated with CuO showed a smaller but notable improvement in thermal performance. This is consistent with findings by (Khanlari et al., 2020), who noted a similar performance gap between CuO and Al_2O_3 coatings. The CuO coating achieved a thermal efficiency of 51.0% without fins, rising to 73.7% with fins, further demonstrating the positive impact of fin integration. However, it is also important to note the diminishing returns seen with increased nanoparticle concentrations beyond 3%, as supported by (Kim et al., 2017). The present study found marginal gains between 3% and 4% concentrations, with a temperature increase of only 1.2 ℃ without fins and 1.4 ℃ with fins. This suggests that nanoparticle agglomeration limits the efficiency of nanocoating at higher concentrations, a conclusion also drawn in previous studies by (Kim et al., 2017) and (Mohammed et al., 2023).
3. **Ventilation rate:** The ventilation rate achieved in the study was significantly lower than the recommended levels. The observed ventilation rate was approximately eighty times lower than the standard recommended by the New Zealand Building Code, which specifies a flow rate of 8 liters per second per person for indoor air quality. This disparity could be attributed to the experimental setup, which lacked insulation and used a low-capacity fan. Improving the ventilation rate would require increasing fan capacity and enclosing the tubes in an insulated structure, as suggested by (Wang et al., 2023). It is difficult to comment on the ventilation rate of nanocoated tubes due to limited research.
4. **Effect of Weather Conditions:** Weather conditions, particularly solar radiation and ambient temperature, significantly influenced the performance of the nanocoated tubes. Higher solar radiation improved thermal efficiency by increasing heat absorption, while cooler ambient temperatures increased the temperature difference (ΔT) between the inlet and outlet. Consistent solar radiation ensured stable performance across test days, which aligns with findings from (Al-Kayiem et al., 2021) that solar thermal systems are sensitive to weather variations. These factors are crucial in optimizing the real-world performance of

solar air heaters. Studies by Janjai and Tung (2005), and (Saxena et al., 2015), strongly support the results of the present study.

The research demonstrated that nanocoating aluminium tubes with Al_2O_3 and CuO significantly improved heat absorption and thermal efficiency, especially with fins. The temperature difference (ΔT) increased by 14.6 ℃ for 4% Al_2O_3 with fins, and thermal efficiency rose to 82.0%. CuO-coated tubes showed similar trends but with lower gains. Ventilation rates were notably lower than recommended, resulting in inadequate air circulation. Weather conditions, particularly solar radiation, played a crucial role, with consistent radiation ensuring stable performance. In conclusion, the study's results strongly support the effectiveness of nanocoating, particularly Al_2O_3, in improving the thermal performance of SAHs.

Summary

In conclusion, the FT-SAH and nanocoated tubes offer a compelling option for enhancing thermal efficiency in solar air heaters, particularly when used in conjunction with fin inserts and nanocoatings. However, the study also underscores the need for further research to enhance the system's ventilation capabilities. The results suggest that while these technologies can significantly improve thermal performance, they should be integrated into a broader, hybrid system to meet heating and ventilation needs in educational and other densely occupied spaces.

7 Conclusion and Recommendation

An IAQ is important for students' health and classroom performance, as students spend the second-longest time in school. Sufficient ventilation could improve the IAQ. As per the compliance document G4 (NZ Building Code compliance document for ventilation) and the New Zealand Standard (NZS) 4303:1990, the recommended flow rate is 8.0 liters per second and per child (28.8 m3/h/child) to maintain a CO_2 level below 1000.0 ppm. The studies found that the comfortable classroom temperature should be between 18.0 ℃ and 25.0 ℃. Several studies show that NZ schools fail to meet the recommended ventilation rate. Studies suggest that SAH could be an alternative and affordable method to ventilate classrooms.

Chapters 3, 4, and 6 report the experimental test results of the SAH's thermal performance and ventilation rate. The results showed positive changes in these parameters from the designed SAH.

7.1 Original contribution

The studies showed that the thermal performance of solar air heaters is low due to internal heat losses. This study found that 60% of research focused on flat-plate SAHs, while 40% focused on tube-type SAHs. These results demonstrated the potential for investigating the performance of tube-type SAHs. Compared with flat panel designs, tube-type solar panels have two theoretical advantages due to the tube's curvature: greater surface area and better orientation to the sun's path during the day. These advantages can be further improved to produce positive effects on thermal efficiency. This background study published a literature review paper (see appendix) titled: “Review of the Thermal Efficiency of a Tube-type Solar Air Heaters.”

The review paper discussed various methods to improve the thermal efficiency of SAHs. One technique suggested was to nanocoat the tubes. Several studies indicate that research on nanocoating tubes for SAH applications was limited. Therefore, an experimental study was conducted to study the effect of nanocoating the tubes on their thermal and ventilation performance.

SOJOL Pvt Ltd provided a finned tube type SAH (FT-SAH) with corrugated fin inserts to test for its thermal performance and ventilation. During the test, it was identified that the designed SAH experiences many heat losses, and an insufficient ventilation rate was achieved from the FT-SAH. A few modifications were suggested to the company, including improved sealing around the aluminum frame and glass, increasing insulation thickness, and increasing fan capacity. Condensation inside the SAH was observed on very cold days. Therefore, it was suggested that the exhaust fan be kept running constantly.

7.2 Conclusions drawn from the research objectives

Objective 1: The overall objective was to investigate the thermal and ventilation performance of the finned-tube solar air heater (FT-SAH) under Wellington, New Zealand, weather conditions at different mass flow rates, and to evaluate the effect of corrugated fin inserts on system performance. The experimental programme consisted of two parts: (i) a 24-day test (June–November 2023) where the FT-SAH with corrugated fins was operated at both high (100%) and low (50%) fan speeds, and (ii) a six-day comparative test in which three tubes were equipped with fin inserts (treatment SAH) and three tubes were left without fins (control SAH), with tubes isolated to prevent cross-flow.

Findings: The FT-SAH demonstrated superior thermal efficiency and outlet temperatures compared with solar air heaters (SAHs) reported in the literature. Thermal efficiency and ventilation performance improved with increasing mass flow rate, reaching a maximum of 95.7% at 0.053 kg/s and 43.6% at 0.024 kg/s. The ventilation performance was nearly five times higher than that reported by Wang et al. (2023). However, as a single unit, the designed FT-SAH could not meet the required classroom ventilation rate, indicating that multiple SAHs or higher fan capacity would be necessary. The comparative test confirmed that fin inserts significantly enhanced thermal performance: the finned SAH achieved an average efficiency of 72.6% (treatment) compared to 44.5% for the unfinned (control), with higher outlet air temperatures (25.4 $^{\circ}$C vs. 22.8 $^{\circ}$C) and greater temperature rise above ambient (7.0 $^{\circ}$C vs. 4.4 $^{\circ}$C). These results clearly demonstrate the positive role of fin inserts and highlight the FT-SAH's potential for improving classroom heating and ventilation.

Objective 2: The second objective was to investigate the nanocoated tube's thermal and ventilation performance under Wellington, NZ, weather conditions at different mass flow rates. For this experiment, one tube was uncoated, one was black paint-coated, four were coated with Al_2O_3/black paint (1%, 2%, 3%, and 4% concentration), and four were coated with CuO/black paint (1%, 2%, 3%, and 4% concentration).

Findings: The tests were conducted in December 2023 (summer). These test results were compared with those of FT-SAH with corrugated fin inserts, and it was found that under the same weather conditions, the thermal performance of the nanocoated tubes was higher than that of FT-SAH with corrugated fin inserts. However, the ventilation rate from nanocoated tubes was nearly 22 times lower than that from FT-SAH. This may be due to the lower fan capacity in nanocoated tubes. For the nanocoated tube study, the tubes were exposed directly to ambient conditions, as they had no casing, cover, or insulation, resulting in high energy losses.

7.3 Limitations of the Study

1) The experimental study was delayed by one and a half years due to technical issues, continuous lockdown during COVID-19, and delays in the shipment of SAH parts. The shipment of nanoparticles was delayed due to a stock shortage at the company. Therefore, assembling and installing the SAH took longer than anticipated.
2) The FT-SAH was heavy and had sharp edges, making installation at the test location difficult. Rubber pads guarded its sharp edges. Since it was mounted on a metal frame in the Massey University, Wellington Campus car park, it was essential to provide safety to the people moving around the SAH location. Therefore, the site had to be isolated using a fence and cones.
3) In the first month of experimental testing, the anemometer was located close to the fan, impacting the test results. Unrealistic values of thermal efficiency were calculated. Later, it was discovered that the anemometer should be placed at least 0.5 to 1 m away from the fan.
4) In the morning, condensation between the glass and tube surface of SAH was observed on cold and rainy days. Frost was formed on the surface of the glass on wet days, and when the temperature dropped below 8° C. Defrosting took one and a half hours when there was bright solar radiation and longer on cloudy days. It would have been interesting to note if this issue existed when the fan was in operation at day and night.
5) The tube holder at each end of the collector was made of wood, and at higher flow rates, the material that settled on the surface of the tubes was chipped. This could shade the collector surface, affecting its thermal efficiency. Air filters should be installed in such cases, as the air will be polluted due to the mixing of the wood chips.
6) The nanocoated tubes were smoother than FT-SAH and exposed to ambient conditions. Unlike FT-SAH, they were not enclosed in an insulated box with a glass cover. Therefore,
7) In this study, aluminium oxide and copper oxide are used in the nanofluid preparation due to their easy availability and low cost. However, other nanoparticles should also be included.
8) Due to time constraints, this research did not study the practical implications of SAH in the classroom. The fieldwork would have proved the usefulness of the designed collector when in operation.
9) This study did not cover the life cycle assessment of the studied SAHs. A life cycle assessment evaluates the environmental impacts of the SAH components over the long term.

10) Using SAH reduces conventional energy consumption, reducing greenhouse gas emissions. This could help achieve the government's announced net zero carbon emissions. However, this report did not cover the decrease in greenhouse gas emissions from operating SAH.
11) The cost-benefit analysis was not studied because the SAH was installed in the carpark rather than the entire campus. Therefore, calculating the benefit of operating SAH from the energy bill was difficult.
12) It is acknowledged that presenting results in terms of energy-based or normalised performance metrics (e.g., ΔT per meter of tube, energy gain per unit mass flow) would improve generalizability and enable broader cross-study comparisons. However, the scope of this study was limited to evaluating practical heating and ventilation performance for classroom applications, and results were therefore expressed in terms of outlet air temperature, ΔT, mass flow rate, and solar radiation. These parameters are directly relevant to the thermal comfort and ventilation objectives that motivated the research. Future studies may extend this work by incorporating generalised energy metrics for benchmarking against a wider range of solar air heater designs.

7.4 Future scope of research

1) The results show that the studied SAHs showed positive results for temperature. However, it does not meet the ventilation rate as per the MOE and ASHRAE standards. Therefore, more research is needed to improve the ventilation performance of the SAH.
2) The FT-SAH's thermal efficiency was higher than the other SAHs studied in the literature. However, further improvement in its efficiency is possible. This can be achieved by sealing the gaps (airtight) to reduce heat loss through the duct, frame, and glass cover. Different shapes, designs, and materials of fin inserts are to be investigated.
3) Combining FT-SAH and nanocoating technology would improve the SAH's thermal efficiency. This technique could be explored. The impact of rain and wind on the SAH's performance needs attention.
4) The FT-SAH was difficult to lift as it was heavy (approximately 80 kg), and its tubes were also difficult to dismantle. There is scope to explore low-cost, lightweight thermal energy storage materials that are eco-friendly and will boost the thermal efficiency of SAH.
5) Various other nanoparticles could be studied for their thermal properties and utilized to improve SAH performance. The effect of hybrid nanofluid (mixing two or more nanoparticles) coating on SAH thermal efficiency could also be studied.

6) It would be interesting to calculate and evaluate a life cycle assessment and greenhouse gas emissions and conduct a cost-benefit analysis.
7) A machine learning model could be developed to predict the thermal and ventilation performance of the studied SAH. This model can be useful in making real-time predictions about solar heater usage.
8) The studied SAHs were tested under NZ weather conditions. Therefore, SAH testing across NZ (cross-usage) must be conducted to check its response under varying weather conditions.

7.5 Significance of the findings

1) The test results showed that the outlet temperature from the FT-SAH was above 18 ˚C for 97.3% and 100 % of the time when SAH is operated under high and low fan speed, respectively. The International Energy Agency reports that space heating in residential and commercial buildings uses around 46% of global energy (*International Energy agency-Cooling*, 2021; *International Energy Agency-Renewables. 2019, Paris.*). A New Zealand study reports that a typical New Zealand uses about one-third of its energy for space heating (BRANZ, 2023). The application of SAH could reduce the dependency on fossil fuels and reduce the purchased energy consumption. SAHs should be encouraged in schools as the government policies provide a 50% subsidy.
2) The SAH can be an alternate solution to supplement building ventilation. As discussed in this thesis, IAQ plays a vital role in students' health and cognitive performance. The SAH can be used in classrooms, offices, hospitals, restaurants, and homes. These are high-density spaces that need sufficient ventilation.
3) The experimental results show that the finned tube type SAH could improve the ventilation rate. The hourly average air volume flow rate was calculated to be 172.1 m^3/kg at an hourly average temperature of 32.2 ˚C. However, the average volume flow rate of air required at 20 ˚C to meet the target airflow rate of 864.0 m^3/h was estimated to be 668.4 m^3/h and 589.0 m^3/h at high and low fan speeds, respectively. Assuming a 30.0% energy loss, 1234.3 m^3/h of air must be supplied to meet the 864.0 m^3/h target at 20.0 ˚C. At least two collectors must supply air at 20.0 ˚C to maintain a ventilation rate of 864.0 m^3/h.

8 References

Abdelkader, T. K., Zhang, Y., Gaballah, E. S., Wang, S., Wan, Q., & Fan, Q. (2020). Energy and exergy analysis of a flat-plate solar air heater coated with carbon nanotubes and cupric oxide nanoparticles embedded in black paint. *Journal of Cleaner Production*, *250*. https://doi.org/10.1016/j.jclepro.2019.119501

Abdullah, A. S., Alawee, W. H., Mohammed, S. A., Alqsair, U. F., Dhahad, H. A., Essa, F. A., & Omara, Z. M. (2022). Performance improvement of tubular solar still via tilting glass cylinder, nano-coating, and nano-PCM: experimental approach. *Environmental Science and Pollution Research*, *29*(43), 65088-65099. https://doi.org/10.1007/s11356-022-20207-z

Abdullah, A. S., Amro, M. I., Younes, M. M., Omara, Z. M., Kabeel, A. E., & Essa, F. A. (2020). Experimental investigation of single pass solar air heater with reflectors and turbulators. *Alexandria Engineering Journal*, *59*(2), 579-587. https://doi.org/https://doi.org/10.1016/j.aej.2020.02.004

Abdullah, A. S., Essa, F. A., Bacha, H. B., & Omara, Z. M. (2020). Improving the trays solar still performance using reflectors and phase change material with nanoparticles. *Journal of Energy Storage*, *31*. https://doi.org/10.1016/j.est.2020.101744

Abi Mathew, A., & Thangavel, V. (2021). A novel thermal storage integrated evacuated tube heat pipe solar air heater: Energy, exergy, economic and environmental impact analysis. *Solar Energy*, *220*, 828-842. https://doi.org/10.1016/j.solener.2021.03.057

Abo-Elfadl, S., Hassan, H., & El-Dosoky, M. F. (2020). Energy and exergy assessment of integrating reflectors on thermal energy storage of evacuated tube solar collector-heat pipe system. *Solar Energy*, *209*, 470-484. https://doi.org/10.1016/j.solener.2020.09.009

Abo-Elfadl, S., Mohamed, Y., El-Dosoky, M. F., & Hassan, H. (2021). Energy, exergy, and economic analysis of tubular solar air heater with porous material: An experimental study. *Applied Thermal Engineering*, *196, 117294*. https://doi.org/10.1016/j.applthermaleng.2021.117294

Abo-Elfadl, S., Yousef, M. S., & Hassan, H. (2021). Energy, exergy, and enviro-economic assessment of double and single pass solar air heaters having a new design absorber. *Process Safety and Environmental Protection*, *149*, 451-464. https://doi.org/10.1016/j.psep.2020.11.020

Abu Hamed, T., & Alkharabsheh, S. (2020). Design and performance analysis of a new evacuated tube solar air heaters equipped with fins and coils. *International Journal of Sustainable Energy*, *39*(10), 997-1008. https://doi.org/10.1080/14786451.2020.1798446

Afshari, F., Sozen, A., Khanlari, A., Tuncer, A. D., & Sirin, C. (2020). Effect of turbulator modifications on the thermal performance of cost-effective alternative solar air heater. *Renewable Energy*, *158*, 297-310. https://doi.org/10.1016/j.renene.2020.05.148

Ahmed, R., Mumovic, D., Bagkeris, E., & Ucci, M. (2022). Combined effects of ventilation rates and indoor temperatures on cognitive performance of female higher education students in a hot climate. *Indoor air*, *32*(2), e13004. https://doi.org/10.1111/ina.13004

Akpinar, E. K., & Kocyigit, F. (2010). Experimental investigation of thermal performance of solar air heater having different obstacles on absorber plates. *International Communications in Heat and Mass Transfer*, *37*(4), 416-421. https://doi.org/10.1016/j.icheatmasstransfer.2009.11.007

Al-Kayiem, H. H., Ismaeel, A. A., Baheta, A. T., & Aurybi, M. A. (2021). Performance enhancement of solar vortex power generator by Al2O3-in-black paint coating. *Journal of Cleaner Production*, *316*. https://doi.org/10.1016/j.jclepro.2021.128303

Alam, T., & Kim, M. H. (2017). Performance improvement of double-pass solar air heater – A state of art of review. *Renewable and Sustainable Energy Reviews*, *79*, 779-793. https://doi.org/10.1016/j.rser.2017.05.087

Alami, A. H., & Aokal, K. (2018). Enhancement of spectral absorption of solar thermal collectors by bulk graphene addition via high-pressure graphite blasting. *Energy Conversion and Management*, *156*, 757-764. https://doi.org/10.1016/j.enconman.2017.11.040

Alexis Sutherland, Aniebietabasi Ackley, Robyn Phipps, Ian Longley, Scott MacKenzie, Jason Chen, Mark Jermy, & Gronert, R. (2022). *The Impact of Natural Ventilation During Winter on Thermal ComfortV4*. https://ir.canterbury.ac.nz/bitstreams/51fe0f2c-24aa-4d99-9d74-97511275e272/download

Algarni, S., Tirth, V., Saxena, A., & Gupta, P. (2022). A comparative study of different low-cost sensible heat storage materials for solar air heating: an experimental approach. *Energy Sources, Part A: Recovery, Utilization, and Environmental Effects*, *44*(1), 912-933. https://doi.org/10.1080/15567036.2022.2050854

Almeida, R. M. S. F., Pinto, M., Pinho, P. G., & de Lemos, L. T. (2016). Natural ventilation and indoor air quality in educational buildings: experimental assessment and improvement strategies. *Energy Efficiency*, *10*(4), 839-854. https://doi.org/10.1007/s12053-016-9485-0

Ansari, M., & Bazargan, M. (2018). Optimization of flat plate solar air heaters with ribbed surfaces. *Applied Thermal Engineering*, *136*, 356-363. https://doi.org/https://doi.org/10.1016/j.applthermaleng.2018.02.099

Arani, R. P., Sathyamurthy, R., Chamkha, A., Kabeel, A. E., Deverajan, M., Kamalakannan, K., Balasubramanian, M., Manokar, A. M., Essa, F., & Saravanan, A. (2021). Effect of fins and silicon dioxide nanoparticle black paint on the absorber plate for augmenting yield from tubular solar still. *Environmental Science and Pollution Research*, *28*(26), 35102-35112. https://doi.org/10.1007/s11356-021-13126-y

ASHRAE. (2021). American Society of Heating, Refrigerating and Air-Conditioning Engineers. In *ASHRAE Handbook—Fundamentals*. *ASHRAE*.

Azuma, K., Yanagi, U., Kagi, N., Kim, H., Ogata, M., & Hayashi, M. (2020). Environmental factors involved in SARS-CoV-2 transmission: effect and role of indoor environmental quality in the strategy for COVID-19 infection control. *Environmental health and preventive medicine*, *25*, 1-16. https://doi.org/https://doi.org/10.1186/s12199-020-00904-2

Bai, L., Su, X., Zhao, D., Zhang, Y., Cheng, Q., Zhang, H., Wang, S., Xie, M., & Su, H. (2018). Exposure to traffic-related air pollution and acute bronchitis in children: season and age as modifiers. *Journal of Epidemiology and Community Health*, *72*(5), 426-433. https://doi.org/10.1136/jech-2017-209948

Bako Biro, Z., Clements Croome, D. J., Kochhar, N., Awbi, H. B., & Williams, M. J. (2012). Ventilation rates in schools and pupils' performance. *Building & Environment*, *48*, 215-223. https://doi.org/10.1016/j.buildenv.2011.08.018

Bassett, M., & Gibson, P. (1999). Indicators of natural ventilation effectiveness in twelve New Zealand schools. Proceedings of the 8th International Conference on Indoor Air Quality and Climate, Eidenburgh, UK.

Bennett, J., Davy, P., Trompetter, B., Wang, Y., Pierse, N., Boulic, M., Phipps, R., & Howden-Chapman, P. (2019). Sources of indoor air pollution at a New Zealand urban primary school; a case study [Article]. *Atmospheric Pollution Research*, *10*(2), 435-444. https://doi.org/10.1016/j.apr.2018.09.006

Bezbaruah, P. J., Das, R. S., & Sarkar, B. K. (2020). Overall performance analysis and GRA optimization of solar air heater with truncated half conical vortex generators [Article]. *Solar Energy*, *196*, 637-652. https://doi.org/10.1016/j.solener.2019.12.057

Bhattacharyya, S., Pathak, M., Sharifpur, M., Chamoli, S., & Ewim, D. R. E. (2020). Heat transfer and exergy analysis of solar air heater tube with helical corrugation and perforated circular disc inserts. *Journal of Thermal Analysis and Calorimetry*, *145*(3), 1019-1034. https://doi.org/10.1007/s10973-020-10215-x

Boulic, M., Wang, Y., Phipps, R., Plagmann, M., Cunningham, C., Theobald, C., Howden-Chapman, P., & Baker, M. (2016). *Increasing the ventilation rate and temperature in New Zealand classrooms using a solar roof collector*.

Branz. (2019). *Indoor air pollution at a New Zealand urban primary school*. https://d39d3mj7qio96p.cloudfront.net/media/documents/BRANZ-RN-Indoor_Air_Quality_6.pdf

BRANZ. (2023). *Energy-Designing homes to conserve energy and use it efficiently, from sources that cause least environmental harm*. Retrieved 22/09/2023 from https://www.level.org.nz/energy/

Building for Climate Change. (2020). https://www.building.govt.nz/

Burch, J., & Casey, R. (2009). *Wind issues in solar thermal performance ratings* American Solar Energy Society National Solar Conference, https://www.nrel.gov/docs/fy09osti/45466.pdf

Calderon-Garciduenas, L., Jewells, V., Galaz-Montoya, C., van Zundert, B., Perez-Calatayud, A., Ascencio-Ferrel, E., Valencia-Salazar, G., Sandoval-Cano, M., Carlos, E., & Solorio, E. (2016). Interactive and additive influences of Gender, BMI and Apolipoprotein 4 on cognition in children chronically exposed to high concentrations of PM2. 5 and ozone. APOE 4 females are at highest risk in Mexico City. *Environmental Research*, *150*, 411-422.

Calderone, L. (2020). Which Renewable Energy Source Has the Most Global Growth? https://www.altenergymag.com/article/2020/08/which-renewable-energy-source-has-the-most-global-growth/33612

Caturwat, N. K., Sukamto, D., & Fauzi, R. (2023). Addition Of Aluminium Oxide Nano Particles To The Absorber Plate Coating To Increase The Productivity Of Solar Distillation. *Trends in Mechanical Engineering Research*, *1*, 1-6. https://jurnal.untirta.ac.id/index.php/timer/article/view/20455/10736

Cengel, Y. A. (2011). Thermodynamics: an engineering approach. In: McGraw-Hill.

Chabane, F., Hatraf, N., & Moummi, N. (2014). Experimental study of heat transfer coefficient with rectangular baffle fin of solar air heater [Original Paper]. *Journal of Advanced Research*, *8*(2), 160. https://doi.org/10.1007/s11708-014-0321-y

Chabane, F., Moummi, N., & Benramache, S. (2014). Experimental study of heat transfer and thermal performance with longitudinal fins of solar air heater. *J Adv Res*, *5*(2), 183-192. https://doi.org/10.1016/j.jare.2013.03.001

Chabane, F., Moummi, N., & Benramache, S. (2014). Experimental study of heat transfer and thermal performance with longitudinal fins of solar air heater. *Journal of Advanced Research*, *5*(2), 183-192. https://doi.org/https://doi.org/10.1016/j.jare.2013.03.001

Chappell, P. (2014). *The Climate And Weather Of Wellington*. https://niwa.co.nz/sites/niwa.co.nz/files/Wellington%20Climate%20WEB_0.pdf

Che Sidik, N. A., Mahmud Jamil, M., Aziz Japar, W. M. A., & Muhammad Adamu, I. (2017). A review on preparation methods, stability and applications of hybrid nanofluids. *Renewable and Sustainable Energy Reviews*, *80*, 1112-1122. https://doi.org/10.1016/j.rser.2017.05.221

Choi, S. U. S., & Eastman, e. A. (1995, November 12-17). *Enhancing thermal conductivity of fluids with nano* International Mechanical Engineering Congress & Exposition, San Francisco, USA.

Choudhury, P. K., & Baruah, D. C. (2017). Solar air heater for residential space heating. *Energy, Ecology and Environment*, *2*(6), 387-403. https://doi.org/10.1007/s40974-017-0077-4

CJ Thomas Renald, P Somasundaram, MM Matheswaran, & N Gnanasekaran. (2022). Analytical investigation on thermo hydraulic performance augmentation of triangular duct solar air heater integrated with wavy fins. *International Journal of Green Energy*, *20*(5), 544-554. https://doi.org/10.1080/15435075.2022.2111215

Cortes, A., & Piacentini, R. (1990). Improvement of the efficiency of a bare solar collector by means of turbulence promoters. *Applied Energy*, *36*(4), 253-261.

Crawley, D. B., Hand, J. W., Kummert, M., & Griffith, B. T. (2008). Contrasting the capabilities of building energy performance simulation programs. *Building and Environment*, *43*(4), 661-673.

Cutler-Welsh, M. (2006a). *Thorrington school classroom energy and climate management* [Final, Canterbury University]. New Zealand.

Cutler-Welsh, M. (2006b). Thorrington school classroom energy and climate management. *Final Report, Christchurch, New Zealand: Natural Resources Engineering, Canterbury University*.

Dabra, V., Yadav, L., & Yadav, A. (2018). The effect of tilt angle on the performance of evacuated tube solar air collector: experimental analysis. *International Journal of Engineering, Science and Technology*, *5*(4), 100-110. https://doi.org/10.4314/ijest.v5i4.9

Daisey, J. M., Angell, W. J., & Apte, M. G. (2003). Indoor air quality, ventilation and health symptoms in schools: an analysis of existing information. *Indoor air*, *13*(1), 53-64. https://doi.org/10.1034/j.1600-0668.2003.00153.x

Daliran, A., & Ajabshirchi, Y. (2018). Theoretical and experimental research on effect of fins attachment on operating parameters and thermal efficiency of solar air collector. *Information Processing in Agriculture*, *5*(4), 411-421. https://doi.org/10.1016/j.inpa.2018.07.004

Denscombe, M., Szulc, H., Patrick, C., & Wood, A. (2014). Ethnicity and friendship: the contrast between sociometric research and fieldwork observation in primary school classrooms. In *Gender and Ethnicity in Schools* (pp. 127-144). Routledge.

Dharmaraj, S. K., Ramasubbu, H., Rajendran, V., & Ravichandran, P. (2023). Effect of graphene nanopaint on performance of solar air heater attached with inclined and winglet baffles. *Environmental Science and Pollution Research*, *30*(37), 87330-87342. https://doi.org/10.1007/s11356-023-28646-y

Dietz, L., Horve, P. F., Coil, D. A., Fretz, M., Eisen, J. A., & Van Den Wymelenberg, K. (2020). 2019 Novel Coronavirus (COVID-19) Pandemic: Built Environment Considerations To Reduce Transmission. *Msystems*, *5*(2). https://doi.org/10.1128/mSystems.00245-20

Doe, F. (2023). *Differences in junior high school students' perception of school, teacher and student factors inhibiting their performance in mathematics*

Duarte, R., Glória Gomes, M. d., & Moret Rodrigues, A. (2017). Classroom ventilation with manual opening of windows: Findings from a two-year-long experimental study of a Portuguese secondary school. *Building and Environment*, *124*, 118-129. https://doi.org/https://doi.org/10.1016/j.buildenv.2017.07.041

Dubey, A. (2014). Pressure drop calculation for perforated solar wall air conditioning system: an analytical approach. *International Journal of Research in Advent Technology*, *2*.

Eggers-Lura, A. (1979). In A. Eggers-Lura (Ed.), *Solar Energy in Developing Countries* (pp. 14-56). Pergamon. https://doi.org/https://doi.org/10.1016/B978-0-08-023253-9.50006-9

Eidan, A. A., Alsahlani, A., Alshukri, M. J., & Alsabery, A. I. (2023). Experimental investigation of a solar evacuated tube collector embedded with a heat pipe using different nanofluids and controlled mechanical exciting pulsations. *International Journal of Thermofluids*, *20*. https://doi.org/10.1016/j.ijft.2023.100415

El-Said, E. M. S., Kabeel, A. E., & Abdulaziz, M. (2016). Theoretical study on hybrid desalination system coupled with nano-fluid solar heater for arid states. *Desalination*, *386*, 84-98. https://doi.org/10.1016/j.desal.2016.03.001

El-Sebaii, A. A., Aboul-Enein, S., Ramadan, M. R. I., Shalaby, S. M., & Moharram, B. M. (2011a). Investigation of thermal performance of-double pass-flat and v-corrugated plate solar air heaters. *Energy*, *36*(2), 1076-1086. https://doi.org/10.1016/j.energy.2010.11.042

El-Sebaii, A. A., Aboul-Enein, S., Ramadan, M. R. I., Shalaby, S. M., & Moharram, B. M. (2011b). Thermal performance investigation of double pass-finned plate solar air heater. *Applied Energy*, *88*(5), 1727-1739. https://doi.org/10.1016/j.apenergy.2010.11.017

Elbrashy, A., Aboutaleb, F., El-Fakharany, M., & Essa, F. A. (2023). Experimental study of solar air heater performance with evacuated tubes connected in series and involving nano-copper oxide/paraffin wax as thermal storage enhancer. *Environmental Science and Pollution Research*, *30*(2), 4603-4616. https://doi.org/10.1007/s11356-022-22462-6

Elbrashy, A. A., Abou-Taleb, F. S., El-Fakharany, M. K., & Essa, F. A. (2022). Experimental study of solar air heater performance by evacuated tubes connected in series and loaded with thermal storage material. *Journal of Energy Storage*, *54*. https://doi.org/10.1016/j.est.2022.105266

Energy, U. S. D. o. (2005). *Basic research needs for solar energy utilization*. http://www.sc.doe.gov/bes/reports/files/SEU_rpt.pd

Fan, W., Kokogiannakis, G., & Ma, Z. (2019). Optimisation of life cycle performance of a double-pass photovoltaic thermal-solar air heater with heat pipes. *Renewable Energy*, *138*, 90-105. https://doi.org/https://doi.org/10.1016/j.renene.2019.01.078

Fang, L., Wyon, D. P., Clausen, G., & Fanger, P. O. (2004). Impact of indoor air temperature and humidity in an office on perceived air quality, SBS symptoms and performance. *Indoor air*, *14 Suppl 7*, 74-81. https://doi.org/10.1111/j.1600-0668.2004.00276.x

Ferreira, A. M., & Cardoso, M. (2014). Indoor air quality and health in schools. *J Bras Pneumol*, *40*(3), 259-268. https://doi.org/10.1590/s1806-37132014000300009

Forns, J., Dadvand, P., Foraster, M., Alvarez-Pedrerol, M., Rivas, I., Lopez-Vicente, M., Suades-Gonzalez, E., Garcia-Esteban, R., Esnaola, M., Cirach, M., Grellier, J., Basagana, X., Querol, X., Guxens, M., Nieuwenhuijsen, M. J., & Sunyer, J. (2016). Traffic-Related Air Pollution, Noise at School, and Behavioral Problems in Barcelona Schoolchildren: A Cross-Sectional Study. *Environmental Health Perspectives*, *124*(4), 529-535. https://doi.org/10.1289/ehp.1409449

Gaihre, S., Semple, S., Miller, J., Fielding, S., & Turner, S. (2014). Classroom carbon dioxide concentration, school attendance, and educational attainment. *Journal of School Health*, *84*(9), 569-574. https://doi.org/10.1111/josh.12183

GaneshKumar, P., Vinothkumar, S., Prasanth, B. M., Kumar, K. S., Kim, S. C., Ramkumar, V., Alodhayb, A. N., & Pandiaraj, S. (2024). Predicting thermal performance in solar air heaters with V-corrugated, shot-blasted absorber plate, and black pebble-based sensible heat storage: A machine learning approach. *Journal of Energy Storage*, *100*. https://doi.org/10.1016/j.est.2024.113450

Ghritlahre, H. K., Sahu, P. K., & Chand, S. (2020). Thermal performance and heat transfer analysis of arc shaped roughened solar air heater – An experimental study. *Solar Energy*, *199*, 173-182. https://doi.org/10.1016/j.solener.2020.01.068

Goldstein, L., & Sparrow, E. M. (1977). Heat/Mass Transfer Characteristics for Flow in a Corrugated Wall Channel. *Journal of Heat Transfer*, *99 (2)*. https://doi.org/10.1115/1.3450667

Goldstein, L., & Sparrow, J. E. M. (1976). Experiments on the Transfer Characteristics of a Corrugated Fin and Tube Heat Exchanger Configuration. *Journal of Heat Transfer*, *98 (1)*. https://doi.org/https://doi.org/10.1115/1.3450464

Guba, E. G., & Lincoln, Y. S. (1994). Competing paradigms in qualitative research. *Handbook of qualitative research*, *2*(163-194), 105.

Gully, F. (2015). Windows and Doors in New Zealand Primary Schools: A Study of Low-Decile Primary Schools in Auckland. *Massey University*.

Gupta, D., Solanki, S. C., & Saini, J. S. (1997). Thermohydraulic performance of solar air heaters with roughened absorber plates. *Solar Energy*, *61*(1), 33-42. https://doi.org/https://doi.org/10.1016/S0038-092X(97)00005-4

Gupta, S., Rajale, S., Raval, F., Sojitra, M., Tiwari, A. K., Joshi, A., & Singh, R. (2021). Comparative performance analysis of flat plate solar collectors with and without aluminium oxide-based nano-fluid. *Materials Today: Proceedings*, *46*, 5378-5383. https://doi.org/10.1016/j.matpr.2020.08.797

Gurbuz, E. Y., Sahinkesen, İ., Kusun, B., Tuncer, A. D., & Kecebas, A. (2023). Enhancing the performance of an unglazed solar air collector using mesh tubes and Fe3O4 nano-enhanced absorber coating. *Energy*, *277*. https://doi.org/10.1016/j.energy.2023.127704

Hama, S., Kumar, P., Tiwari, A., Wang, Y., & Linden, P. F. (2023). The underpinning factors affecting the classroom air quality, thermal comfort and ventilation in 30 classrooms of primary schools in London. *Environmental Research*, *236*. https://doi.org/10.1016/j.envres.2023.116863

Hassan, H., Abo-Elfadl, S., & El-Dosoky, M. F. (2020). An experimental investigation of the performance of new design of solar air heater (tubular). *Renewable Energy*, *151*, 1055-1066. https://doi.org/10.1016/j.renene.2019.11.112

Ho, C.-D., Chang, H., Hsiao, C.-F., & Lin, Y.-C. (2021). Optimizing thermal efficiencies of double-pass cross-corrugated solar air heaters on various configurations with external recycling. *Energies*, *14*(13). https://doi.org/10.3390/en14134019

Holden, K. A., Lee, A. R., Hawcutt, D. B., & Sinha, I. P. (2023). The impact of poor housing and indoor air quality on respiratory health in children. *Breathe (Sheff)*, *19*(2), 230058. https://doi.org/10.1183/20734735.0058-2023

Hussien, S. Q., & Farhan, A. A. (2019). The effect of metal foam fins on the thermo-hydraulic performance of a solar air heater. *International Journal of Renewable Energy Research*, *9*, 840-847.

IEA. (2022). *World Energy Outlook* https://iea.blob.core.windows.net/assets/7e42db90-d8ea-459d-be1e-1256acd11330/WorldEnergyOutlook2022.pdf

Ingham, T., Keall, M., Jones, B., Aldridge, D. R., Dowell, A. C., Davies, C., Crane, J., Draper, J. B., Bailey, L. O., & Viggers, H. (2019). Damp mouldy housing and early childhood hospital admissions for acute respiratory infection: a case control study. *Thorax*, *74*(9), 849-857.

International Energy Agency. (2020).

International Energy agency- Cooling. (2021). https://www.iea.org/reports/cooling

International Energy Agency-Renewables. 2019, Paris. https://www.iea.org/reports/renewables-2019

Isaacs, N., Camiller, M., French, L., Pollard, A., Saville-Smith, K., Fraser, R., Rossouw, P., & Jowett, J. (2006). *Energy use in NZ households*. https://d39d3mj7qio96p.cloudfront.net/media/documents/SR155_Energy_use_in_NZ_households_-_report_on_year_10_of_the_Household_Energy.pdf

Janjai, S., & Tung, P. (2005). Performance of a solar dryer using hot air from roof-integrated solar collectors for drying herbs and spices. *Renewable Energy*, *30*(14), 2085-2095. https://doi.org/10.1016/j.renene.2005.02.006

Jasim Mahmood, A. (2020). Thermal Evaluation of a Double-Pass Unglazed Solar Air Heater with Perforated Plate and Wire Mesh Layers. *Sustainability*, *12*(9). https://doi.org/10.3390/su12093619

Jia, G., Shevliakova, E., Artaxo, P., Noblet-Ducoudré, N. D., Houghton, R., House, J., Kitajima, K., Lennard, C., Popp, A., Sirin, A., Sukumar, R., & Verchot, L. (2019). *Land–climate interactions*. https://www.ipcc.ch/site/assets/uploads/sites/4/2021/07/05_Chapter-2-V6.pdf

John, A. D., & Beckman, W. A. (2013). *Solar Engineering of Thermal Processes, Fourth Edition*

Jurelionis, A., & Seduikyte, L. (2008). Indoor environmental conditions in lithuanian schools.

Kabeel, A. E., Hamed, M. H., Omara, Z. M., & Kandeal, A. W. (2017). Solar air heaters: Design configurations, improvement methods and applications – A detailed review. *Renewable and Sustainable Energy Reviews*, *70*, 1189-1206. https://doi.org/https://doi.org/10.1016/j.rser.2016.12.021

Kabeel, A. E., Omara, Z. M., Essa, F. A., Abdullah, A. S., Arunkumar, T., & Sathyamurthy, R. (2017). Augmentation of a solar still distillate yield via absorber plate coated with black nanoparticles. *Alexandria Engineering Journal*, *56*(4), 433-438. https://doi.org/10.1016/j.aej.2017.08.014

Kabeel, A. E., Sathyamurthy, R., Sharshir, S. W., Muthumanokar, A., Panchal, H., Prakash, N., Prasad, C., Nandakumar, S., & El Kady, M. S. (2019). Effect of water depth on a novel absorber plate of pyramid solar still coated with TiO2 nano black paint. *Journal of Cleaner Production*, *213*, 185-191. https://doi.org/10.1016/j.jclepro.2018.12.185

Kabirikopaei, A., Lau, J., Nord, J., & Bovaird, J. (2021). Identifying the K-12 classrooms' indoor air quality factors that affect student academic performance. *Science of the Total Environment*, *786*, 147498. https://doi.org/10.1016/j.scitotenv.2021.147498

Kalaiarasi, G., Velraj, R., & Swami, M. V. (2016). Experimental energy and exergy analysis of a flat plate solar air heater with a new design of integrated sensible heat storage. *Energy*, *111*, 609-619. https://doi.org/10.1016/j.energy.2016.05.110

Karim, M., & Hawlader, M. (2006). Performance investigation of flat plate, v-corrugated and finned air collectors. *Energy*, *31*(4), 452-470. https://doi.org/10.1016/j.energy.2005.03.007

Karwa, R. (2023). Thermo-hydraulic performance of solar air heater with finned absorber plate forming multiple rectangular air flow passages in parallel under laminar flow conditions. *Applied Thermal Engineering*, *221*. https://doi.org/10.1016/j.applthermaleng.2022.119673

Khanlari, A., Badali, Y., & Tuncer, A. D. (2023). Analysis of a spiral-formed solar air heating system with ceria nanoparticles-enhanced absorber coating. *Journal of Building Engineering*, *71*. https://doi.org/10.1016/j.jobe.2023.106534

Khanlari, A., Sözen, A., Şirin, C., Tuncer, A. D., & Gungor, A. (2020). Performance enhancement of a greenhouse dryer: Analysis of a cost-effective alternative solar air heater. *Journal of Cleaner Production*, *251*. https://doi.org/10.1016/j.jclepro.2019.119672

Khanlari, A., Sözen, A., Tuncer, A. D., Afshari, F., Gürbüz, E. Y., & Bilge, Y. C. (2021). Numerical and experimental analysis of longitudinal tubular solar air heaters made from plastic and metal waste materials. *Heat Transfer Research*, *52*(10).

Khanlari, A., Tuncer, A. D., Sözen, A., Aytaç, İ., Çiftçi, E., & Variyenli, H. İ. (2022). Energy and exergy analysis of a vertical solar air heater with nano-enhanced absorber coating and perforated baffles. *Renewable Energy*, *187*, 586-602. https://doi.org/10.1016/j.renene.2022.01.074

Kim, H., Kim, J., & Cho, H. (2017). Review of Thermal Performance and Efficiency in Evacuated Tube Solar Collector with Various Nanofluids. *International Journal of Air-Conditioning and Refrigeration*, *25*(02). https://doi.org/10.1142/s2010132517300014

Komolafe, C. A., Oluwaleye, I. O., Awogbemi, O., & Osueke, C. O. (2019). Experimental investigation and thermal analysis of solar air heater having rectangular rib roughness on the absorber plate. *Case Studies in Thermal Engineering*, *14*. https://doi.org/10.1016/j.csite.2019.100442

Kulkarni, N., & Grigg, J. (2008). Effect of air pollution on children. *Paediatrics and Child Health*, *18*(5), 238-243. https://doi.org/https://doi.org/10.1016/j.paed.2008.02.007

Kumar, A., & Layek, A. (2020). Nusselt number and friction characteristics of a solar air heater that has a winglet type vortex generator in the absorber surface. *Experimental Thermal and Fluid Science*, *119*. https://doi.org/10.1016/j.expthermflusci.2020.110204

Kumar, R., & Chand, P. (2017). Performance enhancement of solar air heater using herringbone corrugated fins. *Energy*, *127*, 271-279. https://doi.org/10.1016/j.energy.2017.03.128

Kumar, R., Kumar Verma, S., & Kumar Sharma, V. (2020). Performance enhancement analysis of triangular solar air heater coated with nanomaterial embedded in black paint. *Materials Today: Proceedings*, *26*, 2528-2532. https://doi.org/10.1016/j.matpr.2020.02.538

Kumar, R., & Rosen, M. A. (2011). Performance evaluation of a double pass PV/T solar air heater with and without fins. *Applied Thermal Engineering*, *31*(8-9), 1402-1410. https://doi.org/10.1016/j.applthermaleng.2010.12.037

Kumar, R., Verma, S. K., Mishra, S. K., Sharma, A., Yadav, A. S., & Sharma, N. (2022). Performance Enhancement of Solar Air Heater using Graphene/Cerium Oxide and

Graphene-Black Paint Coating on Roughened Absorber Plate. *International Journal of Vehicle Structures and Systems*, *14*(2). https://doi.org/10.4273/ijvss.14.2.23

Kumar, R., Verma, S. K., & Singh, M. (2021). Experimental investigation of nanomaterial doped in black paint coating on absorber for energy conversion applications. *Materials Today: Proceedings*, *44*, 961-967. https://doi.org/10.1016/j.matpr.2020.11.006

Lakshmi, D. V. N., Layek, A., & Kumar, P. M. (2017). Performance Analysis of Trapezoidal Corrugated Solar Air Heater with Sensible Heat Storage Material. *Energy Procedia*, *109*, 463-470. https://doi.org/10.1016/j.egypro.2017.03.069

Li, H., Dai, Y. J., Li, Y., La, D., & Wang, R. Z. (2012). Case study of a two-stage rotary desiccant cooling/heating system driven by evacuated glass tube solar air collectors. *Energy and Buildings*, *47*, 107-112. https://doi.org/10.1016/j.enbuild.2011.11.035

Li, X. (2011). Green Energy for Sustainability and Energy Security. In X. Li (Ed.), *Green Energy: Basic Concepts and Fundamentals* (pp. 1-16). Springer London. https://doi.org/10.1007/978-1-84882-647-2_1

Liaw, F. (2015). Doors and Windows Needs for School. *Massey University, Auckland, New Zealand*.

Lorenc, A., Kesten, J. M., Kidger, J., Langford, R., & Horwood, J. (2021). Reducing COVID-19 risk in schools: a qualitative examination of secondary school staff and family views and concerns in the South West of England. *BMJ Paediatr Open*, *5*(1), e000987. https://doi.org/10.1136/bmjpo-2020-000987

Luca, S., Angelamaria, M., Laura, C., Aldo, R., Alexandro, A., & Marco, D. I. (2019). The Effect of Ventilation Strategies on Indoor Air Quality and Energy Consumptions in Classrooms. *Buildings*, *9*(5), 110-110. https://doi.org/10.3390/buildings9050110

Luo, Q., Li, B., Wang, Z., Su, S., & Xiao, H. (2022). A study of unidirectional spiral tube for air evacuation in a solar heater with phase-change material. *Journal of Building Engineering*, *46*, 103659. https://doi.org/https://doi.org/10.1016/j.jobe.2021.103659

Madhu, B., Kabeel, A. E., Sathyamurthy, R., Sharshir, S. W., Manokar, A. M., Raghavendran, P. R., Chandrashekar, T., & Mageshbabu, D. (2020). Investigation on heat transfer enhancement of conventional and staggered fin solar air heater coated with CNT-black paint-an experimental approach. *Environmental Science and Pollution Research*, *27*(26), 32251-32269. https://doi.org/10.1007/s11356-019-07561-1

Madhulatha, G., Mohan Jagadeesh Kumar, M., & Sateesh, P. (2021). Optimization of tube arrangement and phase change material for enhanced performance of solar air heater- A numerical analysis. *Journal of Energy Storage*, *41*. https://doi.org/10.1016/j.est.2021.102876

Mahamude, A. S. F., Harun, W. S. W., Kadirgama, K., Farhana, K., Ramasamy, D., Samylingam, L., & Aslfattahi, N. (2021). Thermal performance of nanomaterial in solar collector: State-of-play for graphene. *Journal of Energy Storage*, *42*. https://doi.org/10.1016/j.est.2021.103022

Maheshwari, B., Karwa, R., Singhvi, R., Goyal, A., Kumawat, R., Sharma, A., Prajapat, R., Kumawat, D., Rankawat, M., & Bhardwaj, N. (2012). Performance study of solar air heater with baffled duct. *J. Mech. Civil Eng.*, *4*(5), 52-56.

Mandal, S., & Ghosh, S. K. (2020). Experimental investigation of the performance of a double pass solar water heater with reflector. *Renewable Energy*, *149*, 631-640. https://doi.org/10.1016/j.renene.2019.11.160

Manoj Kumar Sain, & Kumawat, G. (2015). performance enhancement of single slope solar still using nanoparticles mixed black paint. *Advanced Nanoscience and Technology: An International Journal*. https://airccj.org/ns/antj/papers/1115antj04.pdf

Matsunaga, J., Kikuta, K., Hirakawa, H., Hayashi, M., & Fukushima, A. (2023). Evaluation of the Primary Energy and Carbon Dioxide Emissions of a Passive Ventilation System with a Solar Air Heater. *Energies*, *16*(14). https://doi.org/10.3390/en16145535

Mazzei, A., & Rodrigues, J. (2000). Alumina-mullite-zirconia composites obtained by reaction sintering: Part I. Microstructure and mechanical behaviour. *Journal of Materials Science*, *35*, 2807-2814.

MBIE. (2017). nzs-43031990. In.

McIntosh, J. (2011a). *The indoor air quality in 35 Wellington primary schools* Wellington]. New Zealand.

McIntosh, J. (2011b). *The Indoor Air Quality in 35 Wellington Primary Schools During the Day: A Thesis Submitted to the Victoria University of Wellington in Partial Fulfilment of the Requirements for the Degree of Masters in Building Science*. Victoria University of Wellington. https://books.google.co.nz/books?id=NCOitwAACAAJ

McNamara, D., Asher, I., & , & Davies, C. (2020). *asthma and respiratory foundation NZ New Zealand child asthma guidelines: a quick reference guide*. https://www.nzrespiratoryguidelines.co.nz/

Mendell, M. J., Eliseeva, E. A., Davies, M. M., & Lobscheid, A. (2016). Do classroom ventilation rates in California elementary schools influence standardized test scores? Results from a prospective study. *Indoor air*, *26*(4), 546. http://ezproxy.massey.ac.nz/login?url=http://search.ebscohost.com/login.aspx?direct=true&db=edb&AN=116816493&site=eds-live&scope=site

Miller, M. D., Marty, M. A., Arcus, A., Brown, J., Morry, D., & Sandy, M. (2002). Differences Between Children and Adults: Implications for Risk Assessment at California EPA. *International Journal of Toxicology*, *21*(5), 403-418. https://doi.org/10.1080/10915810290096630

Ministry of Education, M. (2014). *Designing Quality Learning Spaces: Indoor Air Quality and Thermal Comfort. Wellington, NZ: Ministry of Education*.

Ministry of Education, N. Z. (2014). *Energy use and conservation in schools*

Retrieved 25/09/2023 from https://www.education.govt.nz/school/property-and-transport/school-facilities/energy-water-and-waste-management/energy-use-and-conservation/

Misra, R., Singh, J., Jain, S. K., Faujdar, S., Agrawal, M., Mishra, A., & Goyal, P. K. (2020). Prediction of behavior of triangular solar air heater duct using V-down rib with multiple gaps and turbulence promoters as artificial roughness: A CFD analysis. *International Journal of Heat and Mass Transfer*, *162*. https://doi.org/10.1016/j.ijheatmasstransfer.2020.120376

Mittal, M. K., & Varshney, L. (2006). Optimal thermohydraulic performance of a wire mesh packed solar air heater. *Solar Energy*, *80*(9), 1112-1120. https://doi.org/10.1016/j.solener.2005.10.004

Modi, K. V., Patel, P. R., & Patel, S. K. (2023). Applicability of mono-nanofluid and hybrid-nanofluid as a technique to improve the performance of solar still: A critical review. *Journal of Cleaner Production*, *387*. https://doi.org/10.1016/j.jclepro.2023.135875

MOE. (2017). Retrieved from https://www.education.govt.nz/assets/Documents/Ministry/Publications/Annual-Reports/2017-MOE-Annual-Report-web.pdf

MOE. (2022). *Education Counts- Number of Schools* (Ministry of Education, Issue. https://www.educationcounts.govt.nz/statistics/number-of-schools

Mohammed, M., Oleiwi, J. K., Jawad, A. J. M., Mohammed, A. M., Osman, A. F., Rahman, R., Adam, T., Betar, B. O., Gopinath, S. C. B., & Dahham, O. S. (2023). Effect of zinc oxide surface treatment concentration and nanofiller loading on the flexural properties of unsaturated polyester/kenaf nanocomposites. *Heliyon*, *9*(9), e20051. https://doi.org/10.1016/j.heliyon.2023.e20051

Morawska, L., Tang, J. W., Bahnfleth, W., Bluyssen, P. M., Boerstra, A., Buonanno, G., Cao, J., Dancer, S., Floto, A., Franchimon, F., Haworth, C., Hogeling, J., Isaxon, C., Jimenez, J. L.,

Kurnitski, J., Li, Y., Loomans, M., Marks, G., Marr, L. C., Mazzarella, L., Melikov, A. K., Miller, S., Milton, D. K., Nazaroff, W., Nielsen, P. V., Noakes, C., Peccia, J., Querol, X., Sekhar, C., Seppanen, O., Tanabe, S. I., Tellier, R., Tham, K. W., Wargocki, P., Wierzbicka, A., & Yao, M. (2020). How can airborne transmission of COVID-19 indoors be minimised? *Environment International*, *142*, 105832. https://doi.org/10.1016/j.envint.2020.105832

Morgan, D. L. (2014). Pragmatism as a paradigm for social research. *Qualitative inquiry*, *20*(8), 1045-1053.

Moriyama, M., Hugentobler, W. J., & Iwasaki, A. (2020). Seasonality of Respiratory Viral Infections. *Annual Review of Virology*, *7*(1), 83-101. https://doi.org/10.1146/annurev-virology-012420-022445

Mostafavi, A., & Jain, A. . (2022). Thermal management effectiveness and efficiency of a fin surrounded by a phase change material (PCM). *International Journal of Heat and Mass Transfer*, 191.

Murali, G., Rama Krishna Reddy, K., Sai Kumar, M. T., SaiManikanta, J., & Nitish Kumar Reddy, V. (2020). Performance of solar aluminium can air heater using sensible heat storage. *Materials Today: Proceedings*, *21*, 169-174. https://doi.org/10.1016/j.matpr.2019.04.213

Musolino, A. M., Supino, M. C., Buonsenso, D., Ferro, V., Valentini, P., Magistrelli, A., Lombardi, M. H., Romani, L., D'Argenio, P., & Campana, A. (2020). Lung Ultrasound in Children with COVID-19: Preliminary Findings. *Ultrasound Med Biol*, *46*(8), 2094-2098. https://doi.org/10.1016/j.ultrasmedbio.2020.04.026

Nain, S., Ahlawat, V., Kajal, S., Anuradha, P., Sharma, A., & Singh, T. (2021). Performance analysis of different U-shaped heat exchangers in parabolic trough solar collector for air heating applications. *Case Studies in Thermal Engineering*, *25*. https://doi.org/10.1016/j.csite.2021.100949

Nembhard, M. D., Burton, D. J., & Cohen, J. M. (2020). Ventilation use in nonmedical settings during COVID-19: Cleaning protocol, maintenance, and recommendations. *Toxicol Ind Health*, *36*(9), 644-653. https://doi.org/10.1177/0748233720967528

Norouzi, A. M., Siavashi, M., & Khaliji Oskouei, M. (2020). Efficiency enhancement of the parabolic trough solar collector using the rotating absorber tube and nanoparticles. *Renewable Energy*, *145*, 569-584. https://doi.org/10.1016/j.renene.2019.06.027

Nunez, C. (2019, 03/04/2019). What Are Fossil Fuels? https://www.nationalgeographic.com/environment/article/fossil-fuels

Ozturk, M., & Ciftci, E. (2023). Upgrading the performance of a solar air collector with flexible aluminum air ducts and graphene nanoplatelet-enhanced absorber coating. *Thermal Science and Engineering Progress*, *40*. https://doi.org/10.1016/j.tsep.2023.101760

Pandey, S., Mishra, S. K., Sharma, A., Verma, A. K., & Yadav, L. (2021). Performance analysis of evacuated tube type solar air heater with parabolic trough type collector. *International Journal of Energy and Water Resources*. https://doi.org/10.1007/s42108-021-00158-w

Pardeshi, P. S., Boulic, M., van Heerden, A., Phipps, R., & Cunningham, C. W. (2024). Review of the thermal efficiency of a tube-type solar air heaters. *Renewable and Sustainable Energy Reviews*, *199*. https://doi.org/10.1016/j.rser.2024.114509

Parsa, S. M., Yazdani, A., Dhahad, H., Alawee, W. H., Hesabi, S., Norozpour, F., Javadi Y, D., Ali, H. M., & Afrand, M. (2021). Effect of Ag, Au, TiO2 metallic/metal oxide nanoparticles in double-slope solar stills via thermodynamic and environmental analysis. *Journal of Cleaner Production*, *311*. https://doi.org/10.1016/j.jclepro.2021.127689

Patton, M. Q. 2015. *Qualitative research & evaluation methods: integrating theory and practice*.

Pavlovic, Z. T., & Kostic, L. T. (2015). Variation of reflected radiation from all reflectors of a flat plate solar collector during a year. *Energy*, *80*, 75-84. https://doi.org/10.1016/j.energy.2014.11.044

Paya-Marin, M. A., Lim, J. B. P., Chen, J.-F., Lawson, R. M., & Gupta, B. S. (2015). Large scale test of a novel back-pass non-perforated unglazed solar air collector. *Renewable Energy*, *83*, 871-880. https://doi.org/10.1016/j.renene.2015.05.039

Persily, A. (2020). *Quit Blaming ASHRAE Standard 62.1 for 1000 ppm CO_2* Conference of the International Society of Indoor Air Quality & Climate, https://tsapps.nist.gov/publication/get_pdf.cfm?pub_id=929997

Petersen, S., Jensen, K. L., Pedersen, A. L. S., & Rasmussen, H. S. (2016). The effect of increased classroom ventilation rate indicated by reduced CO2 concentration on the performance of schoolwork by children. In (Vol. 26, pp. 366-379).

Pfeffer, F., Eisenlohr, J., Basch, A., Hermle, M., Lee, B. G., & Goldschmidt, J. C. (2016). Systematic analysis of diffuse rear reflectors for enhanced light trapping in silicon solar cells. *Solar Energy Materials and Solar Cells*, *152*, 80-86. https://doi.org/10.1016/j.solmat.2016.03.028

Poongavanam, G. K., Panchabikesan, K., Leo, A. J. D., & Ramalingam, V. (2018). Experimental investigation on heat transfer augmentation of solar air heater using shot blasted V-corrugated absorber plate. *Renewable Energy*, *127*, 213-229. https://doi.org/10.1016/j.renene.2018.04.056

Prevention, C. f. D. C. a. (2022). *Guidance for School Administrators to Help Reduce the Spread of Seasonal Influenza in K-12 Schools*. https://www.cdc.gov/flu/school/guidance.htm

Priyam, A., & Chand, P. (2016). Thermal and thermohydraulic performance of wavy finned absorber solar air heater. *Solar Energy*, *130*, 250-259. https://doi.org/10.1016/j.solener.2016.02.030

Rahul Kumar, & Verma, S. K. (2021). Exergetic and energetic evaluation of an innovative solar air heating system coated with graphene and copper oxide nanoparticles. *Journal of Thermal Engineering*, *7*, 447-467. https://doi.org/https://doi.org/10.18186/thermal.887023

Rajendran, V., Ramasubbu, H., Rajarathinam, J. V., & Pichandi, R. (2022). Experimental study on the thermal performance of a solar air heater integrated with multi-geometry arrangements over the absorber plate. *Environmental Science and Pollution Research*, *29*(25), 38331-38345. https://doi.org/10.1007/s11356-022-18830-x

Ravi, R. K., & Saini, R. P. (2016a). A review on different techniques used for performance enhancement of double pass solar air heaters [Review Article]. *Renewable and Sustainable Energy Reviews*, *56*, 941-952. https://doi.org/10.1016/j.rser.2015.12.004

Ravi, R. K., & Saini, R. P. (2016b). A review on different techniques used for performance enhancement of double pass solar air heaters [Article]. *Renewable & Sustainable Energy Reviews*, *56*, 941-952. https://doi.org/10.1016/j.rser.2015.12.004

Reardon, C., McGee, C., & Milne, G. (2020). *Australia's guide to environmentally sustainable homes* (6 ed.). https://www.yourhome.gov.au/passive-design

Ritchie, H., Roser, M., & Rosado, P. (2020). Energy. *Our World in Data*. https://ourworldindata.org/energy

Robert, R. A., Kaithari, D. K., Mirza, M. M., & Bhambare, P. S. (2018). Influence Of Nano Al2o3 To Improve The Yield Of Double Slope Solar Still. *International Journal of Students' Research in Technology & Management*, *6*(3), 01-08. https://doi.org/10.18510/ijsrtm.2018.631

Sadrizadeh, S., Yao, R., Yuan, F., Awbi, H., Bahnfleth, W., Bi, Y., Cao, G., Croitoru, C., de Dear, R., Haghighat, F., Kumar, P., Malayeri, M., Nasiri, F., Ruud, M., Sadeghian, P., Wargocki, P., Xiong, J., Yu, W., & Li, B. (2022). Indoor air quality and health in schools: A critical review for developing the roadmap for the future school environment. *Journal of Building Engineering*, *57*. https://doi.org/10.1016/j.jobe.2022.104908

Sahu, M. K., & Prasad, R. K. (2017). Thermohydraulic performance analysis of an arc shape wire roughened solar air heater. *Renewable Energy*, *108*, 598-614. https://doi.org/10.1016/j.renene.2017.02.075

Said, Z., Sabiha, M. A., Saidur, R., Hepbasli, A., Rahim, N. A., Mekhilef, S., & Ward, T. A. (2015). Performance enhancement of a Flat Plate Solar collector using Titanium dioxide

nanofluid and Polyethylene Glycol dispersant. *Journal of Cleaner Production*, *92*, 343-353. https://doi.org/10.1016/j.jclepro.2015.01.007

Saini, R. P., & Verma, J. (2008). Heat transfer and friction factor correlations for a duct having dimple-shape artificial roughness for solar air heaters. *Energy*, *33*(8), 1277-1287. https://doi.org/10.1016/j.energy.2008.02.017

Samneang, H., Kumar, L., Zafar, A., Ali, M. U., Zahid, T., Bibi, S., Ahmad, M. S., Ghafoor, U., & Selvaraj, J. (2021). A Systematic Indoor and Outdoor Study of the Effect of Particle Size and Concentration of TiO2 in Improving Solar Absorption for Solar Still Application. *Frontiers in Materials*, *8*. https://doi.org/10.3389/fmats.2021.683490

Sathyamurthy, R., Kabeel, A. E., Balasubramanian, M., Devarajan, M., Sharshir, S. W., & Manokar, A. M. (2020). Experimental study on enhancing the yield from stepped solar still coated using fumed silica nanoparticle in black paint. *Materials Letters*, *272*. https://doi.org/10.1016/j.matlet.2020.127873

Saxena, A., Srivastava, G., & Tirth, V. (2015). Design and thermal performance evaluation of a novel solar air heater. *Renewable Energy*, *77*, 501-511. https://doi.org/https://doi.org/10.1016/j.renene.2014.12.041

Saxena, R., Pachorkar, P., Jain, A., Majumder, H., Pandey, K. K., Mishra, S. K., Khayum, N., & Kalbande, V. P. (2023). Performance enhancement of solar air heater using artificial roughness. *Materials Today: Proceedings*. https://doi.org/10.1016/j.matpr.2023.05.012

Selimefendigil, F., Sirin, C., Ghachem, K., Kolsi, L., Alqahtani, T., & Algarni, S. (2022). Enhancing the performance of a greenhouse drying system by using triple-flow solar air collector with nano-enhanced absorber coating. *Case Studies in Thermal Engineering*, *34*. https://doi.org/10.1016/j.csite.2022.102011

Senthil, R., Kishore Kumar, K., Rohan Rajendra, K., & Juneja, A. (2020). Enhancement of absorptance of absorber surfaces of a flat plate solar collector using black coating with graphene. *Energy Sources, Part A: Recovery, Utilization, and Environmental Effects*, *43*(20), 2595-2608. https://doi.org/10.1080/15567036.2020.1826016

Sethi, M., Tripathi, R. K., Bhardwaj, P., Kumar, M., Thakur, G., Kumari, A., Hasan, M., & Verma, M. (2023). Review of the impact of nanomaterial on the thermal efficiency of an evacuated tube solar air heater. *Materials Today: Proceedings*. https://doi.org/10.1016/j.matpr.2023.01.229

Shalaby, S. M., Bek, M. A., & El-Sebaii, A. A. (2014). Solar dryers with PCM as energy storage medium: A review. *Renewable and Sustainable Energy Reviews*, *33*, 110-116. https://doi.org/10.1016/j.rser.2014.01.073

Shamshirgaran, S. R., Khalaji Assadi, M., & Viswanatha Sharma, K. (2017). Application of nanomaterials in solar thermal energy storage. *Heat and Mass Transfer*, *54*(6), 1555-1577. https://doi.org/10.1007/s00231-017-2259-1

Shaughnessy, R. J., Haverinen-Shaughnessy, U., Nevalainen, A., & Moschandreas, D. (2006). A preliminary study on the association between ventilation rates in classrooms and student performance [Article]. *Indoor air*, *16*(6), 465-468. https://doi.org/10.1111/j.1600-0668.2006.00440.x

Simon, A. K., Hollander, G. A., & McMichael, A. (2015). Evolution of the immune system in humans from infancy to old age. *Proceedings of the Royal Society B: Biological Sciences*, *282*(1821), 20143085. https://doi.org/doi:10.1098/rspb.2014.3085

Singh, A. K., Agarwal, N., & Saxena, A. (2021). Effect of extended geometry filled with and without phase change material on the thermal performance of solar air heater. *Journal of Energy Storage*, *39*. https://doi.org/10.1016/j.est.2021.102627

Singh, I., & Vardhan, S. (2021). Experimental investigation of an evacuated tube collector solar air heater with helical inserts. *Renewable Energy*, *163*, 1963-1972. https://doi.org/10.1016/j.renene.2020.10.114

Singh, V. P., Jain, S., Karn, A., Kumar, A., Dwivedi, G., Meena, C. S., Dutt, N., & Ghosh, A. (2022). Recent Developments and Advancements in Solar Air Heaters: A Detailed Review. *Sustainability*, *14*(19). https://doi.org/10.3390/su141912149

Sivakumar, S., Siva, K., & Mohanraj, M. (2019). Experimental thermodynamic analysis of a forced convection solar air heater using absorber plate with pin-fins. *Journal of Thermal Analysis and Calorimetry*, *136*(1), 39-47. https://doi.org/10.1007/s10973-018-07998-5

Sivakumar, S., Velmurugan, C., Dhas, D. S. E. J., Solomon, A. B., & Dev Wins, K. L. (2020). Effect of nano cupric oxide coating on the forced convection performance of a mixed-mode flat plate solar dryer. *Renewable Energy*, *155*, 1165-1172. https://doi.org/10.1016/j.renene.2020.04.027

Sivarathinamoorthy, H., & Sureshkannan, G. (2021). The Influence of Internal Heat Storage Material and Longitudinal Fins on a Double-Pass Solar Air Heater Performance. *Journal of Solar Energy Engineering*, *143*(1). https://doi.org/10.1115/1.4047454

Souayeh, B., Bhattacharyya, S., Hdhiri, N., & Hammami, F. (2021). Numerical investigation on heat transfer augmentation in a triangular solar air heater tube fitted with angular-cut varied-length twisted tape. *The European Physical Journal Plus*, *136*(6). https://doi.org/10.1140/epjp/s13360-021-01614-6

Sozen, A., Sirin, C., Khanlari, A., Tuncer, A. D., & Gurbuz, E. Y. (2020). Thermal performance enhancement of tube-type alternative indirect solar dryer with iron mesh modification. *Solar Energy*, *207*, 1269-1281. https://doi.org/10.1016/j.solener.2020.07.072

Sundar, L. S., Sharma, K. V., Naik, M. T., & Singh, M. K. (2013). Empirical and theoretical correlations on viscosity of nanofluids: A review. *Renewable and Sustainable Energy Reviews*, *25*, 670-686. https://doi.org/10.1016/j.rser.2013.04.003

Sunyer, J., Esnaola, M., Alvarez-Pedrerol, M., Forns, J., Rivas, I., Lopez-Vicente, M., Suades-Gonzalez, E., Foraster, M., Garcia-Esteban, R., Basagana, X., Viana, M., Cirach, M., Moreno, T., Alastuey, A., Sebastian-Galles, N., Nieuwenhuijsen, M., & Querol, X. (2015). Association between traffic-related air pollution in schools and cognitive development in primary school children: a prospective cohort study. *PLOS Medicine*, *12*(3), e1001792. https://doi.org/10.1371/journal.pmed.1001792

Sutu, A. (2023). *Solar heat world wide*. http://solarheateurope.eu/2023/09/22/solar-heat-worldwide-report-2023-sheds-light-on-european-market-growth/

Tuncer, A. D., Amini, A., & Khanlari, A. (2023). Developing an infrared-assisted solar drying system using a vertical solar air heater with perforated baffles and nano-enhanced black paint. *Solar Energy*, *263*. https://doi.org/10.1016/j.solener.2023.111958

Tyagi, V. V., Panwar, N. L., Rahim, N. A., & Kothari, R. (2012). Review on solar air heating system with and without thermal energy storage system. *Renewable and Sustainable Energy Reviews*, *16*(4), 2289-2303. https://doi.org/https://doi.org/10.1016/j.rser.2011.12.005

Vasantha Malliga, T., & Jeba Rajasekhar, R. V. (2017). Preparation and characterization of nanographite- and CuO-based absorber and performance evaluation of solar air-heating collector. *Journal of Thermal Analysis and Calorimetry*, *129*(1), 233-240. https://doi.org/10.1007/s10973-017-6155-1

Visagavel, K., & Srinivasan, P. (2010). Experimental investigation on solar air heater assisted natural ventilation in single-sided ventilated room. *Indian Journal of Science and Technology*, *3*(7), 802-806.

Wadhawan, A., Dhoble, A. S., & Gawande, V. B. (2018). Analysis of the effects of use of thermal energy storage device (TESD) in solar air heater. *Alexandria Engineering Journal*, *57*(3), 1173-1183. https://doi.org/10.1016/j.aej.2017.03.016

Wang, Tengyue, D., Yanhua, Zhao, Y., Liang, L., Wang, Z., & Chen, C. (2020). A comparative experimental investigation on thermal performance for two types of vacuum tube solar air collectors based on flat micro-heat pipe arrays (FMHPA). *Solar Energy*, *201*, 508-522. https://doi.org/10.1016/j.solener.2020.03.024

Wang, Zeyu, Diao, Y., Zhao, Y., Chen, C., Liang, L., & Wang, T. (2020). Thermal performance of integrated collector storage solar air heater with evacuated tube and lap joint-type flat micro-heat pipe arrays. *Applied Energy*, *261*. https://doi.org/10.1016/j.apenergy.2019.114466

Wang, P.-Y., Li, S.-F., & Liu, Z.-H. (2015). Collecting performance of an evacuated tubular solar high-temperature air heater with concentric tube heat exchanger. *Energy Conversion and Management*, *106*, 1166-1173. https://doi.org/10.1016/j.enconman.2015.10.058

Wang, T.-y., Diao, Y.-h., Zhu, T.-t., Zhao, Y.-h., Liu, J., & Wei, X.-q. (2017). Thermal performance of solar air collection-storage system with phase change material based on flat micro-heat pipe arrays. *Energy Conversion and Management*, *142*, 230-243. https://doi.org/10.1016/j.enconman.2017.03.039

Wang, T.-y., Zhao, Y.-h., Diao, Y.-h., Ren, R.-y., & Wang, Z.-y. (2019). Performance of a new type of solar air collector with transparent-vacuum glass tube based on micro-heat pipe arrays. *Energy*, *177*, 16-28. https://doi.org/10.1016/j.energy.2019.04.059

Wang, T., Diao, Y., Zhao, Y., Liang, L., Wang, Z., & Chen, C. (2020). A comparative experimental investigation on thermal performance for two types of vacuum tube solar air collectors based on flat micro-heat pipe arrays (FMHPA). *Solar Energy*, *201*, 508-522.

Wang, T., Zhao, Y., Diao, Y., Ma, C., Zhang, Y., & Lu, X. (2021). Experimental investigation of a novel thermal storage solar air heater (TSSAH) based on flat micro-heat pipe arrays. *Renewable Energy*, *173*, 639-651. https://doi.org/10.1016/j.renene.2021.04.027

Wang, Y. (2020). *Effects of operating a solar air heater on the indoor air quality in classrooms during the winter : a case study of Palmerston North primary schools : a thesis submitted in partial fulfilment of the requirements for the degree of Doctor of Philosophy (PhD) in Building Technology at Massey University, Auckland, New Zealand* [Doctoral, Massey University]. http://hdl.handle.net/10179/16397

Wang, Y., Boulic, M., Phipps, R., Plagmann, M., & Cunningham, C. (2019). *Impact on primary classrooms temperature and ventilation from using a roof-mounted solar air heater: a winter case study in New Zealand*. Healthy Buildings 2019 Asia and Pacific Rim (HB2019 Asia).

Wang, Y., Boulic, M., Phipps, R., Plagmann, M., & Cunningham, C. (2020). Experimental performance of a solar air collector with a perforated back plate in New Zealand. *Energies*, *13*(6). https://doi.org/10.3390/en13061415

Wang, Y., Boulic, M., Phipps, R., Plagmann, M., Cunningham, C., & Guyot, G. (2023). Field performance of a solar air heater used for space heating and ventilation – A case study in New Zealand primary schools. *Journal of Building Engineering*, *76*. https://doi.org/10.1016/j.jobe.2023.106802

Wang, Y., Boulic, M., Phipps, R., Plagmann, M., Cunningham, C., Theobald, C., Howden-Chapman, P., & Baker, M. (2016). *Impacts of a solar ventilation unit on temperature and ventilation rate in New Zealand schools: an intervention study*.

Wang, Z., Diao, Y., Zhao, Y., Chen, C., Liang, L., & Wang, T. (2019). Thermal performance investigation of an integrated collector–storage solar air heater on the basis of lap joint-type flat micro-heat pipe arrays: Simultaneous charging and discharging mode. *Energy*, *181*, 882-896. https://doi.org/10.1016/j.energy.2019.05.197

Wargocki, P., Porras-Salazar, J. A., Contreras-Espinoza, S., & Bahnfleth, W. (2020). The relationships between classroom air quality and children's performance in school. *Building and Environment*, *173*. https://doi.org/10.1016/j.buildenv.2020.106749

Wargocki, P., & Wyon, D. P. (2007a). The effects of moderately raised llassroom temperatures and classroom ventilation rate on the performance of schoolwork by children (RP-1257) [Article]. *HVAC&R Research*, *13*(2), 193-220. https://doi.org/10.1080/10789669.2007.10390951

Wargocki, P., & Wyon, D. P. (2007b). The effects of outdoor air supply rate and supply air filter condition in classrooms on the performance of schoolwork by children (RP-1257).

HVAC&R Research, *13*(2), 165. http://ezproxy.massey.ac.nz/login?url=http://search.ebscohost.com/login.aspx?direct=true&db=edb&AN=24818834&site=eds-live&scope=site

Weyant, E. (2022). Research Design: Qualitative, Quantitative, and Mixed Methods Approaches, 5th Edition. *Journal of Electronic Resources in Medical Libraries*, *19*(1-2), 54-55. https://doi.org/10.1080/15424065.2022.2046231

WHO guidelines for indoor air quality:selected pollutants, (2010). https://apps.who.int/iris/bitstream/handle/10665/260127/9789289002134-eng.pdf

WHO. (2021). World Health Organization. In *Roadmap to improve and ensure good indoor ventilation in the context of COVID-19*.

Wolkoff, P. (2018). Indoor air humidity, air quality, and health - An overview. *Int J Hyg Environ Health*, *221*(3), 376-390. https://doi.org/10.1016/j.ijheh.2018.01.015

Wolkoff, P., Azuma, K., & Carrer, P. (2021). Health, work performance, and risk of infection in office-like environments: The role of indoor temperature, air humidity, and ventilation. *Int J Hyg Environ Health*, *233*, 113709. https://doi.org/10.1016/j.ijheh.2021.113709

Yassien, H. N. S., Alomar, O. R., & Salih, M. M. M. (2020). Performance analysis of triple-pass solar air heater system: Effects of adding a net of tubes below absorber surface. *Solar Energy*, *207*, 813-824. https://doi.org/10.1016/j.solener.2020.07.041

Zhang, Q., Zhang, K., Xu, D., Yang, G., Huang, H., Nie, F., Liu, C., & Yang, S. (2014). CuO nanostructures: Synthesis, characterization, growth mechanisms, fundamental properties, and applications. *Progress in Materials Science*, *60*, 208-337. https://doi.org/10.1016/j.pmatsci.2013.09.003

Zhu, T.-t., Diao, Y.-h., Zhao, Y.-h., & Deng, Y.-c. (2015). Experimental study on the thermal performance and pressure drop of a solar air collector based on flat micro-heat pipe arrays. *Energy Conversion and Management*, *94*, 447-457. https://doi.org/10.1016/j.enconman.2015.01.052

Zhu, T.-T., Diao, Y.-H., Zhao, Y.-H., & Li, F.-F. (2016). Thermal performance of a new CPC solar air collector with flat micro-heat pipe arrays. *Applied Thermal Engineering*, *98*, 1201-1213. https://doi.org/10.1016/j.applthermaleng.2016.01.033

Zhu, T., & Zhang, J. (2021). A numerical study on performance optimization of a micro-heat pipe arrays-based solar air heater. *Energy*, *215*. https://doi.org/10.1016/j.energy.2020.119047

Appendices

Appendix A: Solar air heater experimental performance

Appendix : A1 for effective efficiency calculations

The effective efficiency of the solar air heater was calculated by the equation given by Cortes and Piacentini (1990) and Mittal and Varshney (2006).

$$m_{\eta_{eff}} = \frac{Q_u - \frac{P_m}{C}}{I_T A_C}$$

Where,

$m_{\eta eff}$	Effective efficiency of the SAH (%)
Q_u	Useful thermal energy gained by SAH (W)
P_m	Mechanical power is required to force the air through the SAH
C	The conversion factor = 0.18
I_T	Solar radiation on the tilted SAH surface (W/m^2)
A_c	SAH effective area

Useful thermal energy gain (Q_u) was calculated using equation 3.1 given by (John & Beckman, 2013).

$Q_u = \dot{m}C_p(T_o - T_i)$ 3.1

Required mechanical power (P_m) can be calculated from the Equation 3.3 given by Hussien and Farhan (2019).

$$P_m = \frac{\dot{m}\Delta P}{\rho} \quad \textbf{(3.3)}$$

Where,

ΔP	Pressure drops across the SAH, Pa
$\dot{m}$	The mass flow rate of air, kg/s
ρ	Density, kg/m^3

Bernoulli's principle is applied to estimate the pressure drop across the SAH (Dubey, 2014). Assuminimumg that the flow is uniform and there are no significant losses, the pressure drop (ΔP) across the solar air heater can be calculated from Equation 3.4.

$$\Delta P = \rho g(h_2 - h_1)$$

Where,

h_1	Height of SAH (at lower end side) from the base of the metal frame, $h_1 = 0m$
h_2	Height of SAH (at upper-end side) from the base of the metal frame, $h_2 = 1.5m$
g	Acceleration due to gravity, 9.81 m/s^2

Appendix A2: Finned tube type SAH setup, issues and recommendations

1) Anemometer reading

Figure 9-1 displays the annemoter reading. Placing the anemometer close to the fan gives a very high velocity (e.g. 7.7, Fig 9-1) resulting in unrealistic efficiency values (i.e. above 100%). Therefore, it was recommended to place the sensor at least 0.5 m away from the fan (as recommended by Airlab, NZ).

Figure 9-1 Anemometer reading

2) Duct mounting; A. initial position, and B altered position

Figure 9-2: A and B show the duct positioning. Initially, the duct was positioned vertically with a slight inclination at the center, supported on a table, which led to material buildup and caused airflow blockages, resulting in inaccurate data. To resolve this, the duct was later aligned horizontally, with a slight inclination at the solar air heater (SAH) exit, ensuring more consistent airflow and improving the accuracy of the experiment.

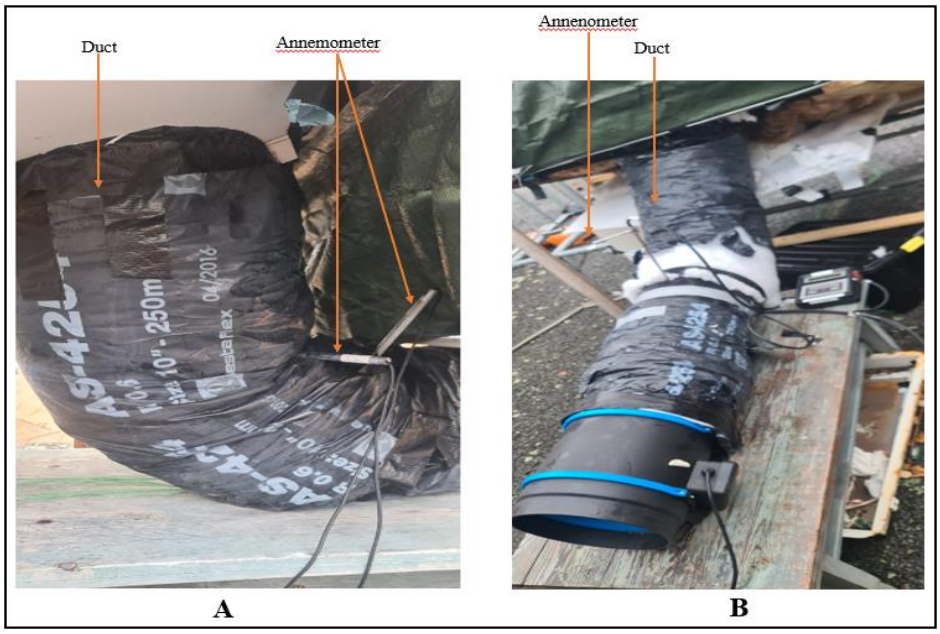

Figure 9-2 Duct mounting; A. initial position, and B altered position

3) Condensation on the solar air heater surface

Figure 9-3 shows the condensation forminimumg on the surface of the solar air heater panel cold days. This condensation was likely results from moisture trapped inside the panel. Therefore, the fan was operated at 8:15 am to mitigate condensation. Running the fan will circulate air inside the solar air heater, preventing moisture from settling on surfaces and allowing any existing condensation to evaporate. This issue could be addressed by improving the sealing of the panel frame, adding a ventilation system, or implementing an anti-condensation layer.

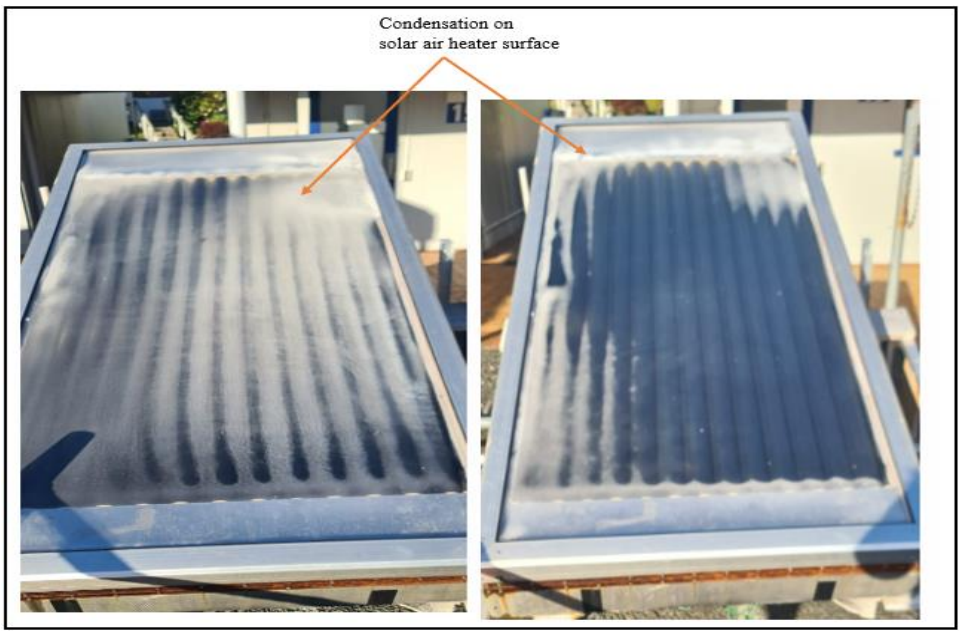

Figure 9-3 Condensation on the solar air heater surface

4) Air drying of nanocoated tubes

After the application of the nanoparticle coating, the tubes underwent a drying process to ensure uniform adhesion of the coating. The drying phase was critical to remove any residual solvents and to stabilize the nanoparticle layer. The tubes were air-dried under controlled conditions to prevent any irregularities or defects in the coating. This step is essential to enhance the durability and performance of the nanocoated tubes.

Figure 9-4 Air drying of nanocoated tubes

5) Coating removal and degradation of Tubes

Tubes experienced coating removal or degradation due to wear, likely from environmental exposure or operational stress. Therefore, stability test is recommended.

Figure 9-5 Coating removal and degradation of Tubes

Approval for attaching review paper in the appendix section

PH **Permissions Helpdesk**

To: pardeshipoonam25@gmail.com <pardeshipoonam25@gmail.com>

Wed 2024-09-25 5:17 AM

How was our service today?

Dear Prof. Poonam Pardeshi,

Thank you so much for sharing.

As an Elsevier journal author, you retain the right to Include the article in a thesis or dissertation (provided that this is not to be published commercially) whether in full or in part, subject to proper acknowledgment; see https://www.elsevier.com/about/policies/copyright for more information. As this is a retained right, no written permission from Elsevier is necessary.

As outlined in our permissions licenses, this extends to the posting to your university's digital repository of the thesis provided that if you include the published journal article (PJA) version, it is embedded in your thesis only and not separately downloadable.

Thank you.

Kind regards,

Thomas Rexson Yesudoss
Copyrights Specialist
ELSEVIER | HCM - Health Content Management

Visit Elsevier Permissions

MASSEY UNIVERSITY
TE KUNENGA KI PŪREHUROA
UNIVERSITY OF NEW ZEALAND

GRADUATE RESEARCH SCHOOL

STATEMENT OF CONTRIBUTION
DOCTORATE WITH PUBLICATIONS/MANUSCRIPTS

We, the candidate and the candidate's Primary Supervisor, certify that all co-authors have consented to their work being included in the thesis and they have accepted the candidate's contribution as indicated below in the *Statement of Originality*.

Name of candidate:	Poonam Subhash Singh Pardeshi
Name/title of Primary Supervisor:	Dr Mikael Boulic
In which chapter is the manuscript /published work:	Appendix

Please select one of the following three options:

(●) **The manuscript/published work is published or in press**

- **Please provide the full reference of the Research Output:**

1) Pardeshi, Poonam S., Mikael Boulic, Andries van Heerden, Robyn Phipps, and Chris W. Cunningham. 2024. "Review of the thermal efficiency of a tube-type solar air heater." Renewable and Sustainable Energy Reviews 199. https://doi.org/10.1016/j.rser.2024.114509.

( ) **The manuscript is currently under review for publication – please indicate:**

- **The name of the journal:**

- **The percentage of the manuscript/published work that was contributed by the candidate:** 85.00

- **Describe the contribution that the candidate has made to the manuscript/published work:**

Conceptualizing- Poonam Subhash Singh Pardeshi, Dr Mikael Boulic, Dr Andries (Hennie) van Heerden, Prof Robyn Phipps
literature review, methodology, writing, and editing- Poonam Subhash Singh Pardeshi
Supervision- Poonam Subhash Singh Pardeshi, Dr Mikael Boulic, Dr Andries (Hennie) van Heerden, Prof Robyn Phipps and Prof Chris Cunningham

( ) **It is intended that the manuscript will be published, but it has not yet been submitted to a journal**

Candidate's Signature:	Poonam Digitally signed by Poonam Date: 2024.09.25 09:36:11 +12'00'
Date:	25-Sep-2024
Primary Supervisor's Signature:	Mikael Boulic Digitally signed by Mikael Boulic Date: 2024.09.25 21:36:58 +12'00'
Date:	25-Sep-2024

This form should appear at the end of each thesis chapter/section/appendix submitted as a manuscript/ publication or collected as an appendix at the end of the thesis.

GRS Version 5 – 13 December 2019
DRC 19/09/10

MASSEY UNIVERSITY
TE KUNENGA KI PŪREHUROA
UNIVERSITY OF NEW ZEALAND

GRADUATE RESEARCH SCHOOL

STATEMENT OF CONTRIBUTION
DOCTORATE WITH PUBLICATIONS/MANUSCRIPTS

We, the candidate and the candidate's Primary Supervisor, certify that all co-authors have consented to their work being included in the thesis and they have accepted the candidate's contribution as indicated below in the *Statement of Originality*.

Name of candidate:	Poonam Subhash Singh Pardeshi
Name/title of Primary Supervisor:	Dr Mikael Boulic
In which chapter is the manuscript /published work:	Appendix

Please select one of the following three options:

○ The manuscript/published work is published or in press

- Please provide the full reference of the Research Output:

◉ The manuscript is currently under review for publication – please indicate:

- The name of the journal:

Renewable Energy

- The percentage of the manuscript/published work that was contributed by the candidate: 90.00

- Describe the contribution that the candidate has made to the manuscript/published work:

Conceptualizing- Poonam Subhash Singh Pardeshi, Dr Mikael Boulic, Dr Andries (Hennie) van Heerden, Prof Robyn Phipps
Methodology, writing, and editing- Poonam Subhash Singh Pardeshi
Supervision- Poonam Subhash Singh Pardeshi, Dr Mikael Boulic, Dr Andries (Hennie) van Heerden, Prof Robyn Phipps and Prof Chris Cunningham

○ It is intended that the manuscript will be published, but it has not yet been submitted to a journal

Candidate's Signature:	Poonam Digitally signed by Poonam Date: 2024.09.25 11:21:27 +12'00'
Date:	25-Sep-2024
Primary Supervisor's Signature:	Mikael Boulic Digitally signed by Mikael Boulic Date: 2024.09.25 21:38:40 +12'00'
Date:	25-Sep-2024

This form should appear at the end of each thesis chapter/section/appendix submitted as a manuscript/ publication or collected as an appendix at the end of the thesis.

GRS Version 5 – 13 December 2019
DRC 19/09/10